UNIVERSITY OF WALES SWANSEA

CIVIL ENGINEERING

FINITE AND INFINITE ELEMENTS IN STATIC AND DYNAMIC STRUCTURAL ANALYSIS

by

José Manuel Mota Couto Marques, Lic.Eng.

Thesis submitted to the University of Wales
in candidature for the degree of
Doctor of Philosophy

C/Ph/78/84 April 1984

T/5

FINITE AND INFINITE ELEMENTS IN STATIC AND DYNAMIC STRUCTURAL ANALYSIS

by

José Manuel Mota Couto Marques

Lic.Eng.

624(043) HARj / FIN
UNIVERSIDADE DO PORTO
Faculdade de Engenharia
BIBLIOTECA
N.º 13726-07
CDU
Data 20 / 9 / 1989
U.N. 5722

T/5

Thesis submitted to the University of Wales

in candidature for the degree

of Doctor of Philosophy

043 D
M 318 f

April 1984

Department of Civil Engineering

University College of Swansea

C/Ph/78/84

To my Mother and to my Father

συνειδὼς ἐμαυτῷ ἀμαθίαν

Σωκρατης

(Πλατων, Φαιδρος, 235)

CERTIFICATE OF RESEARCH

This is to certify that except where specific reference to other investigators is made, the work described in this thesis is the result of the investigation of the candidate.

.....

Candidate

.....

Director of studies

DECLARATION

This is to certify that neither this thesis nor any part of it has been presented or is being concurrently submitted in candidature for any degree at any other University.

.....J. Couto Reyes.....

Candidate

ACKNOWLEDGEMENTS

I wish to express my immense gratitude to Prof. D.R.J. Owen for his attentive and stimulating supervision of my work.

I thank Prof. O.C. Zienkiewicz for having made available the departmental facilities and, in particular, for having provided one of the main themes for my research.

I am obliged to Prof. Joaquim Sarmento for inspiring my interest in structural analysis and to Prof. Rogério Martins for guiding my first steps in the finite element world.

I thank Drs. H.H. Abdel Rahman, P. Bettess, E. Hinton and R.D. Wood for their advice at various stages of my work.

Many thanks are due to S. Azevedo, S. Caldis, F. Damjanić, C. Emson, R. Fejzo, J. Gago, P. Griffin, K. Hatakeyama, M. Honnor, K.H. Leung, D. Mackay and T. Shiomi and, in particular, to Joaquim Figueiras, Orlando Gonçalves Fº and José César de Sá, for their critical support and readiness for many helpful discussions.

My appreciation goes also to all the staff of the Computer Centre for their constant and friendly assistance and, specially, to Mr. P. Gibson and Mr. M. Llewellyn for their valuable advice in developing graphics software and generally "cutting some corners" and to the Computer Advisory team whose expertise helped making fun out of debugging.

I am indebted to the Calouste Gulbenkian Foundation, Instituto Nacional de Investigação Científica and Committee of Vice-Chancellors and Principals of the Universities of the United Kingdom for their financial support.

I am grateful to Mrs. R. Lewis for her patience and care in typing this thesis.

And last, but by no means least, I wish to express my sincere gratitude to my family for constant encouragement throughout my work.

SUMMARY

Finite element techniques are discussed for quasistatic and dynamic materially and geometrically nonlinear analysis of two and three dimensional structures and unbounded domains.

The finite element spatial discretization of the structural dynamic equilibrium equations is presented and a predictor-corrector implicit-explicit direct integration method of the Newmark family is described.

The modelling of elastoplastic behaviour is discussed and various numerical refinements for improved accuracy are proposed.

An elastoviscoplastic algorithm is outlined, with special reference to hardening effects. An implicit-explicit scheme is introduced for quasistatic multimaterial applications.

An Updated Lagrangian formulation is described for geometrically nonlinear problems.

Secant-Newton and BFGS matrix update techniques are presented in association with standard and modified Newton-Raphson methods for efficient incremental-iterative solution of the finite element equations. A novel secant-Newton formula is derived and the potential of line searches as an accelerator is assessed.

The mapped infinite element concept is described and various forms for 2D and 3D analysis are extensively tabulated. Use of finite-infinite element meshes for unbounded domain modelling is illustrated.

CONTENTS

CHAPTER 1 INTRODUCTION

1.1 PRELIMINARY REMARKS 1.1

1.2 SCOPE AND LAYOUT OF THE THESIS 1.2

CHAPTER 2 FINITE ELEMENT DISPLACEMENT FORMULATION IN SOLID MECHANICS

2.1 INTRODUCTION 2.1

2.2 VIRTUAL WORK ANALYSIS 2.1

2.3 FINITE ELEMENT DISCRETIZATION 2.2

2.4 DYNAMIC EQUILIBRIUM EQUATIONS 2.5

2.5 LINEAR ELASTIC MATERIAL MODEL 2.5

2.6 COMPUTATION OF THE STIFFNESS, MASS AND DAMPING MATRICES 2.7

2.7 SOLUTION OF THE DYNAMIC EQUILIBRIUM EQUATIONS 2.9

2.8 PARTITIONING METHODS 2.13

2.9 OPERATOR SPLITTING METHODS 2.14

2.10 CLOSING REMARKS 2.16

2.11 REFERENCES 2.17

CHAPTER 3 THE ELASTOPLASTIC MODEL FOR MATERIAL NONLINEARITY

3.1 INTRODUCTION 3.1

3.2 A HISTORICAL NOTE 3.2

3.3 FUNDAMENTAL PLASTICITY CONCEPTS 3.3

3.4 MATRIX FORMULATION 3.6

3.5 BASIC STEPS FOR STRESS COMPUTATION IN INCREMENTAL ELASTOPLASTIC ANALYSIS 3.9

3.6 DETERMINATION OF THE CONTACT STRESS STATE 3.11

3.7 SUBDIVISION OF THE EXCESS STRESS 3.17

CHAPTER 3 (continued)

3.8	REDUCTION OF THE EXCESS STRESS	3.18
3.9	END-OF-STEP CORRECTION	3.20
3.10	YIELD SURFACES WITH SINGULARITIES	3.21
3.11	PHYSICAL AND NUMERICAL UNLOADING	3.23
3.12	PLANE STRESS PLASTICITY	3.24
3.13	FINAL REMARK	3.27
3.14	REFERENCES	3.28

CHAPTER 4 THE ELASTOVISCOPLASTIC MODEL FOR MATERIAL NONLINEARITY

4.1	INTRODUCTION	4.1
4.2	COMPUTATIONAL PROCEDURE FOR ELASTOVISCOPLASTIC PROBLEMS	4.2
4.3	THE HARDENING CORRECTIVE TERM	4.7
4.4	COMPUTATION OF MATRIX $\underline{H}$	4.8
4.5	TIME STEP DEFINITION	4.10
4.6	IMPLICIT-EXPLICIT TIME INTEGRATION	4.11
4.7	FRONTAL SUBSTRUCTURING IN IMPLICIT-EXPLICIT PROBLEMS	4.11
4.8	NUMERICAL EXAMPLES	4.12
4.9	CONCLUSIONS	4.22
4.10	REFERENCES	4.23

CHAPTER 5 GEOMETRIC NONLINEARITY

5.1	INTRODUCTION -	5.1
5.2	PRELIMINARY CONSIDERATIONS	5.2
5.3	DEFINITIONS OF STRAIN AND RATES OF STRAIN	5.4
5.4	DEFINITIONS OF STRESS AND RATES OF STRESS	5.6
5.5	CONSTITUTIVE RELATIONS	5.7
5.6	VIRTUAL VELOCITY EQUATION	5.7
5.7	RATE FORM OF THE VIRTUAL VELOCITY EQUATION	5.8

CHAPTER 5 (continued).

5.8	UPDATED LAGRANGIAN FINITE ELEMENT FORMULATION	5.9
5.9	STRESS COMPUTATION	5.11
5.10	REFERENCES	5.12

CHAPTER 6 NONLINEAR SOLUTION TECHNIQUES

6.1	INTRODUCTION	6.1
6.2	A NOTE ON EARLY DEVELOPMENTS	6.2
6.3	STANDARD NEWTON-RAPHSON METHOD	6.6
6.4	MODIFIED NEWTON-RAPHSON METHODS	6.7
6.5	LINE SEARCH	6.8
6.6	QUASI-NEWTON METHODS	6.10
6.7	SECANT NEWTON METHODS	6.16
6.8	CONVERGENCE CRITERIA	6.18
6.9	DIVERGENCE AND TERMINATION PROCEDURES	6.19
6.10	CURRENT TRENDS IN SOLUTION TECHNIQUES	6.21
6.11	NUMERICAL EXAMPLES	6.22
6.12	CONCLUDING REMARKS	6.41
6.13	REFERENCES	6.42

CHAPTER 7 MAPPED INFINITE ELEMENTS IN STATIC STRUCTURAL ANALYSIS

7.1	INTRODUCTION	7.1
7.2	NUMERICAL TECHNIQUES FOR UNBOUNDED DOMAIN ANALYSIS	7.2
7.3	MAPPED INFINITE ELEMENTS - THE FUNDAMENTAL CONCEPT	7.4
7.4	ONE-DIMENSIONAL MAPPED INFINITE ELEMENTS	7.5
7.5	TWO-DIMENSIONAL MAPPED INFINITE ELEMENTS	7.7
7.6	THREE-DIMENSIONAL MAPPED INFINITE ELEMENTS	7.11
7.7	POSITIONING OF THE EXPANSION POLES	7.13

CHAPTER 7 (continued)

7.8	COMPUTER IMPLEMENTATION OF MAPPED INFINITE ELEMENTS	7.14
7.9	ELASTOPLASTIC APPLICATIONS	7.16
7.10	ELASTOVISCOPLASTIC APPLICATIONS	7.28
7.11	CONCLUDING REMARKS	7.35
7.12	REFERENCES	7.36

CHAPTER 8 MAPPED INFINITE ELEMENTS IN DYNAMIC STRUCTURAL ANALYSIS

8.1	INTRODUCTION	8.1
8.2	PERIODIC AND TRANSIENT PROBLEMS IN UNBOUNDED DOMAINS	8.1
8.3	MAPPED INFINITE ELEMENTS IN TRANSIENT PROBLEMS	8.2
8.4	INFINITE ELEMENTS IN PERIODIC PROBLEMS	8.2
8.5	NUMERICAL EXPERIMENTS	8.3
8.6	REFERENCES	8.8

CHAPTER 9 CONCLUSIONS

9.1	GENERAL CONSIDERATIONS	9.1
9.2	ACCURACY IN MODELLING OF MATERIAL BEHAVIOUR	9.1
9.3	EFFICIENCY IN NONLINEAR SOLUTION	9.2
9.4	ECONOMY IN UNBOUNDED DOMAIN ANALYSIS	9.2
9.5	DIRECTIONS FOR FURTHER STUDY	9.3
9.6	REFERENCES	9.5

CHAPTER 1

INTRODUCTION

1.1 PRELIMINARY REMARKS 1.1

1.2 SCOPE AND LAYOUT OF THE THESIS 1.2

CHAPTER 1

INTRODUCTION

1.1 PRELIMINARY REMARKS

Since its inception more than thirty years ago, the Finite Element Method (FEM) experienced a steady growth, by deepening the theoretical foundations while widening the applicability range. In its present state of maturity it is considered by both the investigator and the practitioner to be a versatile and reliable numerical tool for research and design.

In many instances the FEM has supplied the means to "make the theory work", thereby putting it to test and stimulating further development. This was for example the case of the mathematical theory of plasticity which was hampered at a certain stage by increasing difficulties in producing analytical solutions for less regular geometries and loading. Geometric and material nonlinearities, as those associated with elastoplastic and elastoviscoplastic behaviour, have nowadays become an indispensable ingredient of many structural analyses and form thus a relevant research topic.

The consideration of inelastic behaviour, combined with large geometry changes and possibly compounded with dynamic effects, constitutes a heavy burden for the solid mechanician, notwithstanding the continuing expansion of computer capacity and speed. The urge for efficient, stable and accurate nonlinear solution methods is therefore strongly felt.

The FEM has proved capable of adequately representing phenomena taking place in a continuum. However, in many practical applications, say in geomechanics, the domain of analysis is essentially unbounded and would therefore require an infinite number of finite elements. This is evidently not a realistic proposal but suffices to show the convenience of extending the method from its standard form in order to cope efficiently with such requirements.

1.2 SCOPE AND LAYOUT OF THE THESIS

The present investigation is centered on the three research areas identified above:

(i) - accuracy in the modelling of structural nonlinearities;

(ii) - efficiency in the solution of the finite element equations;

(iii) - expediency in the modelling of unbounded domains.

The layout of the thesis is now described.

- Chapter 2 introduces the structural dynamic (and static) equilibrium equations, outlines the corresponding finite element spatial discretization and describes methods for time integration of the semi-discrete equations.

- Chapter 3 presents the elastoplastic material model and examines in great detail its computer implementation for associated small strain applications, proposing improved numerical procedures.

- Chapter 4 is devoted to elastoviscoplastic small strain problems. A special reference is made to the representation of hardening behaviour. An implicit-explicit time integration scheme is proposed for efficient solution of problems in multimaterial domains.

- Chapter 5 discusses the nonlinearity introduced by changes of the initial geometry. The governing equations are rederived in rate form and an Updated Lagrangian formulation is outlined.

- Chapter 6 focusses upon methods for the incremental-iterative solution of the nonlinear finite element equation system. The classic standard and modified Newton-Raphson methods are considered and the convenience of adding line searches to the latter is illustrated. Various matrix update (BFGS and secant Newton) techniques are discussed and a novel secant Newton procedure is proposed and assessed.

- Chapter 7 describes the mapped infinite element concept and presents a systematic derivation of two and three dimensional infinite elements. A number of quasistatic materially nonlinear examples is presented that attest to the accuracy and efficiency of combined finite-infinite element meshes for unbounded field modelling.

- Chapter 8 makes a preliminary assessment of the capabilities of the mapped infinite element for dynamic applications in semi--infinite domains.

- Chapter 9 extracts the final conclusions and suggests directions for further study.

CHAPTER 2

FINITE ELEMENT DISPLACEMENT FORMULATION IN SOLID MECHANICS

2.1	INTRODUCTION	2.1
2.2	VIRTUAL WORK ANALYSIS	2.1
2.3	FINITE ELEMENT DISCRETIZATION	2.2
2.4	DYNAMIC EQUILIBRIUM EQUATIONS	2.5
2.5	LINEAR ELASTIC MATERIAL MODEL	2.5
2.6	COMPUTATION OF THE STIFFNESS, MASS AND DAMPING MATRICES	2.7
2.7	SOLUTION OF THE DYNAMIC EQUILIBRIUM EQUATIONS	2.9
2.8	PARTITIONING METHODS	2.13
2.9	OPERATOR SPLITTING METHODS	2.14
2.10	CLOSING REMARKS	2.16
2.11	REFERENCES	2.17

CHAPTER 2

FINITE ELEMENT DISPLACEMENT FORMULATION IN SOLID MECHANICS

2.1 INTRODUCTION

In recent years extensive use has been made of the Finite Element Method by solid and structural mechanicians [1]. The vigorous research activity sustained in this field, coupled with the prodigious development of computer hardware and software, has expanded beyond belief the range and scope of engineering problems amenable to numerical solution.

In this Chapter the structural dynamic equilibrium equations and their finite element spatial discretization are presented. Static analysis is contemplated as a particular case. A preliminary reference is made to nonlinear structural behaviour that will be further developed in Chapters 3 to 5. Methods for time integration of the semi-discrete finite element equations are briefly reviewed and the state-of-the-art in this area is outlined.

2.2 VIRTUAL WORK ANALYSIS

Consider the motion of a body V for which the internal stresses $\underline{\sigma}$ are in equilibrium with surface tractions $\underline{t}$ acting on the portion Γ_t of the boundary Γ and volumetric forces $\underline{z}$ that include body, inertial and damping contributions.

According to the principle of virtual work, if the body is subjected to any virtual displacement field $\delta\underline{u}$ (i.e. one whose components are infinitesimal and compatible with both the boundary constraints and the condition of material continuity), then the net virtual work done by the internal and external forces on the virtual displacements will be zero.

Noting that

$$\underline{z} = \underline{b} - \rho\ddot{\underline{u}} - c\dot{\underline{u}} \tag{2.1}$$

where $\underline{b}$, $\rho\ddot{\underline{u}}$, $c\dot{\underline{u}}$ are, respectively, the body, inertial and damping forces, with ρ the mass density, c the damping parameter and dots denoting time differentiation, we may therefore write

$$\int_V \delta\underline{\varepsilon}^T \underline{\sigma}\, dV - \int_V \delta\underline{u}^T (\underline{b} - \rho\ddot{\underline{u}} - c\dot{\underline{u}})\, dV - \int_{\Gamma_t} \delta\underline{u}^T \underline{t}\, d\Gamma = 0 \tag{2.2}$$

where $\delta\underline{\varepsilon}$ is the virtual strain associated with $\delta\underline{u}$.

2.3 FINITE ELEMENT DISCRETIZATION

Following the standard procedure [1], the spatial domain V is divided into m finite elements interconnected at p nodal mesh points.

Using an isoparametric formulation a single set of functions is employed to interpolate both the geometry and the field variables inside each element from the respective set of nodal values. These functions, the shape functions, are defined for a parent element in a normalized coordinate system onto which the real or distorted element is mapped. All required integration is performed numerically by a Gauss-Legendre rule.

Expressing displacements, velocities and accelerations $\underline{u}$, $\dot{\underline{u}}$, $\ddot{\underline{u}}$ in terms of their nodal values $\underline{d}$, $\dot{\underline{d}}$, $\ddot{\underline{d}}$ by means of the matrix $\underline{N}$ of shape functions we have

$$\begin{aligned}
\underline{u} &= \underline{N}\,\underline{d} = \sum_{i=1}^{p} \underline{N}_i\, \underline{d}_i \\
\dot{\underline{u}} &= \underline{N}\,\dot{\underline{d}} = \sum_{i=1}^{p} \underline{N}_i\, \dot{\underline{d}}_i \\
\ddot{\underline{u}} &= \underline{N}\,\ddot{\underline{d}} = \sum_{i=1}^{p} \underline{N}_i\, \ddot{\underline{d}}_i
\end{aligned} \tag{2.3}$$

where $\underline{N}$ is a diagonal matrix of p submatrices $\underline{N}_i = N_i \underline{I}$, with $\underline{I}$ being a r x r identity matrix and r, the number of variables per node, is r = 2 for plane and axisymmetric problems and r = 3 for three dimensional situations.

Table 2.1 and fig. 2.1 present the shape functions corresponding to the finite elements used in this study.

LINEAR 4-NODE RECTANGULAR ELEMENT

$$N_i = (1 + \xi\xi_i)(1 + \eta\eta_i)/4$$

QUADRATIC 8-NODE RECTANGULAR ELEMENT

$$N_i = (1 + \xi\xi_i)(1 + \eta\eta_i)(\xi\xi_i + \eta\eta_i - 1)/4 \quad \text{- corner nodes}$$

$$N_i = \xi_i^2(1 + \xi\xi_i)(1 - \eta^2)/2 + \eta_i^2(1 + \eta\eta_i)(1 - \xi^2)/2 \quad \text{- midside nodes}$$

QUADRATIC 9-NODE RECTANGULAR ELEMENT

$$N_i = [\xi\xi_i(1 + \xi\xi_i)/2 + (1 - \xi^2)(1 - \xi_i^2)][\eta\eta_i(1 + \eta\eta_i)/2 + (1 - \eta^2)(1 - \eta_i^2)]$$

LINEAR 8-NODE BRICK ELEMENT

$$N_i = (1 + \xi\xi_i)(1 + \eta\eta_i)(1 + \zeta\zeta_i)/8$$

QUADRATIC 20-NODE BRICK ELEMENT

$$N_i = (1 + \xi\xi_i)(1 + \eta\eta_i)(1 + \zeta\zeta_i)(\xi\xi_i + \eta\eta_i + \zeta\zeta_i - 2)/8 \quad \text{- corner nodes}$$

$$N_i = \eta_i^2 \zeta_i^2(1 - \xi^2)(1 + \eta\eta_i)(1 + \zeta\zeta_i)/4$$
$$+ \zeta_i^2 \xi_i^2(1 - \eta^2)(1 + \xi\xi_i)(1 + \zeta\zeta_i)/4 \quad \text{- midside nodes}$$
$$+ \xi_i^2 \eta_i^2(1 - \zeta^2)(1 + \xi\xi_i)(1 + \eta\eta_i)/4$$

TABLE 2.1 – Shape functions for some linear and quadratic 2D and 3D finite elements

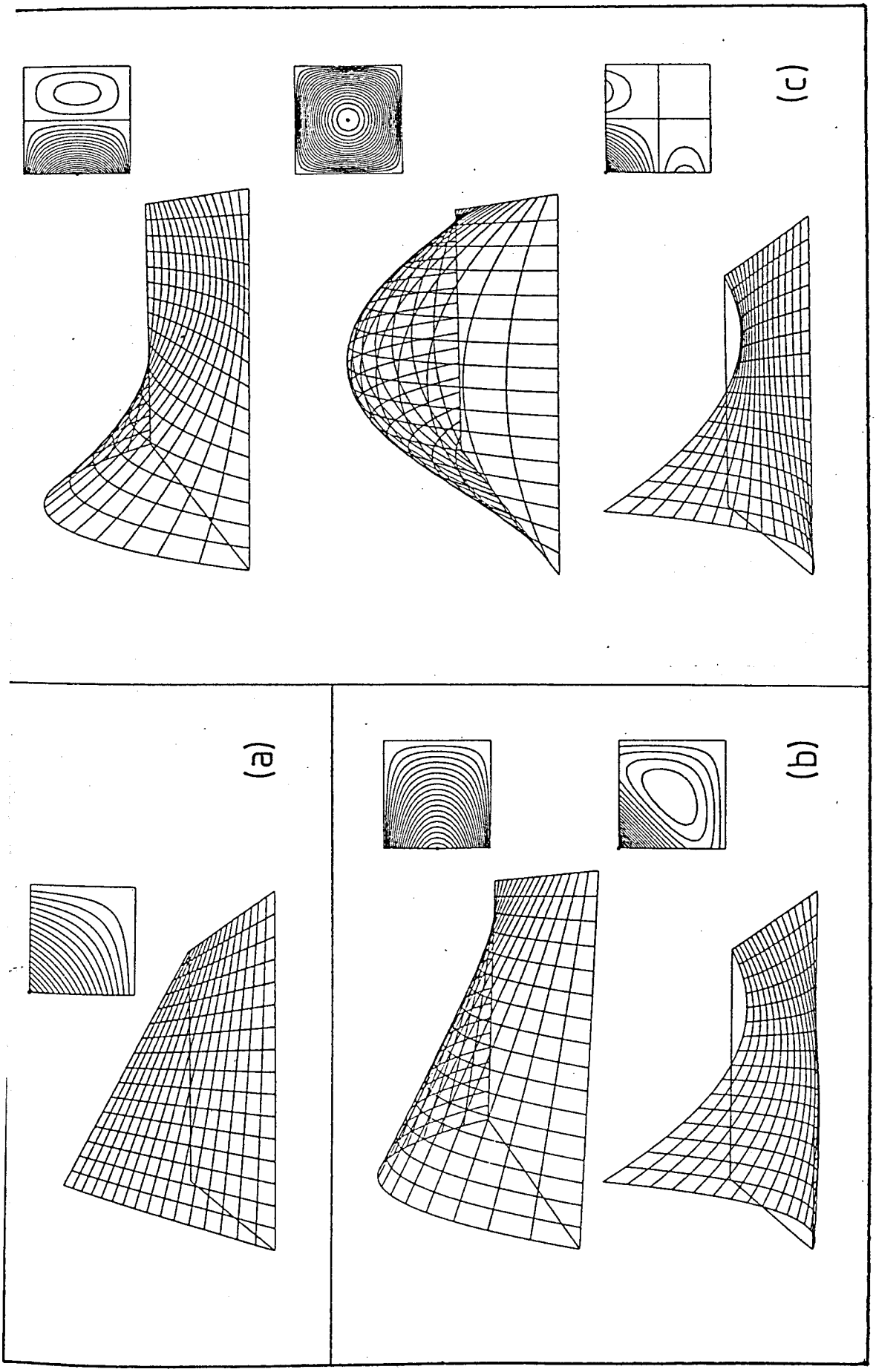

Fig. 2.1 – Typical shape functions for two dimensional finite elements
(a) – 4-node, (b) – 8-node, (c) – 9-node [2]

With the strain-displacement matrix $\underline{B}$ we may relate the virtual strains and displacements by

$$\delta\underline{\varepsilon} = \underline{B}\ \delta\underline{d} = \sum_{i=1}^{p} \underline{B}_i\ \delta\underline{d}_i \tag{2.4}$$

Table 2.2 gives the form of typical submatrices $\underline{B}_i$ for two and three dimensional problems.

2.4 DYNAMIC EQUILIBRIUM EQUATIONS

Substituting (2.3) and (2.4) into (2.2) and noting that the virtual work statement holds for any virtual displacement field, we obtain a system of equations expressing the equilibrium between the external forces $\underline{f}$ including body and surface tractions and the internal forces resulting from resisting, damping and inertial actions, respectively $\underline{F}_S$, $\underline{F}_D$ and $\underline{F}_I$:

$$\underline{F}_I + \underline{F}_D + \underline{F}_S - \underline{f} = \underline{0} \tag{2.5}$$

with

$$\begin{aligned}
\underline{F}_I &= \int_V \underline{N}^T \rho\ \underline{N}\ dV.\ddot{\underline{d}} \\
\underline{F}_D &= \int_V \underline{N}^T c\ \underline{N}\ dV.\dot{\underline{d}} \\
\underline{F}_S &= \int_V \underline{B}^T \underline{\sigma}\ dV.\underline{d} \\
\underline{f} &= \int_V \underline{N}^T \underline{b}\ dV + \int_{\Gamma_t} \underline{N}^T \underline{t}\ d\Gamma
\end{aligned} \tag{2.6}$$

2.5 LINEAR ELASTIC MATERIAL MODEL

In the case of linear elastic material behaviour, the relation between stress and strain is

$$\underline{\sigma} = \underline{D}\ \underline{\varepsilon} \tag{2.7}$$

with the stress-strain matrix $\underline{D}$ as given in Table 2.2. The dynamic equilibrium equations can be rewritten as

$$\underline{M}\ \ddot{\underline{d}} + \underline{C}\ \dot{\underline{d}} + \underline{K}\ \underline{d} - \underline{f} = \underline{0} \tag{2.8}$$

	PLANE STRESS	PLANE STRAIN	AXISYMMETRIC	THREE DIMENSIONAL
STRAIN VECTOR	$[\varepsilon_x \ \varepsilon_y \ \gamma_{xy}]^T$	$[\varepsilon_x \ \varepsilon_y \ \gamma_{xy} \ \varepsilon_z]^T$	$[\varepsilon_r \ \varepsilon_z \ \gamma_{rz} \ \varepsilon_\theta]^T$	$[\varepsilon_x \ \varepsilon_y \ \varepsilon_z \ \gamma_{yz} \ \gamma_{zx} \ \gamma_{xy}]^T$
STRESS VECTOR	$[\sigma_x \ \sigma_y \ \tau_{xy}]^T$	$[\sigma_x \ \sigma_y \ \tau_{xy} \ \sigma_z]^T$	$[\sigma_r \ \sigma_z \ \tau_{rz} \ \sigma_\theta]^T$	$[\sigma_x \ \sigma_y \ \sigma_z \ \tau_{yz} \ \tau_{zx} \ \tau_{xy}]^T$
STRAIN DISPLACEMENT SUBMATRIX, $\underline{B}_i$	$\begin{bmatrix} \partial N_i/\partial x & 0 \\ 0 & \partial N_i/\partial y \\ \partial N_i/\partial y & \partial N_i/\partial x \end{bmatrix}$		$\begin{bmatrix} \partial N_i/\partial r & 0 \\ 0 & \partial N_i/\partial z \\ \partial N_i/\partial z & \partial N_i/\partial r \\ N_i/r & 0 \end{bmatrix}$	$\begin{bmatrix} \partial N_i/\partial x & 0 & 0 \\ 0 & \partial N_i/\partial y & 0 \\ 0 & 0 & \partial N_i/\partial z \\ 0 & \partial N_i/\partial z & \partial N_i/\partial y \\ \partial N_i/\partial z & 0 & \partial N_i/\partial x \\ \partial N_i/\partial y & \partial N_i/\partial x & 0 \end{bmatrix}$
ELASTIC STRESS-STRAIN MATRIX, $\underline{D}$	$\frac{E}{1-\nu^2}\begin{bmatrix} 1 & \nu & 0 \\ & 1 & 0 \\ & & \frac{1-\nu}{2} \end{bmatrix}$	$\frac{E}{(1+\nu)(1-2\nu)}\begin{bmatrix} 1-\nu & \nu & 0 & \nu \\ & 1-\nu & 0 & \nu \\ & & \frac{1-2\nu}{2} & 0 \\ & & & 1-\nu \end{bmatrix}$		$\frac{E}{(1+\nu)(1-2\nu)}\begin{bmatrix} 1-\nu & \nu & \nu & 0 & 0 & 0 \\ & 1-\nu & \nu & 0 & 0 & 0 \\ & & 1-\nu & 0 & 0 & 0 \\ & & & \frac{1-2\nu}{2} & 0 & 0 \\ & & & & \frac{1-2\nu}{2} & 0 \\ & & & & & \frac{1-2\nu}{2} \end{bmatrix}$

TABLE 2.2 - Some vectors and matrices for 2D and 3D problems

where

$$\underline{M} = \int_V \underline{N}^T \rho \, \underline{N} \, dV$$

$$\underline{C} = \int_V \underline{N}^T c \, \underline{N} \, dV \qquad (2.9 \text{ a-c})$$

$$\underline{K} = \int_V \underline{B}^T \underline{D} \, \underline{B} \, dV$$

are the global mass, damping and stiffness matrices, respectively.

In quasistatic problems, where inertia effects are negligible, the terms of (2.8) containing time derivatives of $\underline{d}$ are removed.

2.6 COMPUTATION OF THE STIFFNESS, MASS AND DAMPING MATRICES

The global stiffness, mass and damping matrices are assembled from the respective element contributions $\underline{K}^e$, $\underline{M}^e$ and $\underline{C}^e$ in the standard finite element manner [1].

In the calculation of the element stiffness matrices, the sparsely populated nature of matrix $\underline{B}$ allows for substantial computational savings by adequately organizing the matrix multiplications of (2.9c) in order to avoid operating on zero entries. Gupta's method [11], based on a rearrangement of the strain energy functional, reportedly reduces the computational time for the case of a 20-node 3D brick element with 3x3x3 Gauss points by a factor of 9 [12]. This approach is however applicable only to elastic problems with constant material properties inside each element. Sloan [13], generalizing an algorithm presented by Taylor [14], overcomes this restriction and claims savings in multiplications of about 40% under full yielding for a large sample of 2D elements.

The mass matrices $\underline{M}$ and $\underline{M}^e$ are usually called consistent [1] when calculated by means of (2.9a). Noting that this expression uses the shape functions N while the stiffness computations of (2.9c) involve (in $\underline{B}$) their derivatives, it is therefore evident that the consistent mass matrix provides a more accurate approximation for the stuctural inertia forces than is obtained for the internal

resisting forces from the stiffness matrix [3]. Thus it would make sense to employ lower order interpolation functions in formulating the mass matrix [20] were it not computationally cumbersome.

A more convenient simplification is achieved by resorting instead to lumping of the element mass at the nodes, giving a diagonal matrix. With higher order elements a physically obvious lumping strategy is not always available. Several approaches have been proposed that fall in two main categories.

(i) The sample points for the numerical integration of $\underline{M}^e$ are chosen to coincide with the element nodes, thereby yielding a diagonal matrix. Fried [9] claims no loss of convergence rate if the appropriate order of numerical integration is selected. However, some of the mass matrix terms may be negative and this can lead to the computation of imaginary frequencies of vibration [10].

(ii) The calculation of $\underline{M}^e$ is carried out using a different set of shape functions that are piecewise constant: equal to unity in the vicinity of a node and zero elsewhere. If the non-zero areas do not overlap the final result is diagonal and the total mass is preserved. This method is due to Clough [3] and leads to convergent results [4].

Hinton [5] proposes a simple alternative whereby each term M_i of the diagonal lumped matrix is obtained by scaling the corresponding consistent diagonal term M_{ii} in order to conserve the total element mass M:

$$M_i = M_{ii}\, M/\sum_i M_{ii} \tag{2.10}$$

This technique has proved to be very successful [6-8] and is adopted in the present study.

Since the damping coefficients c for use in (2.9b) are usually not known, recourse is often made to the so-called "Rayleigh damping" whereby $\underline{C}$ is obtained as a linear combination of $\underline{M}$ and $\underline{K}$

$$\underline{C} = a\,\underline{M} + b\,\underline{K} \tag{2.11}$$

2.7 SOLUTION OF THE DYNAMIC EQUILIBRIUM EQUATIONS

Exact analytical solutions are available only for simple linear problems with regular geometry and boundary and loading conditions.

Numerical techniques have therefore to be employed for the transient response analysis of realistic structural systems and the finite element spatial discretization described in the previous Sections is most often complemented by a finite difference time solution. Use of finite elements in both space and time domains has also been proposed [15-18] but is not considered here.

The procedures for numerical solution of the system of second order differential equations given by (2.8) can be divided into two groups, according to the choice of basis [19].

(i) Modal superposition techniques - the dynamic response is obtained by solving separately for each mode of vibration of the structure which are then weighted by the respective modal amplitude and superposed. Practical application is usually limited to linear problems.

(ii) Direct integration methods - a numerical step-by-step procedure is used to advance the solution in time. The dynamic equilibrium equations (formulated directly in terms of nodal displacements, without any preliminary change of basis as in (i)) are satisfied at discrete points Δt apart along the time axis. An assumption is made about the variation of displacement, velocity and acceleration within each time interval Δt, giving rise to several direct integration schemes with different accuracy, stability and efficiency characteristics.

A general division is made between :

(a) explicit integration procedures, such as the central difference method [21], in which the solution at time $t+\Delta t$ is based on the equilibrium conditions at time t. Factorization of the (effective) stiffness matrix is not required in the step-by-step solution but stability is conditional and stringent limits must be imposed on the time step size.

(b) implicit integration procedures, such as the Houbolt [22], Wilson [23] and Newmark [24] methods, that use the equilibrium conditions at $t+\Delta t$ to obtain the corresponding solution.

A full description of the techniques mentioned in (a) and (b) can be found in Reference [19].

The Newmark method, adopted in this study, comprises the following equations (where $\underline{v} = \dot{\underline{d}}$ and $\underline{a} = \ddot{\underline{d}}$)

$$\underline{d}_{n+1} = \underline{d}_n + \Delta t\, \underline{v}_n + \Delta t^2/2.[(1-2\beta)\underline{a}_n + 2\beta\, \underline{a}_{n+1}] \qquad (2.12)$$

$$\underline{v}_{n+1} = \underline{v}_n + \Delta t[(1-\gamma)\, \underline{a}_n + \gamma\, \underline{a}_{n+1}] \qquad (2.13)$$

$$\underline{M}\, \underline{a}_{n+1} + \underline{C}\, \underline{v}_{n+1} + K\, \underline{d}_{n+1} = \underline{f}_{n+1} \qquad (2.14)$$

where $\underline{d}_n$, $\underline{v}_n$, $\underline{a}_n$ are known from the previous step calculations. The step-by-step procedure is started with the given initial values $\underline{d}_0$ and $\underline{v}_0$ from which $\underline{a}_0 = \underline{M}^{-1}(\underline{f}_0 - \underline{K}\, \underline{d}_0 - \underline{C}\, \underline{v}_0)$.

The parameters β and γ control the stability and accuracy characteristics of the algorithm, giving namely [25]:

- unconditional stability - $2\beta \geq \gamma \geq 1/2$
- conditional stability - $\gamma > 1/2$ (2.15)

$$\beta < \gamma/2$$

$$\omega\Delta t \leq \Omega_{CRIT}$$

where $\Omega_{CRIT} = \{\xi(\gamma-1/2) + [\gamma/2 - \beta + \xi^2(\gamma-1/2)^2]^{1/2}\}/(\gamma/2-\beta)$,

ω is the undamped frequency of vibration and ξ the damping ratio (equal to $(a/\omega + b\omega)/2$ for the Rayleigh damping case of (2.11)).

The Newmark family includes as particular cases many well known methods and the properties of a number of them are summarized in Table 2.3 [25]. The average acceleration method (corresponding to $\beta = 1/4$, $\gamma = 1/2$) is one of the most effective and widely used.

Hughes [26-28] has recast Newmark's algorithm in a predictor-corrector form that is most suitable for the purposes to be discussed in the next Section.

Denoting with a bar the predictor values, the Newmark formulas (2.12) and (2.13) can be rewritten as

$$\underline{d}_{n+1} = \bar{\underline{d}}_{n+1} + \Delta t^2 \beta \, \underline{a}_{n+1} \qquad (2.16)$$

$$\underline{v}_{n+1} = \bar{\underline{v}}_{n+1} + \Delta t \, \gamma \, \underline{a}_{n+1}$$

with

$$\bar{\underline{d}}_{n+1} = \underline{d}_n + \Delta t \, \underline{v}_n + \Delta t^2/2.(1-2\beta) \, \underline{a}_n \qquad (2.17)$$

$$\bar{\underline{v}}_{n+1} = \underline{v}_n + \Delta t \, (1-\gamma) \, \underline{a}_n$$

Noting from (2.16) that

$$\underline{a}_{n+1} = (\underline{d}_{n+1} - \bar{\underline{d}}_{n+1})/(\Delta t^2 \beta) \qquad (2.18)$$

$$\underline{v}_{n+1} = \bar{\underline{v}}_{n+1} + (\underline{d}_{n+1} - \bar{\underline{d}}_{n+1})\gamma/(\Delta t \, \beta)$$

and using this result in (2.14), an "effective static problem" is formed in terms of the unknown $\underline{d}_{n+1}$. This is in turn linearized for the general case of a nonlinear transient analysis (in which, broadly, $\underline{K} = \underline{K}(\underline{d}, \underline{v})$, $\underline{C} = \underline{C}(\underline{d}, \underline{v})$ and $\underline{M}\,\underline{a} + \underline{p}(\underline{d}, \underline{v}) = \underline{f}$ with $\underline{p} = \underline{p}(\underline{d}, \underline{v})$ being internal resisting forces). In this case the displacement increment $\Delta\underline{d}$

METHOD	TYPE	β	γ	STABILITY CONDITION
Average acceleration	Implicit	1/4	1/2	Unconditional
Linear acceleration	Implicit	1/6	1/2	$\Omega_{CRIT} = 2\sqrt{3}$
Fox-Goodwin	Implicit	1/12	1/2	$\Omega_{CRIT} = \sqrt{6}$
Central difference	Explicit	0	1/2	$\Omega_{CRIT} = 2$

NOTES - (1) The central difference method is explicit with $\underline{M}$ and $\underline{C}$ diagonal

(2) Stability is based on the undamped case ($\xi = 0$)

TABLE 2.3 - Properties of some members of the Newmark family of direct integration methods

is computed and iteratively corrected within each time step. The algorithm starts with the calculation of $\underline{a}_0$ from given $\underline{d}_0$ and $\underline{v}_0$ (as before) and proceeds as is now described.

(a) - Set the iteration counter i = 0.

(b) - Enter the predictor phase

$$\begin{aligned} \underline{d}_{n+1}^{i} &= \bar{\underline{d}}_{n+1} \\ \underline{v}_{n+1}^{i} &= \bar{\underline{v}}_{n+1} \\ \underline{a}_{n+1}^{i} &= \underline{0} \end{aligned} \tag{2.19}$$

(c) - Solve the incremental "effective static problem"

$$\underline{K}^{*} \Delta \underline{d} = \Delta \underline{r}^{*} \tag{2.20}$$

where

$$\underline{K}^{*} = \underline{M}/(\Delta t^2 \beta) + \underline{C}_T \gamma/(\Delta t \beta) + \underline{K}_T \tag{2.21}$$

$$\Delta \underline{r}^{*} = \underline{f}_{n+1} - \underline{M}\, \underline{a}_{n+1}^{i} - \underline{p}(\underline{d}_{n+1}^{i}, \underline{v}_{n+1}^{i})$$

are, respectively, the effective stiffness matrix and effective residual force vector, with

$$\begin{aligned} \underline{C}_T &= \underline{C}_T(\underline{d}_{n+1}^{i}, \underline{v}_{n+1}^{i}) = \partial \underline{p}/\partial \underline{v} \\ \underline{K}_T &= \underline{K}_T(\underline{d}_{n+1}^{i}, \underline{v}_{n+1}^{i}) = \partial \underline{p}/\partial \underline{d} \end{aligned} \tag{2.22}$$

being the tangential damping and stiffness matrices.

(d) - Perform the corrector phase

$$\begin{aligned} \underline{d}_{n+1}^{i+1} &= \underline{d}_{n+1}^{i} + \Delta \underline{d} \\ \underline{a}_{n+1}^{i+1} &= (\underline{d}_{n+1}^{i+1} - \bar{\underline{d}}_{n+1})/(\Delta t^2 \beta) \\ \underline{v}_{n+1}^{i+1} &= \bar{\underline{v}}_{n+1} + \Delta t\, \gamma\, \underline{a}_{n+1}^{i+1} \end{aligned} \tag{2.23}$$

(e) - If the convergence criterion selected is not satisfied, replace i by i+1 and return to (c).

(f) - The solution at t_{n+1} is

$$\begin{aligned} \underline{d}_{n+1} &= \underline{d}_{n+1}^{i+1} \\ \underline{v}_{n+1} &= \underline{v}_{n+1}^{i+1} \\ \underline{a}_{n+1} &= \underline{a}_{n+1}^{i+1} \end{aligned} \tag{2.24}$$

Substitute n by n+1 and return to (a).

In practice $\underline{K}^*$ is reformed and factorized as infrequently as possible to reduce computation costs. For some types of problems it may be more convenient to form an effective linearized problem in terms of velocity or acceleration rather than displacement as above. The corresponding algorithms can be found in References [2, 28].

2.8 PARTITIONING METHODS

In many interacting media problems time step restrictions for stability and accuracy vary widely throughout the spatial domain of analysis. A very advantageous strategy is to adopt partitioning methods, that combine the best features of explicit and implicit procedures by employing different time integrators on different parts of the system.

In the nodal partition techniques developed by Belytschko [29,30] the nodal variables are divided into two groups, explicit and implicit, the mesh is partitioned into three sets, explicit, implicit and interface. In each time step the explicit nodes are integrated first, supplying the boundary condition for the integration of the implicit nodes.

In the element partition methods proposed by Hughes [26-28] it is the elements rather than the nodes that are identified with different integrators, making computer implementation more simple and concise. Use of the predictor-corrector form described in the previous Section is particularly effective and the algorithm summarized in steps (a) to (f) still applies with the sole modification of the effective stiffness matrix and residual force vector of (2.21) that are now

$$\underline{K}^* = \underline{M}/(\Delta t^2 \beta) + \underline{C}_T^I \gamma/(\Delta t \beta) + \underline{K}_T^I$$

$$\Delta \underline{r}^* = \underline{f}_{n+1} - \underline{M}\, \underline{a}^i_{n+1} - \underline{p}^I(\underline{d}^i_{n+1}, \underline{v}^i_{n+1}) - \underline{p}^E(\bar{\underline{d}}_{n+1}, \bar{\underline{v}}_{n+1}) \qquad (2.25)$$

where the superscripts I and E denote the implicit and explicit parts of the mesh, $\underline{C}_T^I = \partial \underline{p}^I / \partial \underline{v}$ and $\underline{K}_T^I = \partial \underline{p}^I / \partial \underline{d}$.

The effective stiffness matrix has a typical band-profile structure, with diagonal subregions corresponding to the explicit zone and, elsewhere, a profile determined by the connectivity of the implicit elements. This is efficiently exploited by adopting a skyline equation solver [2, 14, 19]. The stability of this method is discussed in References [26, 34]. Chapter 4 describes an implicit-explicit time integration scheme developed for the solution of quasistatic elastoviscoplastic problems.

In the subcycling or time-step mesh partition techniques, due to Belytschko [31, 32], different time step sizing is used throughout the mesh in order to keep as close as possible to the local stability limit for maximum efficiency.

In the mixed-time implicit-explicit methods Liu [33] combines element and time step mesh partitioning by employing different time integrators and time steps simultaneously in different parts of the mesh.

2.9 OPERATOR SPLITTING METHODS

Operator splitting methods attempt to combine the stability of implicit integrators with the efficiency of an explicit scheme.

This approach, already used extensively in finite differences [35], has recently been applied to finite elements by Hughes [36, 37] whose element-by-element (EBE) solution algorithm is designed to take maximum advantage of the typical finite element data structure. Current research in this area is very intense and promising results have been obtained [38-41]. The main features of the EBE method are now briefly outlined.

After discretization in space and time, the finite element equations for a general nonlinear dynamic analysis can be written in the form of (2.20) as

$$\underline{A}\,\underline{x} = \underline{b} \tag{2.26}$$

where $\underline{A}$ is symmetric and positive definite and assembled from element arrays $\underline{A}^e$ which are sparsely populated.

This discrete elliptic problem is then replaced by an associated first order parabolic problem

$$\underline{W}\,\dot{\underline{y}}\,(\tau) + \underline{A}\,\underline{y}\,(\tau) = H(\tau)\,\underline{b} \tag{2.27}$$

$$\underline{y}\,(0) = \underline{0}$$

where $\underline{W}$ is a positive definite diagonal matrix, $H(\tau)$ is a Heaviside function $\left(H(\tau)\right.$ is 1 for $\tau > 0$ and zero otherwise$\left.\right)$, τ is a nondimensional pseudo time and $\dot{\underline{y}} = d\underline{y}/d\tau$.

The asymptotic solution of (2.27) also satisfies (2.26),

$$\underline{x} = \lim_{\tau\to\infty} \underline{y}(\tau) \tag{2.28}$$

A possibility for the selection of $\underline{W}$ is to take the diagonal terms of $\underline{A}$.

A pseudo-time discretization scheme is now applied to (2.27). Using the generalized trapezoidal rule

$$\underline{y} = (1-\alpha)\,\underline{y}_n + \alpha \underline{y}_{n+1} \tag{2.29}$$

$$\dot{\underline{y}} = (\underline{y}_{n+1} - \underline{y}_n)/\Delta\tau$$

where $\Delta\tau = \tau_{n+1} - \tau_n$ is a pseudo-time step and taking $\alpha=1$ for unconditional stability and fast convergence to the asymptotic solution, we arrive at

$$(\underline{W} + \Delta\tau\underline{A})\,\underline{y}_{n+1} = \underline{W}\,\underline{y}_n + \Delta\tau\,\underline{b} \tag{2.30}$$

that can be rewritten as

$$\underline{y}_{n+1} - \underline{y}_n = \Delta\tau\,\underline{W}^{-\frac{1}{2}}\,\underline{V}\,\underline{W}^{-\frac{1}{2}}\,(\underline{b} - \underline{A}\,\underline{y}_n) \tag{2.31}$$

with

$$\underline{V} = (\underline{I} + \Delta\tau\,\underline{W}^{-\frac{1}{2}}\,\underline{A}\,\underline{W}^{-\frac{1}{2}})^{-1} \tag{2.32}$$

where $\underline{I}$ is the identity matrix.

The fundamental idea of the EBE method is to split the global operator $\underline{V}$ into smaller element operators $\underline{V}^e$, approximating $\underline{V}$ in (2.31) by a product of m factors of the form (2.32) (m = no. of elements) but with $\underline{A}$ replaced by $\underline{A}^e$:

$$\underline{V} \approx \underline{V}^{*} = \prod_{e=1}^{m} \underline{V}^{e} = \prod_{e=1}^{m} (\underline{I} + \Delta\tau \underline{W}^{-\frac{1}{2}} \underline{A}^{e} \underline{W}^{-\frac{1}{2}})^{-1} \qquad (2.33)$$

Calculations on the right-hand side of (2.31) can thus be performed in an element-by-element fashion, thereby reducing drastically both core and CPU time requirements, since the global array $\underline{V}$ need not be formed, stored and inverted. Potential savings are even greater in 3D applications.

2.10 CLOSING REMARKS

The introductory exposition of the previous Sections delineates the basic framework for the developments that follow. Material nonlinearity is discussed at length in Chapters 3 and 4, that focus on elastoplastic and elastoviscoplastic behaviour and its numerical treatment.

Nonlinearity arising from changes of geometry is analysed in Chapter 5. Several numerical techniques for use in the iterative solution of the "effective static problem" are described and assessed in Chapter 6. The mapped infinite element is then presented and used in conjunction with standard finite elements for solution of unbounded domain problems.

2.11 REFERENCES

1. ZIENKIEWICZ, O.C., The Finite Element Method, 3rd edition, McGraw-Hill, London, 1977

2. OWEN, D.R.J. and HINTON, E., Finite Elements in Plasticity - Theory and Practice, Pineridge Press, Swansea, 1980

3. CLOUGH, R.W., Analysis of structural vibrations and dynamic response, in Recent Advances in Math. Meth. of Struct. Anal. and Design, 441-485, R.H. Gallagher et al. (eds.), Univ. Alabama Press, 1971

4. TONG, P., PIAN, T.H.H. and BUCIOVELLI, L.L., Mode shapes and frequencies by finite element method using consistent and lumped masses, Comp. & Str., 1, 623-638, 1971

5. HINTON, E., ROCK, T.A. and ZIENKIEWICZ, O.C., A note on mass lumping and related processes in the finite element method, Int. J. Earthq. Engng. Str. Dynamics, 4, 246-249, 1976

6. ROCK, T. and HINTON, E., Free vibration and transient response of thick and thin plates using the finite element method, Int. J. Earthq. Engng. Str. Dynamics, 3, 51-63, 1974

7. SHANTARAM, D., OWEN, D.R.J. and ZIENKIEWICZ, O.C., Dynamic transient behaviour of two and three dimensional structures including plasticity, large deformation effects and fluid interaction, Int. J. Earthq. Engng. Str. Dynamics, 4, 561-578, 1976

8. HINTON, E., OWEN, D.R.J. and SHANTARAM, D., Dynamic transient nonlinear behaviour of thick and thin plates, in MAFELAP II, 423-438, J.R. Whiteman (ed.), Academic Press, London, 1977

9. FRIED, I. and MALKUS, D.S., Finite element mass matrix lumping by numerical integration with no convergence rate loss, Int.J. Sol. Struct., 461-465, 1975

10. COOK, R.D., Remarks about diagonal mass matrices, IJNME, 17, 1427-1429, 1981

11. GUPTA, A.K. and MOHRAZ, B., A method of computing numerically integrated stiffness matrices, IJNME, 5, 83-89, 1972

12. LIGHT, M.F. and LUXMOORE, A.R., Application of the front solution to two and three dimensional elastoplastic crack problems, IJNME, 11, 393-395, 1977

13. SLOAN, S.W., A fast stiffness formulation for finite element analysis of two dimensional solids, IJNME, 17, 1313-1323, 1981

14. TAYLOR, R.L., ch. 24, pp. 677-757 in Reference 1.

15. FRIED, I., Finite element analysis of time dependent phenomena, AIAA J., 7, 1170-1172, 1969

16. ARGYRIS, J.H. and SCHARPF, D.W., Finite elements in space and time, Aeron. J. Roy. Aeron. Soc., 73, 1041-1044, 1969

17. ODEN, J.T., A general theory of finite elements, Part 2. Applications, IJNME, 1, 247-259, 1969

18. ZIENKIEWICZ, O.C. and PAREKH, C.J., Transient field problems - two and three dimensional analysis by isoparametric finite elements, IJNME, 2, 61-71, 1970

19. BATHE, K.J., Finite Element Procedures in Engineering Analysis, Prentice-Hall, Englewood Cliffs, N.J., 1982

20. CLOUGH, R.W. and BATHE, K.J., Finite element analysis of dynamic response, in Adv. in Comp. Meth. in Str. Mech. and Design, 153-179, J.T. Oden et al. (eds.), Univ. Alabama Press, 1972

21. COLLATZ, L., The Numerical Treatment of Differential Equations, Springer Verlag, New York, 1966

22. HOUBOLT, J.C., A recurrence matrix solution for the dynamic response of an elastic aircraft, J. Aeron. Sci., 17, 540-550, 1950

23. WILSON, E.L., FARHOOMAND, I. and BATHE, K.J., Nonlinear dynamic analysis of complex structures, Int. J. Earthq. Engng. Str. Dynamics, 1, 241-252, 1973

24. NEWMARK, N.M., A method of computation for structural dynamics, J. Eng. Mech. Div., ASCE, 85, 67-94, 1959

25. HUGHES, T.J.R. and BELYTSCHKO, T., A précis of developments in computational methods for transient analysis, J. Appl. Mech., 50, 1033-1041, 1983

26. HUGHES, T.J.R. and LIU, W.K., Implicit-explicit finite elements in transient analysis: stability theory, J. Appl. Mech., 45, 371-374, 1978

27. HUGHES, T.J.R. and LIU, W.K., Implicit-explicit finite elements in transient analysis: implementation and numerical examples, J. Appl. Mech., 45, 375-378, 1978

28. HUGHES, T.J.R., PISTER, K.S. and TAYLOR, R.L., Implicit-explicit finite elements in nonlinear transient analysis, Comp. Meth. Appl. Mech. Engng., 17/18, 159-182, 1979

29. BELYTSCHKO, T. and MULLEN, R., Mesh partitions of explicit-implicit time integration, in Formulations and Comput. Algor. in F.E. Analysis, 673-690, K.J. Bathe et al. (eds.), MIT Press, Cambridge, Ma., 1976

30. BELYTSCHKO, T. and MULLEN, R., Stability of explicit-implicit mesh partitions in time integration, IJNME, 12, 1575-1586, 1978

31. BELYTSCHKO, T., Partitioned and adaptive algorithms for explicit time integration, in Nonlinear F.E. Analysis in Structural Mechanics, 572-584, W. Wunderlich et al. (eds.), Springer Verlag, 1980

32. BELYTSCHKO, T., YEN, H.J. and MULLEN, R., Mixed methods for time integration, Comp. Meth. Appl. Mech. Engng., 17/18, 259-275, 1979

33. LIU, W.K. and BELYTSCHKO, T., Mixed-time implicit-explicit finite elements for transient analysis, Comp. & Str., 15, 445-450, 1982

34. HUGHES, T.J.R. and STEPHENSON, R.A., Convergence of implicit-explicit algorithms in nonlinear transient analysis, Int. J. Engng. Sci., 19, 295-302, 1981

35. MARCHUK, G.I., Methods of Numerical Mathematics, Springer Verlag, 1975

36. HUGHES, T.J.R., LEVIT, I. and WINGET, J., Unconditionally stable element-by-element implicit algorithm for heat conduction analysis, J. Eng. Mech. Div., ASCE, 109, 576-585, 1983

37. HUGHES, T.J.R., LEVIT, I. and WINGET, J., An element-by-element solution algorithm for problems of structural and solid mechanics, Comp. Meth. Appl. Mech. Engng., 36, 241-254, 1983

38. HUGHES, T.J.R., WINGET, J., LEVIT, I. and TEZDUYAR, T.E., New alternating direction procedures in finite element analysis based upon EBE approximate factorizations, in Rec. Dev. in Comp. Meth. for Nonlinear Sol. and Struct. Mechanics, 75-109, N. Perrone et al. (eds.), ASME, 1983

39. ORTIZ, M., PINSKY, P.M. and TAYLOR, R.L., Unconditionally stable element-by-element algorithms for dynamic problems, Comp. Meth. Appl. Mech. Engng., 36, 223-239, 1983.

40. ORTIZ, M., PINSKY, P.M. and TAYLOR, R.L., Operator split methods for the numerical solution of the elastoplastic dynamic problem, Comp. Meth. Appl. Mech. Engng., 39, 137-157, 1983

41. LIU, Y.C., Recently developed iterative schemes for finite element analysis, M.Sc. thesis, Univ. College of Swansea, 1983

CHAPTER 3

THE ELASTOPLASTIC MODEL FOR MATERIAL NONLINEARITY

3.1 INTRODUCTION 3.1

3.2 A HISTORICAL NOTE 3.2

3.3 FUNDAMENTAL PLASTICITY CONCEPTS 3.3

3.3.1 Yield criterion

3.3.2 Hardening rule

3.3.3 Flow rule

3.4 MATRIX FORMULATION 3.6

3.5 BASIC STEPS FOR STRESS COMPUTATION IN INCREMENTAL ELASTOPLASTIC ANALYSIS 3.9

3.6 DETERMINATION OF THE CONTACT STRESS STATE 3.11

3.6.1 Method for the computation of the reduction factor R

3.6.2 Numerical example

3.7 SUBDIVISION OF THE EXCESS STRESS 3.17

3.8 REDUCTION OF THE EXCESS STRESS 3.18

3.9 END-OF-STEP CORRECTION 3.20

3.10 YIELD SURFACES WITH SINGULARITIES 3.21

3.11 PHYSICAL AND NUMERICAL UNLOADING 3.23

3.12 PLANE STRESS PLASTICITY 3.24

3.13 FINAL REMARK 3.27

3.14 REFERENCES 3.28

CHAPTER 3

THE ELASTOPLASTIC MODEL FOR MATERIAL NONLINEARITY

3.1 INTRODUCTION

Solid bodies can generally be considered elastic within only a limited load range, beyond which permanent deformations develop. Under certain conditions this irrecoverable straining is practically time independent, as in the case of metals at room temperature and fits into the analytical framework of the mathematical theory of plasticity.

Many structural components are expected to remain elastic under normal working conditions. Nevertheless, an accurate prediction of the behaviour nearing failure allows for a safer as well as more economical design. In addition it must be mentioned that many industrial and manufacturing processes actually rely on a controlled excursion into the plastic state.

The finite element method has been successfully applied to plastic problems since 1960 [1] and has proved to be a versatile and reliable numerical tool.

This Chapter describes the implementation of an elastoplastic model in a typical incremental-iterative structural analysis procedure [2], with detailed reference to the stress computation operations. After a brief historical note, Section 3.3 presents the relevant theoretical background in the context of small strain associated elastoplasticity. The basic finite element expressions are derived in Section 3.4 in a form suitable for numerical treatment. The stress computation procedure, crucial for the reliability and economy of the overall solution, is then reviewed in detail: Sections 3.5 to 3.9 cover the determination of the contact state, subincrementation methods and substep size definition and strategies for redirecting the stress point to the yield surface, illustrating numerical hazards and suggesting simple ways to avoid them. Special attention is devoted to yield functions with singularities. The question of path (in)dependency is also addressed and the Chapter closes with a note on plane stress plasticity. This study is based on References [23] and [41].

3.2 A HISTORICAL NOTE

The first attempts to produce a theoretical prediction of plastic material behaviour were due to Coulomb (1773), Poncelet (1840) and Rankine (1853), for the computation of earth pressure on retaining walls and Tresca (1864), with regard to the extrusion and punching of metals.

Drawing on these early contributions, plasticity studies mobilized the experimental and analytical efforts of such illustrious names as Saint Venant, Levy, von Mises, Hencky, Prandtl, Nadai, von Karman and Reuss.

In the 1930's the mathematical theory of plasticity had reached a certain state of maturity, producing results in substantial agreement with observation, as reported by Hill in his classic monograph [3].

The theory was further elaborated and generalized by Prager, Drucker, Hodge, Koiter and Bland, with important results arrived at in the limit analysis and design of plates, shells and trusses.

However, increasing difficulties in producing analytical solutions for displacement, strain and stress fields for less regular geometries and loadings led to the application of numerical methods, initially finite differences and then finite elements [1].

In this context plasticity effects are first tackled by the "initial strain" method [42], a constant stiffness procedure whereby plastic strains are assimilated to initial thermal strains and converted into "effective plastic loads". This approach fails for ideal plasticity and is superseded by the tangent-modulus method [43] that accounts for plastic deformation by repeatedly adjusting the stress-strain relation. Zienkiewicz [19] proposes the "initial stress" method as a more economic technique and develops a finite element formulation for plasticity taken as a standard in the present study.

3.3 FUNDAMENTAL PLASTICITY CONCEPTS

The mathematical theory of plasticity [3] models the time independent irreversible straining exhibited by many materials (in particular metals) once a certain stress level is reached, and involves the definition of a yield criterion, a hardening rule and a flow rule.

3.3.1 Yield criterion

The yield criterion determines the onset of plastic deformation and can be written in the general scalar form

$$F(\sigma_{ij}, \varepsilon^p_{ij}, k) = f(\sigma_{ij}, \varepsilon^p_{ij}) - Y(k) \qquad (3.1)$$

where the yield function f depends on the stress and plastic strain tensor components, σ_{ij} and ε^p_{ij}, respectively, and the yield stress Y may be related to the past material history via the hardening parameter k, as will be seen in Section 3.3.2. For simplicity only isotropic plasticity is considered here [17] and ε^p_{ij} is dropped in (3.1) giving

$$F(\sigma_{ij}, k) = f(\sigma_{ij}) - Y(k) \qquad (3.2)$$

For a perfectly plastic material (Y(k) = constant), the behaviour is elastic if $F<0$ or if $F=0$ and $\dot{F}<0$, and plastic if $F=0$ and $\dot{F}>0$; hardening materials are elastic for $F<0$ or $F=0$ and $\dot{F}\leq 0$ and yield for $F=0$ and $\dot{F}>0$ [4]. The physical independence of the material behaviour on the coordinate system adopted for its description imposes the yield criterion to be expressable in terms of any set of stress invariants.

In Section 3.4 a set is presented that particularly suits numerical computations [5].

Four yield criteria widely used are now described in terms of principal stresses $\sigma_1 \geq \sigma_2 \geq \sigma_3$:

$$\begin{aligned}
&\text{TRESCA [6]:} && \sigma_1 - \sigma_3 = Y(k) \\
&\text{VON MISES [7]} && \{[(\sigma_1-\sigma_2)^2 + (\sigma_2-\sigma_3)^2 + (\sigma_3-\sigma_1)^2]\}^{1/2} = Y(k) \\
&\text{MOHR-COULOMB[8]} && (\sigma_1-\sigma_3)/2 + \sin\phi(\sigma_1+\sigma_3)/2 = c\cos\phi \\
&\text{DRUCKER-PRAGER[9]:} && \alpha(\sigma_1+\sigma_2+\sigma_3) + \{[(\sigma_1-\sigma_2)^2 + (\sigma_2-\sigma_3)^2 + (\sigma_3-\sigma_1)^2]/6\}^{1/2} = K'
\end{aligned} \qquad (3.3a\text{-}d)$$

with Y(k) being the uniaxial yield stress, c the cohesion,

ϕ the friction angle, $\alpha = 2 \sin \phi / [\sqrt{3}\ (3 \pm \sin \phi)]$ and

$K' = 6c \cos \phi\ / [\sqrt{3}(3 \pm \sin \phi)]$.

A geometrical representation of the above yield surfaces in the principal stress space is presented in fig. 3.1.

3.3.2 Hardening rule

The hardening rule establishes conditions for subsequent yielding from the previous plastic straining history. Two basic models exist: isotropic hardening [3] in which the yield surface is assumed to expand uniformly about the stress space origin during plastic flow and kinematic hardening [10-12], that corresponds simply to a translation preserving the initial shape. More complex hardening rules are obtained by combination [13] and generalization [14] of the above.

Restricting ourselves to isotropic hardening, there are two fundamental ways of relating the yield stress $Y(k)$ to the plastic deformation history, namely work hardening, where k equals the total plastic work, $W_p (= \int \sigma_{ij}\ d\varepsilon^p_{ij})$, and strain hardening, in which Y depends on the effective plastic strain, $\bar{\varepsilon}_p$ $(= \int [2/3\ (d\varepsilon^p_{ij}\ d\varepsilon^p_{ij})]^{1/2})$ [15].

3.3.3 Flow rule

The flow rule relates stress to plastic strain increments. It is most generally established by using the concept of plastic potential Q [16]: the plastic strain is assumed proportional to the stress gradient of Q

$$d\varepsilon^p_{ij} = d\lambda\ \partial Q / \partial \sigma_{ij} \qquad (3.4)$$

where the non-negative factor $d\lambda$ is called the plastic multiplier. Koiter's generalization of (3.4) for singular yield surfaces [4] will be described in Section 3.10.

If Q is made equal to a particular yield function f, then

$$d\varepsilon^p_{ij} = d\lambda\ \partial f / \partial \sigma_{ij} \qquad (3.5)$$

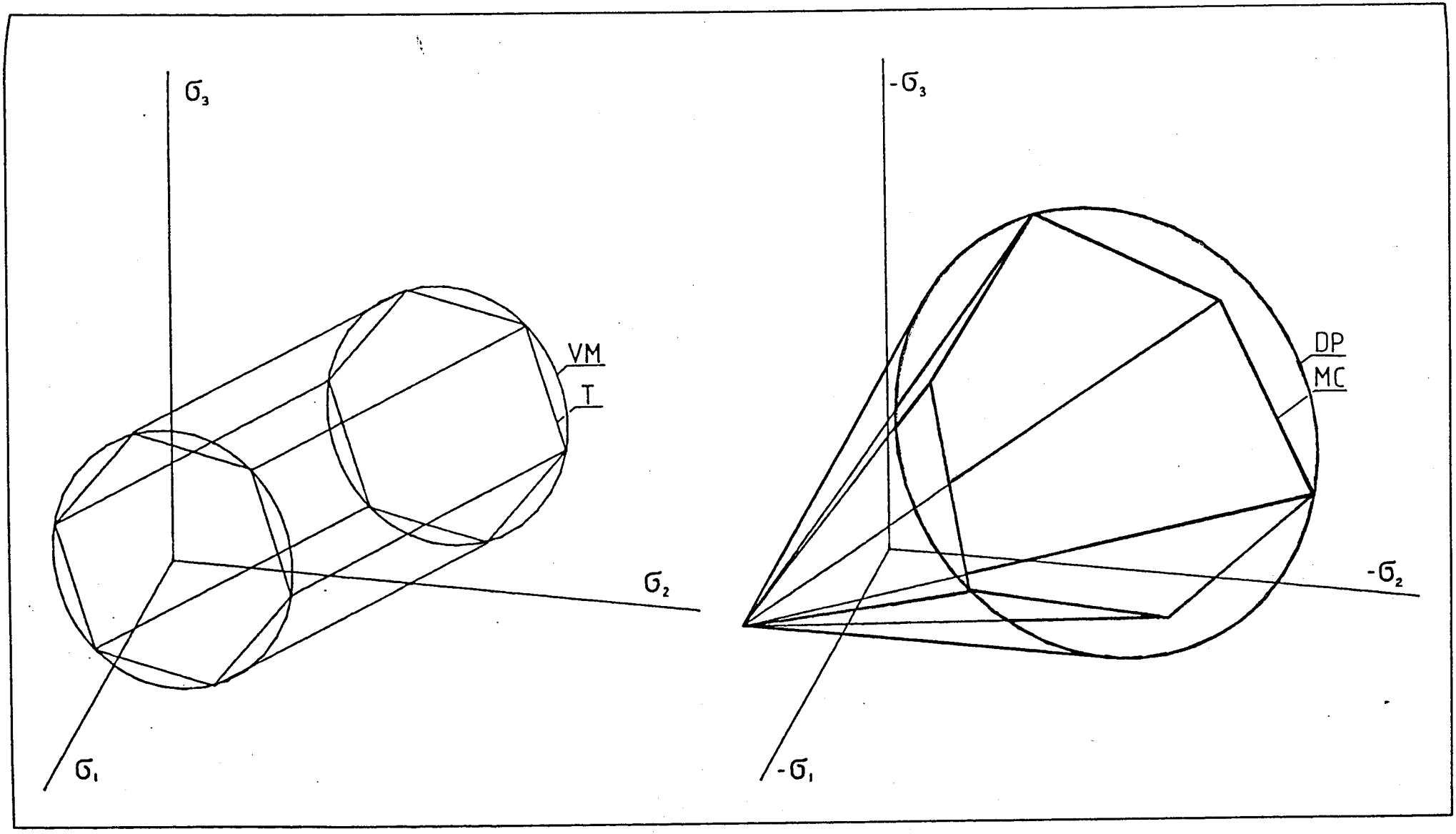

Fig. 3. 1 – Geometrical representation of the Tresca(T), von Mises(VM), Mohr-Coulomb(MC) and Drucker-Prager(DP) yield surfaces in the principal stress space

Equation (3.5) is called the associated flow rule [17] and implies a normality condition between the plastic strain increment and the yield surface in principal stress space.

3.4 MATRIX FORMULATION

Following the approach of References [18-20] we now recast the basic expressions of Section 3.3 in a matrix form suitable for numerical treatment.

During plastic flow (in a 3D isotropic hardening continuum)

$$\begin{aligned} F(\underline{\sigma},k) &= f(\underline{\sigma}) - Y(k) = 0 \\ dF &= (\partial f/\partial \underline{\sigma})^T . d\underline{\sigma} - dY/dk.dk = 0 \\ d\underline{\sigma} &= \underline{D}(d\underline{\varepsilon} - d\underline{\varepsilon}_p) = \underline{D}(d\underline{\varepsilon} - d\lambda\, \partial f/\partial \underline{\sigma}) \end{aligned} \tag{3.6a-c}$$

where $\underline{\sigma} = \{\sigma_x, \sigma_y, \sigma_z, \sigma_{yz}, \sigma_{zx}, \sigma_{xy}\}^T$ and $\underline{D}$ is the usual 3x3 matrix of elastic constants. Making in (3.6)

$$\begin{aligned} \underline{a} &= \partial f/\partial \underline{\sigma} \\ A &= \frac{1}{d\lambda}\,\frac{dY}{dk}\,dk \end{aligned} \tag{3.7a,b}$$

we arrive at

$$d\lambda = \frac{\underline{a}^T \underline{D}\, d\underline{\varepsilon}}{A + \underline{a}^T \underline{D}\, \underline{a}} \quad \text{and}$$

$$d\underline{\sigma} = \underline{D}_{ep}\, d\underline{\varepsilon} \qquad \text{where} \tag{3.8a-c}$$

$$\underline{D}_{ep} = \underline{D} - \frac{\underline{D}\,\underline{a}\,\underline{a}^T\,\underline{D}}{A + \underline{a}^T \underline{D}\, \underline{a}}$$

As pointed out by Nayak [20], work and strain hardening coincide only for von Mises materials. Use of $dk = \bar{\sigma} d\bar{\varepsilon}_p$ and $H' = d\bar{\sigma}/d\bar{\varepsilon}_p$ in (3.7.b), with the effective stress $\bar{\sigma} = [3/2(s_{ij}\, s_{ij})]^{\frac{1}{2}}$ and $s_{ij} = \sigma_{ij} - \delta_{ij}\, \sigma_{kk}/3$ being the deviatoric stress, leads to

$$A = H' \tag{3.9}$$

Considering now strain hardening ($dk = d\bar{\varepsilon}_p$) and a linear law $Y = Y_o + H'\bar{\varepsilon}_p$, where Y_o is the initial yield stress value, we arrive at

$$A = H'\,\bar{a} \qquad \text{with} \qquad (3.10\ a,b)$$

$$\bar{a} = [2/3\ (\partial f/\partial \sigma_{ij})(\partial f/\partial \sigma_{ij})]^{\frac{1}{2}}$$

For a material other than von Mises $\bar{a}$ does not have a unit value and the use of (3.10) in (3.8) is essential to obtain correct results under linear strain hardening, as illustrated by the simple numerical example with a Tresca law in Table 3.1.

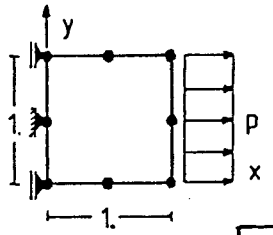

$E = 1E5 \qquad Y_o = 10. \qquad P_1 = 15.$ [UNITS

$\nu = 0.3 \qquad H' = 1.E4 \qquad P_2 = 0.$ [N,m

$Y = Y_o + H'\bar{\varepsilon}p$ - PLANE STRAIN - TRESCA

		ANALYTICAL	WITH A = $H'\bar{a}$	WITH A = H'
p=15.	ε_x	569.513 E-6	569.513 E-6	624.751 E-6
	ε_y	-491.513 E-6	-491.513 E-6	-550.847 E-6
	σ_z	4.5	4.5	4.5
p=0.	ε_x	433.013 E-6	433.013 E-6	488.251 E-6
	ε_y	-433.013 E-6	-433.013 E-6	-492.347 E-6
	σ_z	0.	0	0
ITERATIONS (NEWTON-RAPHSON)			2+1	4+1

TABLE 3.1 - Plane strain bar of linear strain hardening Tresca material

A very convenient formulation for (3.6), (3.7) and (3.8) is achieved by recourse to the set of stress invariants (J_1, J_2', θ)[5] given by

$$\begin{aligned} J_1 &= \sigma_{ii}/3 \\ J_2' &= s_{ij}s_{ij}/2 \\ \theta &= 1/3 \sin^{-1} [-3\sqrt{3}/2 .\ J_3'/(J_2')^{3/2}] \end{aligned} \qquad (3.11\ a\text{-}c)$$

where $J_3' = s_{ij}\, s_{jk}\, s_{ki}/3$. The invariant θ, in essence similar to the Lode parameter [21] μ, is determined by (3.11 c) in the interval $[-30°, +30°]$.

The principal stresses are obtained as

$$\begin{bmatrix} \sigma_1 \\ \sigma_2 \\ \sigma_3 \end{bmatrix} = \frac{2(J_2')^{\frac{1}{2}}}{\sqrt{3}} \begin{bmatrix} \sin(\theta + 2\pi/3) \\ \sin\theta \\ \sin(\theta - 2\pi/3) \end{bmatrix} + \frac{J_1}{3} \begin{bmatrix} 1 \\ 1 \\ 1 \end{bmatrix} \qquad (3.12)$$

and obey therefore the relation $\sigma_1 \geq \sigma_2 \geq \sigma_3$, this fact implying that any state of stress represented in the principal stress space by (3.11) and (3.12), will be projected on the π-plane $(\sigma_1 + \sigma_2 + \sigma_3 = 0)$ in the sextant between the axis σ_1 and $-\sigma_3$, as will be further discussed in Section 3.6.

Use of (3.11) allows the flow vector $\underline{a}$ to be rewritten as

$$\underline{a} = C_1\, \underline{a}_1 + C_2\, \underline{a}_2 + C_3\, \underline{a}_3 \qquad \text{with} \qquad (3.13)$$

$$\begin{aligned} \underline{a}_1 &= \partial J_1/\partial\underline{\sigma} & C_1 &= \partial f/\partial J_1 \\ \underline{a}_2 &= \partial (J_2')^{\frac{1}{2}}/\partial\underline{\sigma} & C_2 &= \partial f/\partial (J_2')^{\frac{1}{2}} - \tan 3\theta/(J_2')^{\frac{1}{2}} .\ \partial f/\partial\theta \\ \underline{a}_3 &= \partial J_3'/\partial\underline{\sigma} & C_3 &= -\sqrt{3}/[2\cos 3\theta (J_2')^{3/2}] \ .\ \partial f/\partial\theta \end{aligned} \qquad (3.14)$$

The yield criteria defined by equations (3.3 a-d) are recast in Table 3.2 in terms of (J_1, J_2', θ) and the corresponding constants C_i are listed in Table 3.3. A change of criterion simply involves switching from one set of constants to another, which allows a considerable generality in computer coding. Further advantages of this strategy will be mentioned while discussing the treatment of singularities in Section 3.10.

3.5 BASIC STEPS FOR STRESS COMPUTATION IN INCREMENTAL ELASTOPLASTIC ANALYSIS

The operations that lead to updating of the state of stress during the ith. iteration of a load (or time) step in an elastoplastic finite element analysis may be summarized as follows [22], for a path dependent algorithm:

- the total strain increment $\Delta\underline{\varepsilon}$ is obtained from the displacement increment $\Delta\underline{d}$ by $\Delta\underline{\varepsilon} = \underline{B}\ \Delta\underline{d}$, where $\underline{B}$ is the strain-displacement matrix;
- an elastic estimate $\Delta\underline{\sigma}^e$ for the stress increment is computed with the aid of the elastic stress-strain matrix $\underline{D}$ as $\Delta\underline{\sigma}^e = \underline{D}\ \Delta\underline{\varepsilon}$;
- a trial stress state $\underline{\sigma}^e = \underline{\sigma}^o + \Delta\underline{\sigma}^e$ is obtained from the value $\underline{\sigma}^o$ at the beginning of the iteration;
- if $f(\underline{\sigma}^e) < Y$ the point is elastic and the estimate is correct; otherwise the yield surface has been trespassed during the trial stress incrementation;
- in this case the contact stress state $\underline{\sigma}^c$ (with $f(\underline{\sigma}^c) = Y$) is first determined;
- the stress point is then brought back to the yield surface and the final value for the stress increment obtained as

YIELD CRITERION	YIELD FUNCTION $f(\sigma)$	YIELD STRESS
TRESCA	$2(J_2')^{\frac{1}{2}} \cos\theta$	$Y(k)$
VON MISES	$\sqrt{3}\ (J_2')^{\frac{1}{2}}$	$Y(k)$
MOHR-COULOMB	$\frac{1}{3}J_1 \sin\phi + (J_2')^{\frac{1}{2}}\left(\cos\theta - \frac{\sin\theta\sin\phi}{\sqrt{3}}\right)$	$c.\cos\phi$
DRUCKER-PRAGER	$\alpha J_1 + (J_2')^{\frac{1}{2}}$	K'

NOTES
1. c is the cohesion, ϕ the friction angle, $Y(k)$ the unlaxial yield stress
2. $\alpha = 2\sin\phi/[\sqrt{3}(3\pm\sin\phi)]$; $k'=6c\cos\phi/[\sqrt{3}(3\pm\sin\phi)]$

TABLE 3.2 - Definition of some common yield criteria employed in elastoplastic problems

YIELD CRITERIA	C1	C2	C3
TRESCA	0	$2\cos\theta(1+\tan\theta\ \tan3\theta)$	$\frac{\sqrt{3}}{J'_2}\ \frac{\sin\theta}{\cos3\theta}$
VON MISES	0	$\sqrt{3}$	0
MOHR-COULOMB	$\frac{1}{3}\sin\phi$	$\cos\theta[(1+\tan\theta\ \tan3\theta) + \sin\phi(\tan3\theta - \tan\theta)/\sqrt{3}]$	$\frac{\sqrt{3}\ \sin\theta+\cos\theta\sin\phi}{2J'_2\cos3\theta}$
DRUCKER-PRAGER	α	1.0	0

TABLE 3.3 - Values of the constants C_i for the yield criteria of TABLE 3.2

$$\Delta\underline{\sigma} = \underline{D}(\Delta\underline{\varepsilon} - \Delta\underline{\varepsilon}^{p}) = \Delta\underline{\sigma}^{e} - d\lambda\ \underline{D}\ \underline{a} \tag{3.15}$$

- to minimize the error due to the substitution of the finite increments in (3.15) for the differentials in (3.6 c), it is possible to adopt a subincrementation procedure whereby the excess stress $\Delta\underline{\sigma}^{exc} = \underline{\sigma}^{e} - \underline{\sigma}^{c}$ is subdivided in K parts and the single step operation (3.15) is replaced by

$$\Delta\underline{\sigma} = \underline{\sigma}^{c} - \underline{\sigma}^{o} + \sum_{j=1}^{K}\left(\Delta\underline{\sigma}_{j}^{exc} - d\lambda_{j}\ \underline{D}\ \underline{a}_{j}\right) \tag{3.16}$$

The following Sections present a detailed analysis and visualization of the above operations, assessing alternative approaches and illustrating some precautions to be taken. Path (in)dependency is further discussed in Section 3.11.

As alternative approaches to the state determination problems we may refer the use of variational inequalities [37], mathematical programming [38] and higher order algorithms such as the fourth order Runge-Kutta method [39].

3.6 DETERMINATION OF THE CONTACT STRESS STATE [23]

The contact stress state is obtained by application of a reduction factor R to the elastic stress increment as

$$\underline{\sigma}^{c} = \underline{\sigma}^{e} - R\ \Delta\underline{\sigma}^{e} \tag{3.17}$$

In Reference [19] a linear interpolation is suggested for R yielding

$$R = [f(\underline{\sigma}^{e}) - Y]/[f(\underline{\sigma}^{e}) - f(\underline{\sigma}^{o})] \tag{3.18}$$

and in [20] an iterative refinement is proposed for cases when f is not a linear function of the stresses.

On use of the invariant set (J_1, J_2', θ) a different approach is however needed in view of the fact that (3.11 c) defines θ in the range $[-30°, +30°]$ only, implying that

$$\sigma_1 \geq \sigma_2 \geq \sigma_3 \tag{3.19}$$

Supposing that the principal stresses of the initial stress state $\underline{\sigma}^o$ have been listed according to (3.19), let us consider the gradual application of an arbitrary stress increment from zero to its full value $\Delta\underline{\sigma}$. For a general nonradial stress path there is a change of the principal stress directions between the initial and the final states $\underline{\sigma}^o$ and $\underline{\sigma}$.

Assuming the naming of the axes to be retained in this incrementation process, it may well happen that on arrival at $\underline{\sigma}$ the relation (3.19) is no longer obeyed by the principal stresses of the final state: we call these the "true" values to distinguish them from those obtained by (3.12) in the sequence (3.19).

Let us now consider a simple numerical example involving the Tresca criterion (fig. 3.2), in which the"true" states $\underline{\sigma}^o$ and $\underline{\sigma}$ are represented in the principal stress space by A(4,3,1) and B(2,6,1). Use of (3.12) would give for $\underline{\sigma}$ the point B'(6,2,1). This is visually equivalent to a reflection of the stress path AB on the axis $-\sigma_3$.

Using the appropriate expressions from Table 3.2 in (3.18) and taking Y = 4, we get R = (5 - 4)/(5 - 3) = 1/2. Equation (3.17) gives $\underline{\sigma}^{c_1}$ with $C_1(3,4.5,1)$ but $f(\underline{\sigma}^{c_1}) = 3.5 < Y$.

Thus a wrong estimate has been obtained for the contact state and this is indeed to be expected whenever A and B in their "true" positions do not share the same sextant delimited by any two axes.

In the above calculations we have in fact interpolated between A and B', obtaining C' on AB' which corresponds to C_1 midway on AB and quite clearly inside the yield surface.

If C_1 is taken as the initial point for the reduction of the "excess" stress C_1B, the inevitable consequence is the appearance of negative values in the computation of $d\lambda$.

Since in (3.15) $\underline{a}$ is directed along the exterior normal to the yield surface (a convex function of $\underline{\sigma}$ according to Drucker's postulate [24]) and $\underline{D}\,\underline{a}$ is colinear with $\underline{a}$ (in the principal stress space in associated plasticity), the algorithm is simply trying to

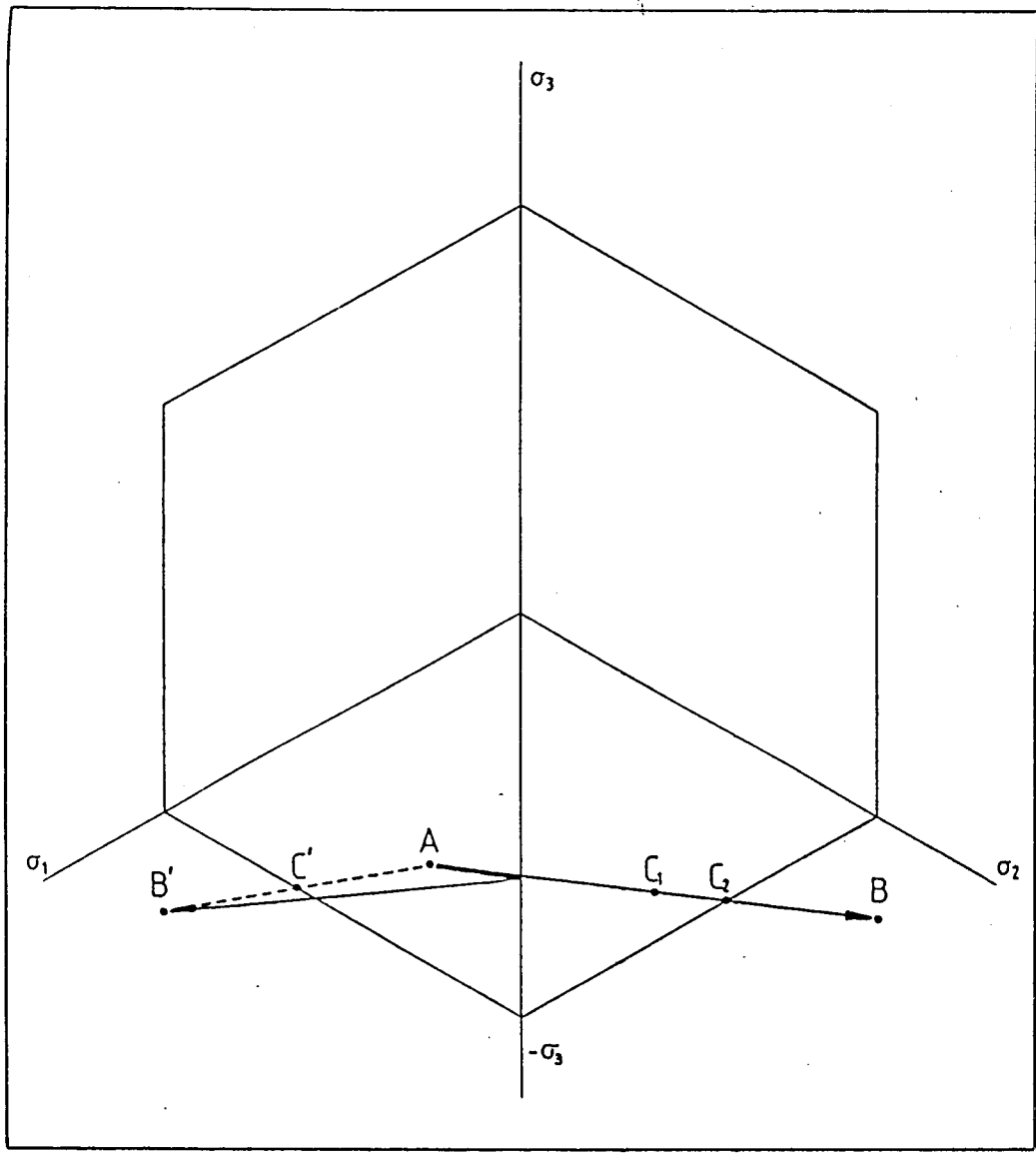

Fig. 3.2 – Stress incrementation paths for the Tresca criterion

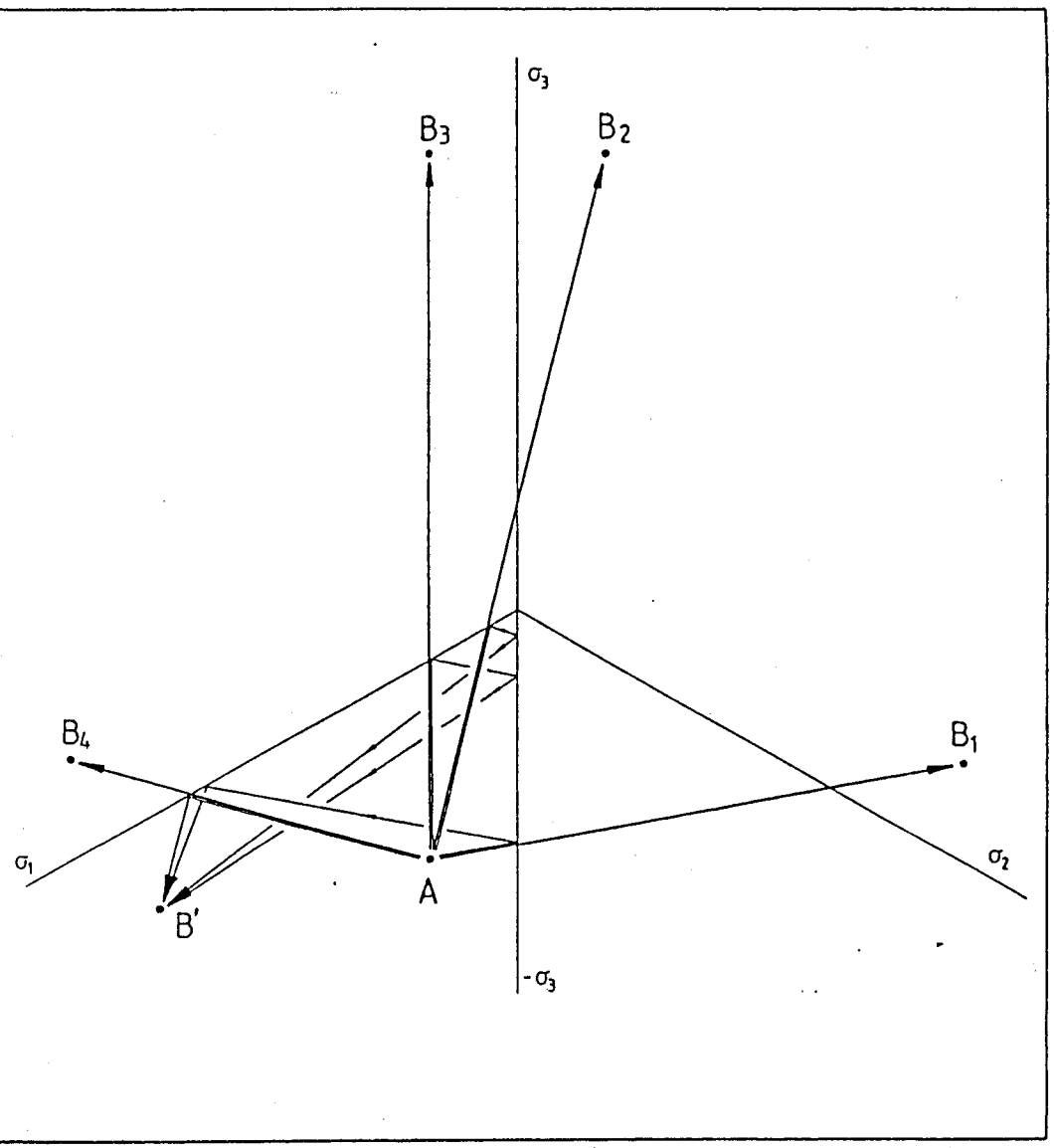

Fig. 3.3 – Further stress incrementation possibilities for the example of fig. 3.2

redirect to the yield surface a "contact" state that is in fact inside it. The zeroing of these negative $d\lambda$ values [20] is an inadequate remedy as the example of Section 3.6.2 shows.

In fig. 3.3 four other possible locations for B obtained by coordinate permutation are considered and the optical analogy is used to show how the stress paths AB_i are reflected on σ_1 and $-\sigma_3$ towards B'.

Returning to the computation of R, expression (3.18) could be again used between C_1 and B and would give the correct result for this example, since the two points now share the same sextant:

$R = (5-4)(5-3.5) = 2/3$ and $f_{c_2} = 4$ with $C_2(2.(6),5,1)$.

This iterative strategy may however be slower as can be seen by applying it between A and B_4 (fig. 3.3) but a stronger objection is that it is entirely misleading whenever the stress point starts from a location on the yield surface and travels across it: considering the path AB_2 (fig. 3.3) as such a case, R_1 is given by (3.18) as 1.0 and the whole elastic stress increment is simply interpreted as excess stress. An accurate method is proposed below.

3.6.1 Method for the computation of the reduction factor R [23]

R is determined by reference to the trial state $\underline{\sigma}$ obtained at B (at the end of the elastic stress increment $\Delta\underline{\sigma}$) as

$$R = [f(\underline{\sigma}) - Y]/\Delta f$$
$$\Delta f = \partial f(\underline{\sigma})/\partial\underline{\sigma}.\Delta\underline{\sigma} \qquad (3.20\ a,b)$$

In our example this gives $\Delta f = \{0,1,-1,0,0,0\}^T.\{-2,3,0,0,0,0\} = 3$ and $R = (5 - 4)/3 = 1/3$; the contact state is $\underline{\sigma}^c = (2,6,1) - (-2,3,0)/3 = (2.(6),5,1)$ and $f(\underline{\sigma}^c) = 4$.

When the yield function f is nonlinear in $\underline{\sigma}$, improved estimates R_i for R are obtained from the initial guess R_o, given by (3.20), as

$$R_i = R_o + \sum_{k=1}^{i} \Delta R_k \qquad \text{where}$$

$$\Delta R_k = \Delta R_{k-1}\,[f(\underline{\sigma}_k) - Y]/[f(\underline{\sigma}_{k-1}) - f(\underline{\sigma}_k)] \qquad (3.21\ a,b)$$

with $f(\underline{\sigma}_0) = f(\underline{\sigma}_B)$ and $\Delta R_o = R_o$. The iterative procedure (3.21) is halted when $\|f(\underline{\sigma}_i) - Y\|/Y$ for the trial contact state $\underline{\sigma}_i$ falls below a specified tolerance.

3.6.2 Numerical Example

A thick cylinder of a perfectly plastic Tresca material with internal and external radii of 1.0 and 10.0 units respectively, is restrained against axial deformation as shown in Table 3.4.

A severe two-step loading program is considered. First an internal pressure p = 2250. is applied, causing plastification to spread at the inner region up to a radial value of 4.347. Then the applied load is completely removed with further yielding being produced.

One elastoviscoplastic (EVP) and two elastoplastic (EP) solutions (RUNS 1 and 2) are compared in Table 3.5 against the analytical values [25]: RUN 1 corresponds to the method proposed in 3.6.1; in RUN 2 the factor R is computed using (3.18) and negative $d\lambda$ values are zeroed. Both EP solutions follow a Newton-Raphson (tangential stiffness) procedure, with the material stiffness being reset to the initial elastic value at the beginning of the second load step.

On the unloading phase, the stress path for the plastic Gauss points is of the type AB_2 of fig. 3.3. The method followed in RUN 2 gives poor results for the zone yielded on unloading, as can be seen from the residual radial displacement at r = 1.0 and longitudinal stress at r = 1.21.

A detailed analysis of intermediate results of RUN 2 reveals that on the first iteration of the unloading step and as a consequence of the zeroing of the negative $d\lambda$ values, the final stress state at r = 1.21 would have been located well inside the yield surface, with a stress level of 766.54. However, a corrective procedure automatically applied to the stress components [22] has relocated the stress point on the yield surface (stress level 1200.). This procedure is

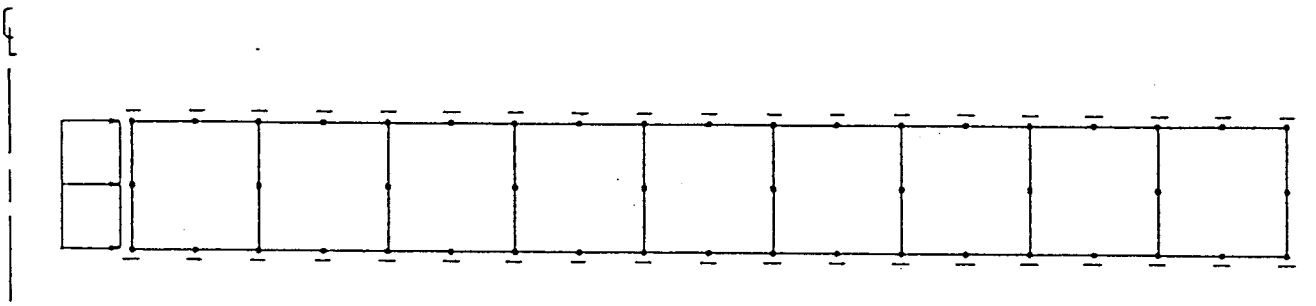

YOUNG MODULUS E = 1.0E7 CAVITY RADIUS R = 1.0
POISSON RATIO ν = 0.33 ELEMENT SIZE 1.0 x 1.0
YIELD STRESS Y = 1200.

TABLE 3.4 - Data for an internally pressurized thick cylinder

		P = 2250.			P = 0. (COMPLETE UNLOADING)			
	RAD.	ANALYT.	RUN 1&2	E. V. P.	ANALYT.	RUN 1	RUN 2	E. V. P.
	1.00	1918.87	1914.05	1909.49	1494.81	1474.21	1432.65	1469.86
RADIAL	1.50	1227.46	1224.41	1221.38	963.54	950.05	946.53	947.13
DISPL.	2.00	882.04	879.77	877.53	683.18	674.94	673.92	672.78
(x1E6)	2.50	678.19	676.46	674.71	517.90	511.36	510.54	509.67
	1.21	-2019.94	-2014.27	-2014.23	-230.05	-260.21	-260.81	-260.48
RADIAL	1.78	-1552.23	-1552.39	-1552.08	-659.58	-619.94	-618.01	-620.03
STRESS	2.21	-1297.69	-1295.23	-1294.68	-723.85	-702.17	-699.22	-701.86
	2.78	-1019.32	-1018.10	-1017.43	-669.45	-658.98	-657.19	-658.45
	1.21	-937.16	-933.42	-933.26	-547.84	-567.74	-842.53	-568.18
AXIAL	1.78	-628.47	-628.58	-628.05	-647.94	-630.00	-624.37	-629.49
STRESS	2.21	-460.48	-458.85	-458.15	-479.95	-478.91	-479.01	-478.19
	2.78	-276.75	-275.95	-275.50	-296.23	-296.00	-296.10	-295.55
	1.21	-819.94	-814.27	-813.84	-1430.06	-1460.21	-1460.81	-1461.29
HOOP	1.78	-352.23	-352.39	-351.11	-1303.89	-1289.14	-1274.03	-1287.52
STRESS	2.21	-97.69	-95.23	-93.64	-730.53	-749.06	-752.32	-747.22
	2.78	180.68	181.90	182.57	-228.20	-238.00	-240.09	-237.16

TABLE 3.5 - Results of the thick cylinder problem of TABLE 3.4

intended to correct minor deviations from the yield surface (after the use of (3.15) or (3.16)) which is clearly not the present case. So a new trial was made using the method of RUN 2 but omitting the correction: this simply failed to converge on step 2. An acceptable solution was obtained only after subdivision of the single shot unloading phase.

The method for contact state definition proposed in 3.6.1 provides results that are in good agreement with both the EVP and analytical solutions and is seen to cope easily with traversals of the yield surface as those due to cyclic load steps of large magnitude.

3.7 SUBDIVISION OF THE EXCESS STRESS

Huffington [26] has first underlined the advantage of using a substepping procedure for the reduction of the excess stress as described in (3.16); many researchers have implemented variations thereof into their codes [2,20,22,27-31]. This technique accounts more closely for the changes in plastic flow direction associated with the movement of the stress point in stress space during each iteration. More accurate and reliable results are obtained and less increments are needed to cover a given load range: savings in the reformulation and inversion of the global coefficient matrix do compensate amply for the extra time required by substepping.

Several criteria have been suggested for the definition of the subincrement size. Nayak [20] and Owen [22] limit the maximum permitted change of the yield function on application of the excess stress to a fraction of Y(k) (typically 5-10% in [20], 12.5% in [22]). Nyssen [31] uses the estimated truncature error of a single step integration. Bushnell [29] limits the effective total strain increment (or, in the presence of primary creep, the effective stress change, with varying step size). Schreyer [30] accounts for the variation of the plastic strain rate direction.

The valuable error analyses of [28] and]30] clearly show that some control is desirable over the tangential component of the excess stress with respect to the yield surface in deviatoric stress space,

in addition to bounding it in the normal direction. We enforce both controls in a simple way by extending Owen's criterion to

$$\text{STEP1} = S_1\ [f(\underline{\sigma}^e) - f(\underline{\sigma}^c)\ ]/f(\underline{\sigma}^c)$$

$$\text{STEP2} = S_2 . f(\underline{\sigma}^e - \underline{\sigma}^c)/f(\underline{\sigma}^c) \qquad (3.22\ a\text{-}c)$$

$$\text{NSTEP} = \text{INT}(\text{AMAX}(\text{STEP1},\ \text{STEP2})) + 1 \quad \text{with } S_1 = S_2 = 12.5\%$$

The procedure is depicted in fig. 3.4 for a von Mises case, comparing a single step solution P_1 with two others, P_2 and P_3, obtained by multistepping based on (3.22 a) only and (3.22 a and b) respectively. The formula (3.22 b) is equivalent to enforcing a limit of approximately S_2 rad. on $\Delta\theta_i$; the value 12.5% ($\approx 7°12$) for S_2 is adequate for most engineering applications.

When a singularity is reached during a step, a subdivision is performed as discussed in Section 3.10.

3.8 REDUCTION OF THE EXCESS STRESS

The computation of the plastic strain increment $\Delta\underline{\varepsilon}_i^p = d\lambda_i \underline{a}_i$ for use in (3.16) can be performed by reference to the stress state $\underline{\sigma}_{i-1}$ at the beginning of the substep or, alternatively, with regard to $\underline{\sigma}_{i-1} + \Delta\underline{\sigma}_i^e/2$ or $\underline{\sigma}_{i-1} + \Delta\underline{\sigma}_i^e$.

In Reference [28] the accuracy of these three methods is thoroughly assessed against an analytical solution [32] for isotropic perfectly plastic von Mises materials and they are named, respectively, tangent [33], secant [34] and radial [35] return methods.

Since only for von Mises-type criteria does the normal to the yield surface coincide with a radial return path in deviatoric stress space, we prefer (with [31]) to call these procedures respectively explicit, midpoint and (fully) implicit. Fig. 3.5 illustrates the differences between the three methods in a single step application: the return path is based on a normal to the yield surface computed at the origin, A, midpoint B, and extremity C of the excess stress vector, giving D, E and F as the corresponding final states.

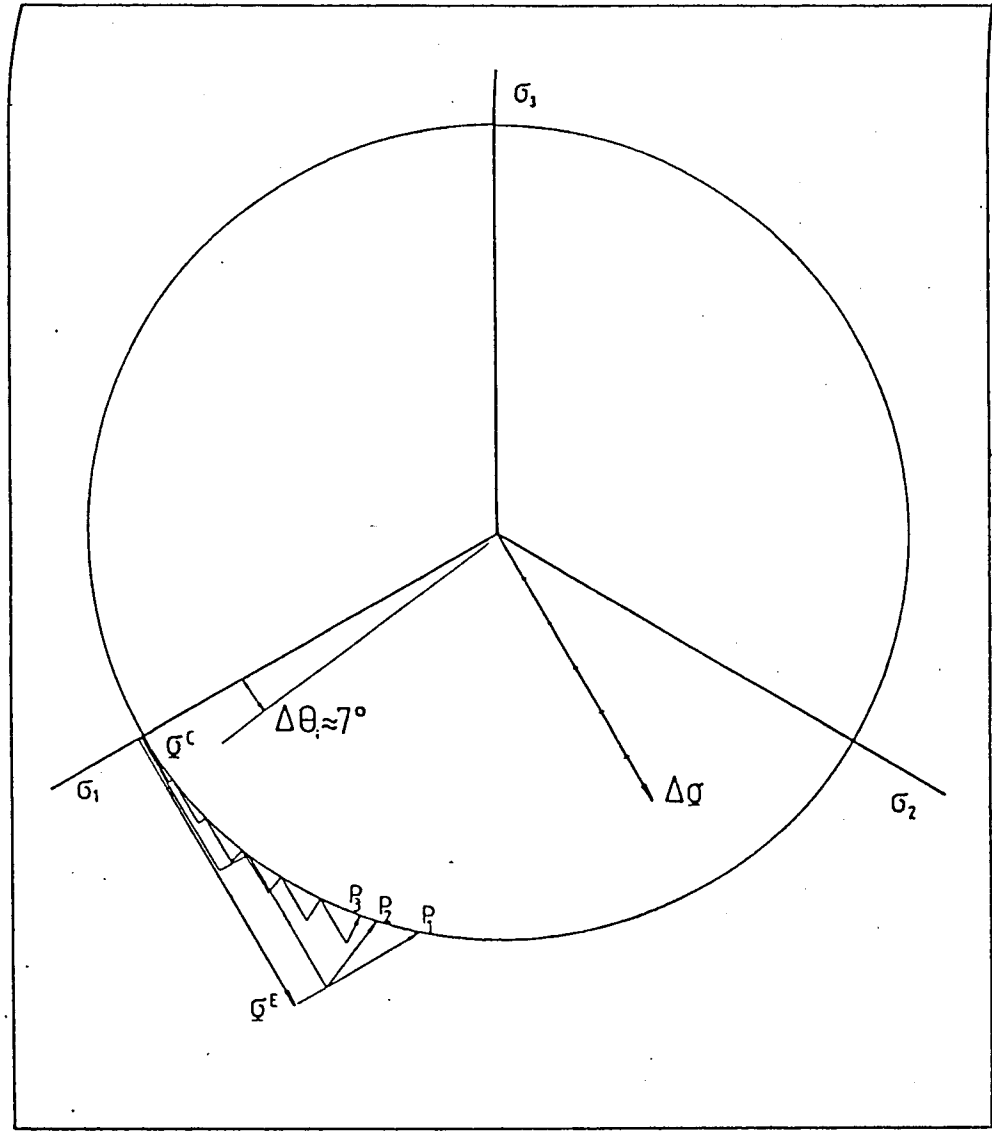

Fig. 3.4 – Comparison of single and multistepping solutions

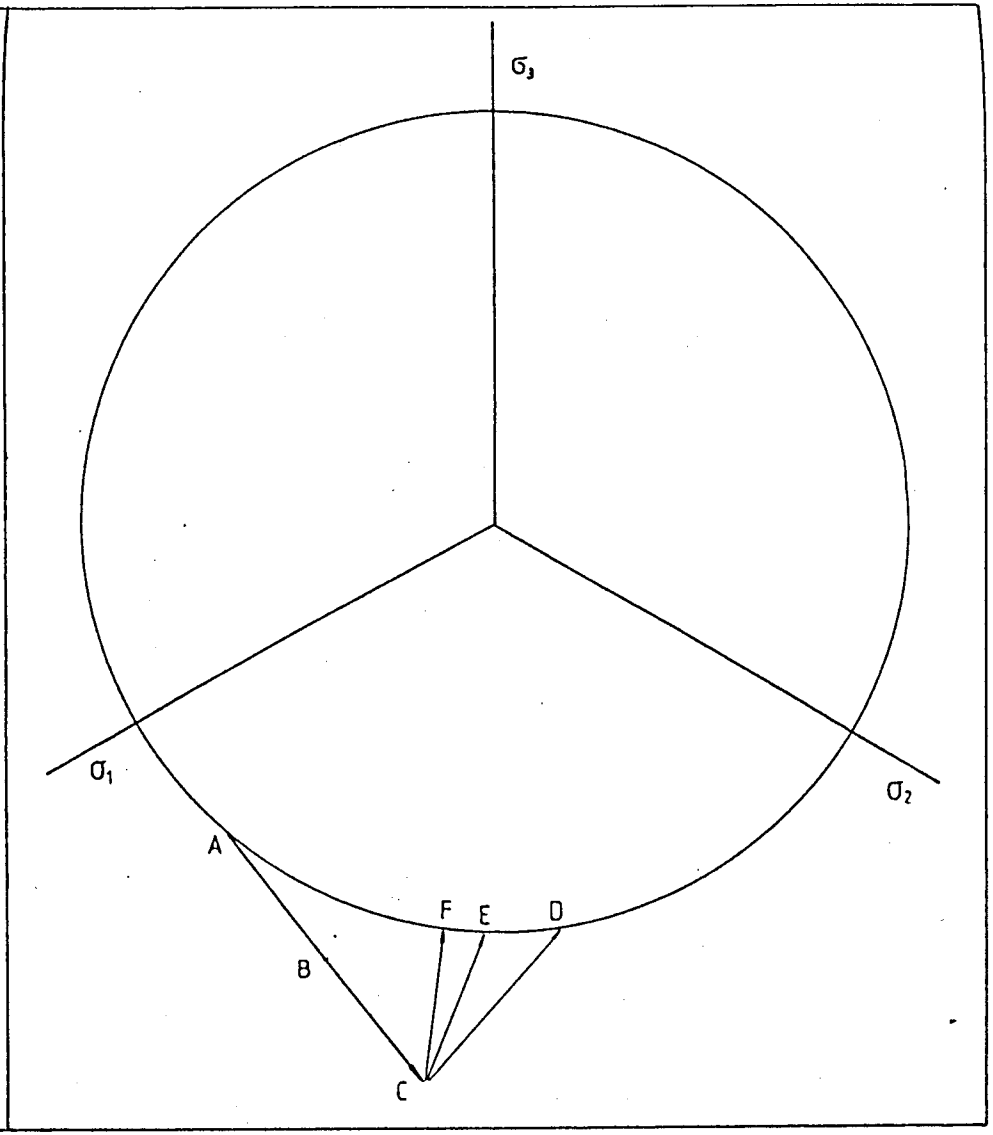

Fig. 3.5 – Single step application of three methods for reduction of the excess stress

The discrepancy observed in this example is greatly reduced by the use of substepping and any of the techniques leads to results considered to be satisfactory for most engineering problems [30].

The explicit method is adopted here for its simplicity and for allowing an easy strategy to detect the arrival to a singularity, as described in Section 3.10; its use in plane stress problems also has certain advantages discussed in Section 3.12.

3.9 END-OF-STEP CORRECTION

If the stress point is not repositioned on the yield surface at the end of a substep, a correction is recommended in order to avoid error accumulation [20,22,28,31]. Here we simply adjust the $d\lambda_i$ just used in the substep, accounting simultaneously for yield surface expansion due to hardening; we compute the corrections

$$\delta(d\lambda_i) = [f(\underline{\sigma}_{i+1}) - Y(k_{i+1})]/(A + \underline{a}_i^T \underline{D}\, \underline{a}_i)$$

$$\delta(\bar{\varepsilon}^p_{i+1}) = \delta(d\lambda_i)\, \bar{a}_i \qquad (3.23\ a\text{-}c)$$

$$\delta(\underline{\sigma}_{i+1}) = -\delta(d\lambda_i)\, \underline{D}\, \underline{a}_i$$

iterating until the corrected stress state $\underline{\sigma}^* = \underline{\sigma}_{i+1} + \Sigma\delta(\underline{\sigma}_{i+1})$ satisfies $[f(\underline{\sigma}^*) - Y(k^*)]/Y(k^*) \leq$ TOLERANCE (say 0.01 - 0.001).

This procedure is consistent with the normality condition and accounts for the extra plastic flow associated with the movement of the stress point.

On use of the criterion (3.22) for definition of the number of subincrements, the end-of-step error is usually very small and most often the procedure (3.23) is not even called into action. In the next Section it is shown how to take advantage of the end-of-step error to flag the advent of a singularity on the yield surface.

3.10 YIELD SURFACES WITH SINGULARITIES

Plastic flow at a singularity can be modelled by recourse to Koiter's generalization [4]

$$d\underline{\varepsilon}^P = \sum_k d\lambda_k \, \partial f_k/\partial \underline{\sigma} \tag{3.24}$$

where k spans only over the active flow mechanisms.

As a precondition to the application of (3.24) one has to prevent undetected stepping past the singularity during the subincrementation process, as illustrated in fig. 3.6 where the excess stress AB is reduced by (3.15) to D outside the yield surface and then "corrected" to Z if automatic activation of (3.23) is allowed.

The occurrence of an excessive departure of the stress point from the yield surface at the end of a step, together with a value for θ close to $\pm 30°$ (to within say 7.5° for $S_2 = 12.5\%$ in (3.22 b)) is taken to indicate that a singularity has been encountered and then procedure (3.23) is not performed. The excess stress AB is instead subdivided (fig. 3.6): the first portion AG is reduced to S at the corner; the remaining part GB is then treated by use of (3.24).

This splitting of the excess stress is easily achieved by first doubling up the size of the step ABD to AHJ (fig. 3.6) and then setting up a linear relation between $F(\underline{\sigma}_J)$, $F(\underline{\sigma}_D)$ and $F(\underline{\sigma}_S)$ (= 0) giving

$$\underline{\sigma}_G = \underline{\sigma}_A + \alpha \, \Delta\underline{\sigma}_i \qquad \text{with}$$

$$\alpha = [F(\underline{\sigma}_J) - 2F(\underline{\sigma}_D)]/[F(\underline{\sigma}_J) - F(\underline{\sigma}_D)] \tag{3.25 a,b}$$

iterating if required to obtain $\theta_s = \pm 30°$.

By reference to fig. 3.6 and considering only two active plastic flow mechanisms we now compute [36]

$$\Delta\underline{\varepsilon}^P = d\lambda_1 \, \partial f_1/\partial\underline{\sigma} + d\lambda_2 \, \partial f_2/\partial\underline{\sigma} = d\lambda_1 \underline{a} + d\lambda_2 \underline{b} \tag{3.26}$$

To calculate the coupled plastic multipliers $d\lambda_1$ and $d\lambda_2$ we note first that

BIBLIOTECA F.E. PORTO

YIELD CRITERIA	C_1	C_2	C_3
TRESCA	0	$2\cos(\theta\pm\pi/3)$ $[1+\tan3\theta\tan(\theta\pm\pi/3)]$	$\frac{\sqrt{3}\sin(\theta\pm\pi/3)}{J'_2\cos3\theta}$
MOHR-COULOMB	$1/3\sin\phi$	$\cos(\theta\pm\pi/3)[1+\tan3\theta\tan(\theta\pm\pi/3)$ $+\sin\phi(\tan3\theta-\tan(\theta\pm\pi/3)/\sqrt{3}]$	$\frac{\sqrt{3}\sin(\theta\pm\pi/3)+\sin\phi\cos(\theta\pm\pi/3)}{2J'_2\cos3\theta}$

TABLE 3.6 – Constants C_i for the definition of $\underline{b}$ at a singularity (the sign of θ governs the ± sign choice)

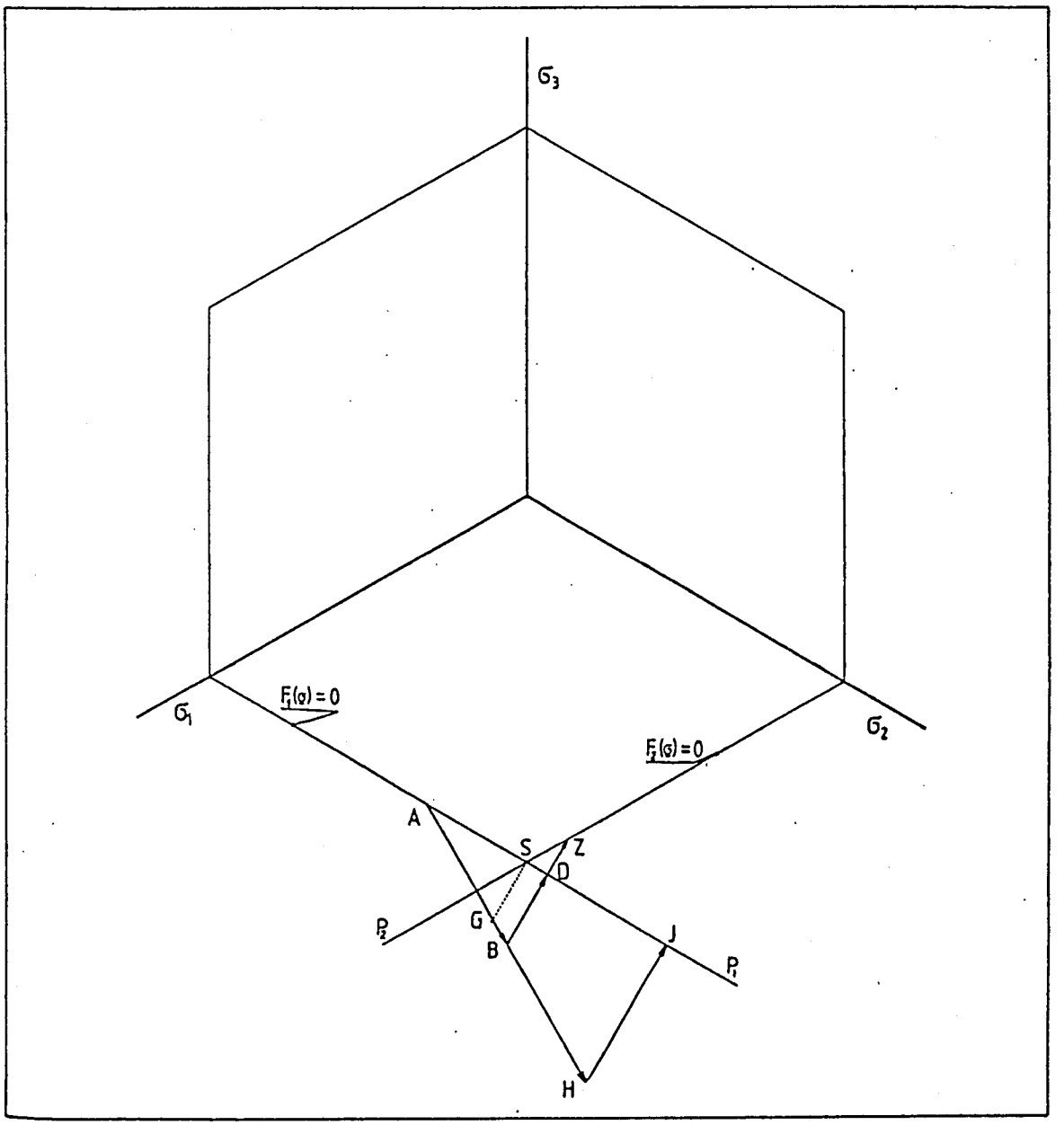

Fig. 3.6 – Substep splitting at a singularity

$$dF_1 = \underline{a}^T d\underline{\sigma} - A\, d\lambda_1 = 0$$

$$dF_2 = \underline{b}^T d\underline{\sigma} - A\, d\lambda_2 = 0 \qquad (3.27\ a\text{-}c)$$

$$d\underline{\sigma} = \underline{D}(d\underline{\varepsilon} - d\lambda_1 \underline{a} - d\lambda_2 \underline{b})$$

Using now (3.8 a) to obtain $\overline{d\lambda}_1$ and $\overline{d\lambda}_2$, the uncoupled multipliers that correspond to the independent activation of each flow mechanism, we derive from (3.27) a compact form for $d\lambda_1$ and $d\lambda_2$ very easy to code.

$$d\lambda_1 = \left[\overline{d\lambda}_1 - \overline{d\lambda}_2 \frac{\underline{b}^T \underline{D}\, \underline{a}}{A + \underline{a}^T \underline{D}\, \underline{a}}\right] \left[1 - \frac{(\underline{b}^T \underline{D}\, \underline{a})^2}{(A + \underline{a}^T \underline{D}\, \underline{a})(A + \underline{b}^T \underline{D}\, \underline{b})}\right] \qquad (3.28\ a,b)$$

$$d\lambda_1 = \left[\overline{d\lambda}_2 - \overline{d\lambda}_1 \frac{\underline{b}^T \underline{D}\, \underline{a}}{A + \underline{b}^T \underline{D}\, \underline{b}}\right] \left[1 - \frac{(\underline{b}^T \underline{D}\, \underline{a})^2}{(A + \underline{a}^T \underline{D}\, \underline{a})(A + \underline{b}^T \underline{D}\, \underline{b})}\right]$$

A negative value for any of the $\overline{d\lambda}_i$ means that $\Delta\underline{\sigma}$ (fig. 3.8) lies outside $P_2 S\, P_1$ and only one plastic flow mechanism is active: computation therefore proceeds by use of (3.8) instead of (3.28).

The flow vector $\underline{b}$ can be obtained in the form (3.13) simply by modifying the constants C_i, as described in Table 3.6 (with $\| \theta \|$ taken as 29.99° for numerical convenience)

The procedure can be easily extended to cope with a singularity involving three flow mechanisms as encountered for instance at the apex of the Mohr-Coulomb pyramid.

3.11 PHYSICAL AND NUMERICAL UNLOADING

Any yielded Gauss point may become elastic due to reduction or reversal of the applied load vector; it is then convenient at the beginning of such a load step, to reset the element tangential stiffnesses to their elastic value to ensure safe numerical handling.

Unloading of a more numerical than physical nature often occurs in path dependent state determination algorithms (where

$\underline{\sigma}_i = \underline{\sigma}_{i-1} + \underline{D}_i^{ep} \underline{B}\, \underline{\Delta d}_i$, as described in Section 3.5), causing deterioration of the solution with oscillations and even divergence.

One possible but expensive remedy is to resort to a path independent strategy (with $\underline{\sigma}_i = \underline{\sigma}_o + D_i^{ep}\, \underline{B}(\sum_{k=1} \underline{\Delta d}_k)$), where trial stress states $\underline{\sigma}_i$ are obtained by reference to the initial stress field $\underline{\sigma}_o$ of the load increment, using the strain variation accumulated up to the current iteration.

An attractive alternative exists [31,40] whereby a principle of "incremental reversibility" is invoked to allow for "plastic" unloading with recovery of plastic strain; negative values for $d\lambda$ are allowed in (3.8) that maintain the stress point on the yield surface while the plastic work at the point is above the value at the beginning of the increment: only then is elastic unloading permitted. Strictly speaking this procedure only ensures path independency in a uniaxial stress-strain context and should therefore be applied with care in other cases.

We compare the three methods in fig. 3.7 and Table 3.7 for the analysis of a 3D tee junction of von Mises material under internal pressure.

3.12 PLANE STRESS PLASTICITY

Starting with a 3D digression we first consider a bar of hardening material yielding under uniaxial load: in a 3D solution that models plane stress conditions by permitting free deformation in the plane normal to the load axis x, the stresses σ_y and σ_z pass by non-zero values during the iteration procedure to become zero only at convergence.

By contrast a much stricter line is followed on a plane stress 2D solution, with σ_z kept zero throughout. Since $\varepsilon_z^p \neq 0$ (although $\sigma_z = 0$), it is not evident how the normality condition is being satisfied.

To clarify this point let us see how to derive the plane stress $\underline{D}_{ep}$ matrix given by

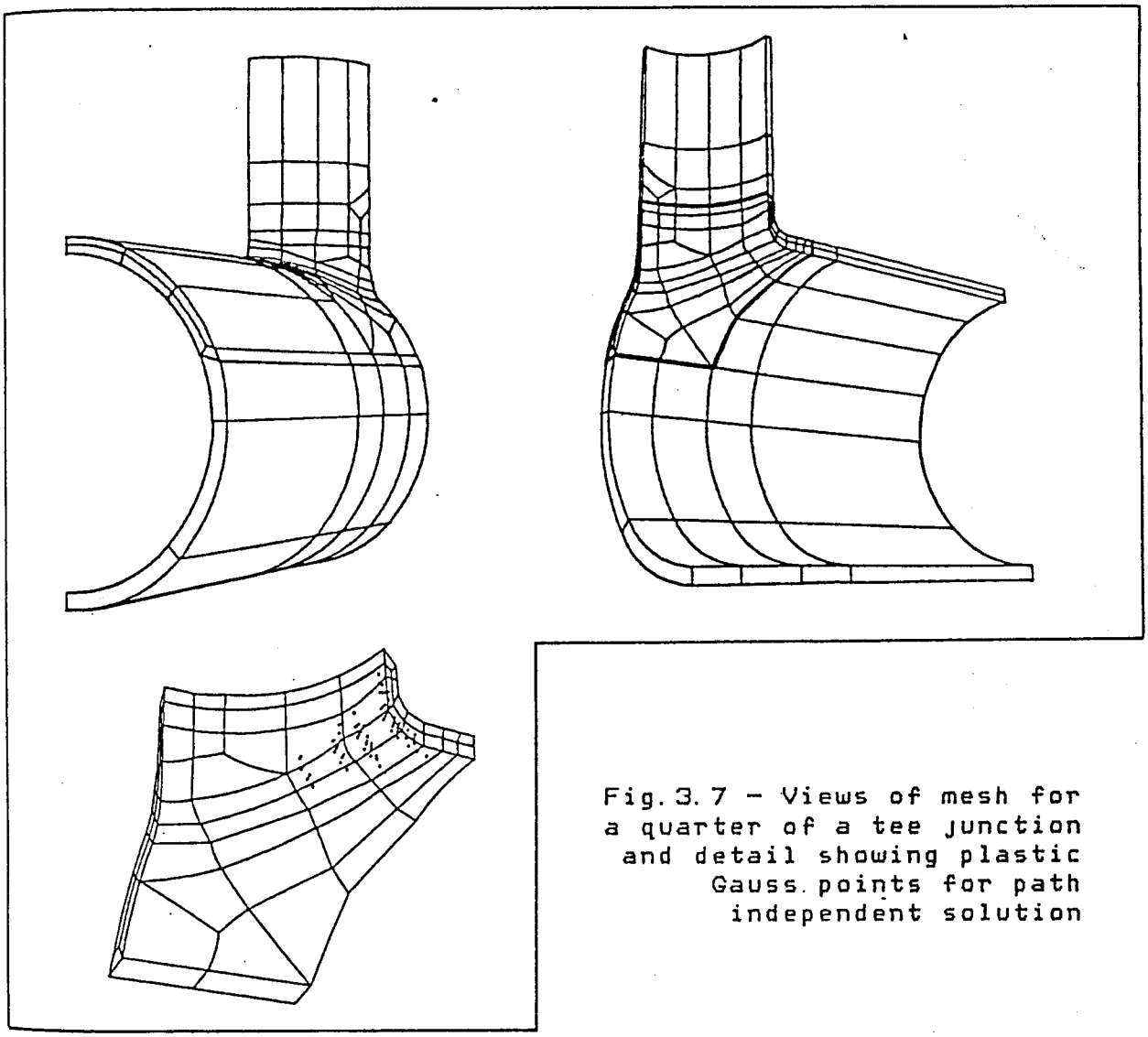

Fig. 3.7 – Views of mesh for a quarter of a tee junction and detail showing plastic Gauss points for path independent solution

E = 3E7	INTERNAL PRESSURE	– 7E4 (1 LOAD STEP)
ν = 0.3	INTERNAL RADII	– 66.5 AND 40.3
Y = 2E5	THICKNESS(VARIABLE)	– 2.3 TO 6.65
V. MISES	ENDS AXIALLY RESTRAINED	
113 ELEMENTS (20 NODED) – 800 NODES – 2*2*2 G.P.		

NEWTON RAPHSON SOLUTIONS	S1 – PATH INDEPENDENT S2 – P. DEPENDENT WITH PLASTIC STRAIN RECOVERY S3 – PATH DEPENDENT

		S1	S2	S3
ITER. 1	PLASTIC G.P.	51	51	51
	Σ SUBSTEPS	132	132	132
ITER. 2	PLASTIC G.P.	68	68	63
	UNLOADING G.P.	--	5	5
	Σ SUBSTEPS	280	209	201
ITER. 3	PLASTIC G.P.	72	72	56
	UNLOADING G.P.	--	17	11
	Σ SUBSTEPS	338	128	112

TABLE 3.7 – Data and results for the tee junction problem of fig 3.7

$$\underline{D}_3^{ep} = \underline{D}_3 - \frac{\underline{D}_3\,\underline{a}_3\,\underline{a}_3^T\,\underline{D}_3}{A + \underline{a}_3^T\,\underline{D}_3\,\underline{a}_3} \qquad \text{with}$$

$$\underline{D}_3 = 2G \begin{vmatrix} 1/(1-\nu) & \nu/(1-\nu) & 0 \\ & 1/(1-\nu) & 0 \\ & & 1/2 \end{vmatrix} \qquad (3.29\ a\text{-}c)$$

$$\underline{a}_3 = \{ a_x, a_y, a_{xy} \}^T$$

where G is the shear modulus and ν the Poisson's ratio. Supposing we knew *a priori* $\Delta\varepsilon_z$ in a plane stress problem we could compute $\Delta\underline{\sigma} = \underline{D}_4\ (\Delta\underline{\varepsilon} - \Delta\underline{\varepsilon}^p)$ as

$$\begin{vmatrix} \Delta\sigma_x \\ \Delta\sigma_y \\ \Delta\tau_{xy} \\ \Delta\sigma_z \end{vmatrix} = 2G \begin{vmatrix} (1-\nu)/(1-2\nu) & \nu/(1-2\nu) & 0 & \nu/(1-2\nu) \\ & (1-\nu)/(1/2\nu) & 0 & \nu/(1-2\nu) \\ & & 1/2 & 0 \\ & & & (1-\nu)/(1-2\nu) \end{vmatrix} \left(\begin{vmatrix} \Delta\varepsilon_x \\ \Delta\varepsilon_y \\ \Delta\gamma_{xy} \\ \Delta\varepsilon_z \end{vmatrix} - d\lambda \begin{vmatrix} a_x \\ a_y \\ a_{xy} \\ a_z \end{vmatrix} \right) \qquad (3.30)$$

Since $\Delta\sigma_z = 0$ we extract $\Delta\varepsilon_z$ as

$$\Delta\varepsilon_z = -\frac{\nu}{1-\nu}\,(\Delta\varepsilon_x + \Delta\varepsilon_y) + d\lambda[\nu/(1-\nu).(a_x+a_y+a_z) + (1-2\nu)/(1-\nu).a_z] \qquad (3.31)$$

Considering incompressible plasticity ($dV_p = d\lambda(a_x+a_y+a_z) = 0$) and taking $d\lambda$ from (3.8a) with $\underline{d} = \underline{D}_4\ \underline{a}_4$ we may express $\Delta\varepsilon_z$ as

$$\Delta\varepsilon_{zz} = R_{xx}\,\Delta\varepsilon_{xx} + R_{yy}\,\Delta\varepsilon_{yy} + R_{xy}\,\Delta\gamma_{xy} \qquad \text{with}$$

$$R_{ij} = [(1-2\nu)\,d_{ij}\,a_{zz}/X - \delta_{ij}\,\nu\,V/X]/(1-\nu) \qquad \text{where} \qquad (3.32\ a\text{-}d)$$

$$X = A + \underline{a}_3^T\,\underline{D}_3\,\underline{a}_3$$

$$V = A + \underline{a}_4^T\,\underline{D}_4\,\underline{a}_4$$

and δ_{ij} is the Kronecker delta.

Eliminating now $\Delta\varepsilon_z$ in $\underline{\Delta\sigma} = \underline{D}_4^{ep}\ \underline{\Delta\varepsilon}$ using (3.32 a), we finally arrive, after some lengthy algebra, to

$$\begin{vmatrix} \Delta\sigma_x \\ \Delta\sigma_y \\ \Delta\tau_{xy} \end{vmatrix} = \underline{D}_3^{ep} \begin{vmatrix} \Delta\varepsilon_x \\ \Delta\varepsilon_y \\ \Delta\gamma_{xy} \end{vmatrix} \tag{3.33}$$

with $\underline{D}_3^{ep}$ given by (3.29 a) as sought.

Equation (3.30) shows that in plane stress we really have $\Delta\sigma_z = \Delta\sigma_z^e + \Delta\sigma_z^p = 0$ but $\Delta\sigma_z^e = -\Delta\sigma_z^p \neq 0$. Use of (3.33), although computationally convenient, hides the fact that a non-zero z component exists in the excess stress, only to vanish after a return to the yield surface that satisfies the normality condition.

This fact should be borne in mind for plane stress computations that resort to a mid-point or an implicit technique.

3.13 FINAL REMARK

Important aspects of the stress computation algorithm in elastoplastic small strain analysis have been examined and refinements were proposed.

Indications will be given in Chapter 5 for extension to finite strain applications.

3.14 REFERENCES

1. TURNER, M.J., DILL, E.H., MARTIN, H.C. and MELOSH, R.J., Large deflections of structures subjected to heating and external loads, J. Aero. Sci., 27, 97-106, 1960

2. ZIENKIEWICZ, O.C., The Finite Element Method, 3rd. edition, McGraw-Hill, London, 1977

3. HILL, R., The Mathematical Theory of Plasticity, Oxford University Press, 1950

4. KOITER, W.T., Stress-strain relations, uniqueness and variational theorems for elastic-plastic materials with a singular yield surface, Q. Appl. Math., 11, 350-354, 1953

5. NAYAK, G.C. and ZIENKIEWICZ, O.C., Convenient form of stress invariants for plasticity, J. Struct. Div., Proc. A.S.C.E., 949-953, 1972

6. TRESCA, H., Mémoire sur l'écoulement des corps solides soumis à de fortes pressions, C. Rend. Acad. Sci. Paris, 59, 754, 1864

7. VON MISES, R., Mechanik der festen Körper im plastisch deformablen Zustand, Götting. Nachr., Math. Phys. Kl., 582-592, 1913

8a. COULOMB, C.A., Essai sur une application des règles de maximis et minimis à quelques problemes de statique rélatifs à l'architecture, Mém. de math. et de phys. prés. à l'Ac. Roy. des Sci. par divers savants, 7, 343, 1773

8b. MOHR, O., Welche Umstände bedingen die Elastizitätsgrenze und den Bruch eines Materials, ZS.d.Vereins Deutscher Ingenieure, 44, 1524 and 1572, 1900

9. DRUCKER, D.C. and PRAGER, W., Soil mechanics and plastic analysis or limit design, Q. Appl. Math., 10, 157-165, 1952

10. PRAGER, W., The theory of plasticity: a survey of recent achievements, Proc. Inst. Mech. Eng., 169, 41-57, 1955

11. PRAGER, W., A new method of analyzing stresses and strains in work hardening plastic solids, J. Appl. Mech., 78, 493-496, 1956

12. ZIEGLER, H., A modification of Prager's hardening rule, Q. Appl. Math., 17, 55-65, 1959

13. HODGE Jr., P.G., Discussion of Ref. 11, J. Appl. Mech., 78, 482-483, 1956

14. EISENBERG, M.A. and PHILIPS, A., On nonlinear kinematic hardening, Acta Mech., 5, 1-13, 1968

15. WHITE Jr., G.N. and DRUCKER, D.C., Effective stress and effective strain in relation to stress theories of plasticity, J. Appl. Phys., 21, 1013-1021, 1950

16. VON MISES, R., Mechanik der plastischen Formänderung von Kristallen, Z.a.M.M., 8, 3, 161-185, 1928

17. BLAND, D.R., The associated flow rule of plasticity, J. Mech. Phys. Sol., 6, 71-78, 1957

18. YAMADA, Y., YOSHIMURA, N. and SAKURAI, T., Plastic stress-strain matrix and its application for the solution of elastic-plastic problems by the finite element method, Int. J. Mech. Sci., 10, 343-354, 1968

19. ZIENKIEWICZ, O.C., VALLIAPPAN, S. and KING, I.P., Elasto-plastic solutions of engineering problems; "initial stress", finite element approach, Int. J. Num. Meth. Engng., 1, 75-100, 1969

20. NAYAK, G.C. and ZIENKIEWICZ, O.C., Elasto-plastic stress analysis. Generalization for various constitutive relations including strain softening, Int. J. Num. Meth. Engng., 5, 113-135, 1972

21. LODE, W., Versuche über den Einfluss der mittleren Hauptspannung auf das Fliessen der Metalle Eisen, Kupfer und Nickel, Z. Phys., 36, 913-939, 1926

22. OWEN, D.R.J. and HINTON, E., Finite Elements in Plasticity: Theory and Practice, Pineridge Press, Swansea, U.K., 1980

23. MARQUES, J.M.M.C. and OWEN, D.R.J., Some reflections on elasto-plastic stress calculation in finite element analysis, Int. J. Num. Meth. Engng. (in press)

24. DRUCKER, D.C., Some implications of work-hardening and ideal plasticity, Q. Appl. Math., 7, 411-418, 1950

25. VENKATRAMAN, B. and PATEL, S.A., Structural Mechanics with Introductions to Elasticity and Plasticity, McGraw-Hill, New York, 1970

26. HUFFINGTON, N.G., Numerical analysis of elastoplastic stresses, Memorandum Report no. 2006, Ballistic Research Laboratories, Aberdeen Proving Ground, Maryland, 1969

27. STRICKLIN, J.A., HAISLER, H.E. and VON RIESSEMANN, W.A., Formulation, computation and solution procedures for material and/or geometric nonlinear structural analysis by the finite element method, SC-CR-72 3102, Sandia Laboratories, Albuquerque, New Mexico, 1972

28. KRIEG, R.D. and KRIEG, D.B., Accuracies of numerical solution methods for the elastic-perfectly plastic model, Trans. A.S.M.E., J. Pr. Vess. Techn., 510-515, 1977

29. BUSHNELL, D., A strategy for the solution of problems involving large deflections, plasticity and creep, Int. J. Num. Meth. Engng., 11, 683-708, 1977

30. SCHREYER, H.L., KULAK, R.F. and KRAMER, J.M., Accurate numerical solutions for elastic-plastic models, Trans. A.S.M.E., J. Pr. Vess. Tech., 226-234, 1979

31. NYSSEN, C., An efficient and accurate iterative method, allowing large incremental steps, to solve elasto-plastic problems, Comp. & Str., 13, 63-71, 1981

32. KEY, S.W., HONDO - A finite element computer program for the large deformation dynamic response of axisymmetric solids, Sandia Laboratories, Albuquerque, N.M., SLA-74-0039, Apr. 74

33. MARCAL, P.V., A stiffness method for elastic-plastic problems, Int. J. Mech. Sci., 7, 229-238, 1965

34. RICE, J.R. and TRACEY, D.M., Computational fracture mechanics, Numerical and Computer Methods in Structural Mechanics, 585-623, S.J. FENVES et al. (eds.), Academic Press, N.Y., 1973

35. WILKINS, M.L., Calculation of elasto-plastic flow, Methods of Computational Physics, Vol. 3, 211-263, B. ALDER et al. (eds.) Academic Press, N.Y., 1964

36. GONÇALVES F°, O.J.A. and OWEN, D.R.J., Incremental elastoplastic stiffness matrix for materials obeying the principal stress yield criterion, Int. J. Num. Meth. Engng. (in press)

37. SAMUELSSON, A. and FRÖIER, M., Finite elements in plasticity - a variational inequality approach, MAFELAP III, WHITEMAN, J.R.(ed.), Academic Press, 1979

38. DONATO, O. de and FRANCHI, A., A modified gradient method for finite element elastoplastic analysis by quadratic programming, Comp. Meth. Appl. Mech. Engng., 2, 107-131, 1973

39. WISSMANN, J.W. and HAUCK, C., Efficient elastic-plastic finite element analysis with higher order stress-point algorithms, Comp. & Str., 17, 89-95, 1983

40. HOLT, J.S. and PARSONS, B., Special problems in incremental finite element plasticity analysis, MAFELAP III, WHITEMAN, J.R. (ed.), Academic Press, 1979

41. MARQUES, J.M.M.C., Stress computation in elastoplasticity, Int. J. Engineering Computations, 1, 42-51, 1984

42. MENDELSON, A. and MANSON, S.S., Practical solution of plastic deformation problems in the elastic-plastic range, NASA TR-R-28, 1959

43. POPE, G.G., A discrete element method for analysis of plane elasto-plastic strain problems, R.A.E., Farnborough, TR 65028, 1965, also Aeron. Q., 17, 83, 1966

CHAPTER 4

THE ELASTOVISCOPLASTIC MODEL FOR MATERIAL NONLINEARITY

4.1	INTRODUCTION	4.1
4.2	COMPUTATIONAL PROCEDURE FOR ELASTOVISCOPLASTIC PROBLEMS	4.2
	4.2.1 The viscoplastic strain rate in Perzyna's model	
	4.2.2 The viscoplastic strain increment	
	4.2.3 The stress increment	
	4.2.4 Equilibrium equations	
	4.2.5 Equilibrium correction	
	4.2.6 Convergence criterion	
4.3	THE HARDENING CORRECTIVE TERM	4.7
4.4	COMPUTATION OF MATRIX $\underline{H}$	4.8
4.5	TIME STEP DEFINITION	4.10
4.6	IMPLICIT-EXPLICIT TIME INTEGRATION	4.11
4.7	FRONTAL SUBSTRUCTURING IN IMPLICIT-EXPLICIT PROBLEMS	4.11
4.8	NUMERICAL EXAMPLES	4.12
	4.8.1 Plane stress compound strip	
	4.8.2 Clamped circular plate	
	4.8.3 Unlined storage cavity	
	4.8.4 Embankment on a stiff layer	
4.9	CONCLUSIONS	4.22
4.10	REFERENCES	4.23

CHAPTER 4

THE ELASTOVISCOPLASTIC MODEL FOR MATERIAL NONLINEARITY

4.1 INTRODUCTION

In many practical problems material behaviour is governed by plastic as well as viscous effects, the latter often becoming even more pronounced once the plastic state has been reached. Such closely associated phenomena were nevertheless subjected to separate theoretical treatment for quite a long time.

The classical theory of plasticity [1], originally motivated by the description of quasi-static metal behaviour at room temperature, makes the fundamental assumption of time independence of the equations of state, thereby providing an acceptable modelling under those types of conditions but failing to accommodate the high temperature, dynamic and long term effects so crucial for many important industrial applications.

On the other hand rheology, under the form of creep and viscoelasticity theories [2,3], confines itself to situations where the stress state does not give rise to significant plastic flow.

The theory of viscoplasticity emerges as an attempt to provide a realistic phenomenological approach to material behaviour combining plastic and creep effects in a unified model. Early developments can be traced back to Bingham [4], Hencky [5], Hohenemser and Prager [5] and Naghdi and Murch [7]; a fundamental generalization of the theory is produced by Perzyna [8,9]; alternative definitions of a viscoplastic material are proposed by Phillips [10,11] and Cristescu [12].

Zienkiewicz and Cormeau [13-20] pioneered the finite element applications of viscoplasticity, emphasizing the numerical simplicity of the computational algorithm and its versatility: one single

program is able to cover an extensive range of problems, spanning from elastic creep to classic plasticity for which an alternative economic solution is obtained in the form of the viscoplastic steady state.

Composite material behaviour involving complex elastic, plastic and rheological effects is easily described by "overlay" viscoplastic models [21-23].

Many successful finite element applications of viscoplasticity have been recently reported for a wide variety of problems such as extrusion and metal forming [24-28], soil [29-33] and rock [34-36], mechanics, plates and shells [37-40], concrete [41] and timber [42] modelling, large displacements [43] and finite strains [44-45], creep and rupture [46-48]. The model has also started to be used with the boundary element method [49].

The present study adopts Perzyna's model, whose basic expressions are reviewed in Section 4.2, in the context of Zienkiewicz and Cormeau's formulation for small strain problems. A detailed mention is made to the representation of hardening behaviour, extending and clarifying the analysis previously made in Reference [51]. The final Section presents an implicit-explicit time integration scheme developed for efficient solution of quasi-static multimaterial domain problems [52,53].

4.2 COMPUTATIONAL PROCEDURE FOR ELASTOVISCOPLASTIC PROBLEMS

4.2.1 The viscoplastic strain rate in Perzyna's model

The main features of the elastoviscoplastic model are clearly illustrated by the simple mechanical device of fig. 4.1:

- the spring E accounts for the elastic deformation;
- the dashpot V supplies the time dependent viscous response, once the stress level $\bar{\sigma}$ in the slider P exceeds a yield value Y.

The concepts of yield criterion and hardening rule, as discussed in Chapter 3 for the elastoplastic model, are again called for.

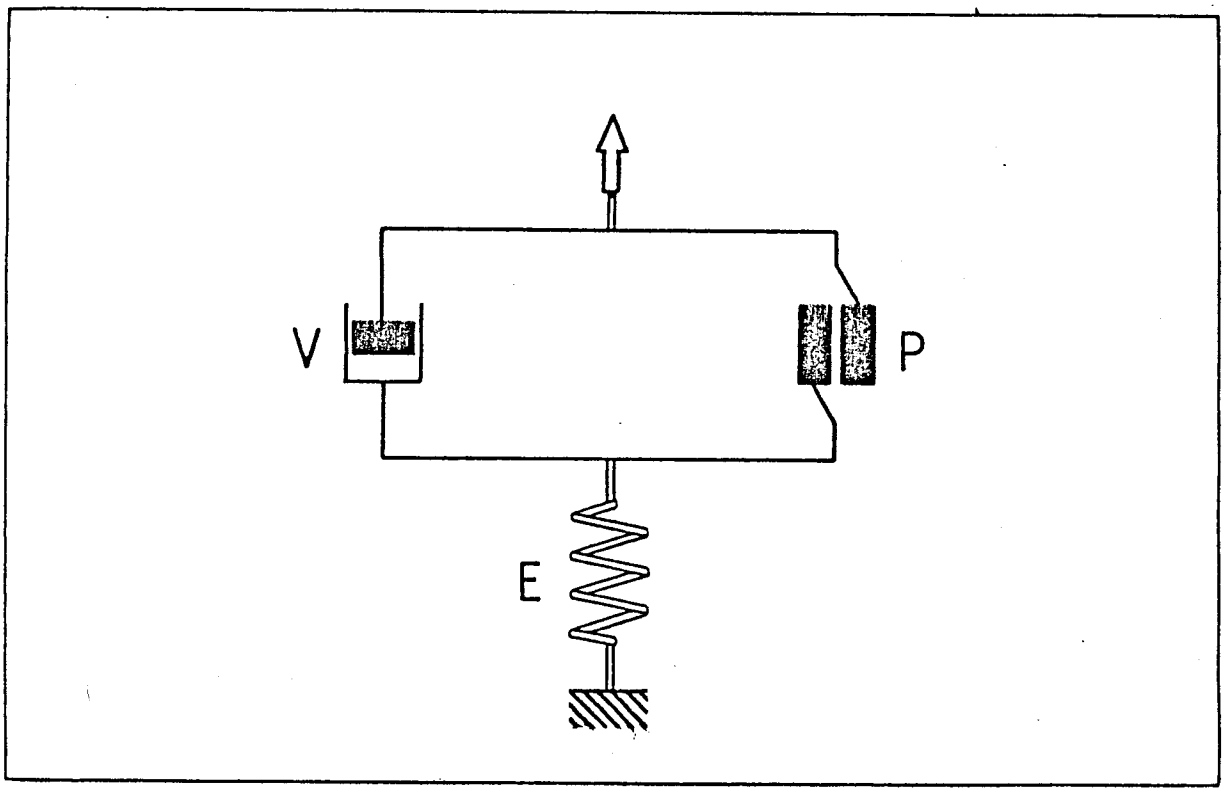

Fig. 4.1 – Basic one dimensional elastoviscoplastic model

The viscoplastic flow rule specific to the Perzyna model is presented below in rate form.

The total strain $\underline{\varepsilon}$ and strain rate $\dot{\underline{\varepsilon}}$ are decomposed into elastic and viscoplastic parts as

$$\underline{\varepsilon} = \underline{\varepsilon}^{e} + \underline{\varepsilon}^{vp}$$
$$\dot{\underline{\varepsilon}} = \dot{\underline{\varepsilon}} + \dot{\underline{\varepsilon}}^{vp} \qquad (4.1)$$

The stress rate $\dot{\underline{\sigma}}$ is related to the elastic strain rate via the elasticity matrix $\underline{D}$ according to

$$\dot{\underline{\sigma}} = \underline{D}\,\dot{\underline{\varepsilon}}^{e} \qquad (4.2)$$

Viscoplastic flow occurs for positive values of a scalar yield condition F which, for isotropic materials, has the form

$$F(\underline{\sigma}, k) = f(\underline{\sigma}) - Y(k) \qquad (4.3)$$

where the yield stress Y depends on a hardening parameter k; common forms for the yield function f may be found in Table 3.2 of Chapter 3.

For associated elastoviscoplasticity Perzyna's flow rule [9] relates the viscoplastic strain rate to the current stresses according to

$$\dot{\underline{\varepsilon}}^{vp} = \gamma < \Phi(F) > \partial f/\partial \underline{\sigma} \qquad (4.4)$$

in which γ is the fluidity parameter, a positive factor which can depend on some state variables (such as time, temperature, total strain invariants or damage)[9,15]; the flow function $\Phi(F)$ is monotonically increasing and positive, with $<\Phi(F) >$ equal to Φ for positive values of F and zero otherwise.

Perzyna [9] presents power and exponential type laws for Φ

$$\begin{aligned} \Phi(F) &= (F/Y)^N \\ \Phi(F) &= \exp(MF/Y) - 1 \end{aligned} \qquad (4.5)$$

where the constants M and N are prescribed so as to fit experimental data.

The inclusion of the flow vector $\partial f/\partial \underline{\sigma}$ in the associated law (4.4) implies that the viscoplastic strain rate vector is normal to what Perzyna calls the "subsequent dynamic loading surface" [9].

4.2.2 The viscoplastic strain increment

The viscoplastic strain increment $\Delta\underline{\varepsilon}_n^{vp}$ in the time interval $\Delta t_n = t_{n+1} - t_n$ can be defined by the formula [43]

$$\Delta\underline{\varepsilon}_n^{vp} = \Delta t_n[(1-\theta)\ \dot{\underline{\varepsilon}}_n^{vp} + \theta\ \dot{\underline{\varepsilon}}_{n+1}^{vp}] \qquad (4.6)$$

The parameter θ ($0 \leq \theta \leq 1$) defines the time integration scheme; well known choices are Euler forward or fully explicit ($\theta=0$), implicit trapezoidal or Crank-Nicholson ($\theta=1/2$), Galerkin ($\theta=2/3$) and Euler backward or fully implicit ($\theta=1$).

Noting from equations (4.4) and (4.5) that $\dot{\underline{\varepsilon}}^{vp} = \dot{\underline{\varepsilon}}^{vp}(\underline{\sigma}, k)$ we may now approximate $\dot{\underline{\varepsilon}}_{n+1}^{vp}$ using a limited Taylor series

expansion

$$\dot{\underline{\varepsilon}}^{vp}_{n+1} = \dot{\underline{\varepsilon}}^{vp}_{n} + \left(\frac{\partial \dot{\underline{\varepsilon}}^{vp}}{\partial \underline{\sigma}}\right)_n \Delta\underline{\sigma}_n + \left(\frac{\partial \dot{\underline{\varepsilon}}^{vp}}{\partial k}\right)_n \Delta k_n \qquad (4.7)$$

or, more concisely,

$$\dot{\underline{\varepsilon}}^{vp}_{n+1} = \dot{\underline{\varepsilon}}^{vp}_{n} + \underline{H}_n \Delta\underline{\sigma}_n + \underline{h}_n \Delta k_n \qquad (4.8)$$

Substitution of (4.8) into (4.6), with $\underline{C}_n = \theta \Delta t_n \underline{H}_n$ yields

$$\Delta\underline{\varepsilon}^{vp}_{n} = \Delta t_n (\dot{\underline{\varepsilon}}^{vp}_{n} + \theta \Delta k_n \underline{h}_n) + \underline{C}_n \Delta\underline{\sigma}_n \qquad (4.9)$$

or in a compact notation

$$\Delta\underline{\varepsilon}^{vp}_{n} = \Delta t_n \dot{\underline{e}}^{vp}_{n} + \underline{C}_n \Delta\underline{\sigma}_n \qquad (4.10)$$

where

$$\dot{\underline{e}}^{vp}_{n} = \dot{\underline{\varepsilon}}^{vp}_{n} + \theta \Delta k_n (\partial \dot{\underline{\varepsilon}}^{vp}/\partial k)_n \qquad (4.11)$$

The second term in (4.11) conveys the effect of yield surface expansion due to hardening during the time step; it affects implicit solutions (where $\theta \neq 0$) and had been disregarded in previous formulations [43,50]. The physical significance of (4.11) and its incidence on numerical results is examined in Section 4.3.

A convenient form for the computation of matrix $\underline{H}$ is described in Section 4.4, taking further advantage of the stress invariant set (J_1, J_2', θ) presented in Chapter 3.

4.2.3 The stress increment

Using (4.10) in the incremental form of equation (4.2) and relating the increments of total strain $\Delta\underline{\varepsilon}_n$ and displacement $\Delta\underline{d}_n$ by the strain-displacement matrix $\underline{B}$, the stress increment is obtained as

$$\Delta\underline{\sigma}_n = \hat{\underline{D}}_n (\underline{B} \Delta\underline{d}_n - \dot{\underline{e}}^{vp} \Delta t_n) \qquad (4.12)$$

where $$\hat{\underline{D}}_n = (\underline{D}^{-1} + \underline{C}_n)^{-1} \qquad (4.13)$$

For associated viscoplasticity $\underline{C}_n$, and therefore $\hat{\underline{D}}_n$, are symmetric matrices.

4.2.4 Equilibrium equations

The equilibrium between internal and external forces at time t_n is expressed by

$$\int_V \underline{B}^T \underline{\sigma}_n \, dv = \underline{f}_n \tag{4.14}$$

where $\underline{f}$ is the vector of nodal loads corresponding to the applied surface tractions, body forces, etc.

Using (4.12) in the incremental form of the equilibrium equations (4.14) and solving for $\Delta\underline{d}_n$ we get

$$\Delta\underline{d}_n = \underline{K}_{Tn}^{-1} \Delta\underline{V}_n \tag{4.15}$$

where the current tangential stiffness matrix $\underline{K}_{Tn}$ and viscous loads $\Delta\underline{V}_n$ are given by

$$\underline{K}_{Tn} = \int_V \underline{B}^T \hat{\underline{D}}_n \underline{B} \, dv \tag{4.16}$$

$$\Delta\underline{V}_n = \int_V \underline{B}^T \hat{\underline{D}}_n \dot{\underline{e}}^{vp} \Delta t_n \, dv + \Delta\underline{f}_n \tag{4.17}$$

The term $\Delta\underline{f}_n$ in (4.17) is non-zero only for the time steps when a new increment of external loading is applied.

The displacement and stress fields at the end of the time step Δt_n are

$$\underline{d}_{n+1} = \underline{d}_n + \Delta\underline{d}_n \tag{4.18}$$

$$\underline{\sigma}_{n+1} = \underline{\sigma}_n + \Delta\underline{\sigma}_n$$

4.2.5 Equilibrium correction

Due to the linearization implicit in (4.6) the equilibrium equations will not in general be exactly satisfied at the end

of the time step. The residual forces can be dissipated by performing a number of equilibrium iteration cycles [54] or, alternatively, they may simply be added to the viscous loads for the next time step [50].

4.2.6 Convergence criterion

Convergence of the time stepping process to steady state conditions is monitored by requiring that the current value of the summation of the viscoplastic strain rates over the Gauss points be less than a specified percentage of that occurring in the first time step of the load increment (typically less than 1.0%).

4.3 THE HARDENING CORRECTIVE TERM

Expression (4.11) for the modified viscoplastic strain rate $\dot{\underline{e}}^{vp}$ with the hardening corrective term $(\theta\ \Delta k\ \partial\dot{\underline{\varepsilon}}^{vp}/\partial k)_n$ is now recast in a form that is more suggestive as to its physical meaning. Differentiating (4.4) we get

$$\frac{\partial\dot{\underline{\varepsilon}}^{vp}}{\partial k} = \gamma \frac{\partial\Phi_n}{\partial Y} \frac{dY_n}{dk} \frac{\partial f_n}{\partial\underline{\sigma}} \tag{4.19}$$

For both laws (4.5) we have

$$\frac{\partial\Phi_n}{\partial Y} = -\frac{f}{Y}\frac{\partial\Phi}{\partial f} \tag{4.20}$$

Using (4.19) and (4.20) the corrective term may be rewritten

$$\left(\theta\ \Delta k \frac{\partial\dot{\underline{\varepsilon}}^{vp}}{\partial k}\right)_n = -\gamma\ \theta\ f_n \frac{\partial\Phi_n}{\partial f}\frac{\Delta Y_n}{Y_n}\frac{\partial f_n}{\partial\underline{\sigma}}. \tag{4.21}$$

Finally we are able to cast $\dot{\underline{e}}^{vp}$ of (4.11) in a form identical to (4.4) as

$$\dot{\underline{e}}^{vp}_n = \gamma < \Phi^*(F_n) > \partial f_n/\partial\underline{\sigma} \tag{4.22}$$

with the modified flow function

$$\Phi^*(F) = \Phi(F) - \theta\ f \frac{\partial\Phi}{\partial f}\ \frac{\Delta Y}{Y} \tag{4.23}$$

The second term on the right-hand side of (4.23) plays a role in implicit problems ($\theta \neq 0$) where the computation of the viscoplastic strain increment during a time step is based on a weighted sum of the known and estimated values of the viscoplastic strain rate, respectively at the beginning and end of the time interval, in the manner of equation (4.6). If the material hardens ($\Delta Y \neq 0$) the effect on the referred estimation induced by the expansion of the yield surface during the time step has to be accounted for. This requirement is readily achieved by adopting the simple modification for the flow function proposed above. Noting that all the factors in the second term of (4.23) are positive (for a hardening case), we are in effect reducing the viscoplastic strain rate, thereby avoiding the overestimation of the final displacement and strain values that would otherwise develop, as illustrated by the numerical examples of Section 4.8.

4.4 COMPUTATION OF MATRIX $\underline{H}$

A convenient form is now presented for the evaluation of matrix $\underline{H}$ with recourse to the stress invariant set (J_1, J_2', θ). As shown in Chapter 3 the flow vector $\underline{a} = \partial f/\partial \underline{\sigma}$ is thereby expressable as $\underline{a} = C_1\underline{a}_1 + C_2\,\underline{a}_2 + C_3\underline{a}_3$ with C_i and $\underline{a}_i$ given by (3.14). A change of yield criterion simply requires a new selection for the constants C_i; Table 3.3 displays the appropriate values for use with four widely used criteria: Tresca, von Mises, Mohr-Coulomb and Drucker-Prager.

Taking this strategy one step further, we first note that

$$\underline{H} = \frac{\partial \dot{\underline{\varepsilon}}^{vp}}{\partial \underline{\sigma}} = \gamma \left(\Phi \frac{\partial \underline{a}^T}{\partial \underline{\sigma}} + \frac{d\Phi}{dF}\, \underline{a}\, \underline{a}^T \right) \qquad (4.24)$$

omitting for clarity the symbols "<>" of 4.4).

Introducing $\underline{a}$ in terms of C_i and $\underline{a}_i$ in (4.24) we arrive, after a lengthy exercise, to the form [55]

$$\underline{H} = \sum_{i=1}^{6} F_i\, \underline{M}_i \qquad \text{with} \qquad (4.25)$$

$$\underline{M}_1 = 6(J_2')^{1/2}\ \partial \underline{a}_2^T/\partial\underline{\sigma}$$

$$\underline{M}_2 = \underline{a}_2\ \underline{a}_2^T$$

$$\underline{M}_3 = 3/2\ \partial \underline{a}_3^T/\partial\underline{\sigma} \qquad (4.26)$$

$$\underline{M}_4 = \underline{a}_3\ \underline{a}_3^T$$

$$\underline{M}_5 = \underline{a}_2\ \underline{a}_3^T + \underline{a}_3\ \underline{a}_2^T$$

$$\underline{M}_6 = \underline{a}\ \underline{a}^T$$

and

$$F_i = \gamma\ \Phi\ \bar{F}_i \qquad \text{for } i \leq 5 \qquad (4.27)$$

with the values of $\bar{F}_i$ given in Table 4.1 for the above mentioned yield criteria, and

	VON MISES	DRUCKER-PRAGER	TRESCA	MOHR-COULOMB
$\bar{F}_1$	$C_2/[6(J_2')^{\frac{1}{2}}]$	$C_2/[6(J_2')^{\frac{1}{2}}]$	$C_2/[6(J_2')^{\frac{1}{2}}]$	$C_2/[6(J_2')^{\frac{1}{2}}]$
$\bar{F}_2$	$-C_2/(J_2')^{\frac{1}{2}}$	$-C_2/(J_2')^{\frac{1}{2}}$	$C_4(1.5C_2-2\cos\theta)$	$C_4(1.5C_2-\cos\theta+\frac{\sin\phi\sin\theta}{\sqrt{3}})$
$\bar{F}_3$	0	0	$2C_3/3$	$2C_3/3$
$\bar{F}_4$	0	0	$3\bar{F}_2/(2J_2')^2$	$3\bar{F}_2/(2J_2')^2$
$\bar{F}_5$	0	0	$C_4C_3(1.5+\cos\theta\cos3\theta)$	$C_4C_3(1.5+\cos\theta\cos3\theta)$ + $C_4\sin\phi(\sin^2\theta-0.75)/J_2'$

TABLE 4.1 – Values of $\bar{F}_i$ for the computation of matrix $\underline{H}$ by (4.25) and (4.27)

$$F_6 = \gamma \, d\Phi/dF \qquad \text{with}$$

$$d\Phi/dF = M(\Phi + 1)/Y \qquad \text{(power law)} \qquad (4.28)$$

$$= N \, \Phi/F \qquad \text{(exponential law)}$$

A similar approach is followed by Damjanić [56] restricted to the Mohr-Coulomb law.

4.5 TIME STEP DEFINITION

The time integration scheme represented by formula (4.6) is conditionally stable for $\theta < 1/2$ [57]. For explicit solutions ($\theta = 0$) with a linear flow function. Cormeau [58] derived theoretical stability limits for some yield criteria, namely

$$\Delta t \leq (1 + \nu)Y/\gamma E \qquad \text{(Tresca)}$$

$$\Delta t \leq 4(1 + \nu)Y/3\gamma E \qquad \text{(von Mises)} \qquad (4.29)$$

$$\Delta t \leq \frac{4(1 + \nu)(1 - 2\nu)Y}{\gamma(1 - 2\nu + \sin^2\phi)E} \qquad \text{(Mohr-Coulomb)}$$

Step sizing criteria that ensure stability and accuracy for implicit integration are presented by Owen and Damjanić [59] based on an eigenvalue analysis of some of the matrices involved.

Empirical methods also exist [50] that control the step increase according to either the size of the previous step with

$$\Delta t_{n+1} \leq k \, \Delta t_n \qquad (4.30)$$

or by limiting the ratio of effective viscoplastic strain increment and effective total strain as

$$\Delta \bar{\varepsilon}^{vp}_n \cong \dot{\bar{\varepsilon}}^{vp}_n \, \Delta t_n \leq \tau \, \bar{\varepsilon}_n \qquad (4.31)$$

where k is in the range 1.0 - 2.0 and τ varies between 0.01 - 0.15 for explicit schemes [15]

Noting that for $\theta=0$, $\hat{\underline{D}}_n$ in (4.13) reduces to $\underline{D}$ and, consequently, $\underline{K}_{In}$ in (4.16) remains constant throughout the time stepping, explicit integration has the attractive feature of requiring the inversion of the global stiffness matrix to be performed once only. Unfortunately

the stringent stability limits imposed on the step size often make the advancement of the solution in time an inordinately lengthy process. Implicit schemes, on the other hand, have no such drawback but require more computational effort per time step.

Situations arise in which the multimaterial nature of the domain defines regions of very different permissible time step lengths. Such is the case in composite material analyses and soil-structure interaction problems. An implicit-explicit strategy is now described that provides substantial economies in computer time [52,53].

4.6 IMPLICIT-EXPLICIT TIME INTEGRATION

Implicit-explicit time integration schemes were first introduced in the context of transient dynamic problems [60], as mentioned in Chapter 2.

The basic idea behind the extension of this concept to the quasistatic analysis of viscoplastic multimaterial domains is to combine the lower expense of explicit rules with the increased stability of implicit schemes. When the time step limits are significantly different for the interacting media under analysis, the step sizing is thereby based upon the larger time limit and the regions that would otherwise have enforced the choice of a smaller value are integrated implicitly. In this way a faster advance along the time axis is achieved but avoiding expensive implicit integration of the whole finite element mesh.

4.7 FRONTAL SUBSTRUCTURING IN IMPLICIT-EXPLICIT PROBLEMS

The basic difference between the two types of elements to be considered in the mesh, is that those in the implicit zone require stiffness updating at every time step whereas the explicit ones retain the initial stiffness value throughout. In all computations concerning the latter the parameter θ of expression (4.6) is taken as zero.

On use of a frontal equation solver [50], maximum economy is achieved if all the explicit elements are processed before the implicit ones. On the first call of the equation solution routine, as soon as the stiffness assembly of all explicit elements is complete, we are in possession of the (invariant) condensed stiffness of an explicit superelement, which is stored for use in all subsequent time steps.

This is in effect only a partial substructuring since we cannot extend the procedure to the element pseudo-load vectors: they must be recomputed and reassembled at every time step regardless of element type, according to (4.17).

If a large portion of the mesh is expected to remain elastic (by experience of physical reasoning), full substructuring gives extra savings in computation times.

To achieve this end the frontal solver is made to process elastic, explicit and implicit elements in sequence. The constant stiffness zone, comprising explicit and elastic elements (which may be considered "non-plastified explicit elements") is dealt with as described above. In the elastic region, (4.17) reduces to $\Delta \underline{V}_n = \Delta \underline{f}_n$ and residual nodal forces are negligibly small. The elastic load vector is then assembled on the first time step only and stored; when a new increment of proportional loading is applied, it is simply scaled to the current load level.

4.8 NUMERICAL EXAMPLES

In this Section are presented four numerical examples:

- the first two examine the numerical significance of the additional hardening term $\underline{h}_n$ of expression (4.8);
- in addition the accuracy and efficiency of the implicit-explicit time integration technique described in Section 4.6 is assessed in examples 1, 3 and 4 against implicit and explicit only solutions. Further use of the implicit-explicit rule will be made in Chapter 7.

All the examples employ parabolic isoparametric elements as well as a linear flow function Φ corresponding to N = 1 in (4.5).

The von Mises, Tresca and Mohr-Coulomb yield criteria and their associated flow rules are considered. The critical time step length Δt_c for explicit time integration is computed by recourse to expressions (4.29).

In the examples that use the implicit-explicit method the Δt_c ratio for the pair of materials involved is equal to or greater than 6 to 1; the conditional stability of the explicit scheme imposes the choice of the smaller Δt_c value; using the implicit-explicit or implicit formulations the larger value or multiples thereof are selected and a constant step size is used for a clear comparison between the three integration techniques.

CPU times are measured in seconds on ICL 1904S, ICL 2966 and CDC 7600 computers, respectively for problems 1, 3 and 4.

4.8.1 Plane stress compound strip

Table 4.2 shows the geometry and material properties of a composite strip subjected to interfacial loading p = 22500 kg/cm^2 and with ends restrained against axial movement. For the load level assumed both regions become plastified in accordance to a von Mises law and steady state conditions are eventually achieved due to the linear strain hardening characteristics of material 1.

The mesh has 8 elements (0.5 x 0.25 cm^2) and a 2 x 2 Gauss rule is used.

The results for explicit, implicit and implicit/explicit time integration schemes are compared in Table 4.2. Implicit integration is performed for both an implicit trapezoidal rule (θ = 0.5) and the Euler backward algorithm (θ = 1.0). It is clearly seen that when the additional hardening factor $\underline{h}_n$ is omitted during implicit solution, the displacements are significantly overestimated. In the coupled implicit-explicit solution, the hardening material is explicitly integrated and therefore the omission of $\underline{h}_n$ has no effect.

4.8.2 Clamped circular plate

The plate of Table 4.3 is subjected to a uniformly distributed vertical load of intensity p = 38.612 kg/cm^2 and then unloaded [20,61].

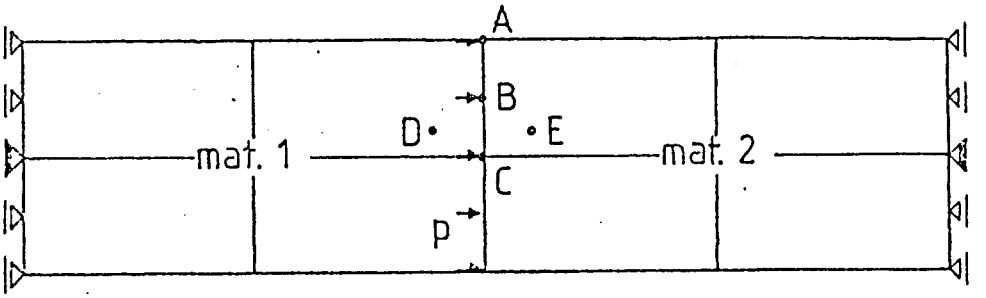

	E(Kg/cm²)	ν	Y_o(Kg/cm²)	H'(Kg/cm²)	γ(/t)
Material 1	20×10^5	0.	2000.	20×10^4	0.0002
Material 2	20×10^6	0.	20000.	0.	0.002

	EXP.	I/E	IMP.	IMP. without $\underline{h}_n$	I/E	IMP.	IMP. without $\underline{h}_n$
θ	0	0. , 0.5	0.5	0.5	0. , 1.0	1.0	1.0
τ	0.15	1.0	1.0	1.	1.0	1.0	1.0
Δt_o	0.(6)	6.(6)	6.(6)	6.(6)	6.(6)	6.(6)	6.(6)
K	1.0	1.0	1.0	1.0	1.0	1.0	1.0
$U_A \times 10^5$	345.529	351.542	351.392	365.172	347.815	346.766	374.281
$U_B \times 10^5$	363.947	370.538	370.365	385.237	366.487	365.353	395.016
$U_C \times 10^5$	370.186	376.993	376.814	392.064	372.810	371.656	402.052
$\bar{\sigma}_D$	2453.1	2464.2	2464.8	2462.6	2457.1	2458.5	2456.8
$\bar{\sigma}_E$	19974.2	19963.0	19959.0	19958.7	19965.8	19969.8	19962.1
TIME STEPS	681	101	101	99	147	146	149
CPU TIME	40.881	9.443	12.481	12.235	13.477	17.532	17.875

TABLE 4.2 – Data and results for the plane stress compound strip problem

The material obeys the von Mises yield criterion and the following hardening law

$$Y = 1260 + 10^5 \bar{\varepsilon}_{vp} + 330\ [1 - \exp(-1453\ \bar{\varepsilon}_{vp})].$$

The mesh has a total of 70 elements with width of 10 mm and height of either 4 or 1 mm and a 2x2 Gauss rule is considered.

It is evident from Table 4.3 that the explicit results and the implicit solutions (including hardening corrective terms) are in close agreement. Omission of the hardening terms leads to over-estimation of the displacements and strains and also residual stresses, particularly at points F and G where more extensive plastification has occurred.

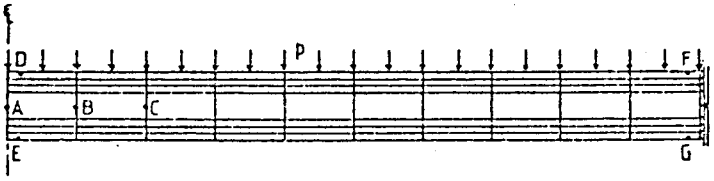

E(Kg/cm²)	ν	γ(/t)	θ	τ	Δt_o	K
70000.	0.33	0.001	0. (EXP.) 1. (IMP.)	0.05	1.	1.5

		p = 38.612 Kg/cm²			LOAD REMOVED		
		EXP	IMP	IMP without $\underline{h}_n$	EXP	IMP	IMP without $\underline{h}_n$
	V_A	- 111898	- 111768	- 114362	- 14928	- 14799	- 17392
	V_B	- 109675	- 109545	- 112089	- 14589	- 14459	- 17004
	V_C	- 103203	- 103092	- 105490	- 13653	- 13541	- 15939
D	σ_R	- 1651.97	- 1615.77	- 1624.36	221.87	258.08	249.48
	σ_Z	- 30.42	- 34.03	- 37.60	10.17	6.56	2.98
	τ_{max}	810.79	790.88	793.38	105.86	125.90	123.28
	ε_R	- 2098.02	- 2094.34	- 2141.57	- 325.41	- 321.72	- 368.95
	ε_Z	2587.11	2611.86	2697.70	876.54	901.29	987.13
	γ_{max}	4685.19	4706.20	4839.28	1201.98	1223.14	1356.08
E	σ_R	1610.84	1602.33	1597.31	- 243.99	- 252.50	- 257.52
	σ_Z	11.01	- 3.95	- 0.27	9.03	- 5.92	- 2.24
	τ_{max}	799.92	803.14	798.80	126.59	123.34	127.64
	ε_R	2096.33	2096.71	2148.72	323.71	324.09	376.11
	ε_Z	- 2630.96	- 2647.90	- 2757.55	- 883.16	- 900.10	-1009.75
	γ_{max}	4727.29	4744.61	4906.32	1206.91	1224.20	1385.88
F	σ_R	2065.50	2085.23	2049.42	- 594.36	- 574.63	- 610.44
	σ_Z	- 38.90	- 39.14	- 39.72	2.80	2.56	1.98
	τ_{max}	1052.23	1062.23	1044.58	300.69	290.55	308.46
	ε_R	5004.59	4991.90	5288.99	1567.01	1554.31	1851.41
	ε_Z	- 3484.89	- 3470.99	- 3774.96	-1789.51	-1775.60	-2079.58
	γ_{max}	8490.67	8464.00	9064.96	3356.58	3330.02	3931.09
G	σ_R	- 2099.04	- 2119.01	- 2030.06	579.84	559.87	648.81
	σ_Z	.22	.56	.35	- 2.87	- 2.52	- 2.74
	τ_{max}	1049.66	1059.83	1015.21	293.48	283.19	328.42
	ε_R	- 4993.00	- 4981.57	- 5318.96	-1555.42	-1543.99	-1881.38
	ε_Z	3424.31	3411.65	3784.77	1766.16	1753.49	2126.62
	γ_{max}	8418.53	8394.35	9104.51	3321.64	3297.58	4008.24

TABLE 4.3 - Data and results for the clamped circular plate problem (with displacements and strains x10⁶)

4.8.3 Unlined storage cavity

Underground cavities are currently used for gas and oil storage, nuclear waste disposal and geothermal energy projects. In the problem considered in fig. 4.2 an axisymmetric unlined cavity is excavated in the zone of contact of two horizontal layers of Mohr-Coulomb soil.

The removal of material disturbs the gravity induced stress field, and the stress relaxation and plastic flow that follow are assumed to start only at completion of the excavation.

The problem parameters are given in Table 4.4 and very similar steady state solutions are obtained by use of explicit, implicit and implicit-explicit time integration schemes, as may be seen in Table 4.5 where the final displacement of point P at the top of the cavity ceiling is registered.

In fig. 4.2 the extent of the yielded zone is also depicted, as well as typical patterns of the principal stress field and of the "plastic" nodal displacements around the cavity, where "plastic" denotes the difference between the final displacement and the instantaneous elastic response. In the principal stress plot, compression is indicated by double lines.

The CPU times of Table 4.5 illustrate the economy of the implicit-explicit technique.

	E	ν	c	ϕ	γ	ρ	Δtc
Material 1	5.E6	0.25	5500.	12.4	1.E-3	35.0	4.918
Material 2	3.E7	0.25	2000.	30.0	1.E-3	35.0	0.192

TABLE 4.4 – Material parameters for the storage cavity problem

	EXP	IMP	IMP	IMP-EXP	IMP-EXP
ΔT(const.)	0.19	4.9	49.0	4.9	14.7
Time steps	421	28	14	26	14
d_v (m)	-1.727	-1.724	-1.745	-1.722	-1.741
CPU(ICL 2966)	938	406	222	279	154

TABLE 4.5 – Vertical displacement of node P(fig.4.2) and CPU time for various solutions of the storage cavity problem

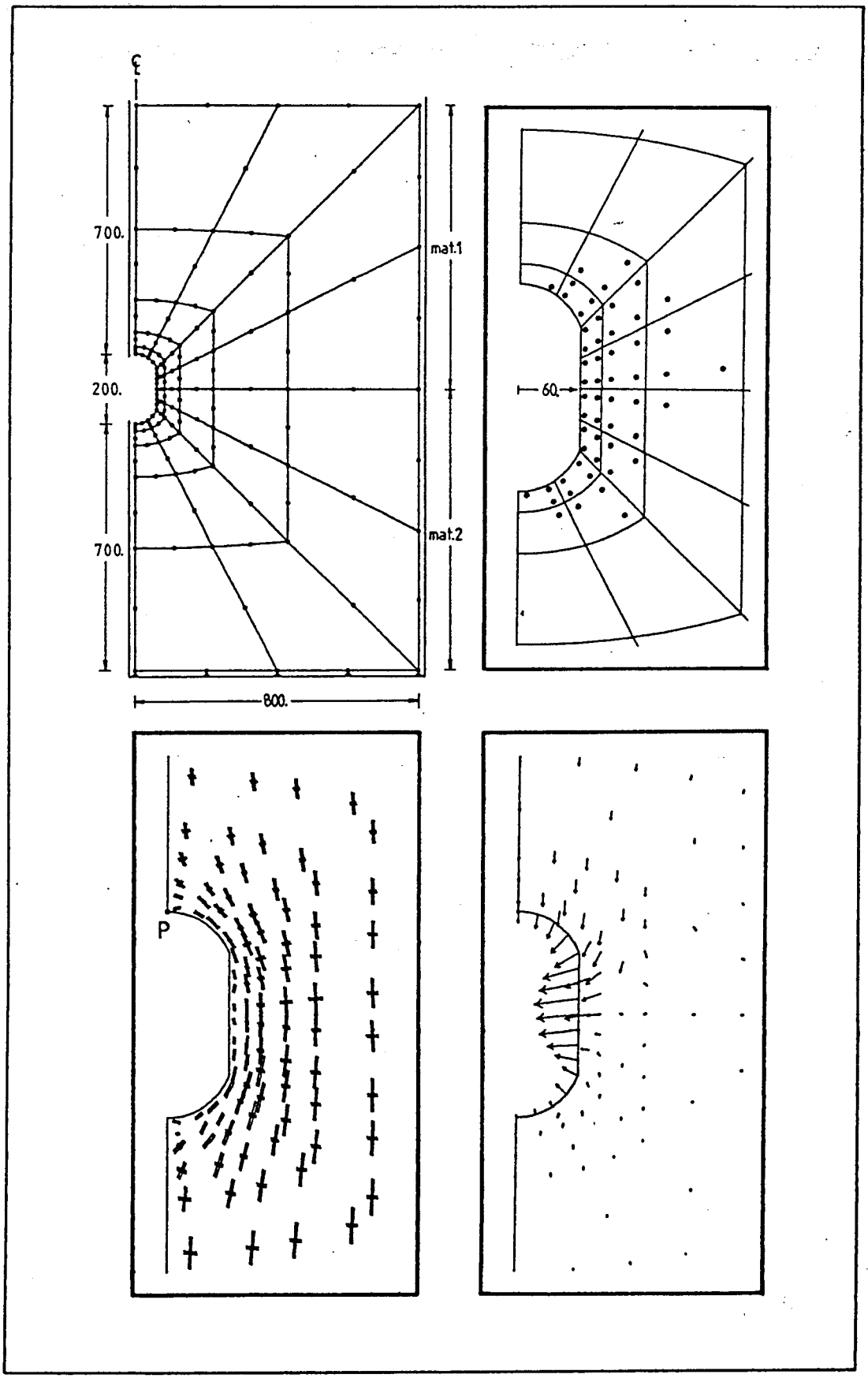

Fig. 4.2 – Mesh geometry, yielded Gauss point map, principal stresses and "plastic" nodal displacements (x150) for the storage cavity problem

4.8.4 Embankment on a stiff layer

An embankment is built on top of a 2.5m thick layer of soil on a horizontal rigid foundation. Plane strain conditions and Mohr-Coulomb material behaviour are assumed: the stiff bottom layer corresponds to material 2 of Table 4.6 and is discretized by a row of 18 square finite elements as shown in fig. 4.3.

Results of the analysis of the slope behaviour under gravity loading are documented in Table 4.7, which contains the displacement components of node N at the crest of the slope.

The good agreement between the various solutions is also evident in fig. 4.4, where the plotted curves of vertical stress at the layer A-B of Gauss points are perfectly coincident.

The deformation pattern is shown in fig. 4.5 where the total displacement is scaled by 100 and in the vector plot of fig. 4.6 where the "plastic" (i.e. total minus instantaneous elastic) displacement is magnified 500 times.

The isometric view of the effective plastic strain (fig. 4.7) and the yielded Gauss point map (fig. 4.3) give a complete picture of the extent of plastification.

In the CPU time comparison of Table 4.7 the implicit-explicit technique proves once more to be competitive.

	E	ν	c	ϕ	γ	ρ	Δtc
Material 1	2.E4	0.35	15.0	10.0	1.E-4	15.0	36.242
Material 2	2.E5	0.25	20.0	20.0	1.E-4	20.0	3.808

TABLE 4.6 – Material parameters for the embankment problem

	EXP	IMP	IMP	IMP-EXP
ΔT(const.)	3.80	36.0	360.0	36.0
Time steps	46	8	4	4
d_H (mm)	-2.012	-2.022	-2.092	-2.071
d_V (mm)	-38.782	-38.872	-39.670	-38.820
CPU(CDC 7600)	37.100	15.876	8.766	6.238

TABLE 4.7 – Horizontal and vertical displacement of node N (fig.4.3) and CPU time for several solutions of the embankment problem

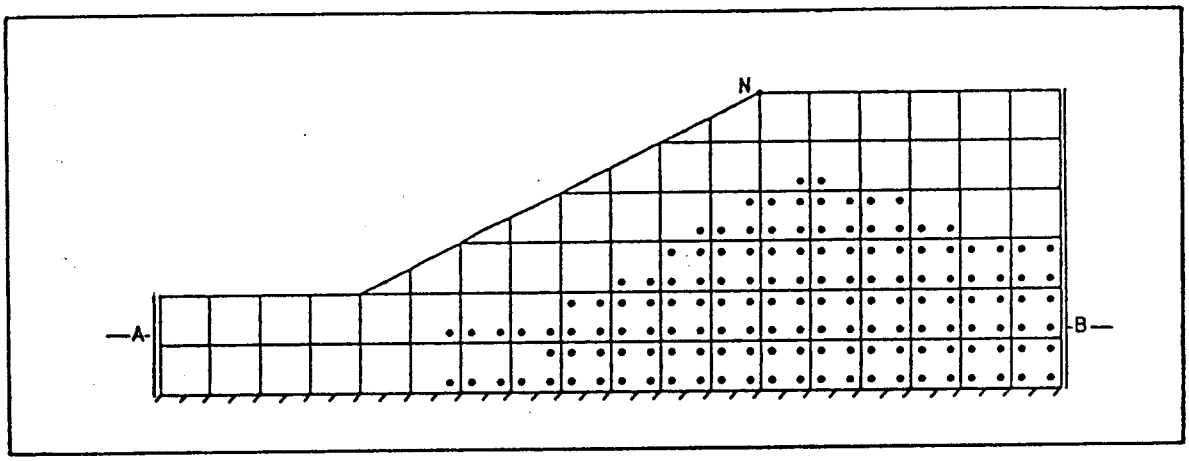

Fig. 4.3 – Mesh geometry and yielded Gauss point map for the embankment problem

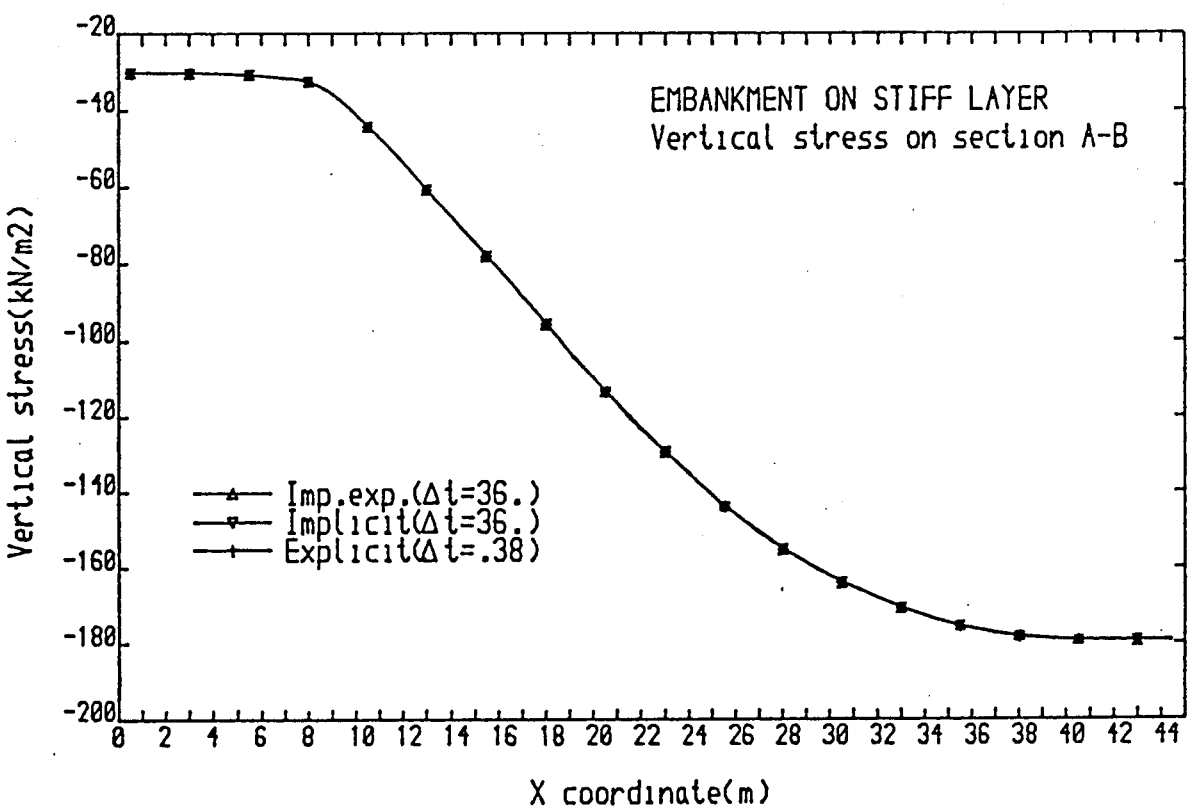

Fig. 4.4 – Vertical stress at the layer A–B of Gauss points (fig. 4.3) in the embankment problem

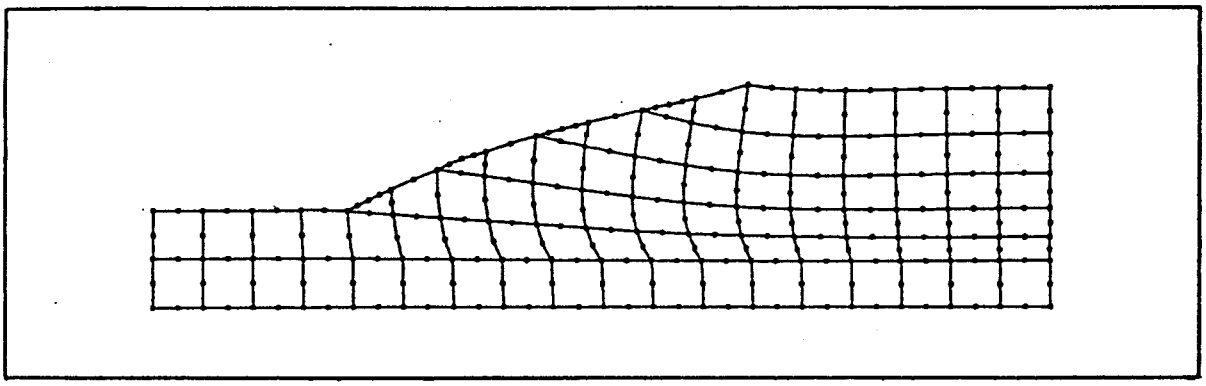

Fig. 4.5 – Deformed embankment mesh (scaling factor 100)

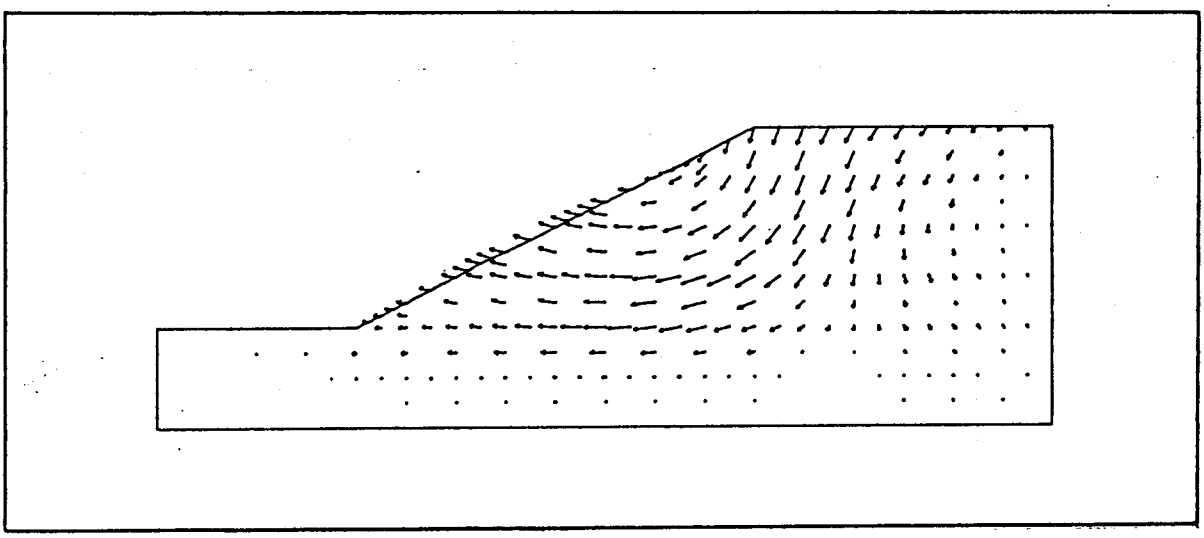

Fig. 4.6 – "Plastic" nodal displacement vectors in the embankment problem

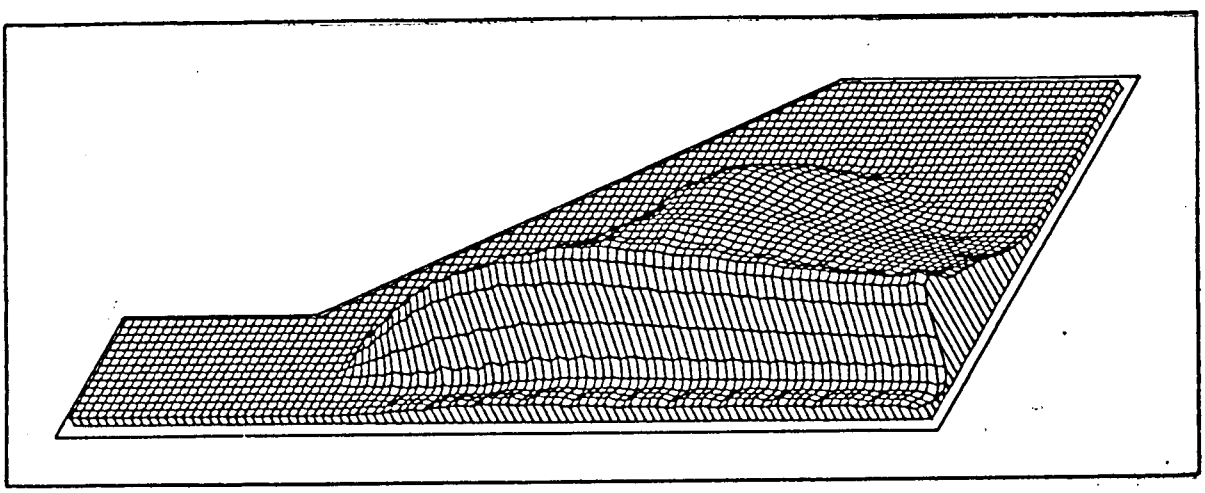

Fig. 4.7 – Isometric view of the effective plastic strain for the embankment problem

4.9 CONCLUSIONS

In our presentation of the elastoviscoplastic model two important questions are considered in detail:

- the correct numerical modelling of viscoplastic materials which exhibit hardening is shown to require the inclusion of additional terms that amount to the adoption of a modified flow function. This is only of consequence when implicit time integration algorithms ($\theta>0$) are considered. Since the permissible time step lengths for implicit time integration can be appreciably large [59], the effects of these hardening correction terms may be significant, particularly so for materials with high hardening rates. Omission of the additional hardening terms results in overestimation of displacements and strains as predicted by our physical interpretation and demonstrated by the numerical examples presented.

- implicit-explicit integration for quasistatic elastoviscoplastic problems proves to be an economic technique particularly well suited for composite domain problems in which the constituent materials exhibit a markedly different time step limit for explicit integration. The technique is easily accommodated in a frontal equation solver and its expedience and accuracy is testified by numerical evidence.

4.10 REFERENCES

1. HILL, R., The Mathematical Theory of Plasticity, Oxford University Press, 1950

2. FINNIE, I. and HELLER, W.R., Creep of Engineering Materials, McGraw-Hill, New York, 1959

3. BLAND, D.R., The Theory of Linear Viscoelasticity, Pergamon Press, Oxford, 1960

4. BINGHAM, E.C., Fluidity and Plasticity, McGraw-Hill, New York, 1922

5. HENCKY, H., Über langsame stationäre Strömungen in plastischen Massen, ZAMM, 5, 115-124, 1925

6. HOHENEMSER, K. and PRAGER, W., Über die Ansätze der Mechanik isotroper Kontinua, ZAMM, 12, 216-226, 1932

7. NAGHDI, P.M. and MURCH, S.A., On the mechanical behaviour of viscoelastic/plastic solids, J. Appl. Mech., 30, 321-328, 1963

8. PERZYNA, P., The constitutive equations for rate sensitive plastic materials, Q. Appl. Math., 20, 321-332, 1963

9. PERZYNA, P., Fundamental problems in viscoplasticity, Adv. in Appl. Mech., 9, 243-377, 1966

10. PHILLIPS, A. and WU, H.C., A theory of viscoplasticity, Int. J. Sol. Struct., 9, 15-30, 1973

11. NICHOLSON, D.W. and PHILLIPS, A., On the structure of the theory of viscoplasticity, Int. J. Sol. Struct., 10, 149-160, 1974

12. CRISTESCU, N., Dynamic Plasticity, North-Holland, Amsterdam, 1967

13. ZIENKIEWICZ, O.C. and CORMEAU, I.C., Visco-plasticity solution by finite element process, Arch. of Mech., 24, 873-889, 1972

14. ZIENKIEWICZ, O.C. and CORMEAU, I.C., Visco-plasticity and plasticity. An alternative for finite element solution of material nonlinearity, Proc. Coll. Méth. Calc. Scientifique et Technique, 179-199, IRIA, 1973

15. ZIENKIEWICZ, O.C. and CORMEAU, I.C., Visco-plasticity - Plasticity and creep in elastic solids - A unified numerical solution approach, IJNME, 8, 821-845, 1974

16. ZIENKIEWICZ, O.C., OWEN, D.R.J. and CORMEAU, I.C., Analysis of viscoplastic effects in pressure vessels by the finite element method, Nuc. Eng. and Design, 28, 278-288, 1974

17. ZIENKIEWICZ, O.C., Viscoplasticity as a computational model for deformation and collapse studies, Symp. Non Lin. Techn. and Behav. in Struct. Analysis, TRRL Publ., 1975

18. ZIENKIEWICZ, O.C., Visco-plasticity, plasticity, creep and visco-plastic flow (problems of small, large and continuing deformation), Proc. Int. Cong. Comput. Meth. in Nonlinear Mechanics, 297-328, J.T. Oden (ed.) Springer Verlag, 1975

19. STAGG, K.G., ZIENKIEWICZ, O.C. and CORMEAU, I.C., On the application of a numerical visco-plastic model to rock mechanics problems, Int. Symp. fur Unteragbau, 327-335, H. Grob et al. (eds.) Luzern, 1972

20. CORMEAU, I.C., Viscoplasticity and plasticity in the finite element method, Ph.D. thesis, Univ. of wales, Swansea, 1976

21. ZIENKIEWICZ, O.C., NAYAK, G.C. and OWEN, D.R.J., Composite and 'overlay' models in numerical analysis of elasto-plastic continua, in Foundations of Plasticity, 107-122, A. Sawczuk (ed.), Noordhoff Press, 1972

22. OWEN, D.R.J., PRAKASH, A. and ZIENKIEWICZ, O.C., Finite element analysis of non-linear composite materials by use of overlay systems, Comp. & Str., 4, 1251-1267, 1974

23. PANDE, G.N., OWEN, D.R.J. and ZIENKIEWICZ, O.C., Overlay models in time-dependent nonlinear material analysis, Comp. & Str., 7, 435-443, 1977

24. ZIENKIEWICZ, O.C., and GODBOLE, P.N., Flow of plastic and visco-plastic solids with special reference to extrusion and forming processes, IJNME, 8, 3-16, 1974

25. DAWSON, P.R. and THOMPSON, E.G., Steady-state thermomechanical finite element analysis of elastoviscoplastic metal forming processes, in Num. Mod. Manufacturing Processes, R.F. Jones et al. (eds.), ASME, 1977

26. THOMPSON, E.G. and BERMAN, H.M., Steady state analysis of elasto-viscoplastic flow during rolling, Proc. Num. Meth. in Industrial Forming Processes, 29-37, J.F.T. Pittman et al. (eds.) Pineridge Press, Swansea, 1982

27. WILLIAMS, J.R., LEWIS, R.W. and MORGAN, K., An elastic-viscoplastic thermal stress model with applications to the continuous casting of metals, IJNME, 14, 1-9, 1979

28. KOBAYASHI, S., Thermoviscoplastic analysis of metal forming problems by the finite element method, Proc. Num. Meth. in Ind. Form. Proc., 17-25, J.F.T. Pittman et al. (eds.), Pineridge Press, Swansea, 1982

29. ZIENKIEWICZ, O.C., HUMPHESON, C. and LEWIS, R.W., A unified approach to soil mechanics including plasticity and viscoplasticity, in F.E. in Geomechanics, 151-177, G. Gudehus (ed.), Wiley, 1976

30. ZIENKIEWICZ, O.C., HUMPHESON, C. and LEWIS, R.W., Associated and non-associated visco-plasticity and plasticity in soil mechanics, Geotechnique, 25, 671-689, 1975

31. ZIENKIEWICZ, O.C. and HUMPHESON, C., Viscoplasticity: a generalized model for description of soil behaviour, F.E.M. in Geomechanics, 116-147, C.S. Desai et al. (eds.), McGraw-Hill, 1977

32. ZIENKIEWICZ, O.C., NORRIS, V.A. and NAYLOR, D.J., Plasticity and viscoplasticity in soil mechanics with special reference to cyclic loading problems, in F.E. in Nonlinear Mechanics, 455-485, P.G. Bergan et al. (eds.), Tapir, Trondheim, 1978

33. MROZ, Z., NORRIS, V.A. and ZIENKIEWICZ, O.C., Elastoplastic and viscoplastic constitutive models for soils with application to cyclic loading, in Soil Mechanics - Transient and Cyclic Loads, 173-217, G.N. Pande et al. (eds.), Wiley, 1982

34. ZIENKIEWICZ, O.C. and PANDE, G.N., Time-dependent multilaminate model of rocks - a numerical study of deformation and failure of rock masses, I.J. Num. An. Meth. Geomech., 1, 219-247, 1977

35. THAKKAR, S.K. and STAGG, K.G., A visco-plastic approach to the problem of stresses in tunnel lining in jointed rock, S.R.C. Report, University College of Swansea, 1974

36. PANDE, G.N., Viscoplastic algorithm for modelling tensile non-linearity in rock and concrete structures, Mech. Bimodulus Materials, AMD-v.33, Ed. C.W.Bert, ASME- 1977

37. DINIS, L.M.J.S., Finite Element Viscoplastic Analysis of Plates, M.Sc. Thesis, Univ. of Wales, Swansea, 1975

38. DINIS, L.M.J.S., Quasi-static and Dynamic Transient Nonlinear Analysis of Plates and Arbitrary Thin Shells by Use of the Semiloof Element, Ph.D. Thesis, Univ. of Wales, Swansea, 1978

39. NAGARAJAN, P.K. and POPOV, E.P., Plastic and viscoplastic analysis of axisymmetric shells, I.J.Sol. Struct., 11, 1-9, 1975

40. OWEN, D.R.J. and DINIS, L.M.J.S., Elasto-viscoplastic analysis of plates by the finite element method, Comp. & Struct., 8, 207-215, 1978

41. DAMJANIC, F.B., Reinforced concrete failure prediction under both static and transient conditions, Ph.D. thesis, Univ. of Wales, Swansea, 1983

42. LEWIS, R.W., SRINATHA, H.R. and THOMAS, H.R., A finite element study of the drying stresses in timber using viscoelastic and elastoviscoplastic rheological models, in Numerical Methods in Coupled Systems, R.W. Lewis et al. (eds.), Wiley, 1983

43. KANCHI, M.B., ZIENKIEWICZ, O.C. and OWEN, D.R.J., The visco-plastic approach to problems of plasticity and creep involving geometric nonlinear effects, IJNME, 12, 169-181, 1978

44. LE MASTER, R.A., A theoretical and numerical comparison of three finite strain finite element formulations for elastic-viscoplastic materials, Comp. & Struct., 16, 215-222, 1983

45. KAWAHARA, M., Large strain viscoelastic and elasto-viscoplastic numerical analysis by means of the finite element method, Nuc. Eng. and Design, 34, 233-246, 1975

46. OWEN, D.R.J. and GONÇALVES F°, O.J.A., A numerical investigation of creep brittle rupture under proportional loading using a state variable theory, in Applicaciones del Método de los Elementos Finitos en Ingenieria, E. Oñate et al. (eds.) Barcelona, 1982

47. GONÇALVES F°, O.J.A. and OWEN, D.R.J., Numerical analysis of creep brittle rupture by the finite element method, paper L12/4, 7th SMiRT, Chicago, 1983

48. GONÇALVES F°, O.J.A. and OWEN, D.R.J., Creep and viscoplastic brittle rupture of structures by the finite element method, in Engineering Approaches to High Temperature Design, 237-277, B. Wilshire et al. (eds.), Pineridge Press, Swansea, 1983

49. TELLES, J.C.F. and BREBBIA, C.A., Elastic/viscoplastic problems using boundary elements, I.J. Mech. Sci., 24, 605-618, 1982

50. OWEN, D.R.J. and HINTON, E., Finite Elements in Plasticity - Theory and Practice, Pineridge Press, Swansea, 1980

51. MARQUES, J.M.M.C. and OWEN, D.R.J., Strain hardening representation for implicit quasistatic elasto-viscoplastic algorithms, Comp. & Struct., 17, 301-304, 1983

52. OWEN, D.R.J. and MARQUES, J.M.M.C., Coupled implicit-explicit time integration with frontal substructuring in two-dimensional quasistatic elastoviscoplasticity, in Numerical Methods for Coupled Problems, 147-160, E. Hinton et al. (eds.), Pineridge Press, Swansea, 1981

53. MARQUES, J.M.M.C. and OWEN, D.R.J., Implicit-explicit time integration in quasistatic elastoviscoplasticity using finite and infinite elements, Comp. Meth. Appl. Mech. Engng., 42, 167-182, 1984

54. OWEN, D.R.J. and GOMES, C.M.B.R., Some recent developments in solution techniques for nonlinear finite element problems, in Aplicaciones del Método de los Elementos Finitos en Ingenieria, E. Oñate et al. (eds.), Barcelona, 1982

55. FEJZO, R., Private communications, Swansea, 1981

56. DAMJANIĆ, F. and OWEN, D.R.J., Implicit time integration of elasto-viscoplastic solids subject to the Mohr-Coulomb yield criterion, IJNME (in press)

57. HUGHES, T.J.R. and TAYLOR, R.L., Unconditionally stable algorithms for quasi-static elasto/visco-plastic finite element analysis, Comp. & Struct., 8, 169-173, 1978

58. CORMEAU, I.C., Numerical stability in quasi-static elasto/visco-plasticity, IJNME, 9, 109-127, 1975

59. OWEN, D.R.J. and DAMJANIĆ, F., Viscoplastic analysis of solids: stability considerations, in Recent Advances in Nonlinear Computational Mechanics, 225-253, E. Hinton et al. (eds.), Pineridge Press, Swansea, 1982

60. BELYTSCHKO, T. and MULLEN, R., Mesh partitions of explicit-implicit time integration, in Formulations and Computational Algorithms in Finite Element Analysis, 673-690, K.J. Bathe et al. (eds.), MIT Press, 1977

61. POPOV, E.P., KHOJASTEH-BAKHT, M. and YAGHMAI, S., Bending of circular plates of hardening material, Int. J. Sol. Struct., 3, 975-988, 1967

CHAPTER 5

GEOMETRIC NONLINEARITY

5.1	INTRODUCTION	5.1
5.2	PRELIMINARY CONSIDERATIONS	5.2
5.3	DEFINITIONS OF STRAIN AND RATES OF STRAIN	5.4
5.4	DEFINITIONS OF STRESS AND RATES OF STRESS	5.6
5.5	CONSTITUTIVE RELATIONS	5.7
5.6	VIRTUAL VELOCITY EQUATION	5.7
5.7	RATE FORM OF THE VIRTUAL VELOCITY EQUATION	5.8
5.8	UPDATED LAGRANGIAN FINITE ELEMENT FORMULATION	5.9
5.9	STRESS COMPUTATION	5.11
5.10	REFERENCES	5.12

CHAPTER 5

GEOMETRIC NONLINEARITY

5.1 INTRODUCTION

In problems involving infinitesimal strain and small displacements the usual engineering approach of neglecting changes in initial geometry is acceptable and provides meaningful accuracy for most purposes. There is, however, a large spectrum of practical applications for which these simplifying assumptions do not hold. Such is, for instance, the case of the ultimate state design of structural components for nuclear power plants, aircraft, automobiles and spacecrafts, metal forming processes (rolling, extrusion, coining, sheet forming), crack tip blunting and cavity coalescence in fracture mechanics, large creep straining of salt layers used for nuclear waste storage, pressure vessel ballooning, pre- and post-buckling analyses of slender structures, such as thin plates and shells.

The presence of large displacements and/or large rotations and/or large strains increases the complexity of the numerical model and demands a rigorous setting within nonlinear continuum mechanics, specially when inelastic material behaviour is simultaneously considered.

The rational, consistent and accurate approach to this problem remains the object of intensive research and continuing controversy. The convenience of a rate-type formulation has nevertheless been generally recognized and is adopted here.

The modification of the initial boundary conditions due to large displacements or extensive deformation, as occurs in contact problems like those associated with pipe whipping and most metal forming operations, is an additional source of nonlinearity, not considered in the present study.

This Chapter opens with a presentation of alternative descriptions of motion and strain and stress measures. Constitutive relations for

various types of time independent material behaviour are briefly described and the incorporation of geometric nonlinear effects in the basic finite element formulation is outlined. The treatment given to this complex topic is necessarily concise and for a thorough description the reader is directed to References [2, 18-21].

For ease of notation, vectors and tensors are denoted by single and double straight underscores. Virtual quantities are indicated by tilde underline(s). A superposed dot or D/Dt designate the material time derivative (i.e., defined with reference to specific particles of the moving continuum [2]). For simplicity only quasistatic loading is considered.

5.2 PRELIMINARY CONSIDERATIONS

The motion of a continuum, from the initial configuration at time t=0 to the current one at time t, can be viewed in two distinct ways with reference to a fixed set of Cartesian axes [2].

(i) The spatial description selects a fixed point $\underline{x}$ in space and analyses the motion of the material particles past that location. A relation of the type

$$\underline{X} = \underline{X}\ (\underline{x},\ t) \tag{5.1}$$

is used to refer the original position $\underline{X}$ of the particle that is passing through $\underline{x}$ at time t.

(ii) The material description chooses a body particle at its initial location $\underline{X}$ and follows it through to the final position $\underline{x}$ at t given by

$$\underline{x} = \underline{x}\ (\underline{X},\ t) \tag{5.2}$$

The spatial and material coordinates were introduced respectively by d'Alembert [14] and Euler [15] but are now currently referred to as Eulerian and Lagrangian, respectively. This historical imprecision apparently derives from erroneous German terminology as pointed out by Truesdell [16].

In the finite element context the spatial approach is mainly used in fluid problems, by treating the mesh as a fixed reference frame

through which the fluid flows, while for solids the mesh is embedded in the body, moving and deforming with it. In fluid-structure interaction studies a mixed strategy named Arbitrary Lagrangian Eulerian has proved to be very convenient [3].

In the finite element analysis of geometrically nonlinear structural problems the solution for the static and kinematic variables is to be advanced from the original undeformed mesh, through the current (or last calculated) configuration at time t, to the neighbouring (but unknown) one at $t+\Delta t$.

The use of the material description for this purpose gives rise to two fundamental formulations, termed Total Lagrangian (TL) [4-7] and Updated Lagrangian (UL) [1,8,9], as the reference mesh for all variables is chosen to be the one at time 0 or t, respectively. Both formulations have advantages and disadvantages. In the TL case the $\underline{B}$ matrix is no longer sparse due to the inclusion of nonlinear terms and so $\underline{K}$ is more costly to compute. In addition the constitutive relation, that is naturally formulated in the current state, requires lengthy transformation. On the other hand, the distortion of the mesh in UL solutions may deteriorate the accuracy, specially when midside nodes of higher order elements drift significantly. This can be overcome by a mesh redefinition procedure [10].

The present study adopts the UL formulation of McMeeking and Rice [1] since it requires minimal adaptations in the basic small strain code described in previous Chapters, besides being computationally efficient.

It must be stressed that although the material description is the basic framework for the following sections, Lagrangian and Eulerian viewpoints will repeatedly emerge whenever convenient for relating the initial and current configurations. However, the UL formulation must in no case be identified with the Eulerian approach as used for instance in steady state flow problems [17].

Finally, it is worth mentioning that as an alternative to fixed Cartesian axes it is possible to use local coordinate systems attached to each element which continuously rotate and translate so as to follow its rigid body motion. Mattiasson [11] presents

TL and UL forms of this approach, known by the names of natural [13], corotational [11] or convected coordinate [12] formulation.

5.3 DEFINITIONS OF STRAIN AND RATES OF STRAIN

Consider two material particles of a deforming body that occupy in the original configuration the positions P and Q defined by $\underline{X}$ and $\underline{X}+d\underline{X}$ with respect to a Cartesian coordinate system fixed in space (fig. 5.1). Let P' and Q' denote their current locations, respectively at $\underline{x}$ and $\underline{x}+d\underline{x}$.

The deformation gradient tensor $\underline{\underline{F}}$ is

$$\underline{\underline{F}} = (\partial \underline{x}/\partial \underline{X}) \tag{5.3}$$

Since the displacement $\underline{u}$ is

$$\underline{u} = \underline{x} - \underline{X} \tag{5.4}$$

$\underline{\underline{F}}$ can be related to the displacement gradients with respect to the original and current configurations respectively by

$$\underline{\underline{F}} = \underline{\underline{I}} + (\partial \underline{u}/\partial \underline{X}) \tag{5.5}$$

$$\underline{\underline{F}}^{-1} = \underline{\underline{I}} - (\partial \underline{u}/\partial \underline{x}) \tag{5.6}$$

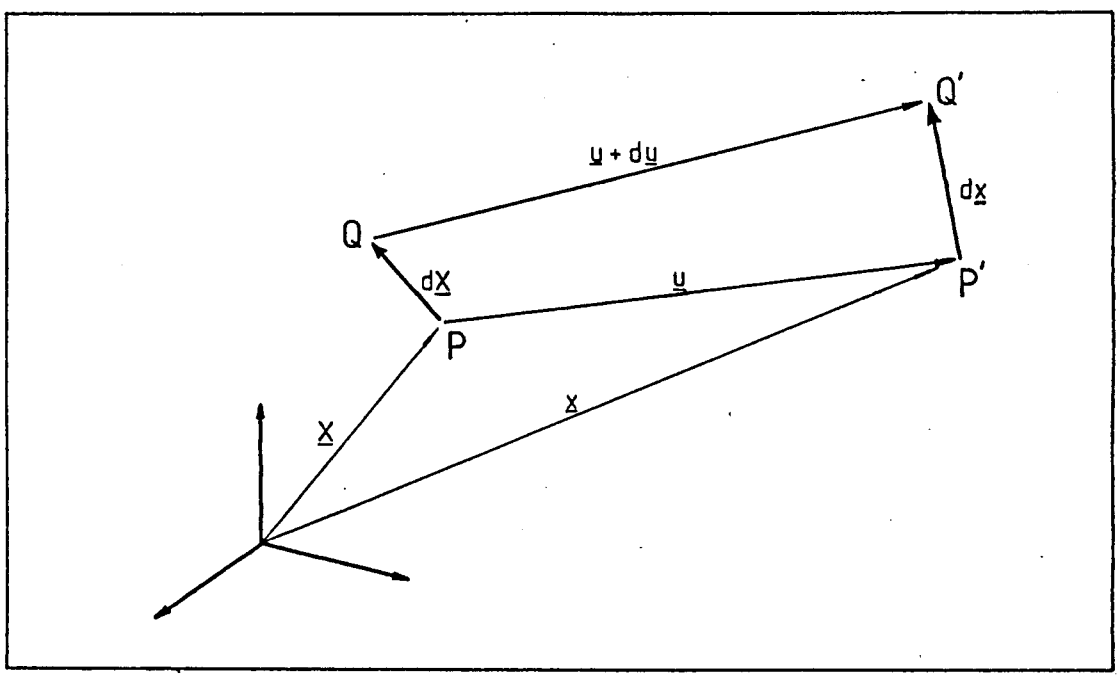

Fig. 5.1 – Original and current positions of a pair of material points of a body

The Lagrangian or Green's strain tensor $\underline{\underline{E}}$ is defined as

$$\underline{\underline{E}} = 1/2\ (\underline{\underline{F}}^T\ \underline{\underline{F}} - \underline{\underline{I}}) \tag{5.7}$$

where $\underline{\underline{I}}$ is the unit tensor or, using (5.5),

$$\underline{\underline{E}} = 1/2[(\partial \underline{u}/\partial \underline{X}) + (\partial \underline{u}/\partial \underline{X})^T + (\partial \underline{u}/\partial \underline{X})^T(\partial \underline{u}/\partial \underline{X})] \tag{5.8}$$

The Eulerian or Almansi's strain tensor $\underline{\underline{E}}'$ is

$$\underline{\underline{E}}' = 1/2(\underline{\underline{I}} - \underline{\underline{F}}^{-T}\ \underline{\underline{F}}^{-1}) \tag{5.9}$$

or, using (5.6),

$$\underline{\underline{E}}' = 1/2[(\partial \underline{u}/\partial \underline{x}) + (\partial \underline{u}/\partial \underline{x})^T - (\partial \underline{u}/\partial \underline{x})^T(\partial \underline{u}/\partial \underline{x})] \tag{5.10}$$

The velocity gradient $\underline{\underline{L}}$ is

$$\underline{\underline{L}} = (\partial \underline{v}/\partial \underline{x}) \tag{5.11}$$

and can be decomposed into symmetric and anti-symmetric parts $\underline{\underline{D}}$ and $\underline{\underline{W}}$, that are called, respectively, rate of deformation and spin tensors.

$$\begin{aligned} \underline{\underline{L}} &= \underline{\underline{D}} + \underline{\underline{W}} \\ \underline{\underline{D}} &= 1/2\ (\underline{\underline{L}} + \underline{\underline{L}}^T) \\ \underline{\underline{W}} &= 1/2\ (\underline{\underline{L}} - \underline{\underline{L}}^T) \end{aligned} \tag{5.12 a-c}$$

Noting that the rate of the deformation gradient is

$$\dot{\underline{\underline{F}}} = \underline{\underline{L}}\,\underline{\underline{F}} \tag{5.13}$$

it can be shown that the material rates of change of the Green and Almansi strain tensors are [2]

$$\dot{\underline{\underline{E}}} = \underline{\underline{F}}^T\ \underline{\underline{D}}\ \underline{\underline{F}} \tag{5.14}$$

$$\dot{\underline{\underline{E}}}' = \underline{\underline{D}} - \underline{\underline{E}}'\underline{\underline{L}} - \underline{\underline{L}}^T\ \underline{\underline{E}}' \tag{5.15}$$

The initial and current values of the mass density and of the elemental volume and surface are related by

$$\begin{aligned} \rho_o/\rho &= \det \underline{\underline{F}} = J \\ dV/dV_o &= J \\ (dA/dA_o)^2 &= J^2/(\underline{n}^T \underline{\underline{F}}^T \underline{\underline{F}} \underline{n}) \end{aligned} \tag{5.16}$$

where $\underline{n}$ is the unit vector normal to dA and the zero subscripts refer to the original configuration.

5.4 DEFINITIONS OF STRESS AND RATES OF STRESS

The components of the Cauchy, Eulerian or true stress tensor $\underline{\underline{\sigma}}$ correspond to those of the traction vectors acting on surface elements considered at a point normally to each of the coordinate axes in the current configuration.

The Kirchhoff stress tensor $\underline{\underline{\tau}}$ is related to $\underline{\underline{\sigma}}$ by

$$\underline{\underline{\tau}} = J \, \underline{\underline{\sigma}} \tag{5.17}$$

The 2nd Piola-Kirchhoff stress tensor $\underline{\underline{S}}$ is defined as

$$\underline{\underline{S}} = J \, \underline{\underline{F}}^{-1} \, \underline{\underline{\sigma}} \, \underline{\underline{F}}^{-T} \tag{5.18}$$

The Cauchy and Kirchhoff stress rates, related by

$$\dot{\underline{\underline{\tau}}} = J \, \dot{\underline{\underline{\sigma}}} + \dot{J} \, \underline{\underline{\sigma}} \tag{5.19}$$

are not invariant under superposed rigid body rotation [2] and thus cannot provide objective constitutive equations relating stress and deformation rates [21]. For this purpose can be employed a spin invariant stress rate definition due to Zaremba [23] and Jaumann [22] whereby the rate of stress is measured with reference to Cartesian axes rigidly rotating locally with an angular velocity given by the spin tensor.

The Jaumann rates of Cauchy and Kirchhoff stress are

$$\overset{\nabla}{\underline{\underline{\sigma}}} = \dot{\underline{\underline{\sigma}}} - \underline{\underline{\sigma}} \, \underline{\underline{W}}^T - \underline{\underline{W}} \, \underline{\underline{\sigma}} \tag{5.20}$$

$$\overset{\nabla}{\underline{\underline{\tau}}} = \dot{\underline{\underline{\tau}}} - \underline{\underline{\tau}} \, \underline{\underline{W}}^T - \underline{\underline{W}} \, \underline{\underline{\tau}} \tag{5.21}$$

5.5 CONSTITUTIVE RELATIONS

A brief description is now given of two classes of time independent material behaviour: elastoplastic and hypoelastic. For large strain formulations in elastoviscoplasticity the reader is directed to References [24-26].

5.5.1 Elastoplastic Materials

As mentioned in Chapter 3, elastoplastic behaviour implies a combination of reversible and irreversible straining. For finite strain problems both additive [27] and multiplicative [28] processes have been proposed for decomposing the velocity gradient into elastic and plastic parts and this topic remains controversial [29-31]. We follow the classic additive approach and adopt here a constitutive law proposed by McMeeking [32] relating the rate of deformation tensor to the Jaumann rate of Kirchhoff stress referred to the current configuration

$$\overset{\nabla}{\underline{\underline{\tau}}} = \underline{\underline{C}}\ \underline{\underline{D}} \tag{5.22}$$

where $\underline{\underline{C}}$ is the constitutive tensor. This law provides a symmetric stiffness matrix (that would not be obtained if $\overset{\nabla}{\underline{\underline{\sigma}}}$ was used instead of $\overset{\nabla}{\underline{\underline{\tau}}}$).

5.5.2 Hypoelastic Materials

By definition [19] a hypoelastic material has the stress rate components as homogeneous linear functions of the components of the rate of deformation. A relation of the type (5.22) is assumed.

5.6 VIRTUAL VELOCITY EQUATION

In the UL formulation the last calculated configuration is taken as reference. Assuming thus the current and reference configurations to coincide instantaneously, the virtual velocity equation is

$$\int_V \underset{\sim}{v}^T\ \underline{\psi}\ dV = \int_V \underline{\underline{D}} : \underline{\underline{\sigma}}\ dV - \int_V \underset{\sim}{v}^T\ \underline{b}\ dV - \int_A \underset{\sim}{v}^T\ \underline{t}\ dA = 0 \tag{5.23}$$

where $\underset{\sim}{v}$ is a virtual velocity field, $\underline{\psi}$ and $\underline{b}$ are out-of-balance and body forces, $\underline{t}$ are surface tractions, and where the scalar tensor

product $\underset{\approx}{D} : \underset{=}{\sigma} = \mathrm{tr}(\underset{\approx}{D}\underset{=}{\sigma})$ gives the rate of virtual internal work per unit current volume [34].

5.7 RATE FORM OF THE VIRTUAL VELOCITY EQUATION

Taking the material time derivative [19] of the terms of (5.23) we obtain the rate form of the virtual velocity equation. Interpreting the arbitrary virtual velocity field as time independent, let us consider first the integral containing $\underset{\approx}{D} : \underset{=}{\sigma}$. We have

$$\frac{D}{Dt}\left(\int_V \underset{\approx}{D} : \underset{=}{\sigma}\, dV\right) = \int_V \underset{\approx}{D} : (\dot{\underset{=}{\sigma}} + \underset{=}{\sigma}\,\dot{J}/J)\, dV + \int_V \dot{\underset{\approx}{D}} : \underset{=}{\sigma}\, dV \qquad (5.24)$$

Using (5.19) and (5.21) and noting that the initial assumption (of Section 5.6) implies $J = 1$ we have

$$\int_V \underset{\approx}{D} : (\dot{\underset{=}{\sigma}} + \underset{=}{\sigma}\,\dot{J}/J)\, dV = \int_V \underset{\approx}{D} : \overset{\nabla}{\underset{=}{\tau}}\, dV + \int_V \underset{\approx}{D} : (\underset{=}{\sigma}\,\underset{=}{W}^T + \underset{=}{W}\,\underset{=}{\sigma})\, dV \qquad (5.25)$$

Taking into account the definition of scalar tensor product and the symmetry of $\underset{\approx}{D}$ and $\underset{=}{\sigma}$ and using (5.12 a,b), the last term of (5.25) is rewritten as

$$\int_V \underset{\approx}{D} : (\underset{=}{\sigma}\,\underset{=}{W}^T + \underset{=}{W}\,\underset{=}{\sigma})\, dV = -\int_V \underset{\approx}{D} : (2\underset{=}{\sigma}\,\underset{=}{D})\, dV + \int_V \underset{\approx}{L} : (\underset{=}{\sigma}\,\underset{=}{L}^T)\, dV + \int_V \underset{\approx}{L}^T : (\underset{=}{\sigma}\,\underset{=}{L}^T)\, dV \qquad (5.26)$$

It can be shown [33] that in (5.24)

$$\int_V \dot{\underset{\approx}{D}} : \underset{=}{\sigma}\, dV = -\int_V \underset{\approx}{L}^T : (\underset{=}{\sigma}\,\underset{=}{L}^T)\, dV \qquad (5.27)$$

Substituting (5.25), (5.26) and (5.27) into (5.24) we arrive at

$$\frac{D}{Dt}\left(\int_V \underset{\approx}{D} : \underset{=}{\sigma}\, dV\right) = \int_V \underset{\approx}{D} : \overset{\nabla}{\underset{=}{\tau}}\, dV - \int_V \underset{\approx}{D} : (2\underset{=}{\sigma}\,\underset{=}{D})\, dV + \int_V \underset{\approx}{L} : (\underset{=}{\sigma}\,\underset{=}{L}^T)\, dV \qquad (5.28)$$

or, on use of (5.22) and after some rearrangement,

$$\frac{D}{Dt}\left(\int_V \underset{\approx}{D} : \underset{=}{\sigma}\, dV\right) = \int_V \underset{\approx}{D} : [(\underset{=}{C} - 2\underset{=}{\sigma})\underset{=}{D}]\, dV + \int_V \underset{\approx}{L} : (\underset{=}{\sigma}\,\underset{=}{L}^T)\, dV \qquad (5.29)$$

Considering now the material time derivatives for the remaining integrals of (5.23) we have

$$\frac{D}{Dt}\left(\int_V \underset{\sim}{v}^T \underline{\psi}\, dV\right) = \int_V \underset{\sim}{v}^T \dot{\underline{\psi}}\, dV + \int_V \underset{\sim}{v}^T \underline{\psi}\, \dot{J}/J\, dV$$

$$\frac{D}{Dt}\left(\int_V \underset{\sim}{v}^T \underline{b}\, dV\right) = \int_V \underset{\sim}{v}^T \dot{\underline{b}}\, dV + \int_V \underset{\sim}{v}^T \underline{b}\, \dot{J}/J\, dV \qquad (5.30)$$

$$\frac{D}{Dt}\left(\int_A \underset{\sim}{v}^T \underline{t}\, dA\right) = \int_A \underset{\sim}{v}^T \dot{\underline{t}}\, dA + \int_A \underset{\sim}{v}^T \underline{t}\, \dot{a}/a\, dA$$

where $a = dA/dA_o$. The integrals containing $\dot{J}/J$ and $\dot{a}/a$ in (5.30) convey the time dependency of the elemental volume and surface. They are discarded prior to the discretization procedure of the next Section (i.e. it is assumed that $\dot{J} = \dot{a} = 0$), on the understanding that the error thereby introduced will be accounted for by the equilibrium iterations to be performed. Non-conservative loading, with configuration dependency of $\underline{b}$ and $\underline{t}$, has not been considered.

5.8 UPDATED LAGRANGIAN FINITE ELEMENT FORMULATION

The standard finite element spatial discretization outlined in Chapter 2 is now applied to the rate form of equation (5.23). Using matrix notation for computational clarity we have

$$\underset{\sim}{v}^T \int_V \underline{N}^T \dot{\underline{\psi}}\, dV = \underset{\sim}{v}^T \int_V \underline{B}^T(\underline{C} - \underline{\hat{\sigma}})\, \underline{B}\, dV.\underline{v} + \underset{\sim}{v}^T \int_V \underline{G}^T\, \underline{\hat{\hat{\sigma}}}\, \underline{G}\, dV.\underline{v}$$

$$- \underset{\sim}{v}^T \int_V \underline{N}^T \dot{\underline{b}}\, dV - \underset{\sim}{v}^T \int_V \underline{N}^T \dot{\underline{t}}\, dA \qquad (5.31)$$

where $\underline{N}$ and $\underline{B}$ are as defined in Chapter 2, $\underline{C}$ is the $\underline{D}$ or $\underline{D}_{EP}$ constitutive matrix of Chapters 2 and 3, $\underline{\hat{\sigma}}$ and $\hat{\hat{\sigma}}$ are given by

$$\underline{\hat{\sigma}} = \begin{bmatrix} 2\sigma_{11} & 0 & 0 & 0 & \sigma_{13} & \sigma_{12} \\ & 2\sigma_{22} & 0 & \sigma_{23} & 0 & \sigma_{21} \\ & & 2\sigma_{33} & \sigma_{32} & \sigma_{31} & 0 \\ & & & (\sigma_{22}+\sigma_{33})/2 & \sigma_{21} & \sigma_{31} \\ & & & & (\sigma_{11}+\sigma_{33})/2 & \sigma_{32} \\ & & & & & (\sigma_{11}+\sigma_{22})/2 \end{bmatrix} \qquad (5.32)$$

$$\hat{\underline{\hat{\sigma}}} = \begin{bmatrix} \sigma_{11}\,\underline{I}_3 & \sigma_{12}\,\underline{I}_3 & \sigma_{13}\,\underline{I}_3 \\ & \sigma_{22}\,\underline{I}_3 & \sigma_{23}\,\underline{I}_3 \\ & & \sigma_{33}\,\underline{I}_3 \end{bmatrix} \tag{5.33}$$

(with $\underline{I}_3$ the 3x3 identity matrix) and $\underline{G}$ has p (= no. of mesh points) submatrices $\underline{G}_i$ of the form

$$\underline{G}_i = \begin{bmatrix} \partial N_i/\partial x\ \underline{I}_3 \\ \partial N_i/\partial y\ \underline{I}_3 \\ \partial N_i/\partial z\ \underline{I}_3 \end{bmatrix} \tag{5.34}$$

Considering a small time step Δt, the displacement increment $\Delta\underline{d}$ can be approximated by Euler integration as

$$\Delta\underline{d} = \underline{v}\,\Delta t \tag{5.35}$$

Noting also that the virtual nodal velocities $\underset{\sim}{v}$ are arbitrary we may recast (5.31) in the form

$$\underline{K}_T\,\Delta\underline{d} = \underline{r} \tag{5.36}$$

where $\underline{r}$ contains the load terms and $\underline{K}_T$ is the tangential stiffness matrix given by

$$\underline{K}_T = \int_V \underline{B}^T(\underline{C}\text{-}\hat{\underline{\sigma}})\,\underline{B}\,dV + \int_V \underline{G}^T\,\hat{\underline{\hat{\sigma}}}\,\underline{G}\,dV \tag{5.37}$$

The last term in (5.37) is called the initial stress or geometric stiffness matrix.

Solution methods for the nonlinear equation system of (5.36) will be discussed in Chapter 6.

5.9 STRESS COMPUTATION

The stress computation procedure [10] is now summarized, in terms of a path independent incremental iterative solution (see Section 3.11), whereby the configuration at the end of the previous load increment is taken as reference and, in addition, the iterative velocity corrections are accumulated within the current load increment (and denoted here by $\underline{v}_i$).

- Calculate $\underline{\underline{D}}$ and $\underline{\underline{w}}$ using $\underline{v}_i$.
- Compute the geometric part of the Cauchy stress rate

$$\dot{\underline{\underline{\sigma}}}_G = \underline{\underline{\sigma}}\,\underline{\underline{W}}^T + \underline{\underline{W}}\,\underline{\underline{\sigma}} \tag{5.38}$$

- Calculate $\overset{\nabla}{\underline{\underline{\tau}}}_E = \underline{\underline{C}}\,\underline{\underline{D}}$ assuming elastic behaviour and the constitutive part of the Cauchy stress rate (from (5.19) and (5.21))

$$\dot{\underline{\underline{\sigma}}}_{CE} = \overset{\nabla}{\underline{\underline{\sigma}}}_E = (\overset{\nabla}{\underline{\underline{\tau}}}_E - \dot{J}\,\underline{\underline{\sigma}})/J \tag{5.39}$$

noting that, since current and reference configurations coincide, $J = 1$ and $\dot{J} = \mathrm{tr}(\underline{\underline{D}})$.

- Add $\dot{\underline{\underline{\sigma}}}_G\,\Delta t$ to $\underline{\underline{\sigma}}$ and store as $\underline{\underline{\sigma}}^*$.
- Compute a trial elastic estimate for the new stress state

$$\underline{\underline{\sigma}}_E = \underline{\underline{\sigma}}^* + \dot{\underline{\underline{\sigma}}}_{CE}\,\Delta t \tag{5.40}$$

- Use the procedures described in Chapter 3 in case the stress point lies outside the yield surface.

5.10 REFERENCES

1. McMEEKING, R.M. and RICE, J.R., Finite-element formulations for problems of large elastic-plastic deformation, Int. J. Sol. Str., 11, 601-616, 1975

2. PRAGER, W., Introduction to Mechanics of Continua, Ginn & Co., Boston, 1961

3. DONEA, J., GUILIANI, S. and HALLEUX, J.P., An Arbitrary-Lagrangian-Eulerian finite element method for transient dynamic fluid-structure interactions, paper 9, Adv. Course on Str. Dynamics, JRC, Ispra , 1983

4. MALLET, R.H. and MARCAL, P.V., Finite element analysis of non-linear structures, J. Struct. Div., ASCE, 94, 2081-2105, 1968

5. NAYAK, G.C., Plasticity and Large Deformation Problems by the Finite Element Method, Ph.D. thesis, Univ. of Wales, Swansea, 1971

6. BATHE, K.J., RAMM, E. and WILSON, E.L., Finite element formulations for large deformation dynamic analysis, IJNME, 9, 353-386, 1975

7. HIBBIT, H.D., MARCAL, P.V. and RICE, J.R., A finite element formulation for problems of large strain and large displacement, Int. J. Sol. Str., 6, 1069-1086, 1970

8. MURRAY, D.W. and WILSON, E.L., Finite element large deflection analysis of plates, J. Eng. Mech. Div., ASCE, 94, 143-165, 1965

9. YAGHMAI, S. and POPOV, E.P., Incremental analysis of large deflections of shells of revolution, Int. J. Sol. Str., 7, 1375-1393, 1971

10. MACKAY, D.C., Finite element investigation of general yield fracture, Ph.D. thesis, Univ. of Wales, Swansea, 1982

11. MATTIASSON, K. and SAMUELSSON, A., Total and updated Lagrangian forms of the co-rotational finite element formulation in geometrically and materially nonlinear analysis, in Num. Meth. for Nonlinear Problems (vol. 2), 134-151, C. Taylor et al. (eds.), Pineridge Press, Swansea, 1984

12. BELYTSCHKO, T. and HSIEH, B.J., Nonlinear transient finite element analysis with convected coordinates, IJNME, 7, 255-271, 1973

13. ARGYRIS, J.H. et al., Finite element method - the natural approach, Comp. Meth. Appl. Mech. Engng., 17/18, 1-106, 1979

14. D'ALEMBERT, J.L., Essai d'une Nouvelle Théorie de la Resistance des Fluides, Paris, 1752

15. EULER, L., Lettre de M. Euler à M. de La Grange, Recherches sur la propagation des ébranlements dans un milieu élastique, Misc. Taur., 2, 1-10, 1762

16. TRUESDELL, C.A., The mechanical foundations of elasticity and fluid dynamics, J. Rat. Mech. Anal., 1, 125-300, 1952

17. KLEIBER, M., KÖNIG, J.A. and SAWCZUK, A., Studies on plastic structures : stability, anisotropic hardening, cyclic loads, Comp. Meth. Appl. Mech. Engng., 33, 487-556, 1982

18. MALVERN, L.E., Introduction to the Mechanics of a Continuous Medium, Prentice-Hall, Englewood Cliffs, N.J., 1969

19. FUNG, Y.C., Foundations of Solid Mechanics, idem, 1965

20. SPENCER, A.J.M., Continuum Mechanics, Longman, London, 1980

21. TRUESDELL, C.A. and NOLL, W., The Non-linear Field Theories of Mechanics, vol. 3, part 3 of Encyclopedia of Physics, S. Flügge (ed.), Springer Verlag, Berlin, 1965

22. JAUMANN, G., Geschlossenes System physikalischer und chemischer Differentialgesetze, Sitzgsber. Akad. Wiss. Wien (IIa), 120, 385-530, 1911

23. ZAREMBA, S., Le principe des mouvements rélatifs et les équations de la mécanique physique, Bull. Int. Acad. Sci. Cracovie, 614-621, 1903

24. KAWAHARA, M., Large strain, viscoelastic and elasto-viscoplastic numerical analysis by means of the finite element method, Nuc. Eng. Design, 34, 233-246, 1975

25. KLEE, K.D. and PAULUN, J.D., On numerical treatment of large elastic-viscoplastic deformations, Arch. Mech., 32, 333-345, 1980

26. LE MASTER, R.A., A theoretical and numerical comparison of three finite strain finite element formulations for elastic-viscoplastic materials, Comp. & Str., 16, 215-222, 1983

27. GREEN, A.E. and NAGHDI, P.M., A general theory of an elastic--plastic continuum, Arch. Rat. Mech. Anal, 18, 251-281, 1965

28. LEE, E.H., Elastic-plastic deformation at finite strains, J. Appl. Mech., 36, 1-6, 1969

29. LEE, E.H. and McMEEKING, R.M., Concerning elastic and plastic components of deformation, Int. J. Sol. Str., 16, 715-721, 1980

30. NEMAT-NASSER, S., Decomposition of strain measures and their rates in finite deformation elastoplasticity, Int. J. Sol. Str., 15, 155-166, 1979

31. LEE, E.H., Some comments on elastic-plastic analysis, Int. J. Sol. Str., 17, 859-872, 1981

32. McMEEKING, R.M., An Eulerian Finite Element Formulation for Problems of Large Displacement Gradients, M.Sc. thesis, Brown University, 1974

33. WOOD, R.D. and HONNOR, M.E., Private communications, Swansea, 1984

34. HILL, R., On constitutive inequalities for simple materials - I, J. Mech. Phys. Sol., 16, 229-242, 1968

CHAPTER 6

NONLINEAR SOLUTION TECHNIQUES

6.1 INTRODUCTION 6.1

6.2 A NOTE ON EARLY DEVELOPMENTS 6.2

6.3 STANDARD NEWTON-RAPHSON METHOD 6.6

6.4 MODIFIED NEWTON-RAPHSON METHODS 6.7

- 6.4.1 Initial stiffness method
- 6.4.2 MNR formula 1
- 6.4.3 MNR formula 2
- 6.4.4 MNR formula 3

6.5 LINE SEARCH 6.8

6.6 QUASI-NEWTON METHODS 6.10

- 6.6.1 Rank one additive updates
- 6.6.1.1 Davidon direct update
- 6.6.1.2 Davidon inverse update
- 6.6.2 Rank two additive updates
- 6.6.2.1 Davidon-Fletcher-Powell direct update
- 6.6.2.2 DFP inverse update
- 6.6.2.3 Broyden-Fletcher-Goldfarb-Shanno direct update
- 6.6.2.4 BFGS inverse update
- 6.6.3 BFGS inverse update in real product form
- 6.6.3.1 Computer implementation of the BFGS method
- 6.6.3.2 Numerical stability of the BFGS inverse update
- 6.6.3.3 Line search in BFGS

6.7 SECANT NEWTON METHODS 6.16

6.7.1 SN formula 1
6.7.2 SN formula 2
6.7.3 SN formula 3
6.7.4 SN formula 4
6.7.5 Numerical stability of the SN method
6.7.6 Line search in SN

6.8 CONVERGENCE CRITERIA 6.18

6.8.1 Residual norm criterion
6.8.2 Energy norm criterion

6.9 DIVERGENCE AND TERMINATION PROCEDURES 6.19

6.10 CURRENT TRENDS IN SOLUTION TECHNIQUES 6.21

6.11 NUMERICAL EXAMPLES 6.22

6.11.1 Thick cylinder under internal and external pressure
6.11.2 Notched bar uniaxially loaded
6.11.3 Tee junction under internal pressure
6.11.4 Snap-through of shallow circular arch
6.11.5 Large deflection analysis of a simply supported plate
6.11.6 Dynamic analysis of a spherical shell

6.12 CONCLUDING REMARKS 6.41

6.13 REFERENCES 6.42

CHAPTER 6

NONLINEAR SOLUTION TECHNIQUES

6.1 INTRODUCTION

The finite element method is being extensively applied in a widening variety of nonlinear structural problems, brought about by continuous advances in new and demanding engineering fields, such as offshore and aerospace exploration or the nuclear, chemical and automotive industries.

In more traditional areas like house, bridge, ship and dam building, nonlinear effects are being more frequently incorporated in the analyses, as imposed by stricter design specifications set to meet higher performance and safety standards at optimum production costs.

The increasing sophistication of theoretical models and the booming expansion of computer power have enabled the finite element analyst to predict more and more accurately the structural and material responses over a broad range of environmental conditions, as required by the enormous risk and responsibility associated with many of the practical applications.

In spite of all the achievements to date, the solution of the system of discretized finite element equations still remains a costly and delicate step in any nonlinear analysis.

This Chapter is therefore dedicated to the description and assessment of some of the more reliable, accurate and efficient nonlinear solution algorithms currently available.

After a brief historical review, the well established Newton-Raphson method and variants thereof are presented; a simple line search procedure is described and its use as an accelerator for modified Newton-Raphson solutions is highlighted; a number of quasi-Newton and secant-Newton methods is then considered and

the relative efficiency of all these procedures is assessed by numerical examples.

Convergence criteria, divergence and termination procedures are also discussed and the Chapter closes with a digression on current trends in nonlinear solution techniques.

6.2 A NOTE ON EARLY DEVELOPMENTS

Soon after the expression "Finite Element" was coined [1] and the first linear structural finite element analyses came to light [2], the method was directly extended to geometric [3] and material [4,5] nonlinearity: the external forces are gradually applied in proportional steps until the desired final level is reached and the structural behaviour is simultaneously linearized.

Early static solutions [3,6] were purely incremental, requiring a large number of very fine load steps but exhibiting nevertheless a tendency to drift away from the true response path (fig. 6.1 a): in general equilibrium is not satisfied at any given load level and errors accumulate; no direct estimate of the solution accuracy is available and repeated runs with decreasing load step sizes must be performed until convergence of two successive trials can be established[7].

Later, the so-called self correcting methods [7] emerge, which are the basis of the incremental-iterative approach widely adopted: a number of iterations is performed during each load step until a convergence criterion is satisfied, usually invoking some norm of the residual or out-of-balance forces (fig. 6.1 b). Equilibrium is therefore pursued throughout the solution and accurate results are achieved with much larger load steps.

Several techniques are employed for the iterative dissipation of the residuals, namely:

- direct iteration [8], in which the previous solution - for the displacements is used to predict the current value of the structural stiffness in a recursive manner (fig. 6.2 a).

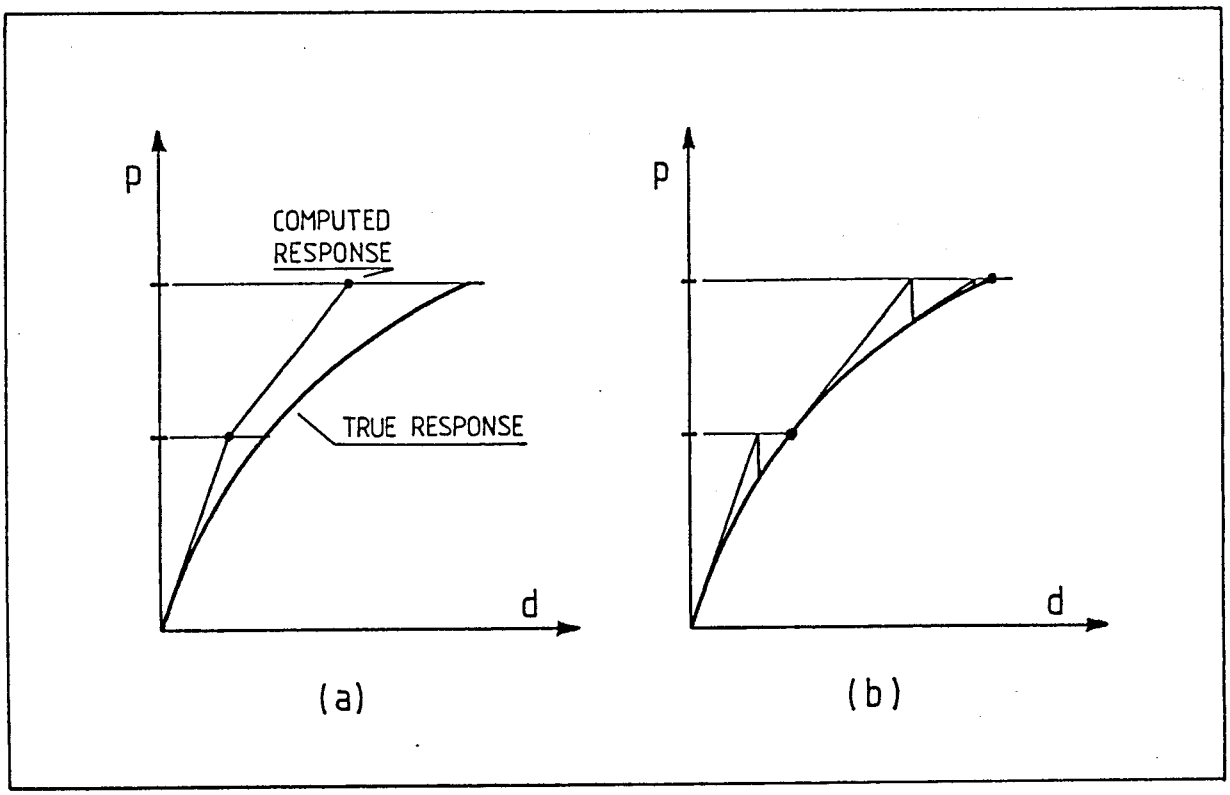

Fig. 6.1 – Purely incremental (a) and incremental iterative (b) methods

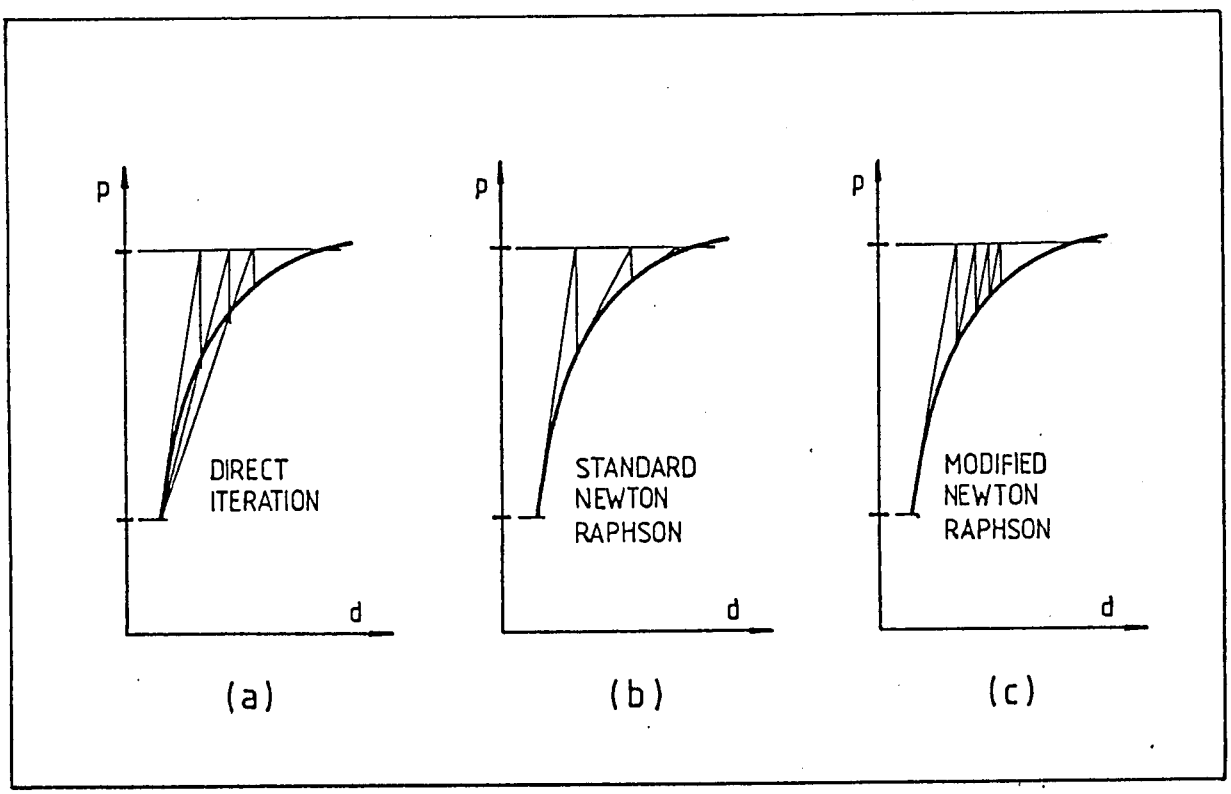

Fig. 6.2 – Various techniques for iterative dissipation of residuals

- standard and modified Newton-Raphson [9] (fig. 6.2 b-c) to be discussed in Section 6.3.

- conjugate Newton [10], that blends conjugate gradient and modified Newton-Raphson procedures, making the best use of both: a new iterative correction for the displacement field is sought in a search direction K-orthogonal to the previous one and is computed by simple re-solution of the global equation system.

- quasi-Newton [11] and secant Newton [12], matrix update techniques fully described in Sections 6.6 and 6.7.

- dynamic relaxation [23], that approaches the static solution as the steady state of a dynamic problem set up by the introduction of special mass and damping matrices. Although computationally simple and economical in core requirements, the method has generally been considered slow [24]. Promising advances were recently achieved in convergence acceleration [25].

Various extrapolation and relaxation procedures have been incorporated in the iterational cycle to guarantee and hasten convergence.

- Bathe [13] advocates Aitken acceleration [14], where each component of the current displacement increment is scaled by an accelerating factor obtained by dividing the previous displacement increment by the difference between itself and the current value.

- modified Aitken schemes have been produced by Irons and Tuck [16] and also Jennings [15], which replace the diagonal acceleration matrix by a scalar, claiming more stable convergence.

- the Alpha-constant stiffness method, introduced by Nayak and Zienkiewicz [17], is an over-relaxation scheme whereby the displacement increment computed using constant stiffness is modified so as to approximate the value that would result from a full Newton-Raphson iteration. Nayak considers his approach to be a quasi-Newton method [18]. Basu [19] simplifies the formulation, Raaser [20] discusses certain implications of the Alpha factor and Cochet [21] proposes a modification beneficial for problems of localized plasticity.

- Line search is another relaxation strategy in which the computed vector of displacement increments is scaled in order to minimize the potential energy [22]; a simple algorithm for the definition of the search parameter is presented in Section 6.5.

In dynamic analyses the difficulties associated with material and geometric nonlinearity are further magnified by the need to monitor the structural response history, which requires advancing the spatial solution along the time axis, as discussed in Chapter 2.

On the use of the displacement formulation of the predictor-multicorrector algorithm [26] adopted in the present study, the dynamic problem is converted into a succession of equivalent static ones, discretely spaced in time, with definition of an effective stiffness matrix and an effective load vector. Predicted values of displacement, velocity and acceleration are iteratively corrected inside each time step.

At this point it is opportune to draw a historical parallel between static and dynamic finite element solution techniques. Dynamic algorithms persisted, much longer than the static ones, in omitting equilibrium corrections, as was indeed favoured by the stabilizing numerical influence of the mass and damping terms included in the effective stiffness matrix, provided that a small enough time step length was chosen. However the accurate solution of the equilibrium equations at each time step is even more important in dynamic than in static analyses, as pointed out by Bathe [27]: namely, any error introduced in the step-by-step dynamic solution will accumulate and cannot be compensated for later, as in many static geometrically nonlinear analyses.

The methods presented in the next Sections apply equally to the equilibrium iterational cycles of both static and dynamic solutions and the word "increment" may denote either a load or a time step. Adaptive step sizing procedures, although not used in this Chapter, are mentioned in Section 6.10.

6.3 STANDARD NEWTON-RAPHSON METHOD (N.R.)

In structural problems the finite element equilibrium equations, formulated in terms of displacements, may be cast in the form

$$\underline{K}\,\underline{d} = \underline{f} \tag{6.1}$$

where $\underline{d}$ is the vector of unknown nodal displacements,
$\underline{f}$ is the vector of nodal applied forces and
$\underline{K}$ is the global stiffness matrix assembled from element contributions in the usual finite element manner [9].

In a linear problem the equation system (6.1) lends itself readily to direct solution, obtained as $\underline{d} = \underline{K}^{-1}\,\underline{f}$. If, however, any source of nonlinearity is present, provoking dependence of the stiffness matrix or the load vector (or both) on the displacements or their derivatives, direct solution is generally impossible and an incremental-iterative scheme is adopted, as mentioned in Section 6.2.

Let $\underline{d}_i$ be the displacement field at iteration i of the current (load or time) increment. Equilibrium between internal and external forces will generally not be satisfied: $\underline{d}_i$ is then an approximate solution for (6.1) and the corresponding residuals $\underline{r}_i$ are

$$\underline{r}_i\,(\underline{d}_i) = \underline{p}_i\,(\underline{d}_i) - \underline{f}_i\,(\underline{d}_i) \neq \underline{0} \tag{6.2}$$

with $\underline{p}_i$, the vector of nodal forces equivalent to the internal stress field $\underline{\sigma}_i$, given by

$$\underline{p} = \int_V \underline{B}^T\,\underline{\sigma}\,dv \tag{6.3}$$

If the true solution exists at $\underline{d}_i + \Delta\underline{d}_i$ then

$$\underline{r}(\underline{d}_i + \Delta\underline{d}_i) = \underline{r}_i(\underline{d}_i) + \left.\frac{\partial \underline{r}}{\partial \underline{d}}\right|_i \Delta\underline{d}_i + \ldots = \underline{0} \tag{6.4}$$

and truncation of the Taylor series expansion gives the iterative correction $\Delta\underline{d}_i$

$$\Delta\underline{d}_i = -\underline{K}_{Ti}^{-1}\,\underline{r}_i \qquad \text{where} \tag{6.5}$$

$$\underline{K}_{Ti} = \left.\frac{\partial \underline{r}}{\partial \underline{d}}\right|_i = \left.\frac{\partial \underline{p}}{\partial \underline{d}}\right|_i - \left.\frac{\partial \underline{f}}{\partial \underline{d}}\right|_i \tag{6.6}$$

is the so-called tangent stiffness matrix. For conservative applied loading there is no dependence of $\underline{f}$ on $\underline{d}$ and the term $\partial \underline{f}/\partial \underline{d}$ in (6.6) vanishes. In deformation dependent loading cases the term is also often omitted in order to preserve symmetry of $\underline{K}_T$ [28].

The improved estimate $\underline{d}_{i+1}$ is now computed as

$$\underline{d}_{i+1} = \underline{d}_i + s_i \, \Delta \underline{d}_i \qquad (6.7)$$

where s_i is the step length or search parameter, a scalar defined by a line search procedure such as described in Section 6.5.

Equations (6.5-7) constitute the standard or full Newton-Raphson method, depicted in fig. 6.2.b for a 1-D example.

6.4 MODIFIED NEWTON-RAPHSON METHODS (M.N.R.)

In order to avoid the expensive reassembly and inversion of the global tangent stiffness matrix at every iteration, several variations on the standard procedure can be considered wherein $\underline{K}_T$ is only occasionally updated.

6.4.1 Initial stiffness method (KO)

The initial elastic stiffness matrix is used throughout the whole solution. The rate of convergence is very slow but may be improved by line search.

6.4.2 M.N.R. formula 1 (KT1)

The stiffness matrix is recalculated at the first iteration of each increment (fig. 6.2.c). When there is a reduction of the applied load level, as for example in proportional cyclic loading programs, it is convenient to reset the stiffness matrix to the initial elastic value, in order to avoid divergence.

6.4.3 M.N.R. formula 2 (KT2)

The reformulation of $\underline{K}_T$ occurs at the second iteration of the increment.

6.4.4 M.N.R. formula 3 (KTN)

Instead of a preset updating pattern for $\underline{K}_T$, an automatic procedure is triggered by monitoring how closely the current tangential matrix is modelling the structural response. The measure utilized is the ratio of work done on the iterative correction $\Delta\underline{d}_i$ by the residual forces at the end and beginning of the iteration

$$\Delta\underline{d}_i^T \ \underline{r}_{i+1} / \Delta\underline{d}_i^T \ \underline{r}_i < \text{TOLKT} \qquad (6.8)$$

where the tolerance TOLKT for re-forming $\underline{K}_T$ is set to, say, 10-30%.

In terms of the 1-D example of fig. 6.3, this criterion is equivalent to limiting the ratio of (shaded) and (shaded + dotted) areas.

To counterbalance the degradation of the quadratic convergence rate of the full NR to a linear one, an acceleration procedure is often incorporated in MNR solutions. The Aitken acceleration [13-16] and the Alpha-constant method [17-21] mentioned before are two possibilities. We have obtained a significant improvement using line search, confirming the findings of Crisfield [51,74]. A simple algorithm is described next.

6.5 LINE SEARCH

The iterative displacement vector $\Delta\underline{d}_i$ defines in n-dimensional solution space what the jargon of optimization calls a search direction. The task of any line search procedure is then to scale $\Delta\underline{d}_i$ optimally in order to minimize (ideally to cancel) the component of the residual force vector $\underline{r}_{i+1}$ with respect to $\Delta\underline{d}_i$, or, in other words, to obtain the local minimum along $\Delta\underline{d}_i$ for the total potential energy

$$\phi(\underline{s}_i) = \Delta\underline{d}_i^T \ \underline{r}(\underline{d}_{i+1}) = 0 \qquad (6.9)$$

Several search procedures have been described in the structural analysis literature.

Irons [10], in the context of conjugate gradient type methods

(that require accurate line searches) computes $\underline{r}_{i+1}$ and ϕ for four trial values of s_i (0.25, 0.85, 2.8 and 4.0) and then interpolates to obtain $\phi(s_i) = 0$.

Matthies [11] and Abdel Rahman [29] use the Illinois algorithm [30], a modified version of the "regula falsi" method, to solve (6.8), after finding a bracketing interval on the zero.

Approximate or slack line searches are considered adequate for use with MNR [51] (and also quasi and secant Newton [11,12]). We apply a "sufficient reduction" criterion defined by Matthies [11] whereby line searches are not performed if

$$\phi(s_i) \;/\; \phi(0) \leq \text{TOLSR} \qquad (6.10)$$

where $\phi(0) = \Delta\underline{d}_i^T \underline{r}(\underline{d}_i)$ corresponds to a zero value of s_i in (6.7) and the search tolerance TOLSR is set within 0.3 - 0.5.

The simple search procedure implemented in our programs comprises two steps:

(i) The values of $\phi(0)$ and $\phi(1)$, that are available at low cost, are used in a linear interpolation for s_L

$$s_L = \phi(0) \;/\; [\phi(0) - \phi(1)] \qquad (6.11)$$

An upper limit of 5. is enforced on s_L to prevent dangerous extrapolations [29].

(ii) If the criterion (6.10) has not yet been satisfied a quadratic fit is now used on $\phi(0)$, $\phi(1)$ and $\phi(s_L)$ to yield s_Q.

We have found this approach to work well; indeed the second step is rarely needed with TOLSR in the range 0.3 - 0.5. The method could be easily extended either by performing a cubic fit on $\phi(0)$, $\phi(1)$, $\phi(s_L)$ and (s_Q) as a third step, or by replacing s_L by s_Q and iterating quadratically.

6.6 QUASI-NEWTON METHODS (QN)

The quasi-Newton methods are a new class of iterative nonlinear solution techniques introduced by Davidon [31] in 1959 for the unconstrained minimization of functionals and utilized by Broyden [32] in 1965 for the solution of nonlinear equation systems. Matthies and Strang [11] in 1979 pioneered their application in the context of structural finite element analysis.

The basic feature of the QN updating procedure is performing a simple modification of the global coefficient matrix at each iteration in order to satisfy the local secant condition (fig. 6.4)

$$\underline{K}_i \ (\underline{d}_i - \underline{d}_{i-1}) = \underline{r}_i - \underline{r}_{i-1} \qquad (6.12)$$

rather than engaging in the costly reformulation and inversion of the tangent stiffness matrix required by the standard NR method.

Expression (6.12) is central to the development of QN methods and therefore is often called the quasi-Newton equation [33].

Three further requirements are usually imposed on the update formula [11,33], namely that both symmetry and positive definiteness of $\underline{K}_{i-1}$ be passed on to $\underline{K}_i$ and that the computation of the new search direction $\Delta\underline{d}_i$ be not expensive. This last condition, crucial for cost effectiveness, is best met by setting an upper limit of two for the rank of the matrix update.

Several such formulas are now presented, both in their direct and inverse forms (in which $\underline{K}_{i-1}^{-1}$ is updated, rather than $\underline{K}_{i-1}$), denoting by $\underline{I}$ the identity matrix and taking, for ease of notation

$$\underline{\delta}_{i-1} = s_{i-1} \ \Delta\underline{d}_{i-1} = \underline{d}_i - \underline{d}_{i-1} \qquad (6.13)$$

$$\underline{\gamma}_i = \underline{r}_i - \underline{r}_{i-1}$$

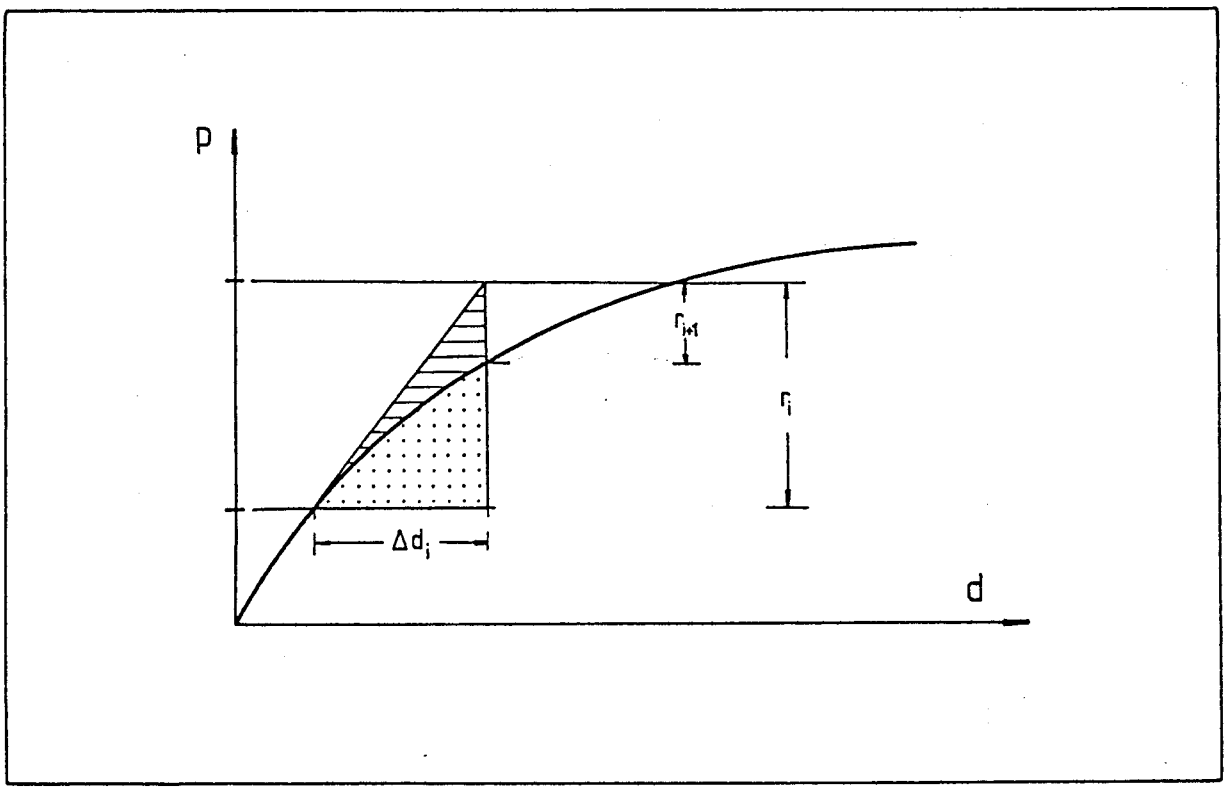

Fig. 6.3 - Work of residual forces on the iterative displacement

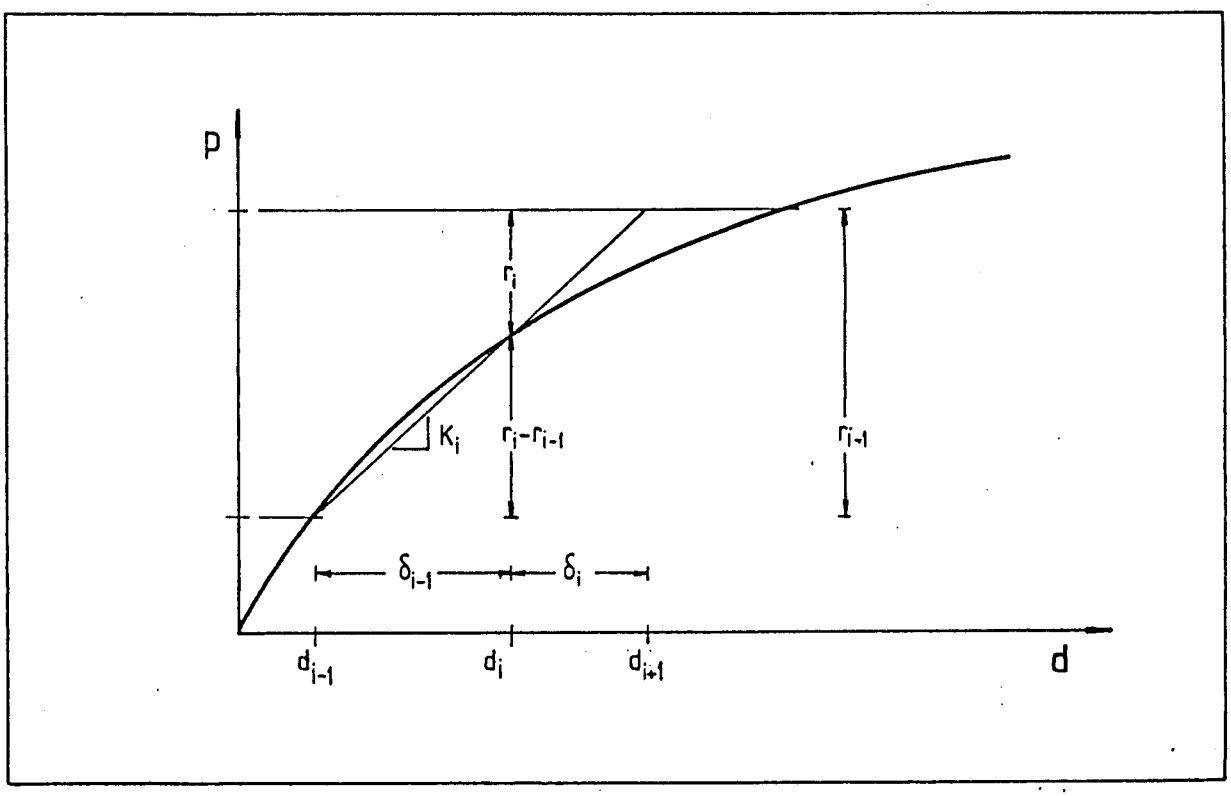

Fig. 6.4 - Local secant condition

6.6.1 Rank one additive updates

6.6.1.1 Davidon direct update

$$\underline{K}_i = \underline{K}_{i-1} + \frac{(\underline{\gamma}_i - \underline{K}_{i-1}\ \underline{\delta}_{i-1})(\underline{\gamma}_i - \underline{K}_{i-1}\ \underline{\delta}_{i-1})^T}{(\underline{\gamma}_i - \underline{K}_{i-1}\ \underline{\delta}_{i-1})^T\ \underline{\delta}_{i-1}} \qquad (6.14)$$

6.6.1.2 Davidon inverse update

$$\underline{K}_i^{-1} = \underline{K}_{i-1}^{-1} + \frac{(\underline{\delta}_{i-1} - \underline{K}_{i-1}^{-1}\ \underline{\gamma}_i)(\underline{\delta}_{i-1} - \underline{K}_{i-1}^{-1}\ \underline{\gamma}_i)^T}{(\underline{\delta}_{i-1} - \underline{K}_{i-1}^{-1}\ \underline{\gamma}_i)^T\ \underline{\gamma}_i} \qquad (6.15)$$

These two updates do not guarantee hereditary positive definiteness and may lead to numerical difficulties [33]. They were first published by Davidon [31] and later rediscovered by Broyden [32] and others [34]. Expression(6.15) is indeed referred by Brodlie [35] as the Murtagh-Sargent formula.

6.6.2 Rank two additive updates

6.6.2.1 Davidon-Fletcher-Powell (DFP) direct update

$$\underline{K}_i = \left(\underline{I} - \frac{\underline{\gamma}_i\ \underline{\delta}_{i-1}^T}{\underline{\gamma}_i^T\ \underline{\delta}_{i-1}}\right) \underline{K}_{i-1} \left(\underline{I} - \frac{\underline{\gamma}_i\ \underline{\delta}_{i-1}^T}{\underline{\gamma}_i^T \underline{\delta}_{i-1}}\right)^T + \frac{\underline{\gamma}_i\ \underline{\gamma}_i^T}{\underline{\gamma}_i^T \underline{\delta}_{i-1}} \qquad (6.16)$$

6.6.2.2 DFP inverse update

$$\underline{K}_i^{-1} = \underline{K}_{i-1}^{-1} + \frac{\underline{\delta}_{i-1}\ \underline{\delta}_{i-1}^T}{\underline{\delta}_{i-1}^T\ \underline{\gamma}_i} - \frac{\underline{K}_{i-1}^{-1}\ \underline{\gamma}_i\ \underline{\gamma}_i^T\ \underline{K}_{i-1}^{-1}}{\underline{\gamma}_i^T\ \underline{K}_{i-1}^{-1}\ \underline{\gamma}_i} \qquad (6.17)$$

Formulas (6.16-17), introduced by Davidon [31] and improved by Fletcher and Powell [36], ensure hereditary symmetry and positive definiteness.

6.6.2.3 Broyden-Fletcher-Goldfarb-Shanno (BFGS) direct update

$$\underline{K}_i = \underline{K}_{i-1} + \frac{\underline{\gamma}_i\ \underline{\gamma}_i^T}{s_{i-1}\ \underline{\delta}_{i-1}^T\ \underline{\gamma}_i} - \frac{\underline{K}_{i-1}\ \underline{\delta}_{i-1}\ \underline{\delta}_{i-1}^T\ \underline{K}_{i-1}}{\underline{\delta}_{i-1}^T\ \underline{K}_{i-1}\ \underline{\delta}_{i-1}} \qquad (6.18)$$

6.6.2.4 BFGS inverse update

$$\underline{K}_i^{-1} = \left(\underline{I} - \frac{\underline{\delta}_{i-1}\, \underline{\gamma}_i^T}{\underline{\delta}_{i-1}^T\, \underline{\gamma}_i} \right) \underline{K}_{i-1}^{-1} \left(\underline{I} - \frac{\underline{\delta}_{i-1}\, \underline{\gamma}_i^T}{\underline{\delta}_{i-1}^T\, \underline{\gamma}_i} \right)^T + \frac{\underline{\delta}_{i-1}\, \underline{\delta}_{i-1}^T}{\underline{\delta}_{i-1}^T\, \underline{\gamma}_i} \qquad (6.19)$$

This update, developed independently by Broyden [37], Fletcher [38], Goldfarb [39] and Shanno [40], is currently considered the best formula for unconstrained minimization [33, 41] and has been extensively applied by structural analysts [11, 13, 29, 42-49]. Expressions (6.14,15), (6.16,19) and (6.17,18) are related by the transformation $\underline{\delta}_{i-1} \leftrightarrow \underline{\gamma}_i$, $\underline{K}_i \leftrightarrow \underline{K}_i^{-1}$. Direct and inverse updates so paired are called dual or complementary [33].

Formulas (6.14-19) involve an additive correction to $\underline{K}_i$ or $\underline{K}_i^{-1}$. Brodlie [35] developed real product forms very convenient for computer implementation of QN methods. The additive forms will be used in Section 6.7 for the derivation of the secant Newton updates.

6.6.3 BFGS inverse update in real product form

The real product forms presented by Brodlie for the inverse updates listed above have the general form

$$\underline{K}_i^{-1} = (\underline{I} + \underline{w}_i\, \underline{v}_i^T)\ \underline{K}_{i-1}^{-1}\ (\underline{I} + \underline{v}_i\, \underline{w}_i^T) \qquad (6.20)$$

The real vectors $\underline{v}_i$ and $\underline{w}_i$ for the BFGS method are given by

$$\underline{v}_i = \underline{r}_{i-1} \left[1 + \left(- \frac{\underline{s}_{i-1}\, \underline{\delta}_{i-1}^T\, \underline{\gamma}_i}{\underline{\delta}_{i-1}^T\, \underline{r}_{i-1}} \right)^{1/2} \right] - \underline{r}_i \qquad (6.21)$$

$$\underline{w}_i = \frac{\underline{\delta}_{i-1}}{\underline{\delta}_{i-1}^T\, \underline{\gamma}_i} \qquad (6.22)$$

6.6.3.1 Computer implementation of the BFGS method

The BFGS inverse update is used in the present study in conjunction with the MNR methods K0, KT1 and KT2 described in 6.4.1 to 6.4.3.

Noting by $\bar{\underline{K}}^{-1}$ the most recently factorized global stiffness matrix, expression (6.20) is expanded for computational purposes into

$$\underline{K}_i^{-1} = \left[\prod_{j=i}^{\ell}\left(\underline{I} + \underline{w}_j\,\underline{v}_j^T\right)\right]\ \bar{\underline{K}}^{-1}\ \left[\prod_{j=\ell}^{i}\left(\underline{I} + \underline{v}_j\,\underline{w}_j^T\right)\right] \tag{6.23}$$

with $i \geq \ell$ and $\ell = 2$ for $\bar{\underline{K}}$ equal to $\underline{K}_0$ or $\underline{K}_{T1}$, or $\ell = 3$ for $\bar{\underline{K}}$ equal to $\underline{K}_{T2}$.

The iterative displacement $\Delta\underline{d}_i = -\underline{K}_i^{-1}\,\underline{r}_i$ is obtained by the following three-step algorithm, that merely involves vector manipulations and one backsubstitution.

(i) Compute the modified load vector $\underline{r}_i^*$ as

$$\underline{r}_i^* = \left[\prod_{j=\ell}^{i}\left(\underline{I} + \underline{v}_j\,\underline{w}_j^T\right)\right]\ \underline{r}_i \tag{6.24}$$

(ii) Extract the corresponding displacement increment $\Delta\underline{d}_i^*$ by backsubstitution from the factorized $\bar{\underline{K}}^{-1}$

$$\Delta\underline{d}_i^* = -\bar{\underline{K}}^{-1}\,\underline{r}_i^* \tag{6.25}$$

(iii) Complete the calculation of $\Delta\underline{d}_i$ as

$$\Delta\underline{d}_i = \left[\prod_{j=i}^{\ell}\left(\underline{I} + \underline{w}_j\,\underline{v}_j^T\right)\right]\ \Delta\underline{d}_i^* \tag{6.26}$$

The pairs $(\underline{v}_j, \underline{w}_j)$ needed for the products in (6.24) and (6.26) are either kept in core or stored on disc. Their maximum number is usually limited to 15-20 [11,44] to avoid an excessive slowing down of the iteration procedure.

When this upper limit is reached, several alternatives are possible such as moving up the pairs discarding the oldest one or simply wiping them all out and starting afresh with a new tangent stiffness matrix.

We note, en passant, that a recursive algorithm also using vector algebra has been presented by Geradin [42] for the Davidon inverse formula (6.15).

6.6.3.2 Numerical stability of the BFGS inverse update

Brodlie [35] proves that $\det(\underline{K}_i^{-1}) \geq 0$ is a necessary and sufficient condition for the recasting of the additive update (6.19) in the real product forms (6.20 - 22) and shows that

$$\frac{\det(\underline{K}_i^{-1})}{\det(\underline{K}_{i-1}^{-1})} = (1 - \underline{w}_i^T \underline{v}_i)^2 \qquad (6.27)$$

Brodlie also gives bounds on the condition numbers C of $\underline{K}_i^{-1}$ and $\underline{K}_{i-1}^{-1}$ as

$$\frac{1}{Q_i^2} \leq \frac{C(\underline{K}_i^{-1})}{C(\underline{K}_{i-1}^{-1})} \leq Q_i^2 \qquad (6.28)$$

with

$$Q_i = \frac{\left\{(\underline{v}_i^T \underline{v}_i)^{\frac{1}{2}} (\underline{w}_i^T \underline{w}_i)^{\frac{1}{2}} + [(\underline{v}_i^T \underline{v}_i)(\underline{w}_i^T \underline{w}_i) + 4(1 + \underline{w}_i^T \underline{v}_i)]^{\frac{1}{2}}\right\}^2}{4 \left|1 + \underline{w}_i^T \underline{v}_i\right|} \qquad (6.29)$$

The real product formulation has therefore the added benefit of allowing for control over the positive definiteness of successive approximations of $\underline{K}^{-1}$: a decision to skip the update and recompute the tangent stiffness is made if either the determinant ratio (6.27) falls below a preset limit (10^{-10}, with [13]) or the estimated increase of the conditioning number given by the ratio of (6.28) exceeds, say, 10^{10} [11].

6.6.3.3 Line search in BFGS

After obtaining the new search direction $\Delta\underline{d}_i$ by (6.24-26), the search parameter s_i for use in (6.7) is computed by means of the procedure described in Section 6.5. The BFGS method is known to perform efficiently without exact line searches [50]; a value of 0.5 for the search tolerance parameter TOLSR is adopted here, as suggested by Matthies [11].

6.7 SECANT NEWTON METHODS (SN)

The SN methods were presented by Crisfield [12] as a memoryless single cycle version of some QN formulas. The SN updates satisfy the QN equation (6.12) but the updating procedure for the computation of $\underline{K}_i^{-1}$ is not applied to $\underline{K}_{i-1}^{-1}$ but instead to $\bar{\underline{K}}^{-1}$, the latest factorized global stiffness matrix, thereby avoiding the storage of the pairs of updating vectors $(\underline{v}_i, \underline{w}_i)$ and associated tape processing operations, which are one major burden with BFGS.

Crisfield [12,60] casts the SN update in the form

$$\Delta \underline{d}_i = A\, \underline{\delta}_i^* + B\, \underline{\delta}_{i-1} + C\, \underline{\delta}_{i-1}^* \qquad (6.30)$$

with $\underline{\delta}_i^* = -\bar{\underline{K}}^{-1}\, \underline{r}_i$ and presents three formulae referred to here as SN1, SN2 and SN3. A fourth formula (SN4) is derived below from the DFP inverse update (6.17).

6.7.1 SN formula 1 (SN1)

This formula is based on the Davidon single rank inverse update (6.15). Replacing $\underline{K}_{i-1}^{-1}$ by $\bar{\underline{K}}^{-1}$ and using $\underline{\delta}_{i-1}$ and $\underline{\gamma}_i$ given by (6.13) and $\underline{\delta}^*$ with the meaning defined above, the factors A,B,C for use in (6.30) are

$$C_1 = \frac{(\underline{\delta}_{i-1} + \underline{\delta}_i^* - \underline{\delta}_{i-1}^*)^T\, \underline{r}_i}{(\underline{\delta}_{i-1} + \underline{\delta}_i^* - \underline{\delta}_{i-1}^*)^T\, \underline{\gamma}_i}\ , \quad A_1 = 1 - C_1,\ B_1 = -C_1 \qquad (6.31)$$

6.7.2 SN formula 2 (SN2)

It is obtained similarly from the BFGS inverse update in the additive form (6.19).

$$C_2 = \frac{\underline{\delta}_{i-1}^T\, \underline{r}_i}{\underline{\delta}_{i-1}^T\, \underline{\gamma}_i}\ , \quad A_2 = 1 - C_2$$

$$B_2 = -C_2 - \frac{(\underline{\delta}_i^* - \underline{\delta}_{i-1}^*)^T\, \underline{r}_i}{\underline{\delta}_{i-1}^T\, \underline{\gamma}_i} + C_2\, \frac{(\underline{\delta}_i^* - \underline{\delta}_{i-1}^*)^T\, \underline{\gamma}_i}{\underline{\delta}_{i-1}^T\, \underline{\gamma}_i} \qquad (6.32)$$

6.7.3 SN formula 3 (SN3)

This formula is also derived from the BFGS expression (6.19) but making the approximation

$$\underline{\delta}_{i-1} \cong - \underline{K}_{i-1}^{-1} \underline{r}_{i-1} \tag{6.33}$$

that is to say, assuming s_{i-1} with unit value in (6.13). This method, previously named "accelerated MNR" [24, 53], does not require the storage of $\underline{\delta}^*_{i-1}$. We have in this case

$$\begin{aligned} C_3 &= 0, \quad A_3 = A_2 \\ B_3 &= - C_2 - A_3 \frac{\underline{\delta}^{*T}_i \underline{\gamma}_i}{\underline{\delta}^T_{i-1} \underline{\gamma}_i} \end{aligned} \tag{6.34}$$

6.7.4 SN formula 4 (SN4)

Using the DFP inverse formula (6.17) to compute $\underline{d}_i = -\underline{K}_i^{-1} \underline{r}_i$, taking $\underline{\delta}^*_i = - \underline{K}_{i-1}^{-1} \underline{r}_i$ (with $\underline{K}_{i-1} = \overline{\underline{K}}$) and noting that $\underline{K}_{i-1}^{-1} \underline{\gamma}_i = \underline{\delta}^*_{i-1} - \underline{\delta}^*_i$, the new search direction is expressed in the form (6.30) with

$$\begin{aligned} C_4 &= \frac{\underline{\gamma}^T_i \underline{\delta}^*_i}{\underline{\gamma}^T_i (\underline{\delta}^*_i - \underline{\delta}^*_{i-1})}, \quad A_4 = 1 - C_4 \\ B_4 &= \frac{\underline{\delta}^T_{i-1} \underline{r}_i}{\underline{\delta}^T_{i-1} \underline{\gamma}_i} \end{aligned} \tag{6.35}$$

Using any of the four SN formulas we make $A = 1, B = C = 0$ for the first iteration and use expressions (6.31-35) thereafter.

6.7.5 Numerical stability of the SN method

As a tentative approach to prevent "bad SN iterations", Crisfield [12, 74] recommends a bound check on the factors A,B,C of (6.30).

$$R_1 > A > 1/R_1$$
$$R_2 > (B+C)/A > -R_2/2 \qquad (6.36)$$

where R_1 is between 2 and 5 and R_2 in the range .2 -.3. If the check (6.36) is not satisfied, the values A = 1, B = C = 0 are used instead.

6.7.6 Line Search in SN

Noting that an approximate line search is already implicit in (6.30) (since in general A differs from unity), the SN method has been found to perform well without recourse to line searches if $\underline{\bar{K}}^{-1}$ is a reasonable guess for the current stiffness [12] and the structure is slowly softening, as for example occurs with steel structures [29]. However, when used in reinforced concrete analysis, the steep strain softening due to concrete cracking makes line searches advisable [51, 52].

6.8 CONVERGENCE CRITERIA

Any convergence criterion has the difficult task of warning the analyst that the iterational cycle has led him close enough to the true solution path, however without knowing where this path lies. An effective criterion used with realistic tolerances is a precondition for accurate but economic solutions.

In nonlinear structural analysis convergence criteria usually rely on displacements, residuals or energy. We leave aside displacement based criteria, because they are sometimes misleadingly triggered by a slow convergence rate (as occurs in some MNR solutions) or by a small value of the search parameter s_i.

6.8.1 Residual norm criterion

The ratio of the Euclidian norms of residuals $\underline{r}_i$ and external forces (i.e. loads plus reactions) $\underline{\bar{f}}_i$ is compared against a tolerance TOLRF typically set in the range 10^{-2} - 10^{-4}.

$$\| \underline{r}_i \| / \| \underline{\bar{f}}_i \| \leq \text{TOLRF} \qquad (6.37)$$

We perform the (correct) computation of the total current value of the reactions in each iteration by reversing the direction of the residual force components at each restrained degree of freedom. Those components of $\underline{r}_i$ are then zeroed and the reactions added to the applied loads to form the total external forces $\overline{\underline{f}}_i$, thereby achieving a quicker decrease of the ratio of the norms in (6.37) than in the original form of Reference [54]. The procedure is also adequate to monitor convergence when there are zero applied loads, such as with thermal loading or with prescribed boundary displacements.

6.8.2 Energy norm criterion

This criterion, proposed by Bathe [13], checks the ratio of the current and initial increments of internal energy, that is the work done by the residuals on the displacement increments

$$(\underline{r}_{i+1}^T \underline{\delta}_i) \; / \; (\underline{r}_2^T \underline{\delta}_1) < \text{TOLEN} \qquad (6.38)$$

and a result less than, say, 10^{-5} is taken to indicate that both displacements and forces are near their equilibrium values.

6.9 DIVERGENCE AND TERMINATION PROCEDURES

The most usual causes for divergence of the iterational cycle are

(i) structural stiffening due to elastic unloading or geometry changes;

(ii) user-specified load level in excess of limit point or collapse loads.

The problem of spurious or numerical unloading has been discussed in Section 3.11 with reference to the question of solution path (in)dependency and it is worth stressing once more the importance of an accurate state determination for a reliable and stable solution.

Secant and quasi-Newton methods, as governed by a local secant condition, seem to adapt quite readily to a stiffening response [11, 13, 48]. MNR techniques are more prone to difficulties.

Bathe [13] distinguishes between the slow geometric stiffening that can be handled by choosing a smaller load increment and so decreasing the linearization error, from the sudden unloading stiffening that requires a resetting of the stiffness matrix to the elastic value [27]. Accordingly, he proposes a divergence procedure, triggered by any increase in the residual forces, whereby $\underline{K}_T$ is reset to $\underline{K}_0$ together with a reduction of the load step.

Another type of control involves the current stiffness parameter [55, 56], a normalized measure of the incremental stiffness in the direction of nodal displacement.

Considering load step n, $\Delta\underline{d}^{nT}\Delta\underline{f}^n$ is the work produced by the current increment of external force $\Delta\underline{f}^n$ on the incremental displacement $\Delta\underline{d}^n$ ($=\Sigma_i\ \underline{\delta}_i^n$) and division of both terms by $\|\Delta\underline{f}^n\|$ yields a value independent of the actual step size.

A measure of the current structural stiffness may be expressed in terms of the inverse quantity: the stiffer the system, the bigger the result. Dividing now by the value corresponding to the initial conditions, the current stiffness parameter S^n is finally obtained as

$$S^n = \frac{\Delta\underline{d}_i^{1\,T}\ \Delta\underline{f}^1}{\Delta\underline{d}^{n\,T}\ \Delta\underline{f}^n}\ \frac{\left\|\Delta\underline{f}^n\right\|^2}{\left\|\Delta\underline{f}^1\right\|^2} \qquad (6.39)$$

The initial configuration corresponds to a unit value for S by definition; stiffening is denoted by an increasing of S and softening by a decrease.

To terminate the computations when the collapse load is reached three combined procedures are used:

(i) a lower bound (0.001 - 0.005 [29] is imposed on the current stiffness parameter;

(ii) three consecutive values of the energy norm (6.38) above 100 are taken to indicate collapse [29];

(iii) a limit is imposed on the maximum number of iterations.

6.10 CURRENT TRENDS IN SOLUTION TECHNIQUES

An intense research effort is being currently devoted to the development of "intelligent" adaptive incremental-iterative procedures that "learn" from the structural response how to optimally steer the solution.

In dynamics, step size restrictions for stability of explicit time integration are overcome by implicit techniques [57] and implicit-explicit schemes [26,59] prove very adequate for multimaterial domains; usually though the advancement of the solution in time employs equally sized steps: effective schemes for automatic step selection have yet to be devised [27] but some progress has already been made [58].

By contrast in statics a host of automatic adaptive procedures has emerged, sparked by research into post-buckling analysis. Numerous strategies have been devised to conduct the solution past limit or bifurcation points: displacement control methods [63-65] switch from load into displacement incrementation; arc-length methods, introduced by Riks and Wempner [66-68] and modified by Crisfield [69-70], constrain the load step size to remain constant in load-deflection space; the correlation between displacement control and arc-length techniques is outlined by Ramm [62]; another way of varying the load level during the iterations is proposed by Bergan [61, 71, 72], using the current stiffness parameter; Bathe [73] outlines a flexible strategy that chooses spherical constant arc-length far from the critical points and then switches to a criterion of constant incremental external work.

Although primarily originated to circumvent the numerical difficulties associated with the analysis of slender structures, all these methods have been shown to improve the convergence characteristics of unconstrained iterative procedures and constitute an important aspect of the continuing search for general, reliable and effective nonlinear solution techniques.

6.11 NUMERICAL EXAMPLES

6.11.1 Thick cylinder under internal and external pressure

A thick cylinder of a perfectly plastic Tresca material is restrained against axial deformation and submitted to internal and external pressure, respectively p and q.

The proportional loading program comprises 9 load increments : p is first set to 1000. and then raised to 1800. in 8 steps of 100. The ratio p/q is kept constant throughout and equal to 4. The geometric and material data is summarized in Table 6.1 together with the analytical values for the radius of plastification c and the radial displacement U of point H at the inner surface (see Ref. [75]). The various finite element solutions undertaken differ widely as to computer time requirements but all agree well with the exact results as typified in fig. 6.5. The convergence tolerances were TOLEN = 1.E-5, TOLRF = 1.E-3.

Table 6.2 assesses the cost of KO, KT1, KT2 and KT runs with relation to the choice between path independency (PI) and path dependency with allowed recovery of plastic strain on spurious unloading (PDR), as described in Section 3.11. It must be said that for the tabulated PDR runs no unloading did occur and so these PDR solutions coincide with pure path dependent (PD) runs. For the lengthier KO case we observe an increase of 243% in the total number of substeps for stress computation and of 20.5% in CPU time by switching to a PI solution. When line searches were added the pure PD strategy failed to converge for KT1 and KT2 at the fifth load step, as opposed to the PDR alternative that was entirely successful.

The PDR results for this problem are as accurate and stable as those supplied by the more expensive PI solutions. However, to keep in line with the caution advocated in Section 3.11, the use of the PDR technique is confined to this exploratory example and all the results presented subsequently are obtained considering path independency.

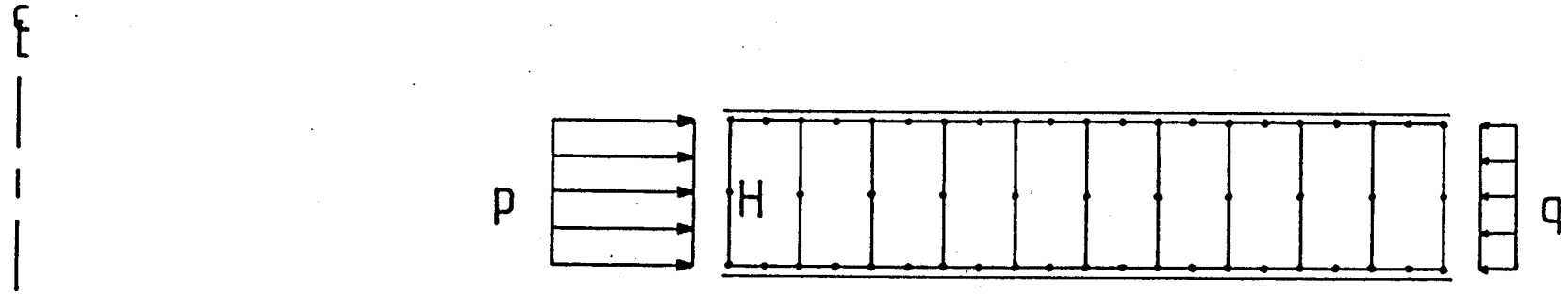

Elastic modulus,	E = 1.E7	Initial yield stress,	Yo = 2000.	Tresca criterion	
Poisson's ratio,	ν = 0.25	Hardening parameter,	H' = 0.	10 el. - 53 nodes	
Internal radius,	a = 100.	External radius,	b = 200.	2x2 Gauss points	

Load step		1	2	3	4	5	6	7	8	9
Int. pressure,	p	1000.	1100.	1200.	1300.	1400.	1500.	1600.	1700.	1800.
Plastic rad.,	c	100.0	105.2	110.9	117.3	124.4	132.6	142.4	154.8	173.7
Displ. (x100),	u_H	1.250	1.388	1.558	1.767	2.028	2.361	2.802	3.432	4.532

TABLE 6.1 - Data and analytical results for the thick cylinder with internal and external pressure

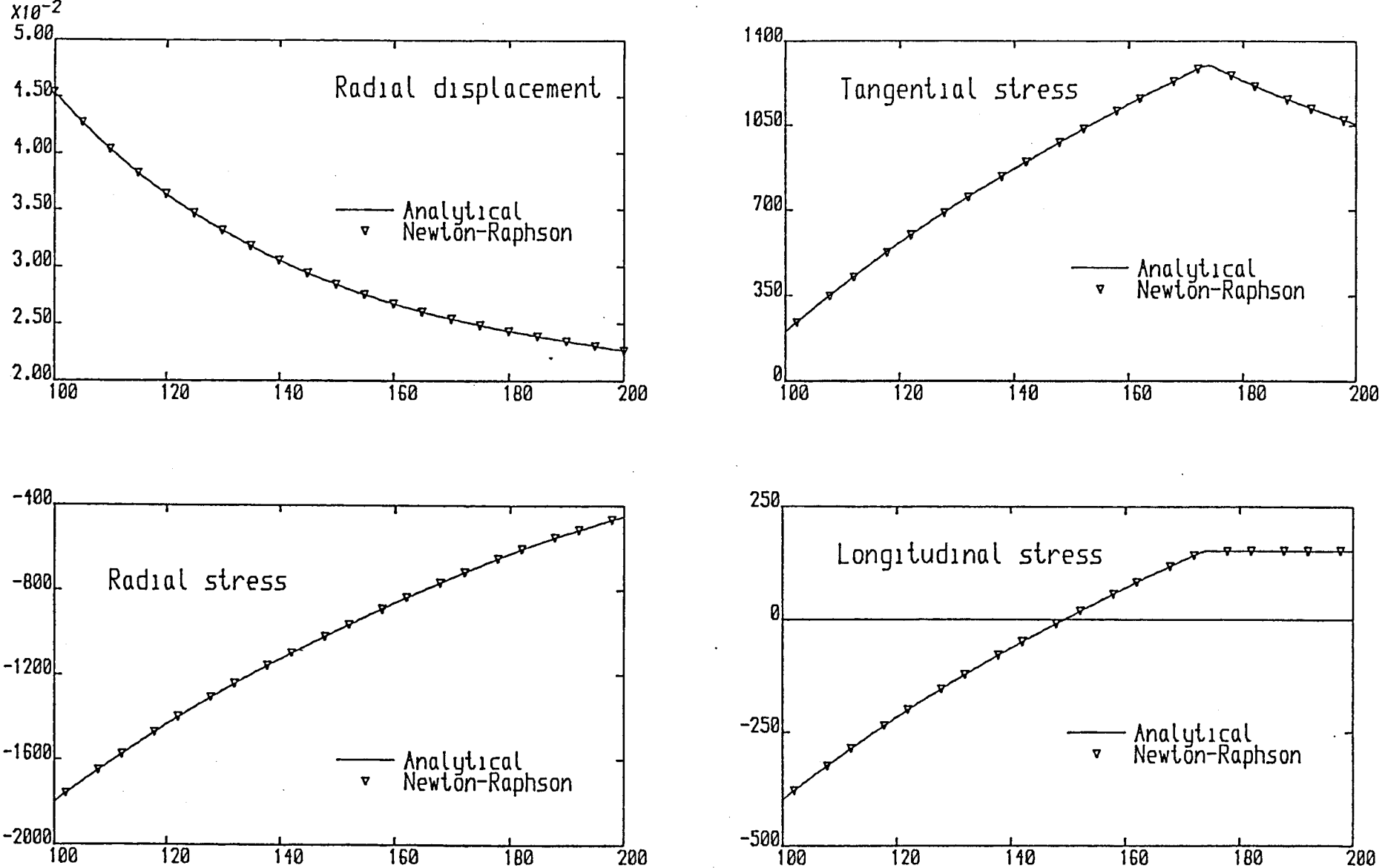

Fig. 6.5 – Comparison of analytical and typical numerical results (KT-PI) for the thick cylinder with internal and external pressure (p=1800.)

	KO		KT1		KT2		KT	
	PDR	PI	PDR	PI	PDR	PI	PDR	PI
CPU time	190	229	93	105	48	54	52	54
Σ substeps	2678	9192	1150	3378	652	2104	508	902

TABLE 6.2 – Cost comparison of path dependent and independent runs for NR and MNR solutions of the thick cylinder with internal and external pressure

Load step	1	2	3	4	5	6	7	8	9	Σ	CPU
KO + BFGS	1	3	4	4	5	5	6	6	8	42	66
KT1 + BFGS	1	3	3	4	5	5	5	5	6	37	67
KT2 + BFGS	1	2	2	2	2	4	4	2	4	23	46

TABLE 6.4 – Iterations per load step for BFGS solutions of the thick cylinder with internal and external pressure

Load step	1	2	3	4	5	6	7	8	9	Σ	CPU
KO + SN1	1	3	5	5	5	6	6	6	7	44	68
KO + SN2	1	3	5	4	5	5	6	6	7	42	64
KO + SN3	1	4	5	4	5	6	6	7	11	49	76
KO + SN4	1	3	4	4	5	6	6	7	7	42	65
KT1 + SN1	1	3	3	3	5	5	5	5	6	36	65
KT1 + SN2	1	3	3	3	5	5	5	5	6	36	64
KT1 + SN3	1	4	4	4	5	5	5	5	7	40	69
KT1 + SN4	1	3	3	3	5	5	5	5	6	36	64
KT2 + SN1	1	2	2	2	2	4	4	2	4	23	46
KT2 + SN2	1	2	2	2	2	4	4	2	4	23	47
KT2 + SN3	1	2	2	2	2	4	4	2	4	23	46
KT2 + SN4	1	2	2	2	2	4	4	2	4	23	46

TABLE 6.5 – Iterations per load step for secant-Newton solutions of the thick cylinder with internal and external pressure

	KT1	KT1+BFGS	KT1+SN1	KT1+SN2	KT1+SN3	KT1+SN4
Iter.	DIV	6	6	65	72	6
CPU	>350	77	76	188	185	74

TABLE 6.6 – Unloading test for the thick cylinder with internal and external pressure

Load step	1	2	3	4	5	6	7	8	9	Σ	CPU
KO											
no LS	1	6	8	9	12	14	18	26	48	142	229
.1	1/ 0	2/ 1	4/ 4	6/ 5	6/ 6	8/ 7	8/ 8	12/11	15/15	62/57	184
.2	1/ 0	2/ 1	3/ 2	6/ 5	6/ 6	8/ 7	6/ 5	8/ 7	10/ 9	50/42	133
.3	1/ 0	2/ 1	3/ 2	4/ 3	5/ 3	5/ 3	6/ 5	8/ 7	10/ 9	44/33	116
.4	1/ 0	2/ 1	5/ 1	5/ 1	6/ 3	6/ 3	7/ 5	10/ 7	18/15	60/36	153
.5	1/ 0	6/ 0	8/ 0	5/ 1	6/ 2	7/ 3	8/ 3	10/ 7	18/15	69/31	160
KT1											
no LS	1	6	6	7	8	7	7	8	13	63	105
.1	1/ 0	2/ 1	2/ 1	2/ 1	4/ 4	4/ 2	3/ 2	4/ 2	6/ 6	28/19	79
.2	1/ 0	2/ 1	2/ 1	2/ 1	4/ 2	4/ 2	3/ 2	4/ 2	6/ 4	28/15	74
.3	1/ 0	2/ 1	2/ 1	2/ 1	4/ 2	4/ 2	3/ 2	4/ 2	6/ 4	28/15	74
.4	1/ 0	2/ 1	2/ 1	2/ 1	5/ 1	4/ 2	3/ 2	5/ 1	6/ 4	30/13	76
.5	1/ 0	6/ 0	6/ 0	7/ 0	8/ 0	7/ 0	7/ 0	5/ 1	7/ 3	57/ 4	97
KT2											
no LS	1	2	2	2	2	5	4	2	6	26	54
.1	1/ 0	2/ 0	2/ 0	2/ 0	2/ 1	3/ 1	3/ 2	2/ 1	3/ 2	20/ 7	52
.2	1/ 0	2/ 0	2/ 0	2/ 0	2/ 0	3/ 1	3/ 1	2/ 0	3/ 1	20/ 3	46
.3	1/ 0	2/ 0	2/ 0	2/ 0	2/ 0	3/ 1	3/ 1	2/ 0	3/ 1	20/ 3	46
.4	1/ 0	2/ 0	2/ 0	2/ 0	2/ 0	3/ 1	3/ 1	2/ 0	3/ 1	20/ 3	46
.5	1/ 0	2/ 0	2/ 0	2/ 0	2/ 0	5/ 0	4/ 0	2/ 0	6/ 0	26/ 0	54

TABLE 6.3 – Iterations/additional state determinations per load step for several TOLSR values for MNR solutions of the thick cylinder with internal and external pressure

In Table 6.3 we analyse the effect of line searches (LS) in the MNR solutions and perform a parametric study of the optimum value for the search tolerance parameter (TOLSR): a value around 0.3 seems most adequate. The remarkable CPU time savings brought about by line searching are 15%, 30% and 49%, respectively for KT2, KT1 and K0 (with TOLSR = 0.3).

Table 6.4 reports on the performance of the BFGS method combined with various MNR possibilities and Table 6.5 presents a similar study for the secant-Newton method: leaving aside the SN1 and, in particular, the SN3 formulas as slower options, the SN2 and SN4 algorithms are very successful and appear to be slightly faster than BFGS.

The inclusion of line searches was also considered and a systematic variation of TOLSR was undertaken but for this particular problem this refinement did not bring any savings.

Our final test examines the ability of the various methods to recover from a bad initial "guess" for the global stiffness matrix. The load is reduced after the ninth load step from 1800. to 1400. and the automatic resetting of $\underline{K}_T$ to $\underline{K}_0$ described in 6.4.2 is intentionally bypassed. Table 6.6 registers the total CPU time and the number of iterations corresponding to the unloading step. The KT1 solution diverges as expected but all the others converge for the correct result, even when requiring many iterations as in the case of SN2 and SN3. Both BFGS and SN (formulas 1 and 4) manage to correct in 6 iterations the tangential elastoplastic stiffness (corresponding to 7.5 plastic elements out of a total of 10) taken as the starting value $\overline{\underline{K}}$. Considering that the unloading phase is elastic this may be considered a quite impressive performance.

6.11.2 Notched bar uniaxially loaded

A bar of length 60. and maximum width 20. has two circular notches of radius 5., as depicted in Table 6.7 where the mesh corresponding to one quarter of the bar is presented, together with the material properties.

A uniaxial loading program of 10 steps is applied under plane strain conditions: the distributed load p increases from 42500. to 77500. in 7 steps of 5000., and then to 82500. in two steps of 2500.

Fig. 6.6 shows the spread of the plastic zone for load steps 2, 4, 6, 8 and 10, and fig. 6.7 presents the corresponding curves of ε_x, ε_y, σ_x and σ_y at Gauss point layer AA.

Table 6.8 compares iterations and additional state determinations per load step and CPU time (in seconds on a CDC7600) required by various solution strategies. Again we note the effectiveness of LS (with TOLSR = 0.3) in speeding up MNR. Once more SN is marginally ahead of BFGS and no improvement resulted from combining these methods with line searches. The divergence of the KT2 solution was obviated by halving the load step size and it is worth stressing the stabilizing effect of the BFGS and SN operations on KT2. The KTN strategy described in section 6.4.4 performs well (with TOLKT = 10%).

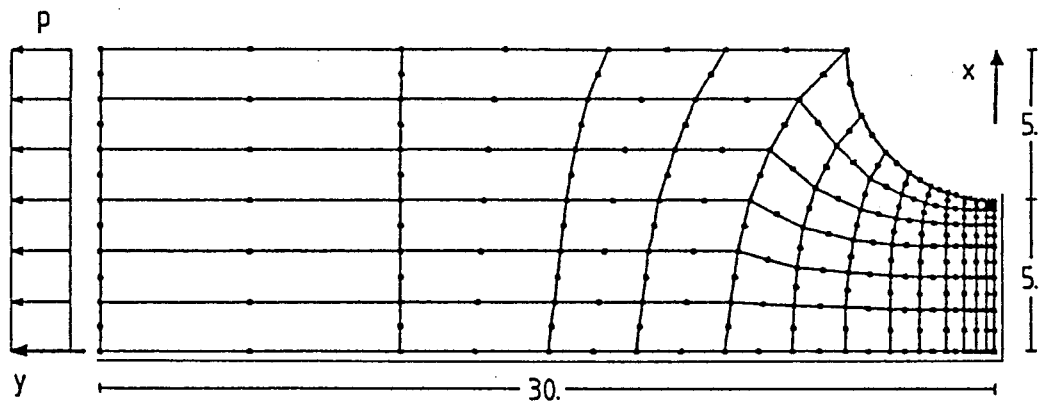

Elastic modulus, E = 2.853E7	von Mises
Poisson's ratio, ν = 0.299	78 elements
Initial yld.st., Yo = 1.210E5	273 nodes
Hardng.paramet., H' = 0.0	2x2 Gauss points

TABLE 6.7 – Mesh and material properties for the notched bar

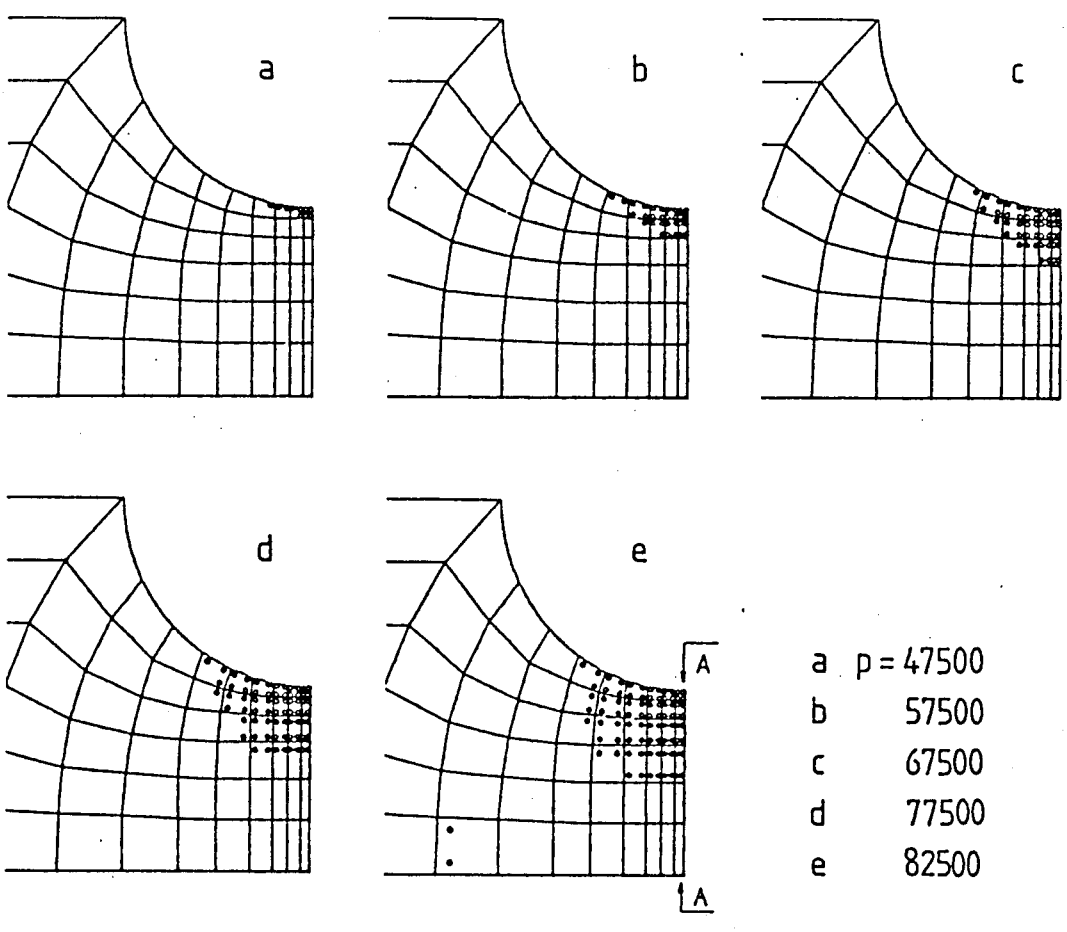

Fig. 6.6 – Plastic Gauss points at load steps 2, 4, 6, 8 and 10 for the notched bar

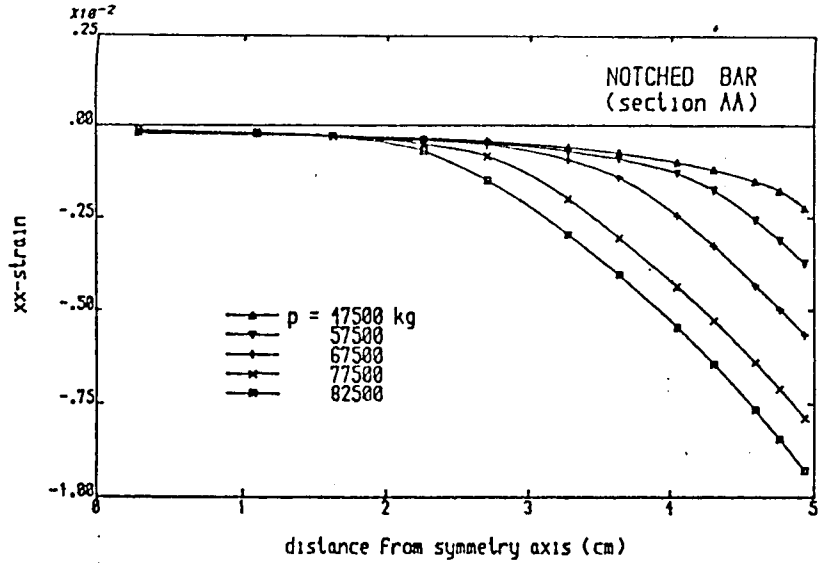

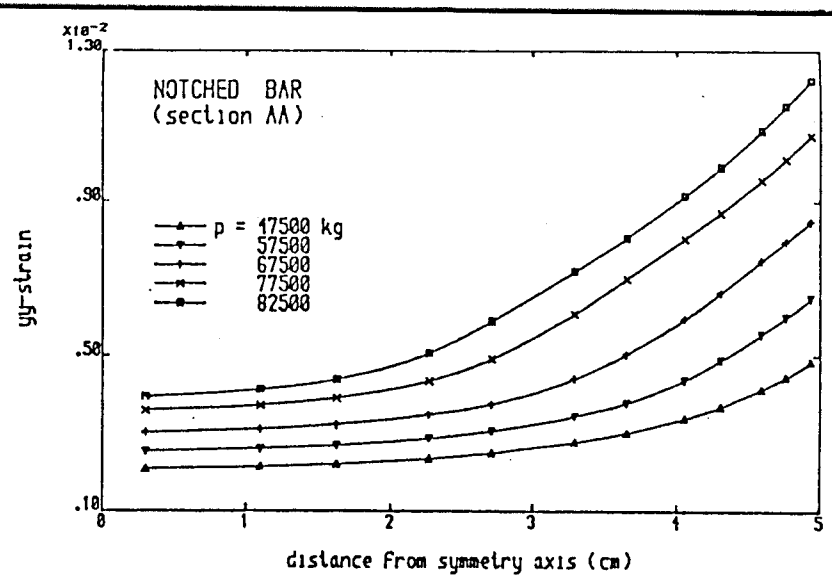

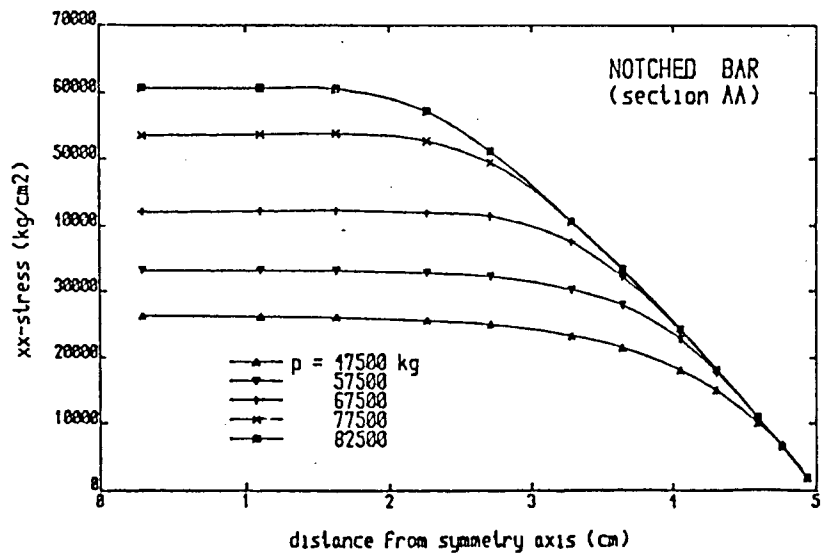

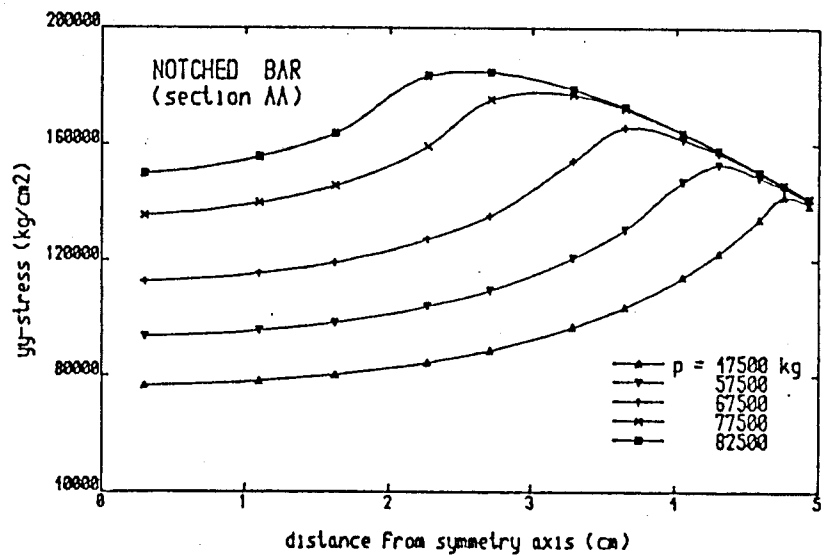

Fig. 6.7 – Curves of ε_x, ε_y, σ_x and σ_y at Gauss point layer AA (fig. 6.6) for load steps 2, 4, 6, 8 and 10 of the notched bar problem

Load step	1	2	3	4	5	6	7	8	9	10	Σ	CPU
KO	1	5	6	8	11	11	14	16	13	15	100	52.1
KO + LS	1/0	2/1	4/2	5/3	6/4	6/4	8/6	8/6	6/4	7/5	53/35	35.5
KO + BFGS	1	3	5	6	7	8	9	9	8	8	64	35.4
KO + SN1	1	3	5	6	7	7	8	10	12	7	66	35.0
KO + SN2	1	3	5	6	7	8	9	11	10	8	68	36.1
KO + SN3	1	3	5	6	7	8	10	10	10	10	70	37.1
KO + SN4	1	3	5	6	7	8	10	8	8	8	64	33.9
KT1	1	5	5	5	5	6	6	8	4	4	49	29.5
KT1 + LS	1/0	2/1	4/1	4/1	5/0	4/1	5/1	4/1	4/0	4/0	37/ 6	24.3
KT1 + BFGS	1	3	4	4	3	4	5	5	3	4	36	23.3
KT1 + SN1	1	3	4	4	3	4	5	6	4	4	38	24.0
KT1 + SN2	1	3	4	4	3	4	5	5	3	4	36	23.0
KT1 + SN3	1	3	4	4	3	4	5	5	3	4	36	23.0
KT1 + SN4	1	3	4	4	3	4	5	5	3	4	36	23.0
KT2	1	2	3	3	3	3	4	DIV.				
KT2 + BFGS	1	2	3	3	3	3	4	4	4	3	30	20.6
KT2 + SN1	1	2	3	3	3	3	4	4	4	3	30	21.3
KT2 + SN2	1	2	3	3	3	3	4	4	4	3	30	20.5
KT2 + SN3	1	2	3	3	3	3	4	4	4	3	30	20.5
KT2 + SN4	1	2	3	3	3	3	4	4	4	3	30	20.5
KTN	1	3	4	3	4	4	4	3	3	3	32	20.9
KT	1	2	3	3	3	3	3	4	4	3	29	26.7

TABLE 6.8 – Iterations/additional state determinations per load step for various solutions of the notched bar problem

6.11.3 Tee junction under internal pressure

A tee junction of von Mises material is subjected to four internal pressure levels of increasing magnitude (p_1= 5000, p_2= 6500, p_3= 8000, p_4= 9000). By virtue of symmetry only one quarter of the tee junction is analysed. Fig. 6.8 presents views of the 3D mesh which comprises 113 twenty-node brick elements with a total of 800 nodes. The internal radii of the cylindrical tubes are 66.5 and 40.3 and their axes coincide respectively with the global x and z axes (z lies vertically in fig. 6.8). In addition to the boundary conditions related to symmetry, zero displacements in the axial direction were prescribed at the tube ends (situated at x = 200. and z = 70.). Yielding starts at the "neck" of the junction and spreads as depicted in the mesh details of fig. 6.8. The number of plastic Gauss points for each load level is 7, 47, 127 and 211. The deformed mesh views presented in fig. 6.8 for p = p_4 help to relate visually the patterns of deformation and yielding. In Table 6.9 are compared the costs of various solutions. As should be expected full NR in 3D is very expensive indeed. Line searches (with TOLSR = 0.3) clearly improve once again the MNR-KT1 solution. The BFGS and the four secant Newton formulas show a similar performance with SN4 slightly faster than the rest.

E = 3E7	Internal pressure	- 4 load levels
ν = 0.3	Internal radii	- 66.5 and 40.3
Yo = 2E5	Thickness(variable)	- 2.3 to 6.65
H' = 0.0	Ends axially restrained	von Mises

113(20-node)elements - 800 nodes - 2*2*2 Gauss points

Load step	1	2	3	4	Σ	CPU
KT	2	2	3	3	10	5943
KT1	2	3	8	6	19	3590
KT1 + LS	2/0	3/1	4/2	3/2	12/5	3285
KT1 + BFGS	2	3	4	4	13	3201
KT1 + SN1	2	3	4	4	13	3215
KT1 + SN2	2	3	4	4	13	3188
KT1 + SN3	2	3	4	4	13	3192
KT1 + SN4	2	3	4	4	13	3160

TABLE 6.9 - Tee junction problem data and comparison of iterations/additional state determinations per load step and CPU times (secs. ICL 2966)

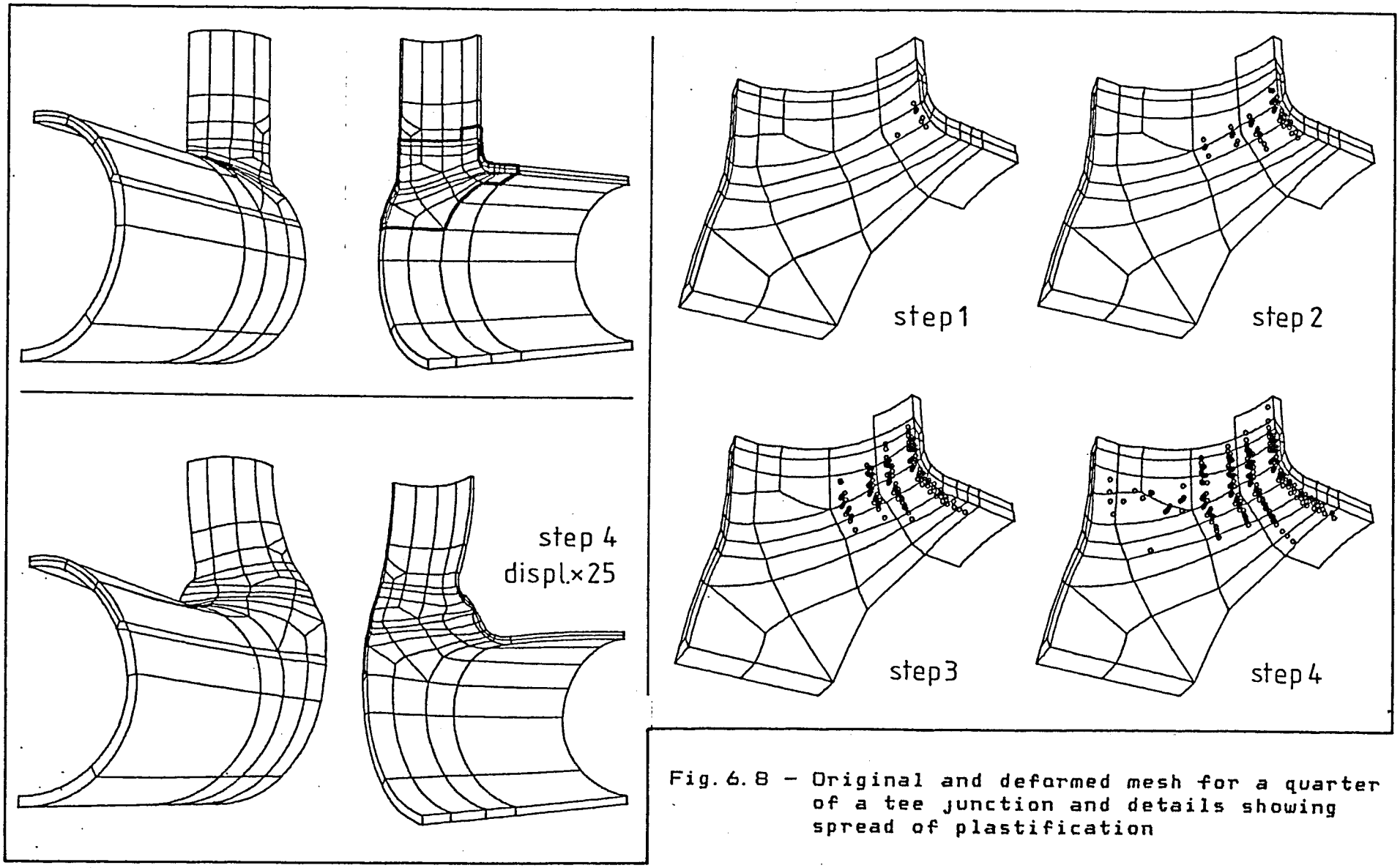

Fig. 6.8 – Original and deformed mesh for a quarter of a tee junction and details showing spread of plastification

6.11.4 Snap-through of shallow circular arch

The shallow circular arch of Table 6.10 has a prescribed vertical displacement δ of 6 mm at node A, applied in 15 equal increments of 0.4 mm. This loading program provokes the snap through of the arch, as documented by fig. 6.9, that relates the vertical displacement and applied load P at the crown A. Fig. 6.10 describes the variation of the horizontal thrust H at the hinged support as a function of the vertical load P at A. The finite element geometrically nonlinear results are seen to agree well with the analytical solution [76].

Values of CPU time and iterations per step are compared in Table 6.10 for various solution strategies. The K0 method diverges when the peak of the load-displacement curve of fig. 6.9 is reached. The KT and KT1 solutions require more iterations between steps 5 and 11, that delimit the branch of P-δ with negative slope in fig. 6.9. The fastest solutions are provided by BFGS, SN2 and SN4 with identical efficiency. Line searches were also tried but no improvement resulted.

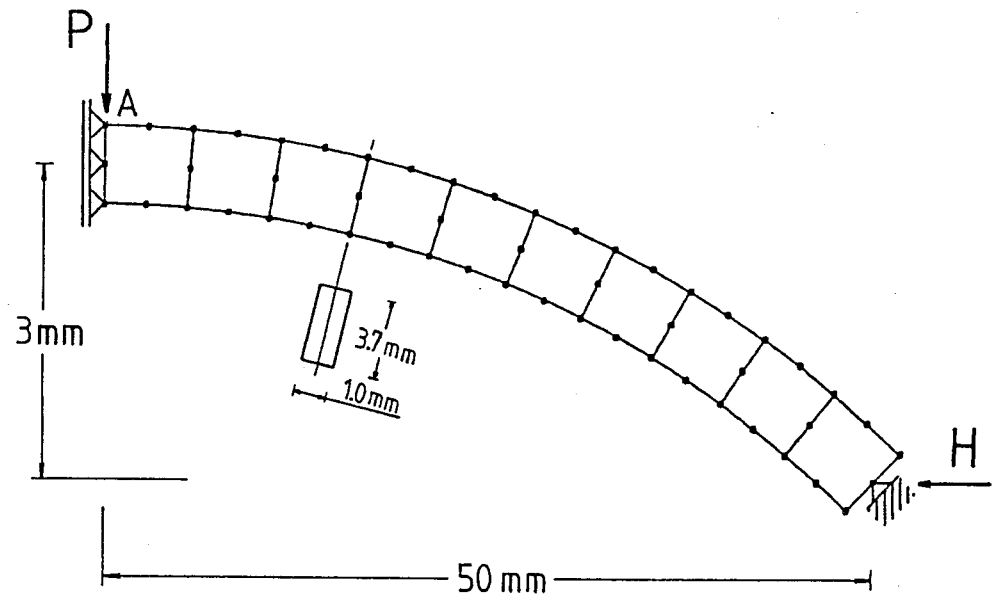

Elastic modulus, E = 1.E4 kN/mm2 — 53 nodes
Poisson's ratio, ν = 0.3 — 10 elements

STEP	KT	KO	KT1	KT1 BFGS	KT1 SN1	KT1 SN2	KT1 SN3	KT1 SN4
1	1	1	1	1	1	1	1	1
2	5	4	4	4	3	4	4	4
3	5	5	4	4	3	4	4	4
4	5	6	5	4	4	4	4	4
5	6	15	5	4	4	4	4	4
6	6	DIV	6	4	4	4	4	4
7	7		6	4	4	4	4	4
8	7		7	4	4	4	5	4
9	7		7	4	4	4	5	4
10	7		7	4	4	4	5	4
11	7		7	4	4	4	5	4
12	6		6	4	6	4	5	4
13	5		6	4	6	4	5	4
14	5		5	4	6	4	4	4
15	4		4	4	5	4	4	4
Σ	83	–	80	57	62	57	63	57
CPU	327	–	144	115	121	115	123	115

TABLE 6.10 – Geometrical and material data, comparison of iterations per step and CPU times (secs. ICL 1904S) for a shallow circular arch

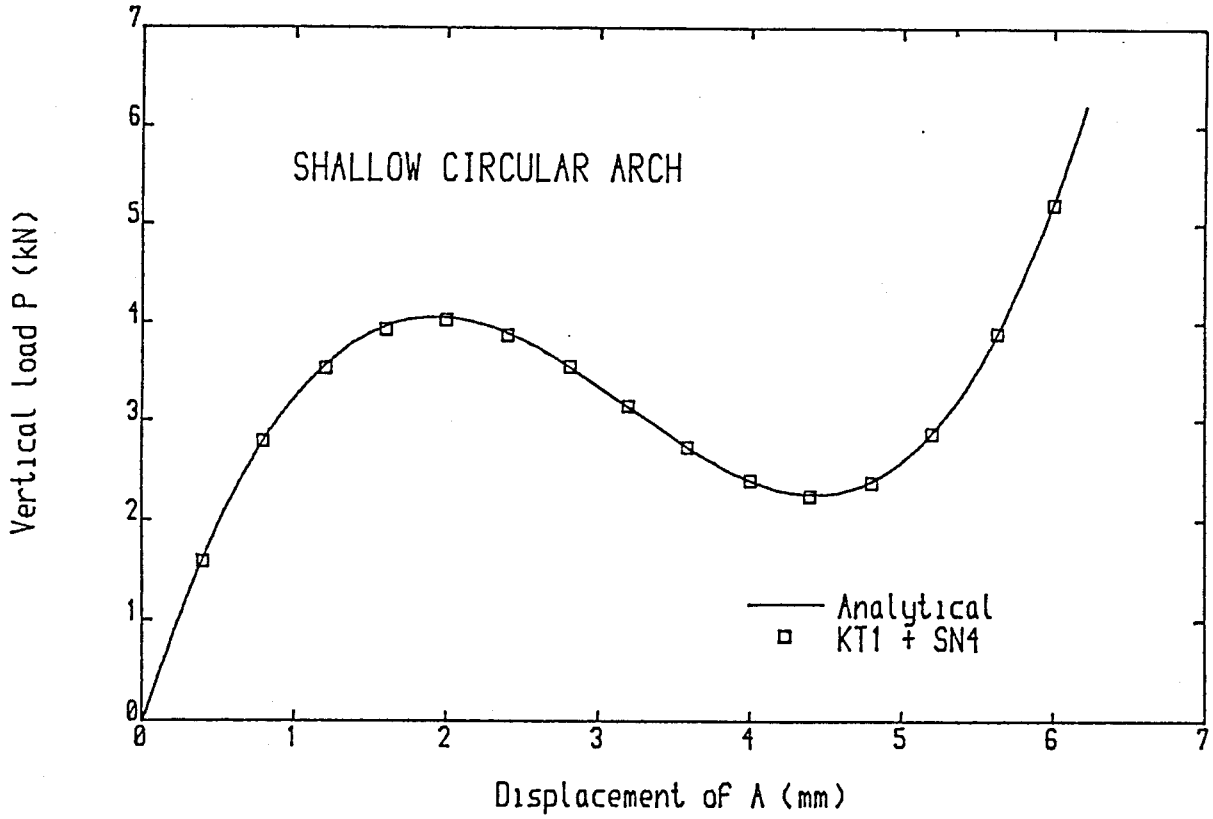

Fig. 6.9 – Applied load vs vertical displacement at crown for a shallow circular arch

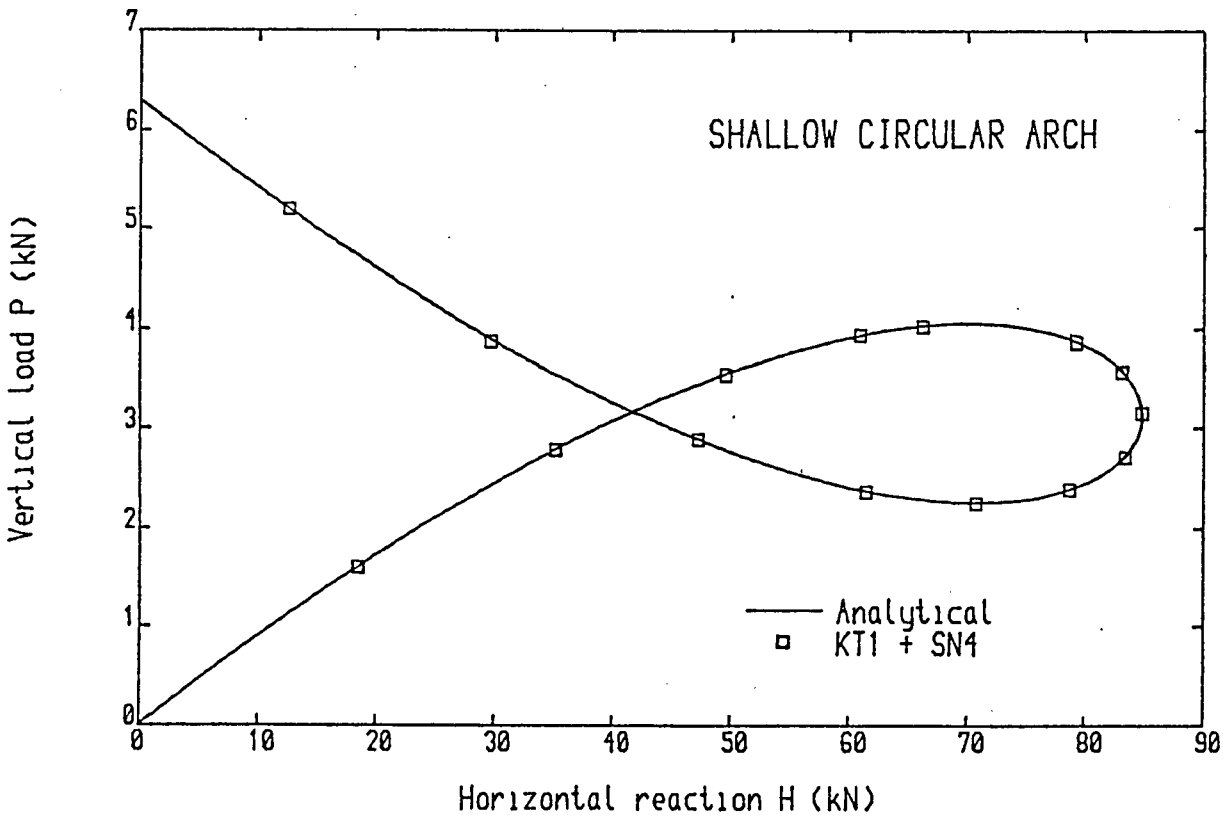

Fig. 6.10 – Applied load at crown vs horizontal reaction for a shallow circular arch

6.11.5 Large deflection analysis of a simply supported plate

The total load applied to the simply supported circular plate of Table 6.11 is raised to 30,000 lb in 30 equal increments and then completely removed after 10 unloading steps of 3,000 lb. The numerical results follow closely the experimental data [77], as shown in fig. 6.11, where can also be detected the change from softening to stiffening response due to the combined effect of material and geometric nonlinearity. This causes the KT1 run to diverge and affects all other solutions to some extent between steps 13 and 23.

The BFGS, SN2 and SN4 methods are the best performers under this severe test, with the SN2 slightly ahead.

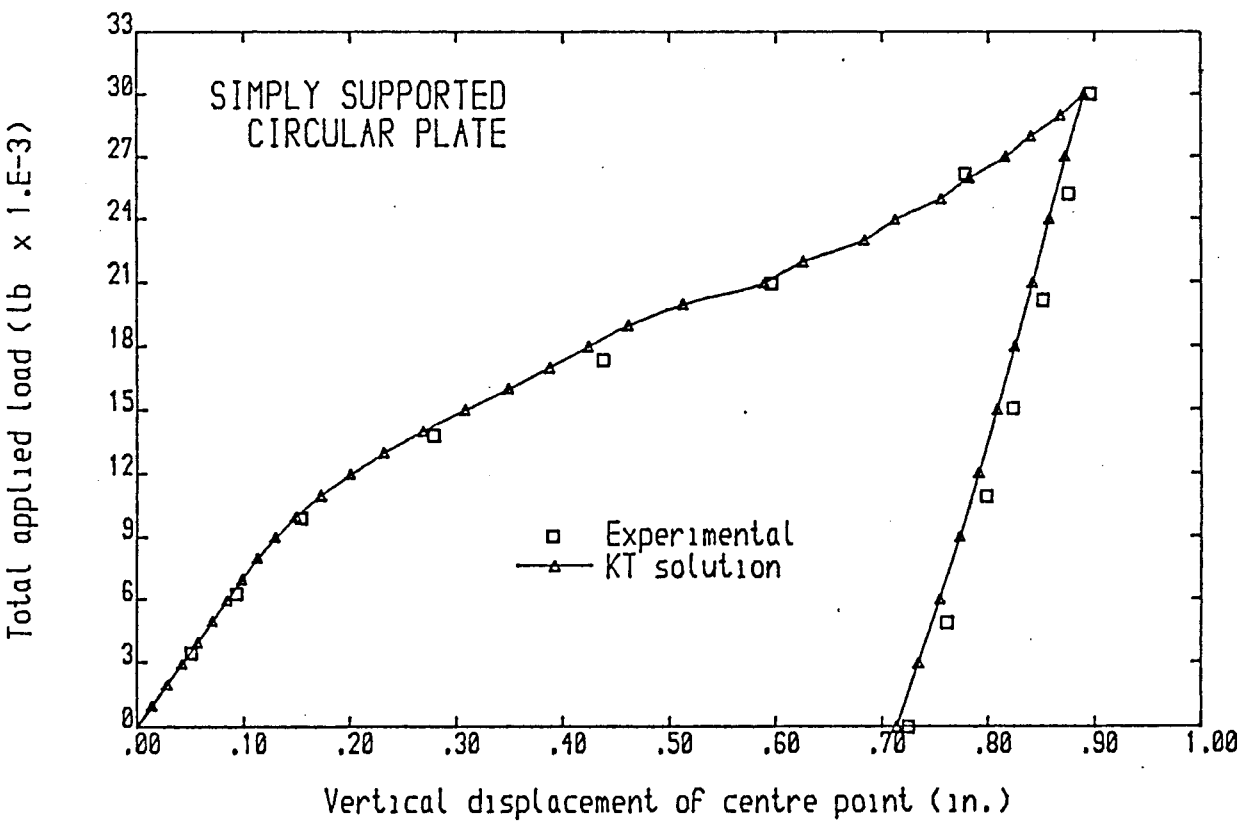

Fig. 6.11 – Load vs deflection for a simply supported circular plate

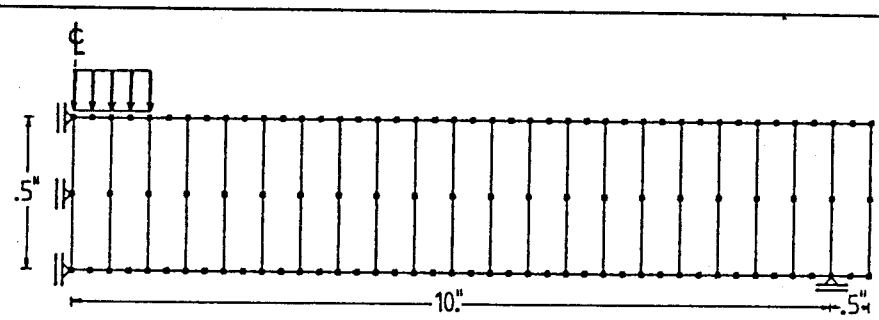

Elastic modulus, E = 3.0E7 psi
Poisson's ratio, ν = 0.3
Initial yld. st., Yo = 32.E3 psi
Hardng. paramet., H' = 1.0E6 psi

von Mises
21 elements
108 nodes
2x2 Gauss points

TOTAL LOAD	KT	KT1	KT1 BFGS	KT1 SN1	KT1 SN2	KT1 SN3	KT1 SN4
1.	1	1	1	1	1	1	1
2.	4	4	4	6	4	4	4
3.	4	4	4	6	4	4	4
4.	4	4	4	6	4	4	4
5.	4	4	4	6	4	4	4
6.	4	4	4	6	4	4	4
7.	4	4	4	6	4	4	4
8.	4	16	7	6	6	7	7
9.	4	12	8	9	8	8	8
10.	5	10	7	8	7	7	7
11.	5	7	5	6	5	5	5
12.	5	7	5	6	5	5	5
13.	5	6	5	10	5	5	5
14.	6	7	5	11	5	5	5
15.	6	DIV.	10	8	12	12	10
16.	6		9	9	9	10	9
17.	7		5	13	5	6	5
18.	6		5	9	5	5	5
19.	7		5	9	5	6	5
20.	12		7	11	7	8	8
21.	16		6	17	7	8	7
22.	10		5	11	6	8	8
23.	11		6	10	6	6	6
24.	7		6	7	6	6	7
25.	9		5	7	5	6	5
26.	5		6	6	6	6	6
27.	8		5	7	5	6	5
28.	4		5	5	5	5	6
29.	7		5	6	5	5	5
30.	5		5	5	5	5	5
27.	4		4	4	4	4	4
24.	4		4	4	4	4	4
21.	4		4	5	4	4	4
18.	4		4	6	4	4	4
15.	4		4	4	4	4	4
12.	4		4	4	4	4	4
9.	4		4	4	4	4	4
6.	4		4	4	4	4	4
3.	4		4	4	4	4	4
0.	5		4	4	4	4	4
Σ	226	-	202	276	209	219	213
CPU	82.4	-	45.0	56.7	44.3	46.0	44.9

TABLE 6.11 - Geometrical and material data, comparison of iterations per step and CPU times (secs. CDC 7600) for a simply supported circular plate

6.11.6 Dynamic analysis of a spherical shell

The clamped spherical shell of Table 6.12 is submitted to a distributed step pressure of 600 psi. The fundamental and smallest time periods of the shell are, respectively, T_f= 0.592E-3 and T_ℓ = 0.776E-6 secs. [54]. A similar shell but with all 10 elements of "soft" material was analysed by Bathe [78] that gives for that problem T_f^*= 0.547E-3 and T_ℓ^*= 1.38E-6 secs. In our case the implicit-explicit technique (with 2 implicit "stiff" elements at the crown) is more economical than the explicit solution. The time step lengths for accurate implicit, explicit and implicit-explicit integration are, respectively, $t_I = T_f/100$ = 0.6E-5, $t_E = T_\ell/\pi$ = 0.25E-6 and $t_{IE} = T_\ell^*/\pi$ = 0.4E-6 secs. The CPU times for analyses by the 3 methods carried out over equal total time are approximately in the ratio IMP : I-E : EXP = 1 : 5 : 7.5. Table 6.12 shows the typical displacement history of the shell crown. For 200 time steps of implicit integration the BFGS, SN2 and SN4 methods (with KT1) require CPU times of 425, 418 and 415 (secs. in ICL 2966) and the total number the iterations performed is 742, 730 and 723 , respectively.

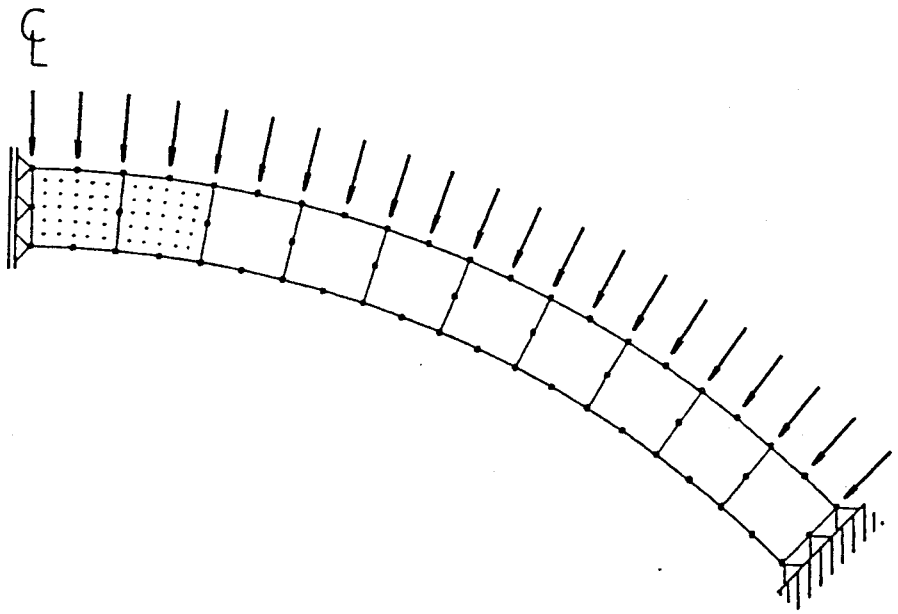

Internal radius, R = 22.27 in		10 elements
Shell thickness, t = 0.41 in		53 nodes
Semi-angle, α = 26°67		von Mises

	Stiff zone (2 elemts.)	Soft zone (8 elmts.)
Elastic modulus, E (psi)	1.05 E+8	1.05 E+7
Poisson's ratio, ν	0.30	0.30
Initial yld. st., Y_o (psi)	0.50 E+5	0.24 E+5
Hardng. paramet., H' (psi)	0.00	2.14 E+5
Mass density, ρ (lb. s^2/in^4)	7.80 E-4	2.45 E-4

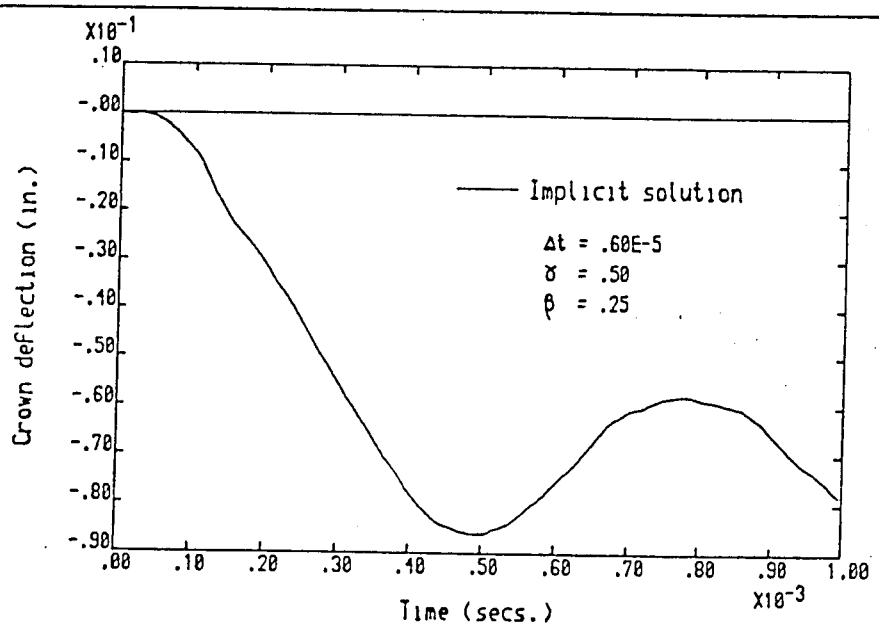

TABLE 6.12 – Geometrical and material data for the spherical shell problem and typical displacement history of the crown

6.12 CONCLUDING REMARKS

Several nonlinear solution techniques have been described and extensively tested in a variety of practical applications that included material and/or geometrical nonlinearities, quasi-static and dynamic loading programs as well as prescribed boundary displacements, in plane stress, plane strain axisymmetric and three-dimensional situations.

The inclusion of line searches in MNR solutions proves beneficial, resulting in substantial savings in computer time (specially evident with KO).

BFGS and SN methods are very efficient. The versions SN2 and SN4 of the latter are the best performers. In particular the newly developed SN4 formula consistently provides expedient solution, showing good recovery from bad initial guesses for the global stiffness. Preliminary investigations have in addition indicated that this new formula has good stability characteristics that allow for a less tight bound check procedure for A, B and C.

6.13 REFERENCES

1. CLOUGH, R.W., The finite element in plane stress analysis, Proc. 2nd ASCE Conf. on Electronic Computation, Pittsburgh, Pa., Sep. 1960

2. TURNER, M.J., CLOUGH, R.W., MARTIN, H.C. and TOPP, L.J., Stiffness and deflection analysis of complex structures, J. Aero. Sci., 23, 805-23, 1956

3. TURNER, M.J., DILL, E.H., MARTIN, H.C. and MELOSH, R.J., Large deflections of structures subjected to heating and external loads, J. Aero. Sci., 27, 97-106, 1960

4. PADLOG,J., HUFF, R.D. and HOLLOWAY, G.F., The unelastic behaviour of structures subjected to cyclic, thermal and mechanical stressing conditions, Bell Aerosystems Company, Report WPADD TR 60-271, 1960

5. GALLAGHER, R.H., PADLOG, J. and BILJAARD, P.P., Stress analysis of heated complex shapes, J. Am. Rocket Soc., 32, 700-707, 1962

6. ARGYRIS, J.H., Recent advances in matrix methods of structural analysis, Progress in Aeronautical Science, Vol. 4, Pergamon Press, N.Y., 1964

7. HAISLER, W.E., STRICKLIN, J.A. and STEBBINS, F.J., Development and evaluation of solution procedures for geometrically nonlinear structural analysis, JAIAA, 10, 264-272, 1972

8. ARGYRIS, J.H., Elastic-plastic matrix displacement analysis of three-dimensional continua, J.R. Aero. Soc., 69, 633-635, 1965

9. ZIENKIEWICZ, O.C., The Finite Element Method, 3rd edition, McGraw-Hill, London 1977

10. IRONS, B. and ELSAWAF, A., The conjugate Newton algorithm for solving finite element equations, in Formulations and Comp. Alg. in F.E. Analysis, 655-672, K.J.Bathe et al. (eds.), MIT Press, 1977

11. MATTHIES, H. and STRANG, G., The solution of nonlinear finite element equations, IJNME, 14, 1613-1626, 1979

12. CRISFIELD, M.A., Incremental/iterative solution procedures for nonlinear structural analysis, in Numerical Methods for Nonlinear Problems, 261-290, C. Taylor et al. (eds.), Pineridge Press, Swansea, 1980

13. BATHE, K.J. and CIMENTO, A.P., Some practical procedures for the solution of nonlinear finite element equations, Comp. Meth. App. Mech. Engng., 22, 59-85, 1980

14. AITKEN, A.C., On Bernoulli's numerical solution of algebraic equations, Proc. Roy. Soc. Edinburgh, 46, 289-305, 1926

15. JENNINGS, A., Accelerating the convergence of matrix iterative processes, J. Inst. Math. App., 8, 99-110, 1971

16. IRONS, B.M. and TUCK, R., A version of the Aitken acceleration for computer iteration, IJNME, 1, 275-277, 1969

17. NAYAK, G.C. and ZIENKIEWICZ, O.C., Note on the 'alpha' - constant stiffness method for the analysis of non-linear problems, IJNME, 4, 579-582, 1972

18. NAYAK, G.C., Plasticity and large deformation by the finite element method, Ph.D. Thesis, Univ. of Wales, Swansea, 1971

19. BASU, A.K., New light on the Nayak technique, IJNME, 6, 152, 1973

20. RAASER, H., A note to Alpha constant stiffness method, IJNME, 9, 252, 1975

21. COCHET, J.F. and DHATT, G.S., A modification of the Alpha constant technique, IJNME, 11, 1053-1054, 1977

22. IRONS, B.M. and AHMAD, S., Techniques of Finite Elements, Ellis Horwood, Chichester, 1980

23. OTTER, J.R.M., Dynamic relaxation, Proc. Inst. Civ. Eng., 35, 633-656, 1966

24. CRISFIELD, M.A., Iterative solution procedures for linear and non-linear structural analysis, TRRL Rep. 900, 1979

25. ZIENKIEWICZ, O.C. and LÖHNER, R., Accelerated 'relaxation' or direct solution? Future prospects for FEM, Report C/R/465/83, Dep. Civ. Eng., Univ. Coll. Swansea, 1983

26. HUGHES, T.J.R. and LIU, W.K., Implicit-explicit finite elements in transient analysis: stability theory,J.Appl. Mech., 45, 371-374, 1978

27. BATHE, K.J., An assessment of current finite element analysis of nonlinear problems in solid mechanics, in Numerical Solution of Partial Differential Equations - III, 117-164, B. Hubbard (ed.), Academic Press, 1976

28. BATHE, K.J., RAMM, E. and WILSON, E.L., Finite element formulations for large deformation dynamic analysis, IJNME, 9, 353-386, 1975

29. ABDEL RAHMAN, H.H., Computational Models for the Nonlinear Analysis of Reinforced Concrete Flexural Slab Systems, Ph.D. Thesis, Univ. of Wales, Swansea, 1982

30. DAHLQUIST, G. and BJÖRCK, Å., Numerical Methods, Prentice-Hall, Englewood Cliffs, N.J., 1974

31. DAVIDON, W.C., Variable metric method for minimization, Rep. ANL-5990 Rev., Argonne Nat. Lab., 1959

32. BROYDEN, C.G., A class of methods for solving nonlinear simultaneous equations, Math. Comp., 19, 577-593, 1965

33. DENNIS, J.E. and MORÉ, J.J., Quasi-Newton methods, motivation and theory, SIAM Rev., 19, 46-89, 1977

34. MURTAGH, B.A. and SARGENT, R.W.H., Computational experience with quadratically convergent minimisation methods, Comput. J., 13, 185-194, 1970

35. BRODLIE, K.W., GOURLAY, A.R. and GREENSTADT, J., Rank-one and rank-two corrections to positive definite matrices expressed in product form, J. Inst. Math. Applics., 11, 73-82, 1973

36. FLETCHER, R. and POWELL, M.J.D., A rapidly convergent descent method for minimization, Comput. J., 6, 163-168, 1963

37. BROYDEN, C.G., A new double-rank minimization algorithm, Notices Amer. Math. Soc., 16, 670, 1969

38. FLETCHER, R., A new approach to variable metric algorithms, Comput. J., 13, 317-322, 1970

39. GOLDFARB, D., A family of variable-metric methods derived by variational means, Math. Comp., 24, 23-26, 1970

40. SHANNO, D.F., Conditioning of quasi-Newton methods for function minimization, Math. Comp., 24, 647-656, 1970

41. DIXON, L.C.W., The choice of step length, a crucial factor in the performance of variable metric algorithms, in Numerical Methods for Nonlinear Optimization, F.A. Lootsma (ed.), Academic Press, London, 1972

42. GERADIN, M., IDELSOHN, S. and HOGGE, M., Nonlinear structural dynamics via Newton and quasi-Newton methods, Nuc. Eng. and Design, 58, 339-348, 1980

43. GERADIN, M., IDELSOHN, S. and HOGGE, M., Computational strategies for the solution of large nonlinear problems via quasi-Newton methods, Comp. & Str., 13, 73-81, 1981

44. PICA, A. and HINTON, E., The quasi-Newton BFGS method in the large deflection analysis of plates, in Numerical Methods for Nonlinear Problems, 355-366, C. Taylor et al. (eds.), Pineridge Press, Swansea, 1980

45. HINTON, E. and ABDEL RAHMAN, H.H., Nonlinear solution algorithms for reinforced concrete plates, paper M3/4, 6th SMiRT, Paris, 1981

46. OWEN, D.R.J. and GOMES, C.M.B.R., An appraisal of numerical solution techniques for nonlinear problems, paper M3/1, 6th SMiRT, Paris, 1981

47. OWEN, D.R.J. and GOMES, C.M.B.R., Some recent developments in solution techniques for nonlinear finite element problems, in Aplicaciones del Método de los Elementos Finitos en Ingenieria, VII 137-153, E. Oñate et al. (eds.), Barcelona, 1982

48. GOMES, C.M.B.R., Matrix update methods in nonlinear analysis of two dimensional and thin shell problems, Ph.D. thesis, Univ. of Wales, Swansea, 1982

49. OWEN, D.R.J., HINTON, E. and ABDEL RAHMAN, H.H., Finite Elements in Nonlinear Stress Analysis: an Introduction, Pineridge Press, Swansea (in preparation)

50. BRODLIE, K.W., Unconstrained minimization, in The State of the Art in Numerical Analysis, D.A.H. Jacobs (ed.), Academic Press, 1977

51. CRISFIELD, M.A., Accelerated solution techniques and concrete cracking, Proc. FENOMECH 2, Comp. Meth. Appl. Mech. Engng., 33, 585-607, 1982

52. HINTON, E., ABDEL RAHMAN, H.H. and ZIENKIEWICZ, O.C., Computational strategies for reinforced concrete slab systems, in Advanced Mechanics of Reinforced Concrete Structures, IABSE Colloquium, Final Report, 303-313, Delft, 1981

53. CRISFIELD, M.A., A faster modified Newton-Raphson iteration, Comp. Meth. Appl. Mech. Engng, 20, 267-278, 1979

54. OWEN, D.R.J. and HINTON, E., Finite Elements in Plasticity - Theory and Practice, Pineridge Press, Swansea, 1980

55. BERGAN, P.G. and SOREIDE, T.H., Solution of large displacement and instability problems using the current stiffness parameter, in Finite Elements in Nonlinear Mechanics, 647-669, P.G. Bergan et al. (eds.), Tapir, Trondheim, 1978

56. BERGAN, P.G., HORRIGMOE, G., KRAKELAND, B. and SOREIDE, T.H., Solution techniques for non-linear finite element problems, IJNME, 12, 1677-1696, 1978

57. OWEN, D.R.J., Implicit finite element methods for the dynamic transient analysis of solids with particular reference to non-linear situations, in Advanced Structural Dynamics, 123-152, J. Donea (ed.), Applied Science Publishers, 1980

58. LIU, W.K. and BELYTSCHKO, T., Mixed-time implicit-explicit finite elements for transient analysis, Comp. & Struct., 15, 445-450, 1982

59. HUGHES, T.R.J., Implicit-explicit finite element techniques for symmetric and nonsymmetric systems, in Recent Advances in Non-linear Computational Mechanics, 255-267, E. Hinton et al. (eds.), Pineridge Press, Swansea, 1982

60. CRISFIELD, M.A., Solution procedures for non-linear structural analysis, idem, 1-39

61. BERGAN, P.G., Automated incremental-iterative solution methods in structural mechanics, idem, 41-62

62. RAMM, E., The Riks-Wempner approach - an extension of the displacement control method in nonlinear analysis, idem, 63-86

63. ARGYRIS, J.H., Continua and discontinua, Proc. 1st. Conf. Matrix Meth. Struct. Mech., 11-189, Wright-Patterson A.F.B., Ohio, 1965

64. ZIENKIEWICZ, O.C., Incremental displacement in nonlinear analysis, IJNME, 3, 587-588, 1971

65. BATOZ, J.L. and DHATT, G., Incremental displacement algorithms for nonlinear problems, IJNME, 14, 1262-1267, 1979

66. RIKS, E., The application of Newton's method to the problem of elastic stability, J. Appl. Mech., 39, 1060-1066, 1972

67. RIKS, E., An incremental approach to the solution of snapping and buckling problems, I.J.Sol. Struct., 15, 529-551, 1979

68. WEMPNER, G.A., Discrete approximations related to nonlinear theories of solids, I.J.Sol.Struct., 7, 1581-1599, 1971

69. CRISFIELD, M.A., A fast incremental/iterative solution procedure that handles "snap-through", Comp. & Struct., 13, 55-62, 1981

70. CRISFIELD, M.A., Variable step-lengths for non-linear structural analysis, TRRL Report 1049, 1982

71. BERGAN, P.G., Solution algorithms for nonlinear structural problems, Comp. & Struct., 12, 497-509, 1980

72. BERGAN, P.G., Automated incremental-iterative solution schemes, in Numerical Methods for Non-linear Problems, 261-290, C. Taylor et al. (eds.), Pineridge Press, Swansea, 1980

73. BATHE, K.J. and DVORKIN, E.N., On the automatic solution of nonlinear finite element equations, Comp. & Struct. (in press)

74. CRISFIELD, M.A., Accelerating and damping the modified Newton-Raphson method, Comp. & Struct., 18, 395-407, 1984

75. BLAND, D.R., Elastoplastic thick-walled tubes of work-hardening material subject to internal and external pressures and to temperature gradients, J. Mech. Phys. Sol., 4, 209-229, 1956

76. BIEZENO, C.B. and GRAMMEL, R., Engineering Dynamics, vol. II, Blackie & Son, Ltd., London and Glasgow, 1956

77. HAYTHORNTHWAITE, R.M. and ONAT, E.T., The load carrying capacity of initially flat circular steel plates under reversed loading, J. Aero. Sci., 22, 867-869, 1965

78. BATHE, K.J. and OZDEMIR, H., Elasto-plastic large deformation static and dynamic analysis, Comp. & Struct., 6, 81-92, 1976

CHAPTER 7

MAPPED INFINITE ELEMENTS IN STATIC STRUCTURAL ANALYSIS

7.1 INTRODUCTION 7.1

7.2 NUMERICAL TECHNIQUES FOR UNBOUNDED DOMAIN ANALYSIS 7.2

7.3 MAPPED INFINITE ELEMENTS - THE FUNDAMENTAL CONCEPT 7.4

7.4 ONE-DIMENSIONAL MAPPED INFINITE ELEMENTS 7.5

7.5 TWO-DIMENSIONAL MAPPED INFINITE ELEMENTS 7.7

- 7.5.1 Singly infinite elements
- 7.5.2 Doubly infinite elements

7.6 THREE-DIMENSIONAL MAPPED INFINITE ELEMENTS 7.11

7.7 POSITIONING OF THE EXPANSION POLES 7.13

7.8 COMPUTER IMPLEMENTATION OF MAPPED INFINITE ELEMENTS 7.14

- 7.8.1 Input data
- 7.8.2 Element stiffness formulation

7.9 ELASTOPLASTIC APPLICATIONS 7.16

- 7.9.1 Internally pressurized cylindrical cavity in an infinite medium
- 7.9.2 Pressure and thermal loading of a cylindrical cavity in an infinitely extended hardening material
- 7.9.3 Spherical cavity in an infinite medium
- 7.9.4 Strip footing on an infinitely extended layer of associated Mohr-Coulomb material

7.10 ELASTOVISCOPLASTIC APPLICATIONS 7.28

- 7.10.1 Lined cylindrical cavity in an infinite medium
- 7.10.2 Strip footing on an infinitely extended double layer of Mohr-Coulomb soil

7.11 CONCLUDING REMARKS 7.35

7.12 REFERENCES 7.36

CHAPTER 7

MAPPED INFINITE ELEMENTS IN STATIC STRUCTURAL ANALYSIS

7.1 INTRODUCTION

Unbounded continua appear in a wide variety of practical engineering problems. Specific examples can be found in fields such as fluid and solid mechanics, acoustics, electromagnetics, heat and mass transfer. Probably the most common situation in which unbounded domains arise is in geomechanical applications where modelling the far field behaviour can often present considerable numerical difficulties.

A common engineering approach is simple truncation in which the infinite domain is terminated at a finite position and the infinite boundary condition tentatively imposed. However, the location of the finite boundary is crucial for accurate solution and the selection of its minimum distance from the region of interest is often a question of experience and intuition.

Several numerical procedures have been used to date for unbounded domain analysis and are briefly reviewed in Section 7.2; a recent development is the mapped infinite element, a powerful and economical alternative based on an elegant mapping technique of impressive simplicity. The fundamental concepts are explained in Sections 7.3 and 7.4, followed by a systematic derivation of two- and three-dimensional families of singly and doubly infinite elements. Details of the computer implementation are provided in Section 7.8 with regard to quasistatic applications. Finally coupled meshes of mapped infinite and conventional finite elements are used in a series of numerical examples involving material nonlinearity for a full assessment of the accuracy and applicability of the method.

7.2 NUMERICAL TECHNIQUES FOR UNBOUNDED DOMAIN ANALYSIS

A number of problems of solid mechanics involving unbounded domains have been solved analytically.

Elastic solutions were developed for the case of a point load applied inside an infinite body (Kelvin [1]), at the boundary of a half-space (Boussinesq [2]) and at the interior of a semi-infinite solid with either free or fixed boundary (Mindlin [3] and Rongved [4]). The infinite plate with a circular hole was also considered either under uniaxial tension (Kirsch [5]) or with the load applied to the interior of the hole surface (Bickley [6]). The case of an elliptical crack in an uniformly stressed infinite plate was presented by Kolosov [7] and Inglis [8]. Marguerre [9] solved the plane strain problem of a line load on the surface of an infinite layer with a rigid base.

In plasticity the indentation of a semi-infinite solid was considered for various punch shapes: rectangular (Shield and Drucker [10]), cylindrical (Hencky [11]) and spherical (Ishlinsky [12]). Hill [13] discussed the expansion of a cylindrical cavity from zero radius in an infinite medium and Murch and Naghdi [14] analysed the infinite wedge under uniform surface load.

The common feature of these and other closed form solutions is the regularity and simplicity of the geometries, loads and boundary constraints assumed. Unfortunately realistic engineering problems seldom comply with such idealized conditions and numerical techniques have to be employed.

Zienkiewicz [15] presents an extensive survey of procedures used for finite element unbounded domain analysis, grouping them in accordance with the nature of the algorithm. The proposed classification is now briefly summarized.

7.2.1 Truncation

This is the simplest and perhaps commonest engineering approach although quite often expensive and misleading. An elegant but costly method was devised by Smith [16] for transient problems, using two sets of solutions with free and clamped boundary to suppress the wave reflection effects.

7.2.2 Matching to analytical solutions

An early example is that of Richardson's far field matching of the finite difference solution of a dam and its foundation [23] to that of Boussinesq quoted above. Recent contributions in this area are due to Lysmer [20] and Waas [24].

7.2.3 Boundary dampers

A number of procedures have been developed to prevent the reflection of the outgoing wave in periodic (and transient) problems by means of boundary dampers, namely by Zienkiewicz [17, 18], Lysmer [19] and Bayliss [21, 22].

7.2.4 Boundary integrals

The coupling of boundary integrals to finite elements has been used for various types of exterior problems in electromagnetism [25, 26], fluid [27, 28] and solid mechanics [29-35] and is extensively surveyed by Zienkiewicz [36-38].

7.2.5 Mappings

Various techniques have been used to map the semi-infinite domain onto a finite one [39-42] and are reviewed by Roach [43]. A further reference to mapping is made below with regard to mapped infinite elements.

7.2.6 Infinite elements

Ungless [44, 45] and Bettess [46] are the independent originators of infinite elements. Recent progress is surveyed by Bettess [48], who describes in detail the development of the two main infinite element formulations.

Decay function infinite elements

Early solutions [44-47] used this type of element, in which the shape functions are multiplied by a decay function of reciprocal or exponential type, as appropriate for the case being considered. A periodic component was included for wave problems [49, 50] and the method applied to potential, dam-reservoir interaction, elastostatic and elastodynamic problems [52-57].

Mapped infinite elements

This element type was introduced by Zienkiewicz [15] and will be extensively dealt with in the following Sections. Applications to date include elastic, electrostatic, plastic, viscoplastic and transient thermal and structural problems [51, 58-65]. Bettess [66] developed useful testing techniques for infinite elements.

As recent contributions to unbounded domain modelling we can mention those of Rukos, Pissanetzky, Curnier and Okabe [67-71].

7.3 MAPPED INFINITE ELEMENTS - THE FUNDAMENTAL CONCEPT

Mapped infinite elements use a simple mapping technique akin to the isoparametric formulation [72] but employing two sets of element trial functions:

(i) the geometry description is performed by means of specially devised mapping functions, suited to the semi-bounded nature of the element domain;

(ii) the field variable modelling is then achieved by recourse to standard shape functions.

This strategy allows for a straightforward incorporation of infinite elements into conventional finite element codes.

The one-dimensional mapped infinite element is now considered in some detail since it forms the basis of the two and three-dimensional versions described subsequently, as well as providing a clear illustration of the fundamental concept.

7.4 ONE-DIMENSIONAL MAPPED INFINITE ELEMENTS

The element of fig. 7.1(a) extending from node 1, through node 2, to node 3 at infinity is mapped onto the parent element defined in fig. 7.1(b) by the local coordinate system $-1 \leq \xi \leq +1$ in the standard finite element manner as

$$x(\xi) = \sum_{i=1}^{2} M_i(\xi)\, x_i \qquad (7.1)$$

where the summation extends over the finite nodes only and the mapping functions M_i, plotted in fig. 7.1(c), are

$$\begin{aligned} M_1(\xi) &= -2\xi \,/\, (1-\xi) \\ M_2(\xi) &= (1+\xi) \,/\, (1-\xi) \end{aligned} \qquad (7.2)$$

It can be seen that $\xi = -1, 0, +1$ correspond respectively to the global positions $x = x_1, x_2, \infty$.

If the origin of the global coordinate system is shifted by Δx, the value for x given by (7.1) should vary by the same amount:

$$x + \Delta x = M_1(x_1 + \Delta x) + M_2(x_2 + \Delta x) = M_1 x_1 + M_2 x_2 + (M_1 + M_2)\Delta x =$$

$$x + (M_1 + M_2)\Delta x$$

For the mapping to be independent of the choice of coordinate system it is therefore required that the summation of the mapping functions equals unity, as is clearly the case with the M_i of (7.2). The position of the pole 0 is arbitrary with $x_0 \leq x_1$ and once chosen, the location of node 2 is defined by

$$x_2 = 2x_1 - x_0 \qquad (7.3)$$

The field variable ϕ (in our case the displacement) is now mapped using standard shape functions, which for the 3-noded element of fig. 7.1 gives

$$\phi = \sum_{i=1}^{3} N_i \phi_i = 0.5\xi(\xi-1)\phi_1 + (1-\xi^2)\phi_2 + 0.5\xi(\xi+1)\phi_3 \qquad (7.4)$$

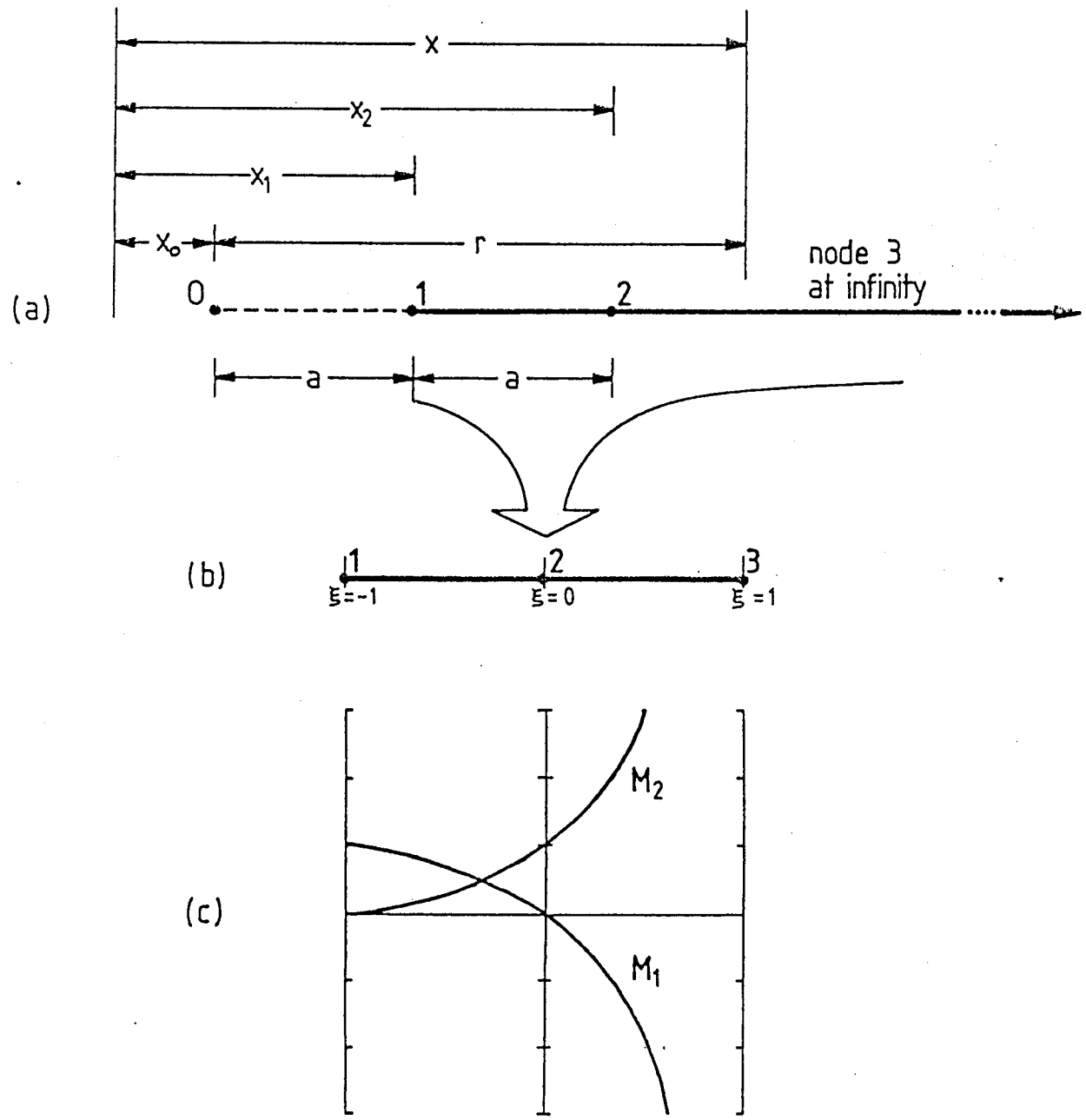

Fig. 7.1 – One dimensional infinite element
(a) Global representation
(b) Local representation
(c) Geometric mapping functions

Solving (7.1) for ξ yields

$$\xi = 1 - 2a/r \qquad (7.5)$$

in which r denotes the distance from the pole, 0, to a general point within the element and $a = x_2 - x_1$ as shown in fig. 7.1. Using (7.5) in (7.4) the unknown ϕ is expressed in terms of the global coordinate, r, as follows

$$\phi = \phi_3 + (-\phi_1 + 4\phi_2 - 3\phi_3)\, a/r + (2\phi_1 - 4\phi_2 + 2\phi_3)a^2/r^2 \qquad (7.6)$$

Thus as r tends to infinity, ϕ approaches ϕ_3. If the value ϕ_3 of ϕ at infinity is zero, this boundary condition is automatically enforced by simply summing only over the "finite" nodes 1 and 2 in expression (7.4). The accuracy with which (7.4) or (7.6) model the decay of ϕ may be improved by including higher order terms in the polynomial expansion. Expression (7.6) also clearly shows the role of the point 0 as pole for the expansion of ϕ.

7.5 TWO-DIMENSIONAL MAPPED INFINITE ELEMENTS

Extension of the procedure described in the previous section to two-dimensional situations can be easily accomplished by taking shape function products. Elements may be generated which are either singly or doubly infinite.

7.5.1 Singly infinite elements

This term is used to denote elements which extend to infinity in one direction only (chosen to be the η direction). Table 7.1 shows the mapping and shape functions for some element types.

6-node Lagrangian element

This element may be regarded as a 9-node Lagrangian element in which the three nodes associated with $\eta = +1$ are positioned at infinity. The mapping functions $M_i(\xi,\eta)$ are a product of Lagrangian quadratic expressions $M'_j(\xi)$ in the ξ direction with singularity functions $M''_k(\eta)$ of the same form as (7.2). In particular

$$
\begin{aligned}
M_1'(\xi) &= (\xi^2 - \xi)/2 \qquad \text{for } \xi_i = -1 \\
M_2'(\xi) &= 1 - \xi^2 \qquad\qquad \xi_i = 0 \\
M_3'(\xi) &= (\xi^2 + \xi)/2 \qquad \xi_i = +1
\end{aligned}
\tag{7.7}
$$

$$
\begin{aligned}
M_1''(\eta) &= -2\eta/(1 - \eta) \quad \text{for } \eta_i = -1 \\
M_2''(\eta) &= (1 + \eta)/(1 - \eta) \quad \eta_i = 0
\end{aligned}
\tag{7.8}
$$

The six shape functions $N_i(\xi,\eta)$ are the appropriate Lagrangian finite element values.

5-node Serendipity element

This element utilises five of the shape functions of the 8-node Serendipity element and the five mapping functions $M_i(\xi,\eta)$ are derived as follows.

M_2 combines $1 - \xi^2$, equal to one at node 2 and zero at the four other nodes, with $1/(1 - \eta)$ which provides the infinite value for $\eta = +1$. ($M_2 = 2(1 - \xi^2)/(1 - \eta)$)

M_4 must contain $1 + \xi$ and $1 + \eta$ to give zero values at nodes 1,5 and 1,2,3 and $1/(1 - \eta)$ as before. ($M_4 = (1 + \xi)(1 + \eta)/2(1 - \eta)$)

M_3 is obtained by applying the technique outlined by Zienkiewicz [57] for the derivation of serendipity shape functions. We start with an auxiliary function $\hat{M}_3 = (1 + \xi)/(1 + \eta)$ linear on ξ and singular for $\eta = +1$ and then enforce zero values at nodes 2 and 4 by sub-tracting M_2 and M_4 appropriately scaled.
($M_3 = \hat{M}_3 - 0.5\, M_2 - 2M_4 = (1 + \xi)(-1 + \xi - \eta)/(1 - \eta)$)

4-node element

This element originates from a 6-node Lagrangian element (linear in ξ, quadratic in η) with the two nodes corresponding to $\eta = +1$ positioned at infinity.

ELEMENT		MAPPING FUNCTIONS	SHAPE FUNCTIONS
2 NODE SUPER PARAM.	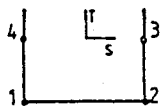	M1 = (1-S)(-T)/ (1-T) M2 = (1+S)(-T)/ (1-T) M3 = (1+S)(1+T)/[2(1-T)] M4 = (1-S)(1+T)/[2(1-T)]	N1 = (1-S)(1-T)/4 N2 = (1+S)(1-T)/4
4 NODE LAGRAN.	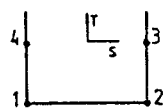	AS FOR THE 2 NODE ELEMENT	N1 = (1-S)(TT-T)/4 N2 = (1+S)(TT-T)/4 N3 = (1+S)(1-TT)/2 N4 = (1-S)(1-TT)/2
5 NODE SEREND.	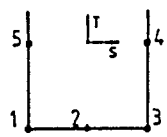	M1 = (1- S)(-1-S-T)/(1-T) M2 = (1-SS) 2 /(1-T) M3 = (1+ S)(-1+S-T)/(1-T) M4 = (1+ S)(1+T)/[2(1-T)] M5 = (1- S)(1+T)/[2(1-T)]	N1 = (1- S)(1- T)(-1-S-T)/4 N2 = (1-SS)(1- T) /2 N3 = (1+ S)(1- T)(-1+S-T)/4 N4 = (1+ S)(1-TT) /2 N5 = (1- S)(1-TT) /2
6 NODE LAGRAN.	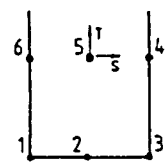	M1 = (SS-S)(-T)/ (1-T) M2 = (1-SS)(-2T)/ (1-T) M3 = (SS+S)(-T)/ (1-T) M4 = (SS+S)(1+T)/[2(1-T)] M5 = (1-SS)(1+T)/ (1-T) M6 = (SS-S)(1+T)/[2(1-T)]	N1 = (SS-S)(TT-T)/4 N2 = (1-SS)(TT-T)/2 N3 = (SS+S)(TT-T)/4 N4 = (SS+S)(1-TT)/2 N5 = (1-SS)(1-TT) N6 = (SS-S)(1-TT)/2

TABLE 7.1 - Mapping and shape functions for 2D singly infinite elements
(S = xi, T = eta, SS = S*S, TT = T*T)

ELEMENT		MAPPING FUNCTIONS	SHAPE FUNCTIONS
1 NODE SUPER PARAM.	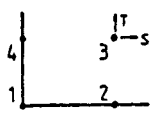	M1 = 4ST /[(1-S)(1-T)] M2 = (1+S)(-2T)/[(1-S)(1-T)] M3 = (1+S)(1+T)/[(1-S)(1-T)] M4 = (-2S)(1+T)/[(1-S)(1-T)]	N1 = (1-S)(1-T)/4
3 NODE SEREND.	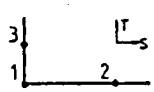	M1 = [ST+3(-1-S-T)]/[(1-S)(1-T)] M2 = 2(1+S) /[(1-S)(1-T)] M3 = 2(1+T) /[(1-S)(1-T)]	N1 = (1- S)(1- T)(-1-S-T)/4 N2 = (1-SS)(1- T) /2 N3 = (1- S)(1-TT) /2
4 NODE LAGRAN.	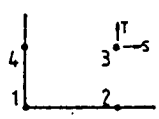	AS FOR THE 1 NODE ELEMENT	N1 = (SS-S)(TT-T)/4 N2 = (1-SS)(TT-T)/2 N3 = (1-SS)(1-TT) N4 = (SS-S)(1-TT)/2

TABLE 7.2 - Mapping and shape functions for 2D doubly infinite elements
(S = xi, T = eta, SS = S*S, TT = T*T)

2-node Superparametric element

When forming a 2-node infinite element from the 4-node linear finite element, it appears difficult to enforce simultaneously the singularity at $\eta = +1$ and the invariance requirement under change of coordinate origin. This problem can be overcome by the inclusion of two extra nodes for geometric mapping only, so that this superparametric element employs 4 nodes for geometric modelling and 2 nodes for field variable description. The four mapping functions are those of the 4-node infinite element described above and the two shape functions are taken from the 4-node linear finite element.

All the above elements may be connected to finite elements having the appropriate number of nodal points along the common edge.

7.5.2 Doubly infinite elements

This term is used to denote elements which extend to infinity in two directions. They can be used as "corner" elements in a mesh where transition is needed between zones extending to infinity along different directions. The mapping and shape functions for some typical versions are listed in Table 7.2.

4-node Lagrangian element

The auxiliary functions $M'_j(\xi)$ and $M''_k(\eta)$ now both exhibit a singular value for ξ or η equal to 1 and are given, from (7.2) by

$$
\begin{aligned}
M'_1(\xi) &= -2\xi/(1-\xi) \quad \text{for } \xi_i = -1 \\
M'_2(\xi) &= (1+\xi)/(1-\xi) \quad \xi_i = 0 \\
M''_1(\eta) &= -2\eta/(1-\eta) \quad \eta_i = -1 \\
M''_2(\eta) &= (1+\eta)/(1-\eta) \quad \eta_i = 0
\end{aligned}
\tag{7.9}
$$

Products of these functions give $M_i(\xi,\eta)$ and the shape functions are appropriately selected from the 9-node Lagrangian finite element.

3-node Serendipity element

This element (as the 5-noded singly infinite version) originates from the 8-node finite element whose shape functions are used for field modelling as well as for derivation of the mapping functions.

1-node superparametric element

As for the singly infinite case, three additional nodes are required to define the geometric mapping. The four mapping functions are taken from the 4-node doubly infinite element described above and the single shape function from the 4-node linear finite element.

7.6 THREE-DIMENSIONAL MAPPED INFINITE ELEMENTS

The principles discussed in the previous section readily extend to three-dimensional situations. Table 7.3 lists the mapping and shape functions for some typical versions which extend to infinity along the ζ direction.

18-node Lagrangian element

The 27 node Lagrangian finite element supplies the shape functions for this element. The mapping functions $M_i(\xi,\eta,\zeta)$ are products of functions $M'_j(\xi)$ and $M''_k(\eta)$ as in (7.7) and $M'''_\ell(\zeta)$ as in (7.8).

16-node superparametric element

This element utilises two additional nodes for geometry mapping, thereby using the 18 mapping functions of the 18-node infinite element described above. The 16 shape functions are derived from those of the 8-node two-dimensional Serendipity finite element which are multiplied by $(\zeta^2 - \zeta)/2$ and $1 - \zeta^2$ respectively for $\zeta_i = -1$ and 0. The element has therefore a field variable modelling of the Serendipity type in ξ and η and is Lagrangian in ζ.

ELEMENT	MAPPING FUNCTIONS	SHAPE FUNCTIONS
4 NODE SUPER PARAM. 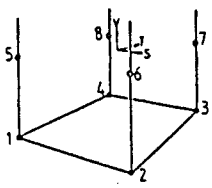	M1 = (1-S)(1-T)(-V)/[2(1-V)] M2 = (1+S)(1-T)(-V)/[2(1-V)] M3 = (1+S)(1+T)(-V)/[2(1-V)] M4 = (1-S)(1+T)(-V)/[2(1-V)] M5 = (1-S)(1-T)(1+V)/[4(1-V)] M6 = (1+S)(1-T)(1+V)/[4(1-V)] M7 = (1+S)(1+T)(1+V)/[4(1-V)] M8 = (1-S)(1+T)(1+V)/[4(1-V)]	N1 = (1-S)(1-T)(1-V)/8 N2 = (1+S)(1-T)(1-V)/8 N3 = (1+S)(1+T)(1-V)/8 N4 = (1-S)(1+T)(1-V)/8
8 NODE 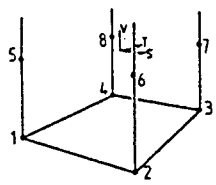	AS FOR THE 4 NODE ELEMENT	N1 = (1-S)(1-T)(VV-V)/8 N2 = (1+S)(1-T)(VV-V)/8 N3 = (1+S)(1+T)(VV-V)/8 N4 = (1-S)(1+T)(VV-V)/8 N5 = (1-S)(1-T)(1-VV)/4 N6 = (1+S)(1-T)(1-VV)/4 N7 = (1+S)(1+T)(1-VV)/4 N8 = (1-S)(1+T)(1-VV)/4
12 NODE SEREND. 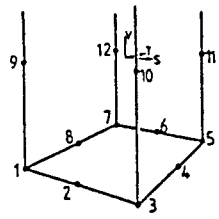	M1 = (1- S)(1- T)(-S-T-V-2)/[2(1-V)] M2 = (1-SS)(1- T) / (1-V) M3 = (1+ S)(1- T)(+S-T-V-2)/[2(1-V)] M4 = (1+ S)(1-TT) / (1-V) M5 = (1+ S)(1+ T)(+S+T-V-2)/[2(1-V)] M6 = (1-SS)(1+ T) / (1-V) M7 = (1- S)(1+ T)(-S+T-V-2)/[2(1-V)] M8 = (1- S)(1-TT) / (1-V) M9 = (1- S)(1- T)(1+ V) /[4(1-V)] M10 = (1+ S)(1- T)(1+ V) /[4(1-V)] M11 = (1+ S)(1+ T)(1+ V) /[4(1-V)] M12 = (1- S)(1+ T)(1+ V) /[4(1-V)]	N1 = (1- S)(1- T)(1- V)(-S-T-V-2)/8 N2 = (1-SS)(1- T)(1- V) /4 N3 = (1+ S)(1- T)(1- V)(+S-T-V-2)/8 N4 = (1+ S)(1-TT)(1- V) /4 N5 = (1+ S)(1+ T)(1- V)(+S+T-V-2)/8 N6 = (1-SS)(1+ T)(1- V) /4 N7 = (1- S)(1+ T)(1- V)(-S+T-V-2)/8 N8 = (1- S)(1-TT)(1- V) /4 N9 = (1- S)(1- T)(1-VV) /4 N10 = (1+ S)(1- T)(1-VV) /4 N11 = (1+ S)(1+ T)(1-VV) /4 N12 = (1- S)(1+ T)(1-VV) /4
16 NODE SUPER PARAM. 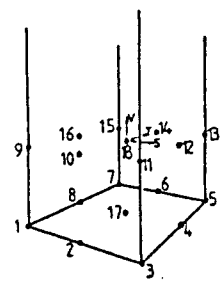	M1 = (SS-S)(TT-T)(-V)/[2(1-V)] M2 = (1-SS)(TT-T)(-V)/ (1-V) M3 = (SS+S)(TT-T)(-V)/[2(1-V)] M4 = (SS+S)(1-TT)(-V)/ (1-V) M5 = (SS+S)(TT+T)(-V)/[2(1-V)] M6 = (1-SS)(TT+T)(-V)/ (1-V) M7 = (SS-S)(TT+T)(-V)/[2(1-V)] M8 = (SS-S)(1-TT)(-V)/ (1-V) M9 = (SS-S)(TT-T)(1+V)/[4(1-V)] M10 = (1-SS)(TT-T)(1+V)/[2(1-V)] M11 = (SS+S)(TT-T)(1+V)/[4(1-V)] M12 = (SS+S)(1-TT)(1+V)/[2(1-V)] M13 = (SS+S)(TT+T)(1+V)/[4(1-V)] M14 = (1-SS)(TT+T)(1+V)/[2(1-V)] M15 = (SS-S)(TT+T)(1+V)/[4(1-V)] M16 = (SS-S)(1-TT)(1+V)/[2(1-V)] M17 = (1-SS)(1-TT)(-2V)/ (1-V) M18 = (1-SS)(1-TT)(1+V)/ (1-V)	N1 = (1- S)(1- T)(VV-V)(-S-T-1)/8 N2 = (1-SS)(1- T)(VV-V) /4 N3 = (1+ S)(1- T)(VV-V)(+S-T-1)/8 N4 = (1+ S)(1-TT)(VV-V) /4 N5 = (1+ S)(1+ T)(VV-V)(+S+T-1)/8 N6 = (1-SS)(1+ T)(VV-V) /4 N7 = (1- S)(1+ T)(VV-V)(-S+T-1)/8 N8 = (1- S)(1-TT)(VV-V) /4 N9 = (1- S)(1- T)(1-VV)(-S-T-1)/4 N10 = (1-SS)(1- T)(1-VV) /2 N11 = (1+ S)(1- T)(1-VV)(+S-T-1)/4 N12 = (1+ S)(1-TT)(1-VV) /2 N13 = (1+ S)(1+ T)(1-VV)(+S+T-1)/4 N14 = (1-SS)(1+ T)(1-VV) /2 N15 = (1- S)(1+ T)(1-VV)(-S+T-1)/4 N16 = (1- S)(1-TT)(1-VV) /2
18 NODE LAGRAN. 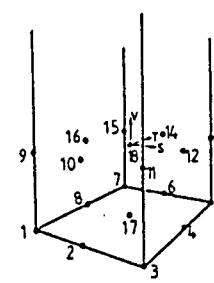	AS FOR THE 16 NODE ELEMENT	N1 = (SS-S)(TT-T)(VV-V)/8 N2 = (1-SS)(TT-T)(VV-V)/4 N3 = (SS+S)(TT-T)(VV-V)/8 N4 = (SS+S)(1-TT)(VV-V)/4 N5 = (SS+S)(TT+T)(VV-V)/8 N6 = (1-SS)(TT+T)(VV-V)/4 N7 = (SS-S)(TT+T)(VV-V)/8 N8 = (SS-S)(1-TT)(VV-V)/4 N9 = (SS-S)(TT-T)(1-VV)/4 N10 = (1-SS)(TT-T)(1-VV)/2 N11 = (SS+S)(TT-T)(1-VV)/4 N12 = (SS+S)(1-TT)(1-VV)/2 N13 = (SS+S)(TT+T)(1-VV)/4 N14 = (1-SS)(TT+T)(1-VV)/2 N15 = (SS-S)(TT+T)(1-VV)/4 N16 = (SS-S)(1-TT)(1-VV)/2 N17 = (1-SS)(1-TT)(VV-V)/2 N18 = (1-SS)(1-TT)(1-VV)

TABLE 7.3 - Mapping and shape functions for 3D singly infinite elements
(S = xi, T = eta, V = zeta, SS = S*S, TT = T*T, VV = V*V)

12-node Serendipity element

The twelve shape and mapping functions are taken or derived from the 20 node brick finite element.

8-node Langrangian element

This element is derived from a 12-node Lagrangian finite element, bilinear in ξ and η and quadratic in ζ.

4-node Superparametric element

If the nodes at $\zeta = 1$ of an 8-node brick finite element are translated to infinity, a 4-node superparametric infinite element is obtained which requires four extra nodes for geometry mapping. Therefore the eight mapping functions are those of the 8-node infinite element described above.

Once again these three-dimensional elements may be attached to appropriate three-dimensional finite elements.

The two- and three-dimensional superparametric elements described in this section have been derived as a result of a systematic search of infinite element equivalents to some of the more common isoparametric finite elements. For each superparametric version an "isoparametric" alternative has been also presented and should be preferred: by using the same nodes for the two sets of element trial functions not only is the coding more straightforward but more information is also available regarding the far field behaviour.

7.7 POSITIONING OF THE EXPANSION POLES

The geometry and field variable expansions involved in the mapped infinite element technique are both referred to the same point, or set of points, termed the pole(s) as discussed in Section 7.4. Therefore the geometric and physical characteristics of the problem must both be taken into account when positioning the pole(s).

The pole(s) must be exterior to the infinite element. Also element edges or faces extending to infinity must be either parallel or divergent, since convergence would lead to overlapping of elements and non-uniqueness of mapping. The effects of shifting the pole positions may be explored in an attempt to improve the fit to the decay pattern expected [62].

In order to ensure continuity across the boundary between infinite and finite elements (or adjacent infinite elements) the number and location of the connecting nodes must coincide.

7.8 COMPUTER IMPLEMENTATION OF MAPPED INFINITE ELEMENTS

The changes necessary to implement the mapped infinite elements described in the previous sections into an existing finite element code for elastoplastic or elasto-viscoplastic analysis are relatively few. The essential modifications are detailed below assuming that a frontal process is employed for equation solution [73].

7.8.1 Input data

The element numbering is not conditioned by the inclusion of infinite elements in the mesh and is done as usual in order to minimise the frontwidth. The connecting data for an infinite element is input according to the nodal sequence depicted in Tables 7.1-3 (i.e. with the additional nodes of superparametric versions being listed last). The number of nodes per element now variable throughout the mesh, is registered in a column array, with additional superparametric nodes not being counted. For example the 16-node three-dimensional infinite element is regarded as having 16 nodes, but the connectivity data comprises the numbers of the 18 nodes required for geometric mapping.

Point loads on infinite elements present no difficulty. Distributed edge or face loading can only be applied to the face common to the infinite element and the finite element to which

it is connected and for frontal solution can be arbitrarily assigned to the finite element. Distributed loading along any edge or face extending to infinite is incompatible with the assumption of vanishing displacements at infinity. For gravity type loading, the mapping functions perform the geometry description required by the volume integrals involved.

7.8.2 Element stiffness formulation

The element stiffness matrix, given as usual by

$$\underline{K}^e = \int_V \underline{B}^T \underline{D} \underline{B} \, dv \tag{7.10}$$

is obtained for an infinite element as follows:

The integration in (7.10) is performed numerically using Gaussian quadrature. Looping over each such integration point:

* evaluate the Gauss abscissae and weights, w_i

* call the mapping function subroutine which evaluates $\underline{M}$, $\partial\underline{M}/\partial\xi$, $\partial\underline{M}/\partial\eta$, $\partial\underline{M}/\partial\zeta$ using the appropriate functions defined in Tables 7.1-3.

* compute the coordinate Jacobian matrix $\underline{J}$ as

  $\underline{J} = [\underline{x}\ \underline{y}\ \underline{z}]^T\ [\partial\underline{M}/\partial\xi\ \partial\underline{M}/\partial\eta\ \partial\underline{M}/\partial\zeta]$

  where the first array contains the element nodal coordinates

* compute the determinant, det $\underline{J}$, and the inverse, $\underline{J}^{-1}$

* call the shape function routine which evaluates $\underline{N}$, $\partial\underline{N}/\partial\xi$, $\partial\underline{N}/\partial\eta$, $\partial\underline{N}/\partial\zeta$ using the appropriate functions defined in Tables 7.1-3

* compute the Cartesian derivatives

  $[\partial\underline{N}/\partial x\ \partial\underline{N}/\partial y\ \partial\underline{N}/\partial z] = [\partial\underline{N}/\partial\xi\ \partial\underline{N}/\partial\eta\ \partial\underline{N}/\partial\zeta].\underline{J}^{-1}$

* use these Cartesian derivatives to evaluate $\underline{B}$

* also evaluate the $\underline{D}$ matrix

* evaluate $\underline{B}_i^T \underline{D} \underline{B}_j w_i w_j \det \underline{J}$ and sum into K^e_{ij}

Thus, in summary, the geometric mapping functions $\underline{M}$ are used to relate the local and global coordinates in the computation of the Jacobian $\underline{J}$. This Jacobian is then inverted and used to obtain the Cartesian shape function derivatives needed to express the $\underline{B}$ matrix.

7.9 ELASTOPLASTIC APPLICATIONS

In this section the results of four numerical examples are presented which illustrate the benefits of using a combined finite/infinite element approach for the solution of elastoplastic problems.

7.9.1 Internally pressurised cylindrical cavity in an infinite medium

The problem to be analysed is detailed in Table 7.4. Plane strain conditions are assumed in the axial direction and the elasto-plastic material obeys the Tresca yield criterion. Four solutions were performed using finite elements only, with meshes of 9 and 21 eight-node isoparametric elements. The outermost nodes were considered to be either radially free (meshes 9FFR and 21FFR) or fixed (9FFX and 21FFX). Three solutions were also performed using one 5-node mapped infinite element and either one, two or three 8-node finite elements (meshes 1F1I, 2F1I and 3F1I respectively). Table 7.4 displays the various meshes, the material properties, the computational cost of solution and the extent of plastification for each of the five load increments.

Table 7.5 shows the distribution of radial stresses for the various solutions undertaken and Fig. 7.2 shows the residual tangential stress variation after removal of load. All the results are compared with the analytical solution for this problem [74]

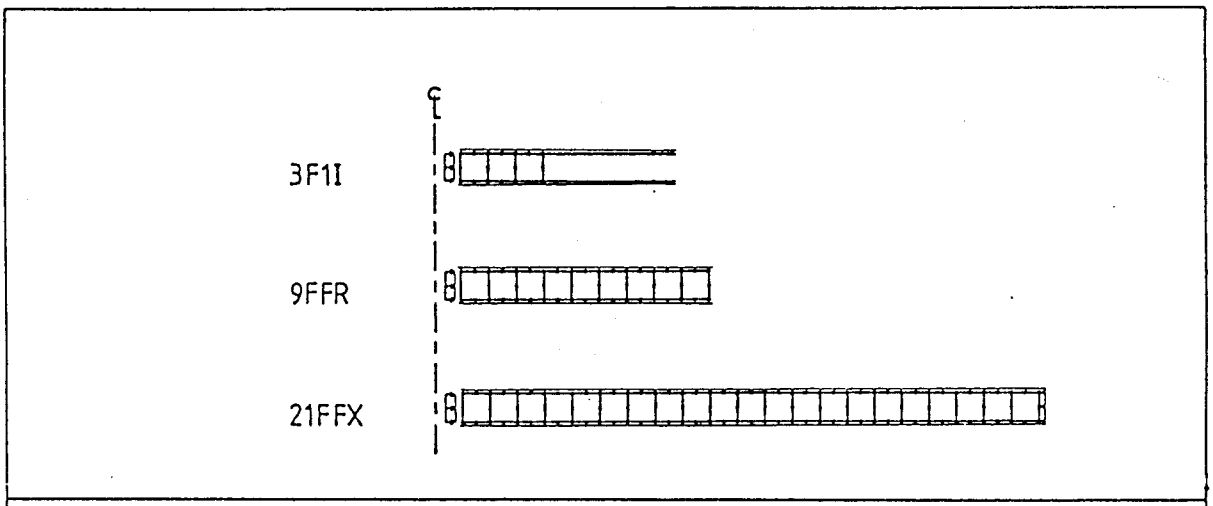

Elastic modulus, E = 1.E7				Initial yield stress, YO = 1200.			
Poisson's ratio, ν = 0.33				Hardening parameter , H' = 0.			
Cavity radius , a = 1.00				Finite element size , 1.0 x 1.0			
Load step	1	2	3	4	5		
Internal pressure p	500.	1250.	1750.	2250.	0.		
Plastic zone radius c	-	1.71887	2.60735	3.95508	1.54883		
Mesh	1F1I	2F1I	3F1I	9FFX	9FFR	21FFX	21FFR
CPU time (ICL 2966)	9	13	17	28	30	53	59

TABLE 7.4 - Geometric, material and loading data for a cylindrical cavity in an infinite medium

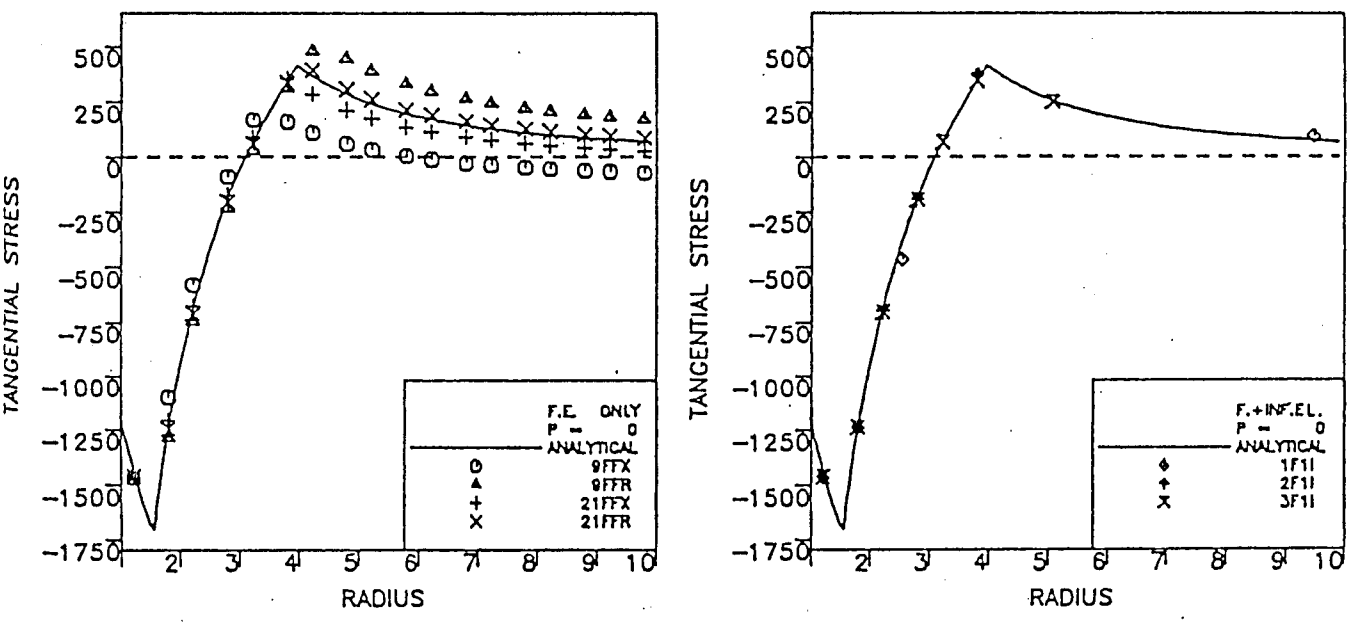

Fig. 7.2 - Residual tangential stress distribution for the example of TABLE 7.4 for various finite and finite/infinite element solutions

		ANALYT	FINITE ELEMENTS ONLY					ANALYT	FIN. + INFINITE ELEM.		
INC	RAD		9FFX	9FFR	21FFX	21FFR	RAD		1F1I	2F1I	3F1I
1	1.21	-340.76	-350.62	-344.67	-347.15	-345.91	1.21	-340.76	-346.23	-346.23	-346.23
	1.79	-156.28	-163.67	-150.28	-155.87	-153.06	1.79	-156.28	-153.78	-153.78	-153.78
	3.21	-48.48	-61.44	-43.98	-51.27	-47.61	5.07	-19.44			-19.44
	9.21	-5.89	-20.01	-0.90	-8.88	-4.87	9.46	-5.58	-5.58		
	14.21	-2.48			-5.48	-1.45	14.20	-2.48		-2.48	
	18.79	-1.42			-4.43	-0.38	18.93	-1.40			-1.40
2	1.21	-1019.94	-1006.15	-1010.70	-1008.74	-1009.72	1.21	-1019.94	-1009.47	-1009.47	-1009.47
	1.79	-554.08	-578.16	-563.73	-569.94	-566.86	1.79	-554.08	-567.65	-567.65	-567.65
	3.21	-171.90	-210.56	-158.91	-181.14	-170.09	5.07	-68.91			-69.25
	9.21	-20.89	-68.58	-3.26	-31.37	-17.40	9.46	-19.79	-19.89		
	14.21	-8.78			-19.36	-5.17	14.20	-8.80		-8.84	
	18.79	-5.02			-15.64	-1.37	18.93	-4.95			-4.97
3	1.21	-1519.94	-1514.27	-1514.27	-1514.27	-1514.27	1.21	-1519.94	-1514.27	-1514.27	-1514.27
	1.79	-1052.23	-1052.39	-1052.39	-1052.39	-1052.39	1.79	-1052.23	-1052.39	-1052.39	-1052.39
	3.21	-395.53	-437.48	-381.96	-407.85	-395.41	5.07	-158.57			-159.65
	9.21	-48.07	-142.49	-7.84	-70.63	-40.45	9.46	-45.54	-40.94		
	14.21	-20.20			-43.60	-12.01	14.20	-20.24		-20.38	
	18.79	-11.55			-35.23	-3.19	18.93	-11.38			-11.46
4	1.21	-2019.94	-2014.27	-2014.27	-2014.27	-2014.27	1.21	-2019.94	-2014.27	-2014.27	-2014.27
	1.79	-1552.23	-1552.39	-1552.39	-1552.39	-1552.39	1.79	-1552.23	-1552.39	-1552.39	-1552.39
	3.21	-849.98	-844.36	-848.02	-847.88	-848.02	5.07	-364.87			-363.73
	9.21	-110.62	-277.60	-20.21	-152.68	-94.05	9.46	-104.79	-150.26		
	14.21	-46.47			-94.26	-27.92	14.20	-46.57		-41.53	
	18.79	-26.59			-76.15	-7.42	18.93	-26.20			-26.11
5	1.21	-230.06	-267.78	-260.21	-263.46	-261.85	1.21	-230.06	-262.26	-262.26	-262.26
	1.79	-652.47	-595.90	-619.94	-609.59	-614.73	1.79	-652.47	-613.41	-613.41	-613.41
	3.21	-570.84	-493.74	-583.40	-546.25	-564.78	5.07	-252.96			-248.41
	9.21	-76.69	-163.41	-14.78	-100.45	-65.08	9.46	-72.65	-117.14		
	14.21	-32.22			-62.01	-19.32	14.20	-32.29		-26.81	
	18.79	-18.43			-50.10	-5.13	18.93	-18.16			-17.83

TABLE 7.5 - Comparison of the radial stresses for the example of TABLE 7.4 for various finite and finite/infinite element solutions

and the following general conclusion can be drawn:

For solutions based on finite elements only the two types of boundary conditions (radially fixed or free) bound the analytical solution as expected. These bounds are close in the near field region, but differ significantly in the far field. The finite/infinite element solutions provide consistently good results in both the near and far field regions, provided that the zone of plastic yielding does not invade the infinite element. This deterioration in solution is evident in meshes 1F1I and 2F1I after load steps 2 and 3 respectively. The values obtained (with plastification confined to the finite element region) are always within the upper and lower bounds given by the finite element only solutions. The results obtained with mesh 3F1I are not only much more accurate than those given by 21 finite elements, but the execution time is also reduced by a factor of 3.5.

7.9.2 Pressure and thermal loading of a cylindrical cavity in an infinitely extended hardening material

This plane strain example illustrates the applicability of infinite elements to a problem with complex loading and material properties and also indicates that an inadequate representation of the thermal loading can lead to inaccurate solutions. The loading is applied in one step and consists of an internal pressure, $p = 2400$ together with an axisymmetric temperature variation, $T = 500\ a/r$, where a is the cavity radius. The material properties are included in Table 7.6 and a Tresca yield criterion is adopted. A linear strain hardening response is assumed, with the variation in yield stress given by $Y = 1200 + 10^6\ \bar{\varepsilon}_p$ where $\bar{\varepsilon}_p$ is the effective plastic strain. The mesh employed in solution contains three 8-node finite elements and one 6-node infinite element and the distribution of elements is the same as for mesh 3F1I in Table 7.4. The thermal loading is specified in three ways:

RADIUS		1.21	1.79	2.21	2.79	3.21	3.79	5.07	18.93
TEMPERATURE VARIATION PROFILE	RUN 1	419.39	275.05	226.83	178.72	155.88	131.82	98.58	26.42
	RUN 2	412.77	279.54	226.11	179.30	155.70	131.97	98.58	26.42
	RUN 3	400.00	285.71	222.22	181.82	153.85	133.33	83.33	9.26
RADIAL STRESS	ANAL.	-2039.73	-1435.46	-1149.89	-857.71	-687.74	-524.12	-329.69	-52.53
	RUN 1	-2036.76	-1427.47	-1141.82	-850.86	-680.71	-518.34	-273.86	-105.12
	RUN 2	-2036.58	-1427.40	-1141.89	-850.93	-680.76	-518.37	-273.89	-105.12
	RUN 3	-2038.52	-1431.76	-1146.39	-855.15	-684.21	-520.79	-311.28	-52.08
LONGITUDINAL STRESS	ANAL.	-1183.91	-764.67	-556.46	-340.91	-232.39	-196.97	-147.14	-39.43
	RUN 1	-1495.08	-791.17	-552.68	-336.52	-232.65	-196.75	-112.29	-74.28
	RUN 2	-1467.65	-795.38	-551.97	-337.16	-232.39	-196.97	-112.29	-74.28
	RUN 3	-1216.55	-785.77	-550.42	-342.32	-229.62	-199.01	-113.50	-24.70
TANGENTIAL STRESS	ANAL.	-297.06	-34.62	148.83	367.97	455.35	327.14	182.55	13.11
	RUN 1	-272.67	-25.57	154.41	372.70	448.06	321.59	232.32	-39.91
	RUN 2	-271.95	-26.63	154.44	372.55	448.37	321.39	232.35	-39.91
	RUN 3	-282.64	-34.83	151.86	368.79	454.59	321.78	219.88	6.36

Elastic modulus, $E = 1.E7$ — Initial yield stress, $YO = 1200.$
Poisson's ratio, $\nu = 0.33$ — Coeff. therm. expansion, $\alpha = 1.E-7$
Cavity radius , $a = 1.00$

TABLE 7.6 – Problem parameters and solution comparison for a pressure and thermally loaded cylindrical cavity in an infinitely extended hardening material

Run 1. The nodal temperatures are prescribed and the Gauss point values interpolated using the shape functions in the usual way.

Run 2. The temperature at the Gauss points is calculated directly from the specified temperature variation.

Run 3. For numerical integration of the thermal loads, the temperature field is approximated by a constant value within each integration zone which is equal to the value at the corresponding Gauss point. This inaccuracy is magnified in the infinite element since the domain of integration is considerably extended. In order to improve the temperature curve fitting, the Gauss point temperatures for the third solution are defined as the average of the temperature field over each integration domain, r_1- r_2, so that

$$T_{GP} = \int_{r_1}^{r_2} 2\pi r \; 500/r \, dr \Big/ \int_{r_1}^{r_2} 2\pi r \, dr = 500 \; / \; [(r_1 + r_2)/2]$$

The results of all three solutions are compared in Table 7.6 with the analytical solution of Ref. [75]. The superior results of Run 3 are immediately apparent, with Runs 1 and 2 being significantly in error in the far field region.

7.9.3 Spherical cavity in an infinite medium

An internally pressurised spherical cavity in an infinite medium is analysed as a three-dimensional problem. The problem parameters are listed in Table 7.7 and the material is assumed to obey the von Mises yield criterion. Two finite element meshes, of three-dimensional 20-noded elements, are used to model one eighth of the continuum. Each mesh contains three layers each of 12 elements, the layers being defined by the radial values 1, 2, 3, 4 for case A and by 1, 2, 4, 8 for case D. The distribution of elements in a typical layer is shown in Table 7.7. The outermost nodes are considered to be either fixed or free (mesh codes FX and FR respectively).

Elastic modulus, E = 1.E7 Poisson's ratio, ν = 0.33 Yield stress , YO = 1200. Hardening fact., H' = 0. Cavity radius , a = 1.		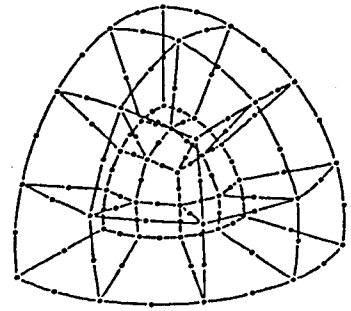 Typical element layer
Load step	1	2
Internal pressure p	750.	2250.
Plastic radius c	-	1.8297

Mesh	FFXA	FFRA	FFXB	FFRB	F12IA	F12IB	F12IC	F16IA	F16IB	F16IC
CPU time CDC 7600	57.4	74.1	57.5	62.3	52.2	52.2	32.0	56.1	57.6	37.5

TABLE 7.7 – Geometric, material and loading data for a spherical cavity in an infinite medium

SPHERICAL CAVITY – RADIAL DISPLACEMENTS(*1.E6)

		FINITE ELEMENTS ONLY				FINITE+INFINITE ELEMENTS						ANALYT
						12 NODE INF. EL.			16 NODE INF. EL.			
INC	RAD	FFXA	FFRA	FFXB	FFRB	F12IA	F12IB	F12IC	F16IA	F16IB	F16IC	
1	1.00	47.10	50.47	48.92	49.35	49.30	49.22	49.26	49.29	49.21	49.31	49.87
	1.50	19.98	22.69	21.45	21.79	21.74	21.68	21.77	21.75	21.68	21.75	22.17
	2.00	10.55	13.42	12.10	12.46	12.40	12.34	12.50	12.42	12.35	12.39	12.47
	4.00	0.00	4.75	2.69	3.28		3.12	3.09		3.09	3.09	3.12
	6.00			0.78	1.66	1.37			1.37			1.39
	8.00			0.00	1.18		0.77			0.77		0.78
2	1.00	365.66	476.25	411.17	422.78	421.37	419.14	421.23	421.30	419.09	421.64	416.01
	1.50	125.78	173.25	145.17	150.14	149.53	148.56	149.64	149.54	148.56	149.59	153.77
	2.00	64.44	97.75	79.31	83.15	82.66	81.87	83.15	82.79	81.94	82.56	81.47
	4.00	0.00	34.55	17.53	21.83		20.63	20.55		20.41	20.58	20.37
	6.00			5.06	11.04	9.08			9.11			9.05
	8.00			0.00	7.85		5.09			5.10		5.09

TABLE 7.8 – Radial displacement comparison for the spherical cavity example of TABLE 7.7 for various finite and finite/infinite element solutions

SPHERICAL CAVITY - RADIAL STRESSES

		ANALYT	FINITE ELEMENTS ONLY					ANALYT	FINITE+INFINITE ELEMENTS					
										12 NODE INF. EL.			16 NODE INF. EL.	
INC	RAD		FFXA	FFRA	FFXB	FFRB	RAD		F12IA	F12IB	F12IC	F16IA	F16IB	F16IC
1	1.21	-422.38	-431.74	-416.97	-423.76	-421.89	1.21	-422.38	-422.10	-422.47	-422.17	-422.12	-422.48	-422.08
	1.79	-131.19	-143.80	-115.65	-128.59	-125.04	1.79	-131.19	-125.47	-126.15	-125.46	-125.47	-126.16	-125.48
	3.21	-22.67	-43.82	-11.02			5.07	-5.75		-5.68			-5.69	
	3.79	-13.80	-35.27	-2.07			9.46	-0.89			-0.88			-0.88
	4.84	-6.60			-9.39	-5.15	14.19	-0.26	-0.26			-0.26		
	7.15	-2.05			-4.77	-0.51	18.92	-0.11		-0.11			-0.11	
2	1.21	-1790.67	-1788.37	-1821.47	-1809.62	-1815.09	1.21	-1790.67	-1814.44	-1813.32	-1814.62	-1814.52	-1813.36	-1814.49
	1.79	-855.25	-907.61	-863.13	-879.25	-871.99	1.79	-855.25	-872.90	-874.28	-872.95	-872.85	-874.30	-873.18
	3.21	-148.12	-266.46	-80.06			5.07	-37.60		-37.62			-37.64	
	3.79	-90.20	-214.50	-15.04			9.46	-5.79			-5.83			-5.82
	4.84	-43.12			-61.39	-34.30	14.19	-1.71	-1.73			-1.72		
	7.15	-13.39			-31.22	-3.38	18.92	-0.72		-0.73			-0.72	

TABLE 7.9 - Radial stress comparison for the spherical cavity example of TABLE 7.7

SPHERICAL CAVITY - TANGENTIAL STRESSES

		ANALYT	FINITE ELEMENTS ONLY					ANALYT	FINITE+INFINITE ELEMENTS					
										12 NODE INF. EL.			16 NODE INF. EL.	
INC	RAD		FFXA	FFRA	FFXB	FFRB	RAD		F12IA	F12IB	F12IC	F16IA	F16IB	F16IC
1	1.21	211.19	199.79	243.87	223.62	229.18	1.21	211.19	228.50	227.44	228.57	228.52	227.44	228.64
	1.79	65.59	32.93	69.26	52.56	57.15	1.79	65.59	56.60	55.71	56.63	56.60	55.70	56.73
	3.21	11.33	-11.06	23.25			5.07	2.88		2.85			2.84	
	3.79	6.90	-15.46	18.66			9.46	0.44			0.44			0.44
	4.84	3.30			0.74	5.02	14.19	0.13	0.13			0.13		
	7.15	1.02			-1.94	2.34	18.92	0.06		0..06			0.05	
2	1.21	-590.67	-587.94	-621.22	-609.12	-614.58	1.21	-590.67	-613.95	-612.82	-614.15	-614.01	-612.85	-614.02
	1.79	344.75	130.38	337.31	263.57	297.63	1.79	344.75	293.42	286.83	293.96	293.46	286.82	294.47
	3.21	74.06	-67.20	168.91			5.07	18.80		18.87			18.82	
	3.79	45.10	-94.00	135.56			9.46	2.89			2.93			2.92
	4.84	21.56			4.81	33.46	14.19	0.86	0.87			0.86		
	7.15	6.70			-12.69	15.57	18.92	0.36		0.37			0.36	

TABLE 7.10 - Tangential stress comparison for the spherical cavity example of TABLE 7.7

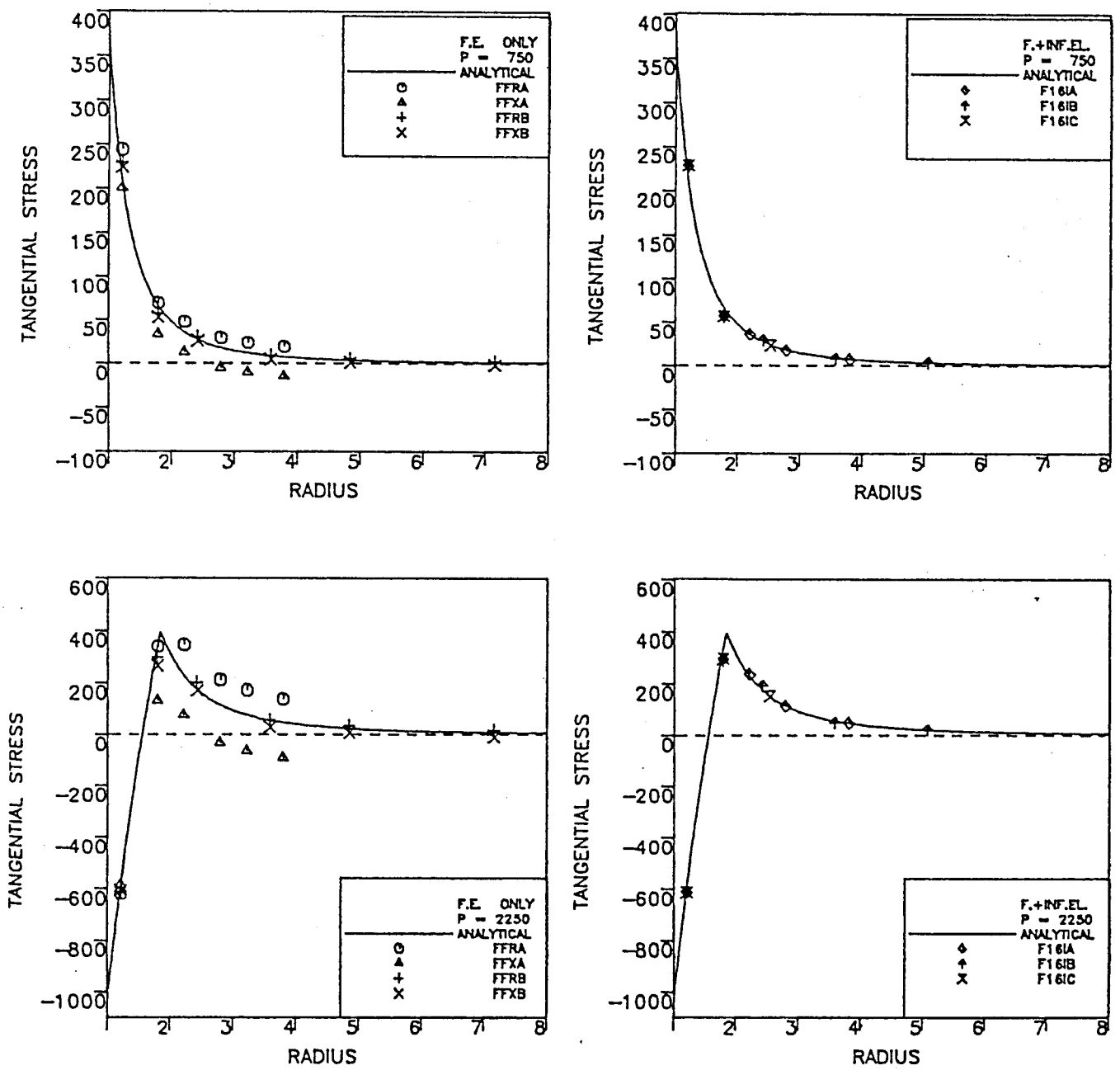

Fig. 7.3 – Tangential stress variation for the spherical cavity example of TABLE 7.7 for various finite and finite/infinite element solutions

Six other situations are also considered, in which an external layer of either 12-node or 16-node mapped infinite elements is attached to a finite element mesh. In meshes F12IA and F16IA there are 12 infinite elements attached to two layers of 12 finite elements whose boundaries are defined by the radial values 1, 2 and 3. The corresponding radial values for meshes F12IB and F16IB are 1, 2 and 4. In meshes F12IC and F16IC there are 12 infinite elements and one layer of 12 finite elements bounded by the radial values 1 and 2. Two load levels (p_1 = 750 and p_2 = 2250) are considered and the solution time for each analysis is included in Table 7.7.

The radial displacement and the radial and tangential stresses are compared with the analytical solution [74] in Tables 7.8-10. The tangential stress distribution is shown in Fig. 7.3 for both finite element and finite/infinite element solutions. The results obtained for all the finite/infinite element solutions are seen to be accurate. The effects of the presence of a finite boundary in the finite element only solutions are immediately apparent. From Tables 7.7-10 it is seen that for comparably accurate results (e.g. meshes FFRB and F12IA), the use of infinite elements approximately halves the computation costs.

7.9.4 Strip footing on an infinitely extended layer of associated Mohr-Coulomb material

This final example assesses the influence of the positioning of the far field boundary on the numerical solution to a strip footing situated on an infinitely extended layer of elastoplastic material. This problem was previously considered in Ref.[76]. Table 7.11 lists the problem parameters and illustrates both the finite element meshes and the finite/infinite element meshes employed in solution. In particular two finite element meshes containing 32 and 36 eight-node isoparametric elements (and coded 32F and 36F respectively) are considered as well as two meshes of 28 finite elements and 4 infinite elements with either 5 or 6 nodes (codes 28F415 and 28F416 respectively). The applied loading is incremented in steps of 20 up to a value of 140 and thereafter in smaller increments of 4, 2 and 1 as shown in Fig. 7.4(a) where the vertical displacement response of the point A is indicated. The

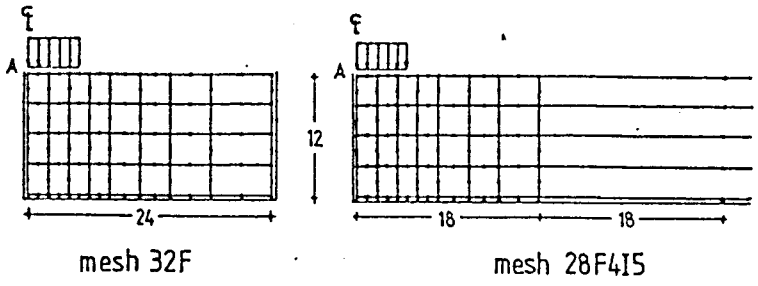

Elastic modulus, E = 30000.		Cohesion , C = 10.		
Poisson's ratio, ν = 0.3		Friction angle, ϕ = 20.		
Mesh	32F	36F	28F4I5	28F4I6
CPU time of 10 load steps (CDC 7600)	35.0	37.8	32.7	27.6

TABLE 7.11 – Geometric and material data for a strip footing on an infinitely extended layer of Mohr-Coulomb material

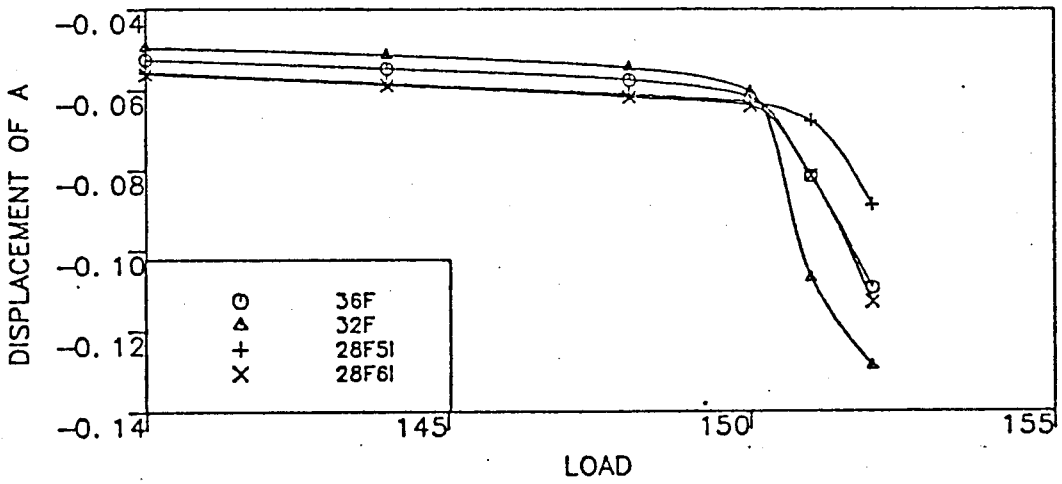

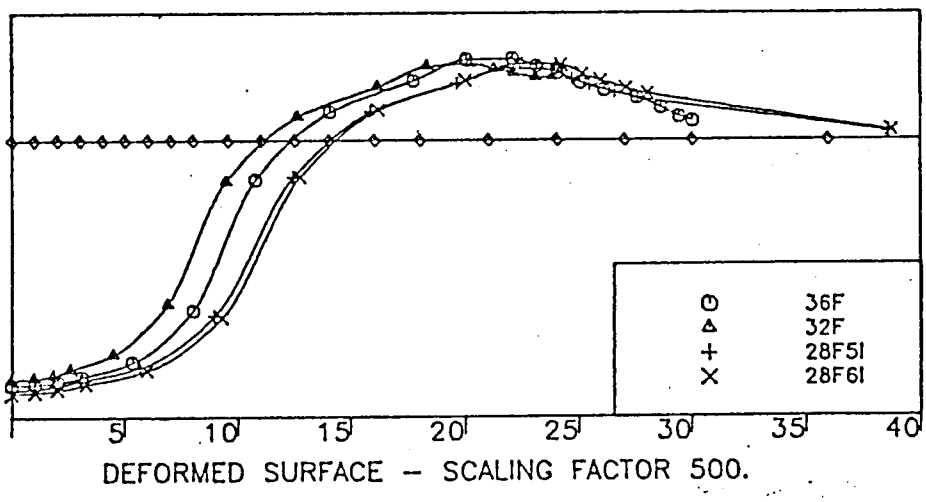

Fig. 7.4 – Displacement responses for the strip footing of TABLE 7.11
(a) Vertical displacement of point A with increasing applied load
(b) Profile of the deformed soil surface for an applied load p = 150

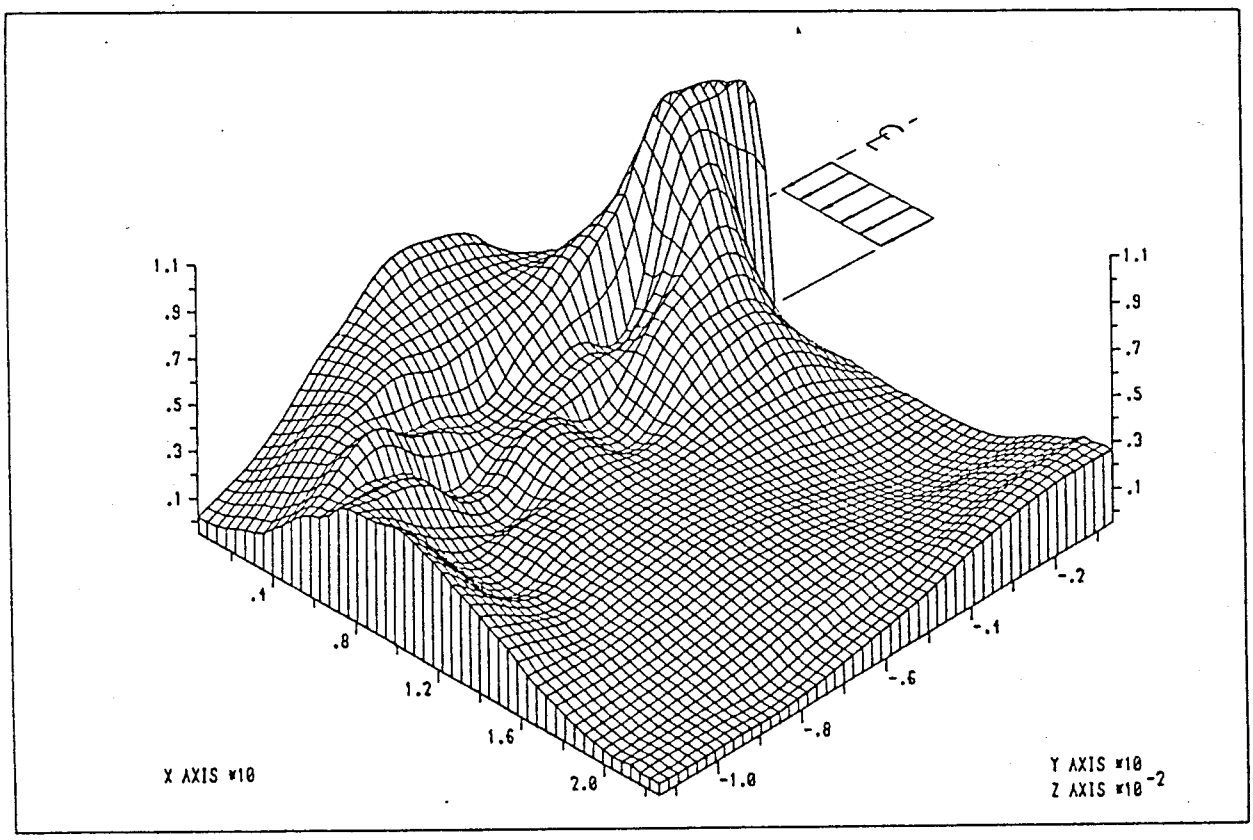

Fig. 7.5(a) - Isometric plot of the effective plastic strain for the strip footing problem of TABLE 7.11(finite element solution - 32 elements)

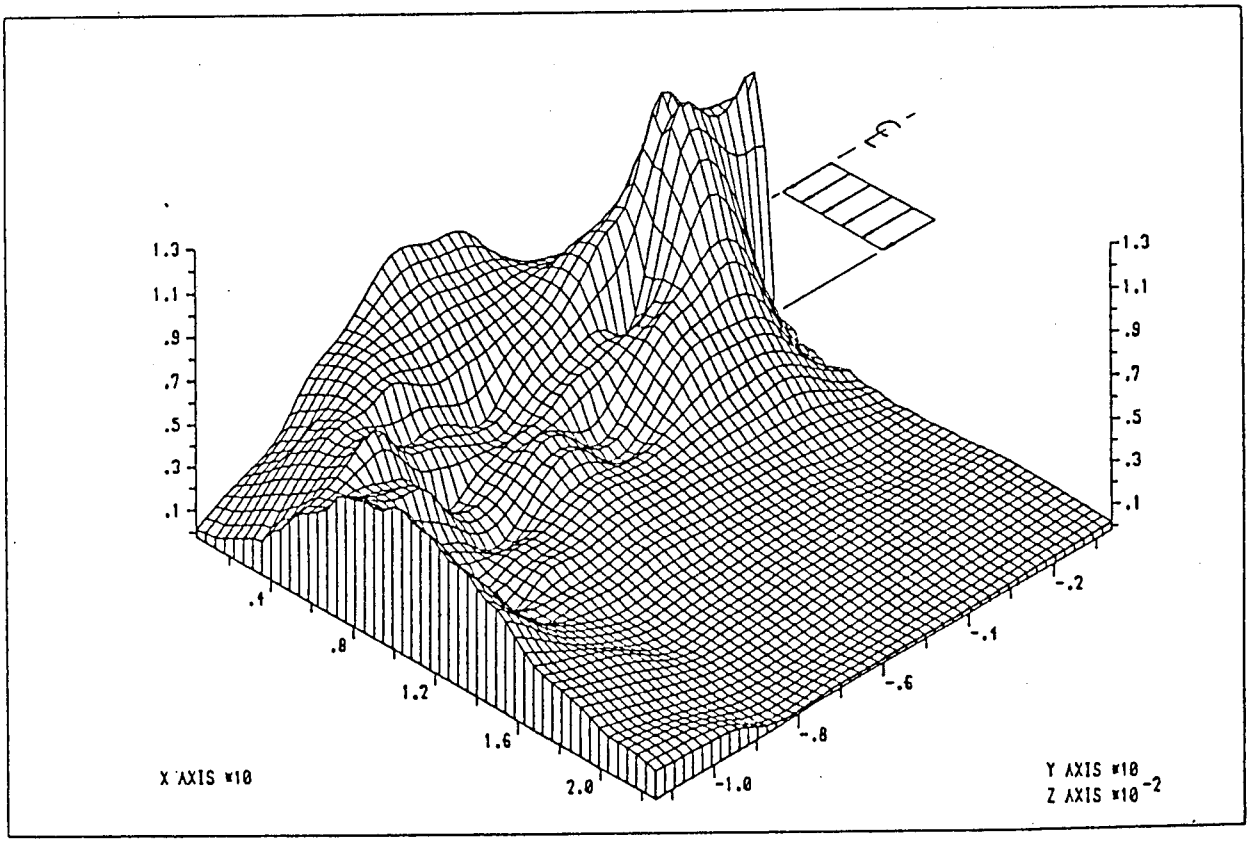

Fig. 7.5(b) - Isometric plot of the effective plastic strain for the strip footing problem of TABLE 7.11(finite/infinite element solution - 28 finite and 4 five noded mapped infinite elements)

profile of the deformed soil surface (magnified by 500) is shown in Fig. 7.4(b) for a load level p = 150. Both these displacement diagrams indicate a stiffening of the response as the distance of the far field boundary from the applied load is decreased.

Fig. 7.5(a) and (b) show an isometric view of the effective plastic strain over the same area for the 32 finite element solution and the finite/infinite solution with mesh 28F415. The excessive plastic deformation in the far field region predicted by the finite element only solution can be readily seen.

The finite/infinite element solutions give collapse loads which are in good agreement with Ref. [76]. Table 7.11 also shows that for a given total number of elements (either finite or infinite) the use of infinite elements leads to a reduction in the computation time required to achieve a converged solution.

7.10 ELASTOVISCOPLASTIC APPLICATIONS

In this section we employ the infinite element technique together with the explicit, implicit and implicit-explicit schemes described in Chapter 4 in the analysis of the following two-material elastoviscoplastic problems:

* internal pressure loading of a lined cylindrical cavity in an infinite medium;
* strip footing on an infinitely extending double horizontal layer.

The Mohr-Coulomb and Tresca yield criteria and their associated flow rules, as well as a linear flow function $\Phi = (f-Y)/Y$, are used. We recall that the critical time step length Δt_c for explicit time integration is $\Delta t_c = (1+\nu)Y/E\gamma$ for the Tresca case, while for the Mohr-Coulomb example we have

$$\Delta t_c = 4(1 + \nu)(1 - 2\nu)c \cos \phi/[(1 - 2\nu + \sin^2 \phi) E\gamma]$$

where E is the elastic modulus, ν Poisson's ratio, c the cohesion, ϕ the friction angle, Y the uniaxial yield stress and γ the fluidity parameter.

A constant time step size is used throughout each run for a clear comparison between the time integration techniques. The Δt_c ratio for the pair of materials involved in each of the problems presented is equal to or greater than 6 to 1; the conditional stability of the explicit scheme imposes the choice of the smaller Δt_c value; using the implicit-explicit or implicit formulations the larger value or multiples thereof are selected. The time integrations are performed with θ values of 0.0 and 1.0 respectively for the explicit and implicit elements.

The units used are m and kN, γ is /year and ρ denotes density; CPU times are measured in seconds on CDC 7600 or ICL 2966 computers.

The results presented illustrate once more the expedience and accuracy of the implicit-explicit scheme which make it an economic alternative for the solution of quasistatic viscoplastic problems in multi-material domains.

7.10.1 Lined cylindrical cavity in an infinite medium

Internal pressure is applied to the lining of a cylindrical cavity in an infinitely extending medium, where plane strain conditions and a perfectly plastic Tresca law are considered.

The material parameters and mesh geometry are given in Table 7.12 and the applied pressure is $p = 14250\ kN/m^2$.

To assess the steady state elastoviscoplastic results an elasto-plastic analytical solution has been derived from [75] by considering the displacement and pressure compatibility at the interface between the lining and the surrounding region.

In the discretization of this unbounded domain problem 6-node mapped infinite elements are coupled with isoparametric finite elements. The quality of the far field description can be judged from the numerical evidence of Table 7.13.

The implicit-explicit scheme leads to accurate steady state results in both the near and the far field regions as is also evident from the plots of radial displacement and stress components of fig. 7.6.

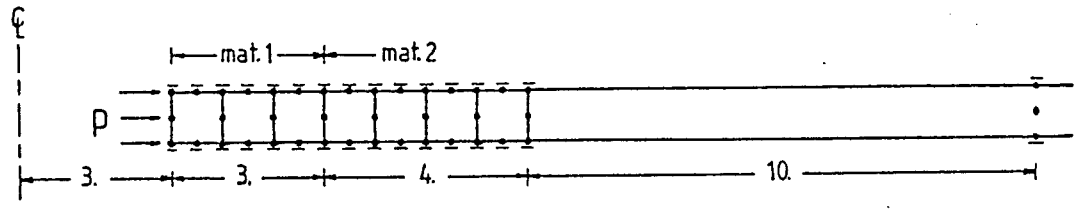

	E	ν	Y	γ	Δtc
Material 1	2.5E8	0.25	10000.	1.E-4	0.5
Material 2	2.5E7	0.25	10000.	1.E-4	5.0

TABLE 7.12 - Mesh geometry and material parameters for the lined cylindrical cavity in infinite medium problem

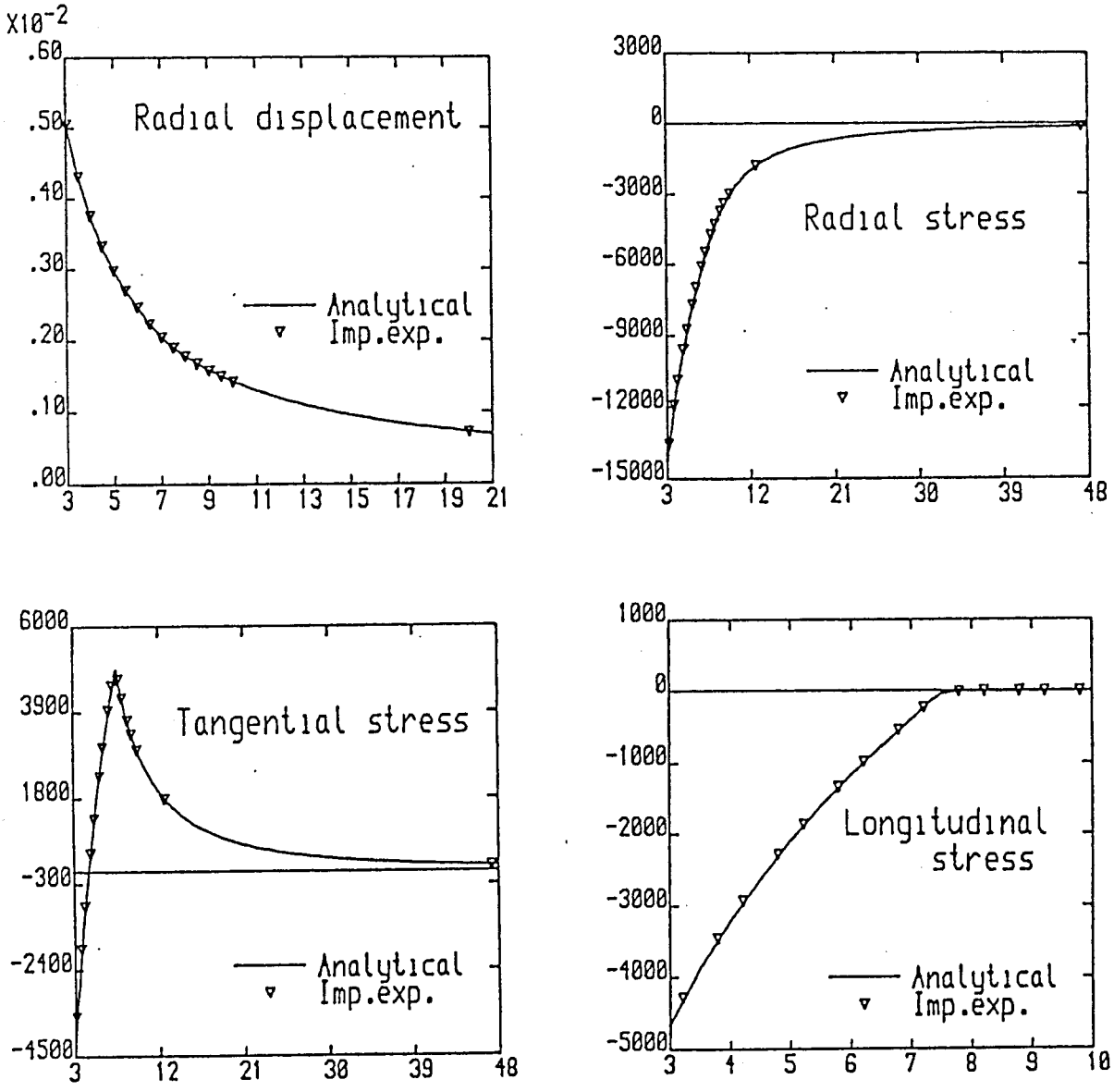

Fig. 7.6 - Implicit-explicit results (Δt=5.0) for the lined cylindrical cavity problem (with the radius measured on the horizontal axis)

	Radius	Analyt.	Imp. exp.	Imp. exp.	Implicit	Implicit	Explicit
T. step			5.00	10.00	5.00	50.00	0.50
Radial displ.(x1.E6)(m)	3.00	5071.92	5060.11	5117.78	5062.51	5075.21	5060.28
	3.50	4327.77	4317.69	4367.11	4319.75	4330.60	4317.84
	4.00	3770.36	3761.59	3804.82	3763.39	3772.86	3761.72
	4.50	3337.83	3330.08	3368.49	3331.67	3340.06	3330.20
	5.00	2993.00	2986.07	3020.63	2987.50	2995.02	2986.18
	5.50	2712.20	2705.95	2737.35	2707.24	2714.05	2706.05
	6.00	2479.62	2473.93	2502.70	2475.11	2481.33	2474.02
	6.50	2243.02	2238.26	2261.62	2239.34	2244.74	2238.39
	7.00	2055.36	2051.41	2069.27	2052.41	2057.10	2051.58
	7.50	1908.09	1904.58	1920.35	1905.34	1909.41	1904.62
	8.00	1788.70	1784.76	1799.48	1785.46	1789.25	1784.79
	8.50	1683.48	1679.78	1693.62	1680.43	1684.00	1679.81
	9.00	1589.95	1586.46	1599.53	1587.08	1590.45	1586.48
	9.50	1506.27	1502.96	1515.35	1503.54	1506.74	1502.98
	10.00	1430.96	1427.81	1439.58	1428.37	1431.40	1427.83
	20.00	715.48	713.90	719.79	714.18	715.70	713.92
Radial stress(kN/m2)	3.21	-13569.29	-13564.43	-13565.17	-13564.67	-13566.21	-13564.40
	3.79	-11915.96	-11910.13	-11912.31	-11910.84	-11915.39	-11910.04
	4.21	-10858.35	-10847.69	-10850.56	-10848.63	-10854.63	-10847.58
	4.79	-9573.58	-9562.48	-9566.03	-9563.63	-9571.04	-9562.34
	5.21	-8727.78	-8714.21	-8718.11	-8715.48	-8723.63	-8714.05
	5.79	-7677.09	-7663.28	-7667.55	-7664.67	-7673.59	-7663.11
	6.21	-6972.38	-6957.11	-6969.57	-6958.47	-6967.91	-6956.81
	6.79	-6083.56	-6068.06	-6102.29	-6069.27	-6079.39	-6067.49
	7.21	-5479.60	-5459.27	-5501.65	-5460.88	-5471.55	-5459.00
	7.79	-4717.70	-4711.25	-4750.45	-4713.17	-4723.30	-4711.39
	8.21	-4244.54	-4235.53	-4270.45	-4237.19	-4246.19	-4235.61
	8.79	-3705.19	-3696.74	-3727.22	-3698.19	-3706.04	-3696.81
	9.21	-3372.97	-3365.74	-3393.49	-3367.06	-3374.21	-3365.80
	9.79	-2986.82	-2980.08	-3004.65	-2981.25	-2987.58	-2980.13
	12.68	-1780.14	-1776.22	-1790.86	-1776.91	-1780.69	-1776.25
	47.32	-127.81	-127.53	-128.58	-127.58	-127.85	-127.53
Tangential stress(kN/m2)	3.21	-3569.29	-3531.01	-3541.94	-3534.57	-3557.40	-3530.56
	3.79	-1915.96	-1886.17	-1895.66	-1889.26	-1909.07	-1885.78
	4.21	-858.35	-828.27	-837.06	-831.13	-849.50	-827.91
	4.79	426.41	452.52	444.40	449.88	432.92	452.85
	5.21	1272.22	1298.46	1290.70	1295.93	1279.71	1298.78
	5.79	2322.91	2346.98	2339.59	2344.58	2329.12	2347.29
	6.21	3027.62	3052.94	2803.92	3053.44	3035.58	3056.58
	6.79	3916.43	3940.35	3652.56	3940.70	3923.49	3943.71
	7.21	4520.40	4561.40	4523.71	4547.96	4531.15	4550.93
	7.79	4717.70	4702.30	4740.70	4704.06	4713.93	4702.33
	8.21	4244.54	4235.53	4270.45	4237.19	4246.19	4235.61
	8.79	3705.19	3696.74	3727.22	3698.19	3706.04	3696.81
	9.21	3372.97	3365.74	3393.49	3367.06	3374.21	3365.80
	9.79	2986.82	2980.08	3004.65	2981.25	2987.58	2980.13
	12.68	1780.14	1776.22	1790.86	1776.91	1780.69	1776.25
	47.32	127.81	127.53	128.58	127.58	127.85	127.53
Longitudinal stress(kN/m2)	3.21	-4284.64	-4273.86	-4276.78	-4274.81	-4280.90	-4273.74
	3.79	-3457.98	-3449.08	-3451.99	-3450.02	-3456.12	-3448.96
	4.21	-2929.17	-2918.99	-2921.91	-2919.94	-2926.03	-2918.87
	4.79	-2286.79	-2277.49	-2280.41	-2278.44	-2284.53	-2277.37
	5.21	-1863.89	-1853.94	-1856.85	-1854.89	-1860.98	-1853.82
	5.79	-1338.54	-1329.07	-1331.99	-1330.02	-1336.12	-1328.95
	6.21	-986.19	-976.04	-1041.41	-976.26	-983.08	-975.06
	6.79	-541.78	-531.93	-612.43	-532.14	-538.98	-530.94
	7.21	-239.80	-224.47	-244.48	-228.23	-235.10	-227.02
	7.79	0.00	-2.24	-2.44	-2.28	-2.34	-2.26
	8.21	0.00	0.00	0.00	0.00	0.00	0.00

TABLE 7.13 - Solution comparison for the lined cylindrical cavity in an infinite medium

This problem illustrates how to make the most of two efficient techniques: the finite/infinite element coupling, to model economically the unbounded domain, combines with implicit-explicit time integration, to overcome expediently unequal time step size restrictions.

7.10.2 Strip footing on an infinitely extended double layer of Mohr-Coulomb soil

A strip footing applies a distributed load $p = 40kN/m^2$ on two horizontal layers of associated Mohr-Coulomb soil that extend infinitely as described in Table 7.14. Plane strain conditions are assumed and four 5-node isoparametric infinite elements model the far field. The finite-infinite element association has been previously used in this context in the example of Section 7.9.4, where a series of tests carried out against finite element only meshes of increasing width assesses the realism of the infinite element far field mapping.

The displacement components of the surface nodes are plotted in fig. 7.7 for various solutions and are seen to agree well.

The area corresponding to the 28 finite elements of Table 7.14 is shown in fig. 7.8 where a typical pattern of "plastic" (i.e. final minus instantaneous elastic) displacements is magnified 2500 times. An isometric view of the effective plastic strain on the same area is depicted in fig. 7.9 showing a peak for the plastic flow on the layer interface below the load.

Computer times are compared in Table 7.15 and the economies provided by the use of implicit-explicity integration are again evident.

	Mat. 1	Mat. 2
E	2.0E4	3.5E4
ν	0.25	0.35
c	10.0	3.0
ϕ	20.0	20.0
γ	1.E-4	1.E-4
Δtc	19.04	3.13

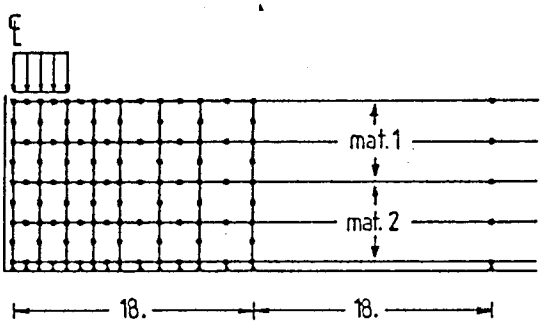

TABLE 7.14 - Mesh geometry and material parameters for the strip footing on layered soil problem

	EXP	IMP	IMP	IMP--EXP	IMP-EXP
ΔT(const.)	3.1	19.0	190.0	19.0	28.5
Time steps	55	19	11	15	8
dv (mm)	-13.571	-13.620	-13.772	-13.624	-13.733
CPU(ICL 2966)	244	222	124	132	76

TABLE 7.15 - Vertical displacement of node S(fig.7.8) and CPU time for various solutions of the footing problem

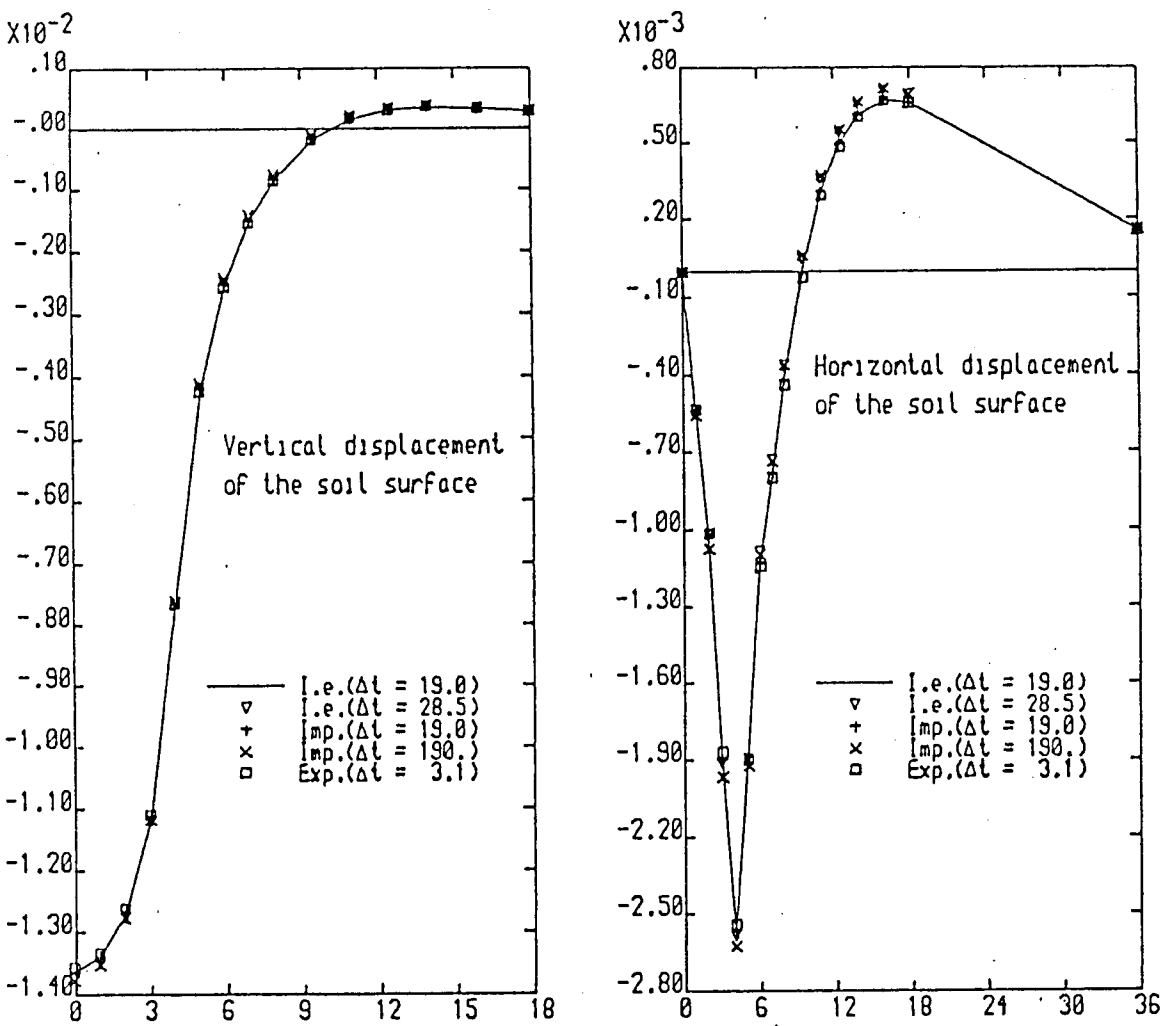

Fig. 7.7 - Displacement components of the surface nodes for various solutions of the strip footing problem

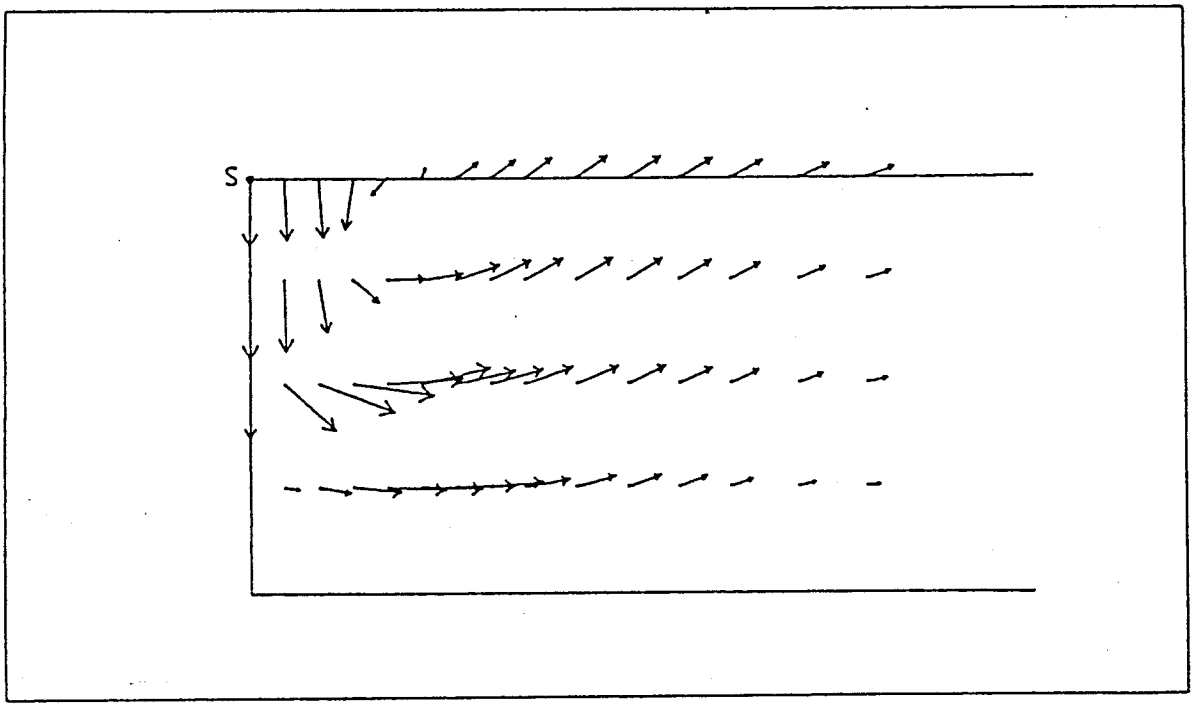

Fig. 7.8 – "Plastic" nodal displacement vectors for the strip footing on layered soil problem

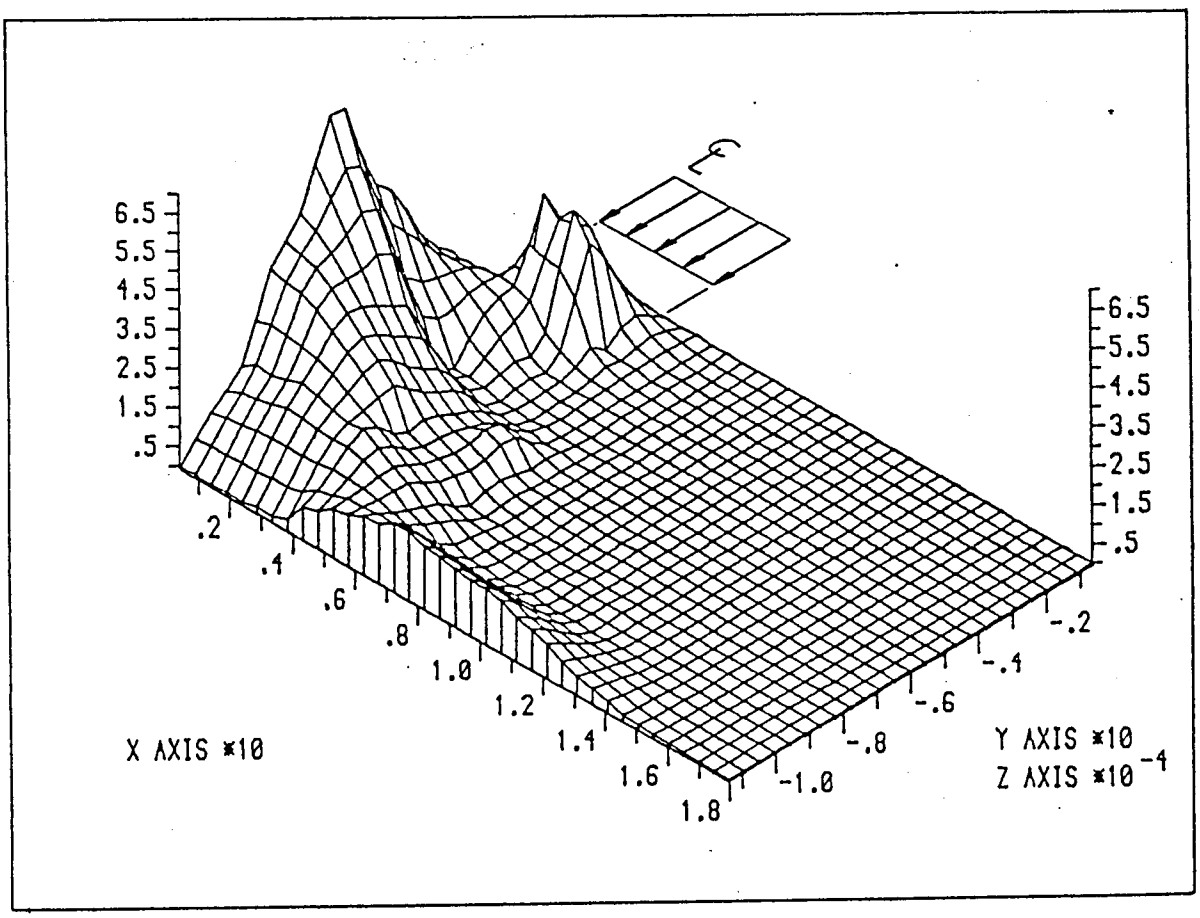

Fig. 7.9 – Isometric view of the effective plastic strain in the strip footing on layered soil problem

7.11 CONCLUDING REMARKS

We have examined the use of both two- and three-dimensional mapped infinite elements in quasistatic problems with anelastic deformation.

The numerical examples presented indicate that a combined finite-infinite element approach to unbounded domains results in substantial savings in both computer time and storage, arising from the reduced number of degrees of freedom required for accurate solution. This is particularly important in three-dimensional problems where an expedient handling of far field regions has a dramatic incidence in reducing the total costs of analysis.

Furthermore the examples presented show that, for a given number of degrees of freedom, a combined finite-infinite element approach provides more accurate solutions than a simple finite element modelling, with the sole constraint that the plastic deformation zone should not invade any infinite element.

In addition the viscoplastic solutions illustrate the accrued advantages of the combined use of implicit-explicit and finite-infinite coupling techniques.

7.12 REFERENCES

1. THOMSON, W. (LORD KELVIN), Note on the integration of the equations of equilibrium of an elastic solid, Cambridge and Dublin Math. J., 3, 87-89, 1848 (also Mathematical and Physical Papers, 1, 37, Cambridge Univ. Press, 1882).

2. BOUSSINESQ, J., Application des potentiels à l'étude de l'équilibre et du mouvement des solides élastiques, Gauthier-Villars, Paris, 1885

3. MINDLIN, R.D., Force at a point in the interior of a semi-infinite solid, Physics, 7, 195-202, 1936

4. RONGVED, L., Force at a point in the interior of a semi-infinite solid with fixed boundary, J. Appl. Mech., 545-546, 1955

5. KIRSCH, G., Die Theorie der Elastizität und die Bedürfnisse der Festigkeitslehre, Z. der Ver. deutscher Ingenieure, 42, 797, 1898

6. BICKLEY, W.G., The distribution of stress round a circular hole in a plate, Trans. Roy. Soc. (London) A, 227, 383-415, 1928

7. KOLOSOV, G.V., On the application of complex function theory to a plane problem in the mathematical theory of elasticity (in Russian), Dissertation at Dorpat Univ., 1909 (also Über einige Eigenschaften des ebenen Problems der Elastizitätstheorie, Z. Math. Phys., 62, 383-409, 1914)

8. INGLIS, C.E., Stresses in a plate due to the presence of cracks and sharp corners, Proc. Inst. Nav. Arch., 60, 1913

9. MARGUERRE, K., Druckverteilung durch eine elastiche Schicht auf starrer rauher Unterlage, Ing. Arch., 2, 108-117, 1931

10. SHIELD, R.T. and DRUCKER, D.C., The application of limit analysis to punch indentation problems, J. Appl. Mech., 20, 453-460, 1953

11. HENCKY, H., Über einige statisch bestimmte Fälle des Gleichgewichts in plastischen Körpern, ZAMM, 3, 211-251, 1923

12. ISHLINSKY, A.Y., The axially-symmetric problem of the theory of plasticity and the Brinell's test (in Russian), Prikl. Mat. Mekh., 8, 3, 1947

13. HILL, R., General features of elastic-plastic problems as exemplified by some particular solutions, J. Appl. Mech., 16, 295-300, 1949

14. MURCH, S.A. and NAGHDI, P.M., On the infinite elastic, perfectly plastic wedge under uniform surface tractions. Proc. 3rd U.S. Nat. Congr. of Appl. Mech., 611-624, ASME, 1958

15. ZIENKIEWICZ, O.C., BETTESS, P., CHIAM, T.C. and EMSON, C., Numerical methods for unbounded field problems and a new infinite element formulation, Winter Annual Meeting of the A.S.M.E., Washington, D.C., 1981, The Applied Mechanics Division, 115-148, 1981

16. SMITH, W.D., A non reflecting plane boundary for wave propagation problems, J. Comp. Phys., 15, 493-503, 1974

17. ZIENKIEWICZ, O.C. and NEWTON, R.E., Coupled vibrations of a structure immersed in a compressible fluid, Proc. Symp. on Finite Element Techniques, Stuttgart, 1969

18. ZIENKIEWICZ, O.C., KELLY, D.W. and BETTESS, P., The Sommerfeld (radiation) condition on infinite domains and its modelling in numerical procedures, in Computing Methods in Applied Sciences and Engineering, R. Glowinski et al. (eds.), 169-203, Springer Verlag, 1979

19. LYSMER, J. and KUHLEMEYER, R.L., Finite dynamic model for infinite media, J. Eng. Mech. Div., Proc. ASCE, 859-877, 1969

20. LYSMER, J. and WAAS, G., Shear waves in plane infinite structures, J. Eng. Mech. Div., Proc. ASCE, 85-105, 1972

21. BAYLISS, A., GUNZBERGER, M. and TURKEL, E., Boundary conditions for the numerical solution of elliptic equations in exterior regions, ICASE Report No. 80-1, NASA, Langley, 1978

22. BAYLISS, A. and TURKEL, E., Radiation boundary conditions for wave-like equations, ICASE Report No. 79-26, NASA, Langley, 1979

23. RICHARDSON, L.F., The approximate arithmetical solution by finite differences of physical problems involving differential equations, with an application to the stresses in a masonry dam, Trans. Roy. Soc. London. Ser. A210, 307-357, 1910

24. WAAS, G., Linear two dimensional analysis of soil dynamics problems in semi-infinite layered media. Ph.D. Thesis, Univ. of California, Berkeley, 1972

25. SILVESTER, P. and HSIEH, M.S., Finite element solution of two dimensional exterior field problems, Proc. I.E.E. V.118, 1743-1747, Dec. 1971

26. McDONALD, B.H. and WEXLER, A., Finite element solution of unbounded field problems, I.E.E.E. Transactions on microwave theory and techniques, Vol. MTT-20, No.12, 841-847, 1972

27. BERKHOFF, J.C.W., Computation of combined refraction-diffraction, Proc. 13th Int. Conf. on Coastal Engineering, Vancouver, 1972

28. KARAIOSIFIDIS, S., A comparison of solution methods for exterior surface wave problems. M.Sc. Thesis, University of Wales, 1976

29. BREBBIA, C.A., The Boundary Element Method for Engineers, Pentech Press, 1980

30. BEER, G. and MEEK, J.L., The coupling of boundary and finite element methods for infinite domain problems in elastoplasticity, Proc. 3rd Int. Sem. on Boundary Element Methods, C.A. Brebbia (ed.) Irvine, California, 1981

31. BALAS, J. and SLADEK, J., Method of boundary integral equations for analysis of three dimensional crack problems, idem.

32. OTTENSTREUER, M. and SCHMID, G., Boundary elements applied to soil-foundation interaction, idem.

33. TELLES, J.C.F. and BREBBIA, C.A., New developments in elastoplastic analysis, idem.

34. TELLES, J.C.F. and BREBBIA, C.A., Boundary element solution for half-plane problems, Int. J. Sol. Struct. (In press)

35. BEER, G. and MEEK, J.L., Coupled infinite element-boundary element analysis of infinite domain problems in geomechanics, Proc. Int. Conf. on Num. Meth. for Coupled Problems, E. Hinton et al. (eds.), Pineridge Press, Swansea, 1981

36. ZIENKIEWICZ, O.C., KELLY, D.W. and BETTESS, P., The coupling of the finite element and boundary solution procedures, Int. J. Num. Meth. Engng., 11, 355-375, 1977

37. ZIENKIEWICZ, O.C., KELLY, D.W. and BETTESS, P., Marriage à la mode - the best of both worlds (finite elements and boundary integrals), Int. Symp. on Innovative Num. Anal. in Appl. Engng. Science, Versailles, France, 1977

38. KELLY, D.W., MUSTOE, G.G. and ZIENKIEWICZ, O.C., Coupling Boundary Element Methods with other numerical methods, in Developments in Boundary Element Methods - 1, 251 - 285, Applied Science Publishers, London, 1979

39. NATH, B., The w-plane finite element method for the solution of scalar field problems in two dimensions, Int. J. Num. Meth. Engng., 15, 361-379, 1980

40. NATH, B., The w-plane finite element method for the solution of the steady-state scalar wave equation in two dimensions, Earthquake Engng. and Str. Dyn., 8, 181-191, 1980

41. GARTLING, D. and BECKER, E.B., Computationally efficient finite element analysis of viscous flow problems, Proc. Int. Conf. on Computational Methods in Non-linear Mechanics, Univ. of Texas, Austin, Texas, 1974

42. DENNIS, S.C.R. and WALKER, J.D.A., Steady flow past a sphere at low and moderate Reynolds numbers, J. Fluid Mech., 48, 771-789, 1971

43. ROACH, P.J., Computational Fluid Dynamics, Hermosa Publishers, Albuquerque, New Mexico, 1976

44. UNGLESS, R.L., An infinite finite element, M.A.Sc. Thesis, Univ. of British Columbia, 1973

45. ANDERSON, D.L. and UNGLESS, R.L., Infinite finite elements, Int. Symp. on Innovative Numerical Analysis in Applied Engineering Science, Versailles, France,1977

46. BETTESS, P., Infinite elements, Int. J. Num. Meth. Engng., 11, 53-64, 1977

47. BETTESS, P., More on infinite elements, Int. J. Num. Meth. Engng., 15, 1613-1626, 1980

48. BETTESS, P. and BETTESS, J.A., Infinite elements for static problems, Int. J. Engng. Computations, 1, 4-16, 1984

49. BETTESS, P. and ZIENKIEWICZ, O.C., Diffraction and refraction of survace waves using finite and infinite elements, Int. J. Num. Meth. Engng., 11, 1271-1290, 1977

50. ZIENKIEWICZ, O.C. and BETTESS, P., Infinite elements in the study of fluid structure interaction problems, Lecture Notes in Physics, Springer Verlag, 58, 133-172, 1976

51. LYNN, P.P. and HADID, H.A., Infinite elements with $1/r^n$ type decay, Int. J. Num. Meth. Engng., 17, 347-355, 1981

52. SAINI, S.S., BETTESS, P. and ZIENKIEWICZ, O.C., Coupled hydro-dynamic response of concrete gravity dams using finite and infinite elements, Earthquake Eng. and Structural Dynamics, 16, 363-374, 1978

53. CHOW, Y.K., Dynamic behaviour of piles, Ph. D. Thesis, Univ. of Manchester, 1981

54. CHOW, Y.K., and SMITH, I.M., Static and periodic infinite solid elements, Int. J. Num. Meth. Engng. 17, 503-526, 1981

55. MEDINA-MELO, F.J., Modelling of soil-structure interaction by finite and infinite elements. Ph.D. Thesis, Univ. of California, Berkeley, 1981.

56. MEDINA, F., An axisymmetric infinite element, Int. J. Num. Meth. Engng., 17, 1177-1185, 1981

57. MEDINA, F., Direct finite element method for linear soil-structure interaction, Proc. Int. Conf. on Numerical Methods for Coupled Problems, E. Hinton et al. (eds.), Pineridge Press, Swansea, 1981

58. BEER, G. and MEEK, J.L., Infinite domain elements, Int. J. Num. Meth. Engng., 17, 43-52, 1981.

59. MARQUES, J.M.M.C. and OWEN, D.R.J., Infinite elements in quasistatic materially nonlinear problems, Comp. & Str., 18,739-751,1984

60. MARQUES, J.M.M.C. and OWEN, D.R.J., Implicit-explicit time integration in quasistatic elastoviscoplasticity using finite and infinite elements, Comp. Meth. Appl. Mech. Engng., 42, 167-182, 1984

61, EMSON, C. and BETTESS, P., Application of infinite elements to external electromagnetic field problems, Proc. Int. Conf. on Num. Meth. for Coupled Problems, E. Hinton et al. (eds.), Pineridge Press, Swansea, 1981

62. ZIENKIEWICZ, O.C., EMSON, C. and BETTESS, P., A novel boundary infinite element, Submitted to Int. J. Num. Meth. Engng., 1982

63. BETTESS, P., EMSON, C. and CHIAM, T.C., A new mapped infinite element for exterior wave problems, Internal Report C/R/403/82, Dept. Civil Eng., University College of Swansea, 1982.

64. DAMJANIC, F., Reinforced concrete failure prediction under both static and transient conditions. Ph.D. Thesis, University of Wales, 1983.

65. DAMJANIC, F. and OWEN, D.R.J., Mapped infinite elements in transient thermal analysis, Computers and Structures (in press)

66. BETTESS, P., EMSON, C. and BANDO, K., Some useful techniques for the testing of infinite elements, Internal Report C/R/411/82, Dept. Civil Eng., University College of Swansea, 1982

67. RUKOS, E.A., Continuous elements in the finite element method, Int. J. Num. Meth. Engng., 12, 11-33, 1978

68. PISSANETZKY, S., An infinite element and a formula for numerical quadrature over an infinite interval, IJNME, 19, 913-928, 1983

69. PISSANETZKY, S., A simple infinite element, COMPEL, Boole Press, to be published

70. CURNIER, A., A static infinite element, IJNME, 19, 1479-1488, 1983

71. OKABE, N., Generalised Lagrange family for the cube with special reference to infinite domain interpolations, Comp. Meth. Appl. Mech. and Engng., 38, 153-168, 1983

72. ZIENKIEWICZ, O.C., The Finite Element Method, 3rd edition, McGraw-Hill, 1977

73. OWEN, D.R.J. and HINTON, E., Finite Elements in Plasticity - Theory and Practice, Pineridge Press, Swansea, 1981

74. VENKATRAMAN, B. and PATEL, S.A., Structural Mechanics with Introductions to Elasticity and Plasticity, McGraw-Hill

75. BLAND, D.R., Elastoplastic thick-walled tubes of work-hardening material subject to internal and external pressures and to temperature gradients, J. Mech. Phys. Sol., 4, 209-229, 1956

76. ZIENKIEWICZ, O.C., HUMPHESON, C. and LEWIS, R.W., Associated and non-associated visco-plasticity and plasticity in soil mechanics, Geotechnique, 25, 671-689, 1975

CHAPTER 8

MAPPED INFINITE ELEMENTS IN DYNAMIC STRUCTURAL ANALYSIS

8.1	INTRODUCTION	8.1
8.2	PERIODIC AND TRANSIENT PROBLEMS IN UNBOUNDED DOMAINS	8.1
8.3	MAPPED INFINITE ELEMENTS IN TRANSIENT PROBLEMS	8.2
8.4	INFINITE ELEMENTS IN PERIODIC PROBLEMS	8.2
8.5	NUMERICAL EXPERIMENTS	8.3
8.6	REFERENCES	8.8

CHAPTER 8

MAPPED INFINITE ELEMENTS IN DYNAMIC STRUCTURAL ANALYSIS

8.1 INTRODUCTION

Spatial domains extending to infinity are the natural setting for many transient phenomena of engineering significance. Such is the case with most instances of structural interaction with soil and/or fluid media, as those pertaining to foundation and earthquake analysis, coastal and offshore engineering, design of floating or flying structures.

As mentioned in Chapter 7, several approaches have been proposed that contemplate particular forms of the problem, but no method of general applicability is as yet available.

In view of the excellent quasistatic performance of the mapped infinite element, a logical development is to assess its potential for transient dynamic unbounded domain problems. This Chapter gives an account of the preliminary results of a continuing investigation.

8.2 PERIODIC AND TRANSIENT PROBLEMS IN UNBOUNDED DOMAINS

In dynamic unbounded domain problems the so called finiteness [1] and (Sommerfeld) radiation [1,2] conditions respectively demand that in the far field both displacements and stresses remain finite and that only outward travelling waves be present.

Truncation of the domain of analysis at a finite location introduces a reflective boundary, thereby causing a build up of energy that can lead to numerical instabilities [8]. The boundary dampers of Lysmer and Kuhlemeyer [3], recently generalized by Bayliss [4], aim at absorbing the outgoing wave. Smith [5] cancels the reflecting effect by alternating between Neumann and Dirichlet

boundary conditions in a costly total of 2^h solutions, where n is the number of wave reflections. Dasgupta [15] presents a "cloning algorithm" that accommodates the Sommerfeld condition. Zienkiewicz [6,7] shows that the radiation condition amounts to the introduction of a damping term that ensures constant energy loss from the system.

8.3 MAPPED INFINITE ELEMENTS IN TRANSIENT PROBLEMS

Truncation can be avoided and the external region included in the analysis by resorting to infinite elements. This gives conceivably the means of reproducing the "geometric damping" [8] experienced by the waves when travelling outwards through an increasingly larger volume. On the other hand, the material damping present in many nonlinear problems [8] can be tentatively modelled via the damping matrix of the infinite element. We note that the procedure for the computation of the infinite element stiffness matrix described in Section 7.8.2 is readily adapted for the calculation of the consistent or lumped mass matrix as given by expressions (2.9a) and (2.10). And so at least a Rayleigh damping matrix of the form (2.11) can be constructed.

In relation to this approach it is interesting to note that Pedro [9] (quoted in [8]) suggests a combination of mass, stiffness and damping imposed at a finite boundary to simulate the exterior domain. It appears therefore tempting to assess how far can the representation of such characteristics of the external region, automatically supplied by the infinite element mapping, be a physically acceptable basis for such purpose.

This is in brief the intuitive motivation for this study. Other approaches also related to infinite elements are described in the next Section.

8.4 INFINITE ELEMENTS IN PERIODIC PROBLEMS

Infinite elements have been successfully applied to periodic exterior wave problems. The first such solutions employed decay function infinite element that combine the standard finite element shape function with an exponential decay term and a periodic

component [10,11]. Chow and Smith [12] used that element for periodic elastic wave applications, assuming a special split between the shear and dilatational wave components.

Recently an infinite wave element has been formulated by incorporating an oscillatory term in the mapped infinite element and employing a special integration rule [13].

Bettess [14] suggests the use of Heaviside transform type techniques to enable the periodic infinite element to cope with fully transient situations.

8.5 NUMERICAL EXPERIMENTS

The mapped infinite element in the basic form described in Chapter 7 cannot be expected to provide a detailed rendition of transient conditions on the far field. For that purpose the infinite wave element [13] is a better suited tool.

The aim of the numerical investigation reported below is twofold:

(i) examine the effect of expanding a finite element only mesh by adding infinite elements in order to detect at an early stage any impending numerical difficulties and also to obtain some insight into the meaning of the corresponding results;

(ii) assess the sensitivity of the solution to the material properties assigned to the infinite element.

Point load on an elastic half space

A vertical point load is applied on the horizontal boundary of an elastic half space with a constant unit value during a time interval of one second and is then removed.

The assumed material properties are Young modulus, E= 1., Poisson's ratio, ν = 0.1 and mass density, ρ = 1.E-5.

A 20-element axisymmetric mesh is obtained by combining four 6-node mapped infinite elements with 16 (8-node) finite

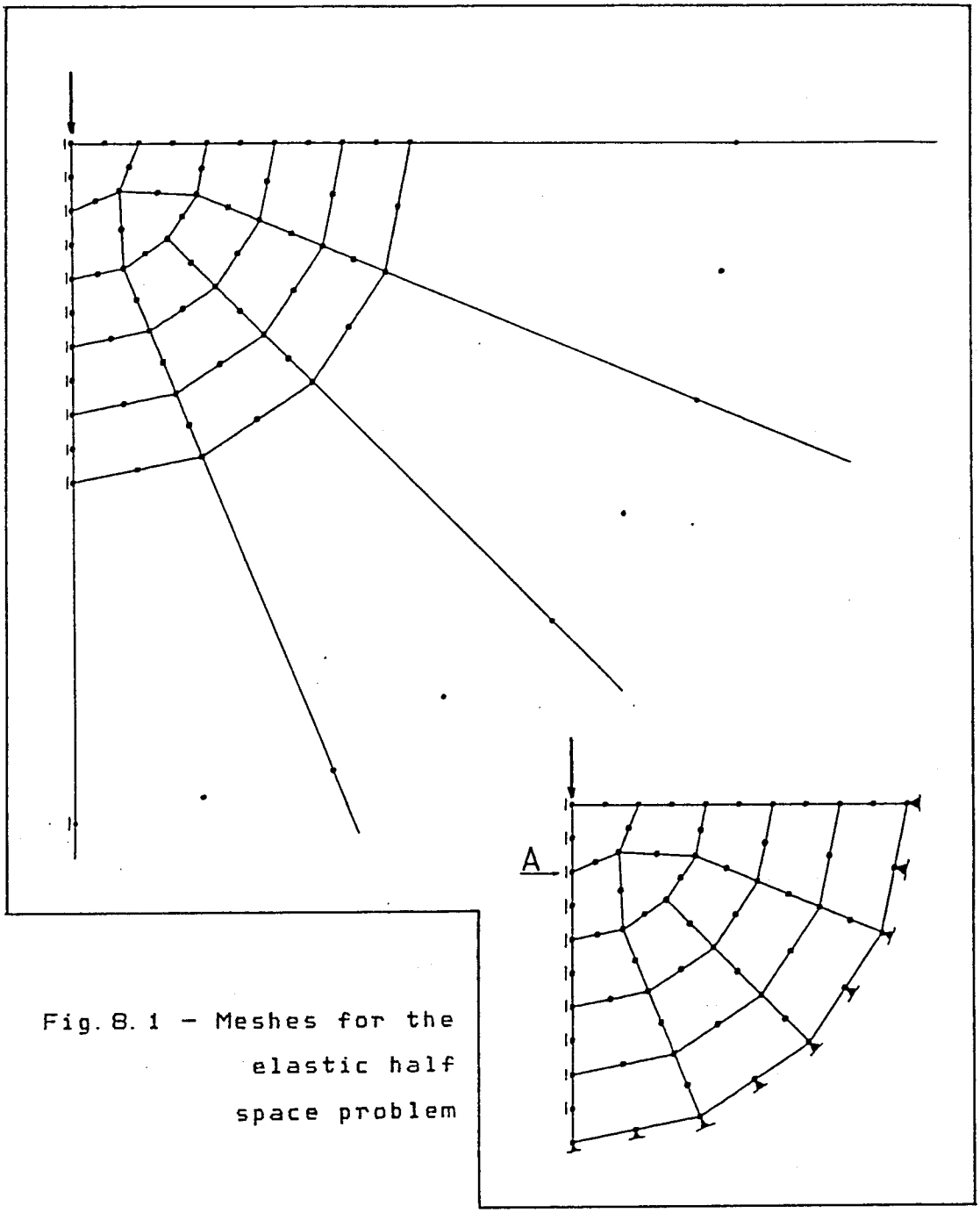

Fig. 8.1 – Meshes for the elastic half space problem

elements as shown in fig.8.1, where node A is at a depth below the surface of value 1.

In fig.8.2 the static solution for the vertical displacement of points on the axis of symmetry obtained with the two meshes is compared with the Boussinesq analytical values [16]. For node A the F.E. only mesh gives -0.37469, the coupled F.E.+I.E. mesh yields

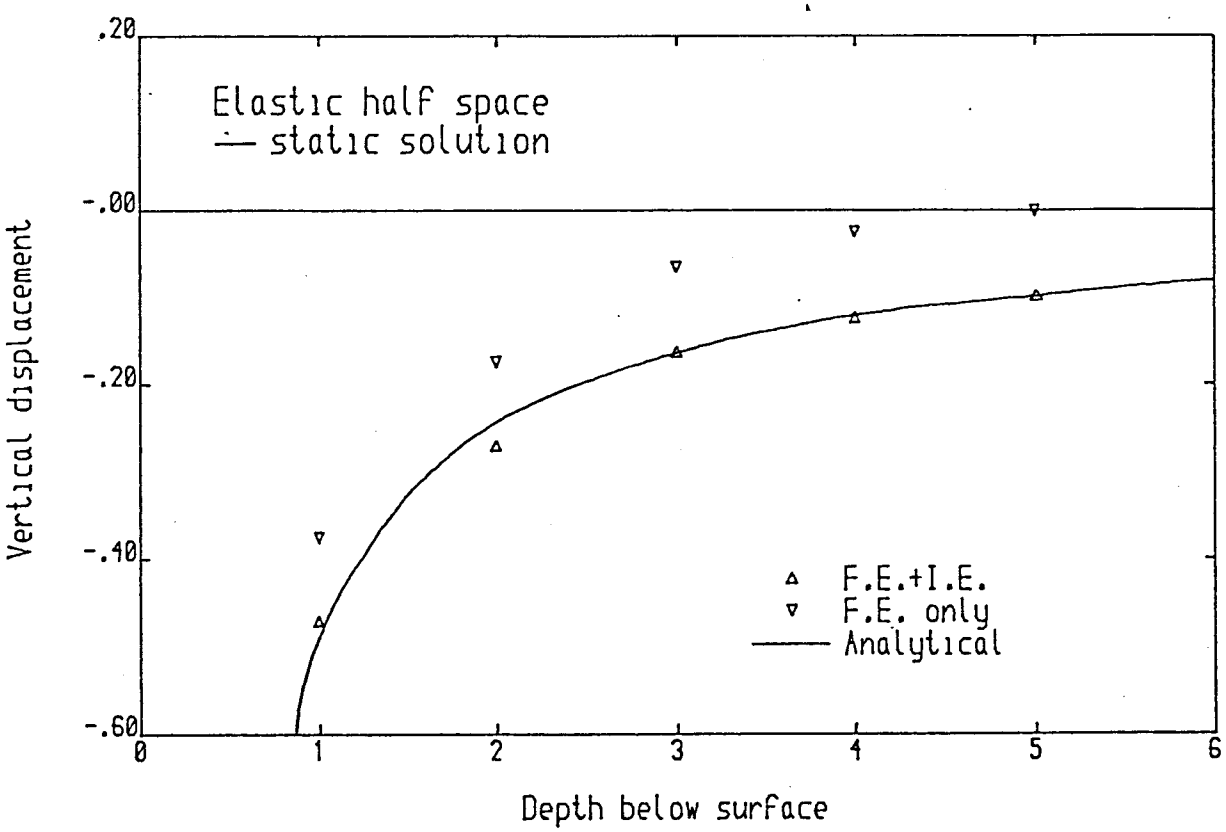

Fig. 8.2 - Plot of the vertical displacement below the load for static solutions of the elastic half space problem

-0.47039 and the exact solution is -0.49020.

In fig.8.3 the vertical displacement history of node A is plotted during a time interval of 10 seconds that extends well beyond the moment of load removal at t= 1.

Comparing the F.E. only and F.E.+I.E. results a pattern is discernible in both cases: the curves oscillate during the first second around the respective static solution values (indicated by arrows in the plots) and then fluctuate around zero.

Having therefore succeeded in our first aim, we now consider the effect of multiplying the mass density of the infinite element zone by a factor R. The results corresponding to values of R of 1.E+3 and 1.E-3 are presented in fig.8.3. Increasing the inertia of the infinite element zone (R= 1.E+3) induces a perceptible sinusoidal pattern after t= 1. Reducing R to 1.E-3

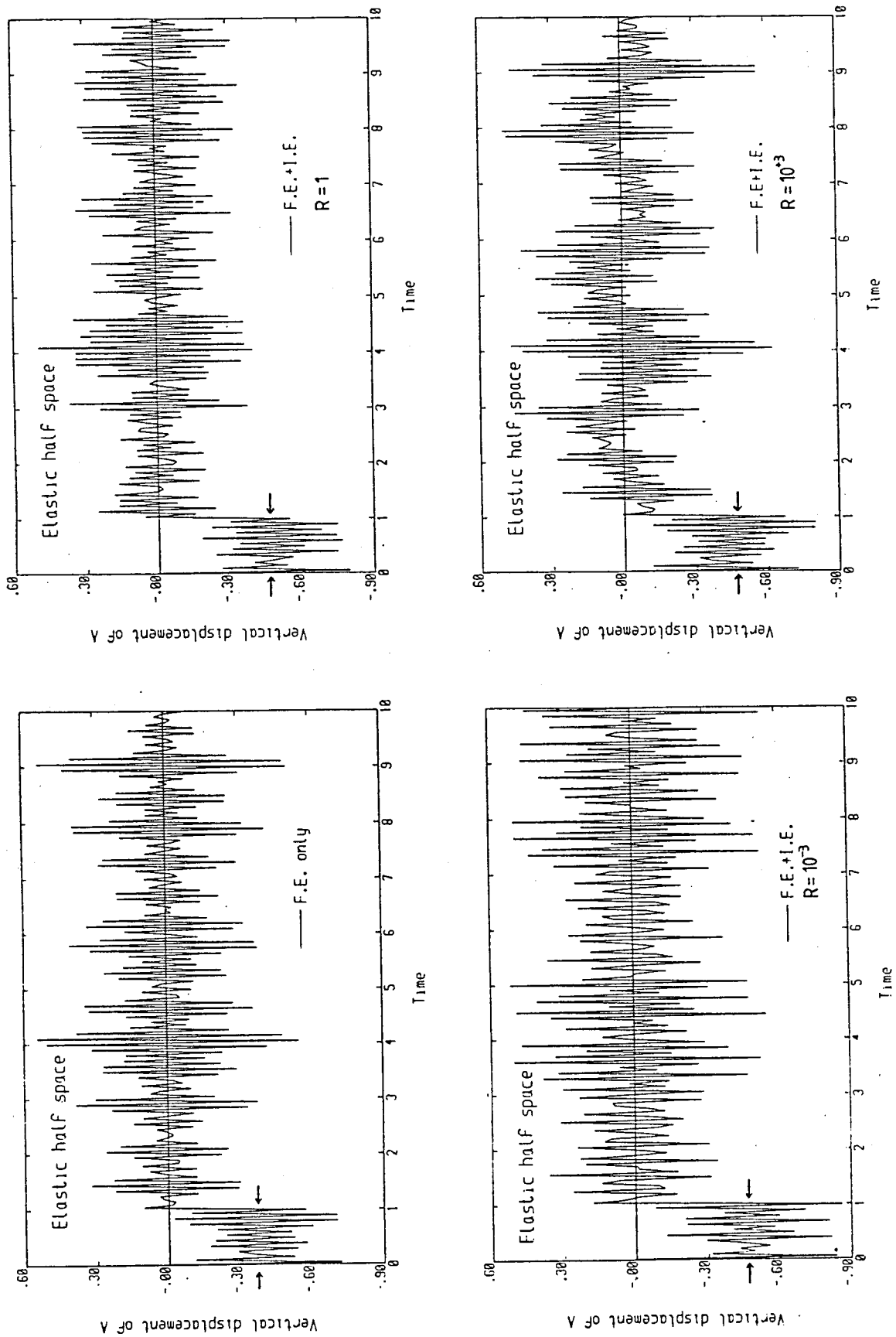

Fig. 8.3 – Plots of the vertical displacement history of node A for various solutions of the elastic half space problem

leads to a wider spacing for the "spikes" along the time axis.

Other experiments to be considered are the use of a lumped mass matrix instead of the consistent matrix used above, the adoption of different time integration rules for the finite and the infinite zone, the selection of different choices for damping matrix, the use of integration parameters giving increased numerical damping.

Summing up it may be said that the use of the mapped infinite element for transient analysis deserves further attention.

8.6 REFERENCES

1. FUNG, Y.C, Foundations of Solid Mechanics, Prentice-Hall, Inc., Englewood Cliffs, N.J., 1965

2. SOMMERFELD, A., Partial Differential Equations in Physics, Academic Press, N.Y., 1949

3. LYSMER, J. and KUHLEMEYER, R.L., Finite dynamic model for infinite media, J. Eng. Mech. Div., ASCE, 859-877, 1969

4. BAYLISS, A., GUNZBERGER, M. and TURKEL, E., Boundary conditions for numerical solution of elliptic equations in exterior regions, ICASE Report no. 80-1, NASA, Langley, 1978

5. SMITH, W.D., A non reflecting plane boundary for wave propagation problems, J. Comp. Phys., 15, 493-503, 1974

6. ZIENKIEWICZ, O.C. and NEWTON, R.E., Coupled vibrations of a structure submerged in a compressible fluid, Proc. Symp. F.E. Techniques, 359-371, Stuttgart, 1969

7. ZIENKIEWICZ, O.C. and BETTESS, P., Infinite elements in the study of fluid-structure interaction problems, Lecture Notes in Physics, 58, 133-172, Springer Verlag, 1976

8. ZIENKIEWICZ, O.C., KELLY, D.W. and BETTESS, P., The Sommerfeld (radiation) condition on infinite domains and its modelling in numerical procedures, in Comp. Meth. in Appl. Sc. and Engng., 169-203, R. Glowinski et al. (eds.), Springer-Verlag, 1979

9. PEDRO, J.O., Finite element stress analysis of arch dams, LNEC, Proc. 46/11/5272, Lisbon, 1976

10. BETTESS, P. and ZIENKIEWICZ, O.C., Diffraction and refraction of surface waves using finite and infinite elements, IJNME, 11, 1271-1290, 1977

11. SAINI, S.S., BETTESS, P. and ZIENKIEWICZ, O.C., Coupled hydrodynamic response of concrete gravity dams using finite and infinite elements, Int. J. Earthq. Engng. Str. Dynamics, 6, 363-374, 1978

12. CHOW, Y.K. and SMITH, I.M., Static and periodic infinite solid elements, IJNME, 17, 503-526, 1981

13. BETTESS, P., EMSON, C. and CHIAM, T.C., A new mapped infinite element for exterior wave problems, Internal Report C/R/403/82, Dep. Civ. Eng., Univ. Coll of Swansea, 1982

14. BETTESS, P., Private communications, Swansea, 1984

15. DASGUPTA, G., A finite element formulation for unbounded homogeneous continua, J. Appl. Mech., 49, 136-140, 1982

16. TIMOSHENKO, S.P. and GOODIER, J.N., Theory of elasticity, Mc Graw-Hill

CHAPTER 9

CONCLUSIONS

9.1	GENERAL CONSIDERATIONS	9.1
9.2	ACCURACY IN MODELLING OF MATERIAL BEHAVIOUR	9.1
9.3	EFFICIENCY IN NONLINEAR SOLUTION	9.2
9.4	ECONOMY IN UNBOUNDED DOMAIN ANALYSIS	9.2
9.5	DIRECTIONS FOR FURTHER STUDY	9.3
9.6	REFERENCES	9.5

CHAPTER 9

CONCLUSIONS

9.1 GENERAL CONSIDERATIONS

Finite element techniques for solution of quasistatic and transient dynamic materially and geometrically nonlinear structural problems in two-and three-dimensional bounded and unbounded domains have been investigated.

A critical assessment of current computational procedures and underlying assumptions has been systematically conducted to cover the fundamental aspects of the global formulation and many original improvements and refinements have been introduced and evaluated.

The main achievements and the more significant conclusions are now summarized.

9.2 ACCURACY IN MODELLING OF MATERIAL BEHAVIOUR

The elastoplastic state determination algorithm traditionally used in Swansea and familiar to many researchers elsewhere was carefully analysed. The use of Nayak's invariant set, although providing compactness in the coding and flexibility in the choice of yield criteria, was shown to suffer from some subtle drawbacks. An optical analogy [1] was proposed to help visualize possible troublesome situations which may arise when the stress point changes sextant in the stress space and which can provoke erroneous determination of the stress state of contact with the yield surface. An efficient numerical procedure was proposed that completely overcomes this problem. The investigation was further extended [2] to contemplate substepping techniques and an improved criterion for step sizing was established. An efficient way to detect the approach of yield surface singularities was developed and it was shown how to accommodate Koiter's generalization in the coding by taking in both cases full advantage of the use of Nayak's invariant set. A useful clarification of the question of normality in plane stress plasticity was produced.

The accurate modelling of hardening effects in elastoviscoplasticity was shown to require the inclusion of additional terms if an implicit integration scheme is selected [3]. This was interpreted as being equivalent to the adoption of a modified flow function that accounts for the expansion of the yield surface during the time step. The overestimation of displacements predicted on omission of the corrective terms became clearly apparent in the numerical experiments undertaken.

9.3 EFFICIENCY IN NONLINEAR SOLUTION

A detailed review of numerical methods for incremental-iterative solution of materially and geometrically nonlinear structural problems was produced. The formulation and computer implementation of full and modified Newton-Raphson methods was presented and a simple line search algorithm was developed that proved to be an effective accelerator of MNR solutions. It has therefore been agreeable to acknowledge the emergence in recent publications [7] of a renewed interest in this strategy, as the present research had indeed anticipated.

A careful assessment of matrix update techniques was undertaken, covering BFGS and, in particular, secant-Newton methods. A novel SN procedure has been derived from the inverse Davidon-Fletcher-Powell additive update, and the numerical comparisons carried out to date consistently attest to its superior efficiency and stability characteristics.

Special attention was devoted to elasto-viscoplastic quasistatic problems in multimaterial domains. An implicit-explicit time integration scheme was developed that proved instrumental in reducing computation costs [4,5]. Added benefits were obtained from the implementation of full and partial substructuring techniques in the frontal equation solver.

9.4 ECONOMY IN UNBOUNDED DOMAIN ANALYSIS

An extensive research effort has been invested upon Zienkiewicz's mapped infinite element. A new and simpler method of organizing the mapping between the finite parent domain and the semi-infinite

element domain was devised that emphasizes the formal similarities between finite and infinite mapped elements.

A systematic development and testing of 2D and 3D families of linear, serendipity and Lagrangian mapped infinite elements was carried out [6].

The performance of the element in the far field modelling of quasistatic unbounded domain problems with material nonlinearity was assessed in a series of numerical examples where both elastoplastic and elastoviscoplastic behaviour were considered [5,6]. In order to supply a term of comparison both with respect to accuracy and cost, alternative runs with finite-element-only meshes were undertaken for various mesh extents and types of boundary conditions. The coupled finite/infinite element solutions were always, and by far, the most economical and precise. In elastoviscoplastic multimaterial unbounded domains compounded benefits were obtained by the simultaneous use of finite/infinite elements and implicit/explicit time integration.

A preliminary investigation was carried out in transient dynamic problems mainly aimed at assessing the potential of the mapped infinite element as a nonreflective boundary damper. The results obtained so far seem promising but more extensive experimentation is required.

The ease of implementation, accuracy and expediency of the mapped infinite element make it a desirable feature for inclusion in multipurpose finite element packages.

9.5 DIRECTIONS FOR FURTHER STUDY

Brief outlines of the current state-of-the-art and research trends have been presented at several stages throughout the thesis. Merging that information with the valuable experience accumulated in the course of this investigation, a number of priorities for further research can be established.

(i) In the context of elastoplastic material modelling fourth-order Runge-Kutta methods [8] seem very accurate and fast and are certainly worth considering.

The very elementary elastoviscoplastic algorithm employed can be vastly improved, namely in what concerns the time integration of the constitutive relation. Iteration loops within each time step [9] besides ensuring more realistic results could be also beneficial for stability, in particular for implicit-explicit schemes, for which an efficient step sizing criterion remains to be established.

In large deformation applications a continuing effort is needed to translate into efficient coding the subtleties of the formulation, keeping nevertheless a clear understanding of the scope and meaning of the simplifying assumptions relevant to the actual degree of geometric nonlinearity presented by each category of problems. Recently published material [10-12] reportedly uses the Green-Naghdi stress rate based on rotated Cauchy stress, together with the polar decomposition of the velocity gradient and an improved response at large shear strains is achieved.

(ii) As to nonlinear solution procedures, the trend towards adaptive algorithms which automatically define the optimum load or time step size continues to register significant advances [13,14]. A very interesting "cross-fertilization" between quasi-Newton and dynamic relaxation methods has also been proposed [15]. A recent progress report on the element-by-element method demonstrates its effectiveness for large 3D problems. Viscous relaxation and multigrid techniques with the use of hierarchical element forms seem particularly apt to explore optimally the superior efficiency of vector processors [17]. As demonstrated by this compact overview of recent achievements, a wide variety of comparative testing and creative merging of methods is continuing and makes this research area a very exciting one.

(iii) Regarding efficient modelling of unbounded domains, there is still room for improvement in the generalization of concepts [18]. In particular in the case of transient dynamic analysis, more extensive numerical experimentation is required to provide a more distinct picture of the mapped infinite element capabilities.

9.6 REFERENCES

1. MARQUES, J.M.M.C. and OWEN, D.R.J., Some reflections on elastoplastic stress calculation in finite element analysis, Int. J. Num. Meth. Engng. (in press)

2. MARQUES, J.M.M.C., Stress computation in elastoplasticity, Int. J. Engineering Computations, 1, 42-51, 1984

3. MARQUES, J.M.M.C. and OWEN, D.R.J., Strain hardening representation for implicit quasistatic elasto-viscoplastic algorithms, Comp. & Str., 17, 301-304, 1983

4. OWEN, D.R.J. and MARQUES, J.M.M.C., Coupled implicit-explicit time integration with frontal substructuring in two-dimensional quasistatic elastoviscoplasticity, in Num Meth. for Coupled Problems, 147-160, E. Hinton et al. (eds.), Pineridge Press, Swansea, 1981

5. MARQUES, J.M.M.C. and OWEN, D.R.J., Implicit-explicit time integration in quasistatic elastoviscoplasticity using finite and infinite elements, Comp. Meth. Appl. Mech. Engng., 42, 167-182, 1984

6. MARQUES, J.M.M.C. and OWEN, D.R.J., Infinite elements in quasistatic materially nonlinear problems, Comp. & Str., 18,739-751, 1984

7. CRISFIELD, M.A., Accelerating and damping the modified Newton-Raphson method, Comp. & Str., 18, 395-407, 1984

8. WISSMANN, J.W. and HAUCK, C., Efficient elastic-plastic finite element analysis with higher order stress-point algorithms, Comp. & Str., 17, 89-95, 1983

9. LABORDE, P., Approximation en viscoplasticité, J. Méc. Théor. Appl., 1, 419-428, 1982

10. HALLEUX, J.P. and CASADEI, F., Transient large strain analysis of plane and axisymmetric structures by means of biquadratic finite elements, in Num. Meth. for Nonlinear Problems (vol. 2), 586-599, C. Taylor et al. (eds.), Pineridge Press, Swansea, 1984

11. BATHE, K.J., CHAUDARY, A., DVORKIN, E.N., ALMEIDA, C.A., HO, L.W. and LARSSON, G., Some advances in finite element procedures for non-linear analysis, idem, 488-500

12. MOLENKAMP, F. and TEUNISSEN, J.A.M., Incremental updating of large material rotation and deformation, idem, 182-190

13. BERGAN, P.G. and MOLLESTAD, E., Static and dynamic solution strategies in nonlinear analysis, idem, 3-17

14. CRISFIELD, M.A., Overcoming limit points with material softening and strain localisation, idem, 244-277

15. FELIPPA, C.A., Dynamic relaxation and quasi-Newton methods, idem, 27-38

16. HUGHES, T.J.R., RAEFSKY, A., MULLER, A., WINGET, J.M. and LEVIT, I., A progress report on EBE solution procedures in solid mechanics, idem, 18-26

17. ZIENKIEWICZ, O.C., Numerical methods for nonlinear problems - a look at future prospects, idem, 1

18. OKABE, N., Generalised Lagrange family for the cube with special reference to infinite domain interpolations, Comp. Meth. Appl. Mech. Engng., 38, 153-168, 1983

FACULDADE DE ENGENHARIA
UNIVERSIDADE DO PORTO
BIBLIOTECA
0000005872